SCUOLA INTERNAZIONALE SUPERIORE DI STUDI AVANZATI

DOCTORAL THESIS

Symmetry Resolution of Entanglement Measures in Free Fermionic Systems and Conformal Field Theories

Author:
Riccarda BONSIGNORI

Supervisor:
Prof. Pasquale CALABRESE



A thesis submitted in fulfillment of the requirements
for the degree of Doctor of Philosophy
in the

Statistical Physics Group
SISSA

Acknowledgements

I thank in advance the members of the Examination Committee for their comments and suggestions on the manuscript. The other acknowledgements will be present in the printed version of the Thesis.

List of publications

The Thesis is based on the following publications:

- [1] R. Bonsignori, P. Ruggiero and P. Calabrese,
Symmetry resolved entanglement in free fermionic systems,
J. Phys. A **52**, 475302 (2019).

- [2] R. Bonsignori and P. Calabrese,
Boundary effects on symmetry resolved entanglement,
J. Phys. A: Math. Theor. **54**, 015005 (2020).

- [3] G. Parez, R. Bonsignori and P. Calabrese,
Quasiparticle dynamics of symmetry resolved entanglement after a quench: the examples of conformal field theories and free fermions,
Phys. Rev. B **103**, L041104 (2020).

- [4] S. Murciano, R. Bonsignori and P. Calabrese,
Symmetry decomposition of negativity of massless free fermions,
SciPost Phys. **10**, 111 (2021)

- [5] G. Parez, R. Bonsignori and P. Calabrese,
Exact quench dynamics of symmetry resolved entanglement in a free fermion chain,
arXiv:2106.13115

The following work is in progress and is not discussed in this Thesis:

- [6] G. Parez, R. Bonsignori and P. Calabrese,
Quench dynamics of symmetry resolved entanglement negativity in a free fermion chain,
In preparation

Contents

Acknowledgements i

List of publications iii

Introduction ix

I Preliminary notions xvii

1 Entanglement 1

1.1 Entanglement in Quantum mechanics . . . 1
1.1.1 Pure and mixed states . . . 1
1.1.2 Bipartite systems . . . 3
1.1.3 An example: the Qbit . . . 4
1.1.4 Definition of entanglement . . . 5
1.1.5 Separability criteria . . . 6
1.1.6 Operational definition of entanglement . . . 8
1.2 Entanglement measures . . . 9
1.2.1 von Neumann and Rényi Entropies . . . 9
1.2.2 Mutual information . . . 10
1.2.3 Negativity . . . 11
1.3 Replica approach . . . 12
1.3.1 Replicas and entanglement entropy . . . 12
1.3.2 Replicas and entanglement negativity . . . 13
1.3.3 Path Integral approach for the entanglement entropy . . . 14
1.3.4 Twist Fields . . . 16
1.3.5 Path Integral approach for the negativity . . . 18
1.4 Entanglement Entropy and Conformal Field theory . . . 20
1.4.1 Entanglement entropy in CFT: single interval . . . 21
1.4.2 Systems with boundaries . . . 28
1.4.3 Disjoint intervals . . . 30
1.4.4 Entanglement negativity in conformal field theory . . . 31
1.5 Entanglement spreading in integrable systems out of equilibrium . . . 33
1.5.1 Dynamics of a system after a quench . . . 34
1.5.2 CFT approach to global quantum quenches . . . 35
1.5.3 Correlation functions following a global quench . . . 36
1.5.4 Evolution of the entanglement entropy after a global quench . . . 37

1.5.5 Quasiparticle picture . . . 38
1.6 Free fermions on the lattice . . . 40
1.6.1 Correlation matrix techniques . . . 42

II Results **45**

2 Symmetry resolved entanglement in free fermionic systems **47**
2.1 Introduction . . . 47
2.2 Symmetry resolution and flux insertion . . . 48
2.2.1 Replica method and results from QFT . . . 49
2.3 Free fermions on a lattice: flux insertion and charged entropies . . . 50
2.3.1 Charged entropies via the generalised Fisher-Hartwig conjecture . . . 52
2.4 Free fermions on a lattice: symmetry resolved entropies . . . 58
2.4.1 Q_A-resolved moments via Fourier trasform . . . 59
2.4.2 Symmetry resolved Rényi and entanglement entropy . . . 61
2.5 Charged and symmetry resolved entanglement for the Fermi gas . . . 63
2.6 Concluding remarks . . . 64
2.A Appendix: Details of calculations . . . 65

3 Boundary effects on symmerty resolved entanglement **67**
3.1 Introduction . . . 67
3.2 Entanglement entropy, CFT, and boundaries . . . 69
3.3 Semi-infinite chain of free fermions: the block $A = [1, \ell]$ . . . 71
3.3.1 A generalised Fisher-Hartwig formula and charged entropies . . . 72
3.3.2 Symmetry resolved moments and entropies . . . 76
3.4 A general relation between Toeplitz+Hankel matrices and block Toeplitz ones . . . 78
3.5 Disjoint intervals in the infinite chain . . . 79
3.6 Block away from the boundary . . . 81
3.6.1 Symmetry resolution . . . 83
3.7 Concluding remarks . . . 84

4 Symmetry decomposition of negativity of massless free fermions **87**
4.1 Introduction . . . 87
4.2 Charge imbalance resolved negativity . . . 88
4.2.1 The fermionic partial time reversal density matrix . . . 89
4.2.2 Imbalance entanglement via bosonic partial transpose . . . 90
4.2.3 Imbalance entanglement of fermions via partial TR . . . 94
4.3 Replica approach . . . 95
4.3.1 Charged moments of the reduced density matrix . . . 96
4.3.2 Charged moments of the partial transpose . . . 99
4.4 Charged and symmetry resolved negativities in a tripartite geometry . . . 100
4.4.1 Low and high temperature limits. . . . 105
4.4.2 Symmetry resolution . . . 107
4.5 Charged and symmetry resolved negativities in a bipartite geometry . . . 109
4.5.1 Low and high temperature limits . . . 111
4.5.2 A semi-infinite system . . . 113
4.5.3 Symmetry resolution . . . 114

4.6 Concluding remarks . . . 116
4.A Appendix: Numerical methods . . . 117
4.B Appendix: Mode expansion of charged moments of ρ_A and $\rho_A^{R_1}$ . . . 118
4.C Appendix: Lattice-dependent terms and Fisher-Hartwig conjecture . . . 119
4.D Appendix: Twisted partial transpose . . . 123

5 Exact quench dynamics of symmetry resolved entanglement in a free fermion chain 125
5.1 Introduction . . . 125
5.2 Symmetry resolution and flux insertion . . . 126
5.3 Free fermions . . . 127
5.4 Quench from the Néel state . . . 130
5.4.1 Single interval . . . 130
5.4.2 Disjoint intervals . . . 139
5.5 Quench from the dimer state . . . 144
5.5.1 Single interval . . . 144
5.5.2 Disjoint intervals . . . 149
5.6 Conformal field theory results . . . 153
5.7 Quasiparticle picture for the charged moments . . . 154
5.7.1 Dynamics of the entanglement entropies . . . 154
5.7.2 Discussion about the dynamics of the mutual information . . . 155
5.8 Concluding remarks . . . 156
5.A Evaluation of $\mathrm{Tr} J_A(t)^{2n}$ . . . 158

A Conformal Field Theory 163
A.1 The conformal group . . . 163
A.1.1 Conditions for conformal invariance . . . 163
A.1.2 Conformal group in $d \geq 3$ . . . 165
A.1.3 Constraints of conformal invariance in d dimensions . . . 166
A.1.4 Conformal group in $d = 2$ . . . 167
A.2 The energy-momentum tensor . . . 170
A.2.1 Energy-momentum tensor for $d = 2$ . . . 171
A.3 Radial Quantization . . . 171
A.4 Operator product expansion . . . 172
A.4.1 Operator product expansion of the energy-momentum tensor . . . 173
A.4.2 Conformal transformations of the energy-momentum tensor . . . 174
A.5 Conformal Ward identity . . . 175
A.6 Two-point function . . . 176

Bibliography 178

Introduction

Since the early stages of Quantum Mechanics, it appeared evident that the common interpretation of the physical world had to be questioned and reformulated. In particular, *entanglement*, first coined by Schrödinger as "Verschränkung" in 1935, is the phenomenon that better encodes the counter-intuitive nature of the quantum realm [7]:

> *"When two systems, of which we know the states by their respective representatives, enter into temporary physical interaction due to known forces between them, and when after a time of mutual influence the systems separate again, then they can no longer be described in the same way as before, viz. by endowing each of them with a representative of its own. I would not call that one but rather the characteristic trait of quantum mechanics, the one that enforces its entire departure from classical lines of thought. By the interaction the two representatives [the quantum states] have become entangled."*

The peculiarity of entanglement is not only due to the fact that it has no analog in classical physics, but also to the fact that when two or more systems are entangled, a local action on one of them *immediately* affects the state of the others. This vision was initially rejected by part of the scientific community, in particular Einstein referred to entanglement as "spooky action at distance". In fact, it implies that information between systems can be transmitted faster than light, which is forbidden by the theory of relativity. In the famous 1935 paper by Einstein, Podolsky and Rosen [8], a series of arguments was proposed to show that the quantum state is simply an incomplete characterization of a quantum system. The missing parameters are sometimes referred to as "hidden parameters" or "hidden variables". According to the authors, the reason why entanglement seems nonlocal is because the wave function failed to give enough information. This in turn implies the hidden variables theory, namely the existence of hidden variables or parameters that precludes the scientist from knowing everything about the state of the system.

In 1964 Bell [9] proved that the assumption of the existence of hidden variables, supported by Einstein's view of local realism, leads to algebraic predictions, known as Bell's inequalities, that are violated by the Quantum Mechanics. Thanks to these inequalities, the problem of the physical reality of quantum systems was shifted from the realm of philosophy to the domain of experimental physics. In 1982 an experiment by Aspect *et al.* [10], showed an unambiguous violation of Bell's inequalities, disproving the existence of hidden variables. Therefore, entan-

glement played a central role in the discovery of the non-local nature of quantum theory, and its understanding was a necessary step to test its foundations.

It was only in the 1980s that physicists and computer scientists started to consider the non-local correlations of entangled quantum states as a new kind of non-classical physical resource. They realized that it could be used to perform tasks that cannot be accomplished with classical information tools, such as quantum teleportation and quantum cryptography [11, 12]. Since then, the interest in quantum entanglement has grown significantly in several previously disconnected areas of physics, unveiling unexpected connections between them. In high energy physics, for instance, entanglement between degrees of freedom both inside and outside of a black hole is expected to explain the properties of Hawking's radiation, especially for the associated Beckenstein– Hawking entropy [13, 14]. In condensed matter physics, entanglement is a key ingredient in the study of the dynamics of many-body quantum systems [15]. Moreover, it is the mechanism at the basis of many interesting phenomena in topologically ordered phases (as fractional quantum Hall states and spin liquid states), which include fractional charge, fractional statistics and protected gapless boundary excitations [16]. In statistical physics, that is the main perspective of this Thesis, entanglement is a tool to detect and classify quantum critical points. Progress in the study of entanglement does not come only from the theoretical community but also from the experimental ones. Recently, thanks to the developments in cold-atom and ion-trap experiments, it has been possible to measure the many-body entanglement of non-equilibrium quantum states [17, 18, 19].

In order to characterize and manipulate entanglement in quantum systems, it is also necessary to properly quantify it. The definition of suitable entanglement measures represented a nontrivial challenge for the quantum information community as they are not in principle uniquely defined. Nowadays, several definitions of entanglement measures are available, and a lot has been understood in the context of low-dimensional many body quantum systems, both from the theoretical [15, 20, 21, 22] and experimental side [23, 18, 24, 19]. For bipartite pure states described by a density matrix ρ, the most useful measure is the *entanglement entropy*, defined as the von Neumann entropy of the reduced density matrix $\rho_A = \mathrm{Tr}_B \rho$ associated to one of the two subsystems (denoted by A and B, respectively)

$$S = -\mathrm{Tr}\rho_A \ln \rho_A. \tag{0.0.1}$$

The entanglement entropy S is the limit for $n \to 1$ of a larger family of entropies, known as Rényi entropies

$$S_n = \frac{1}{1-n} \ln \mathrm{Tr}\rho_A^n. \tag{0.0.2}$$

In many-body quantum systems with gapped local hamiltonian, the entanglement entropy of a subsystem is observed to obey the so-called *area law*. For such systems, quantum correlations generally occur between degrees of freedom close to the boundary separating the subsystem A from its complement. As a consequence, the entanglement entropy for a d-dimensional system is expected to scale with the area of the boundary ∂A, that is $S \sim Area(\partial A)/a^{d-1}$, where a is an ultraviolet cutoff. This idea was developed starting from the analogy with the black hole entropy, that is proportional to the area of the boundary surface of the black hole, as expressed by the Bekenstein-Hawking formula [21]. Exceptions to the area law are represented for example by one-dimensional critical systems, where the entanglement entropy is found to scale as the logarithm of the subsystem size [25, 26].

Within quantum field theory both Eqs. (0.0.1) and (0.0.2) are usually obtained from the integer moments $Z_n = \mathrm{Tr}\rho_A^n$ of ρ_A, which are in turn easily expressed in the path integral formalism as partition function on suitable n-sheeted Riemann surfaces [25, 26]. This approach, when applied to critical systems, whose low energy physics is described by $(1+1)$ dimensional conformal field theory, leads to the famous scaling results [27, 25, 26, 28]

$$S = \frac{c}{3}\ln\frac{\ell}{a}, \qquad S_n = \frac{c}{6}\frac{(n+1)}{n}\ln\frac{\ell}{a}, \tag{0.0.3}$$

for a subsystem A made of a single interval of length ℓ embedded in an infinite one-dimensional system, and similarly for finite systems, systems at finite temperature, and other situations: it is sufficient to replace ℓ with the relevant length in the considered regime, see e.g. [26]. As previously discussed, this logarithmic scaling with ℓ is an example of violation of the area law.

For a mixed state, the entanglement entropies are no longer good measures of entanglement since they mix quantum and classical correlations (e.g. in a high temperature state, S gives the extensive result for the thermal entropy that has nothing to do with entanglement). However, they can be used to construct a measure of the total correlations between the subsets. Let us denote two subsystems A_1 and A_2 such that $A = A_1 \cup A_2$. The *mutual information*

$$I^{A_1:A_2} \equiv S^{A_1} + S^{A_2} - S^{A_1\cup A_2}, \tag{0.0.4}$$

is a very useful measure of the total correlation between A_1 and A_2 [29]. This definition can be readily generalised to a Rényi mutual information

$$I_n^{A_1:A_2} = S_n^{A_1} + S_n^{A_2} - S_n^{A_1\cup A_2} = \frac{1}{n-1}\log\left(\frac{\mathrm{Tr}\rho^n_{A_1\cup A_2}}{\mathrm{Tr}\rho^n_{A_1}\mathrm{Tr}\rho^n_{A_2}}\right). \tag{0.0.5}$$

However, as a very important difference compared to the von Neumann mutual information (0.0.4), $I_n^{A_1:A_2}$ is not a measure of the correlations (e.g., it can be negative for some states [30]). The definition of a proper and calculable Rényi mutual information is a long standing problem, see, e.g., the discussion in the recent manuscript [31].

A computable measure for entanglement in mixed states is the so called *entanglement negativity* [32]. Denoting as $\rho_A^{T_1}$ the partial transpose of the reduced density matrix ρ_A with respect only to A_2, the entanglement negativity is defined as

$$\mathcal{N} = \frac{||\rho_A^{T_2}|| - 1}{2}, \tag{0.0.6}$$

where the trace norm $||\cdot||$ is the sum of the absolute values of the eigenvalues of $\rho_A^{T_2}$. A related measure of entanglement for mixed states is the *logarithmic negativity*

$$\mathcal{E} = \log||\rho_A^{T_2}|| = \log\mathrm{Tr}|\rho_A^{T_2}|. \tag{0.0.7}$$

For a detailed characterization of entanglement measures we refer to Chap. 1 and Sect. 1.2.

In recent years, the interplay between entanglement and symmetries of a quantum system gained a lot of attention. The goal of this investigation is to have access to the "internal symmetry structure" of the entanglement [33, 34, 35]. This interest is motivated by the experimental observation conducted by Lukin et al [19] who revealed, in the context of many-body disordered systems, that a finer description of the many body dynamics comes from the knowledge

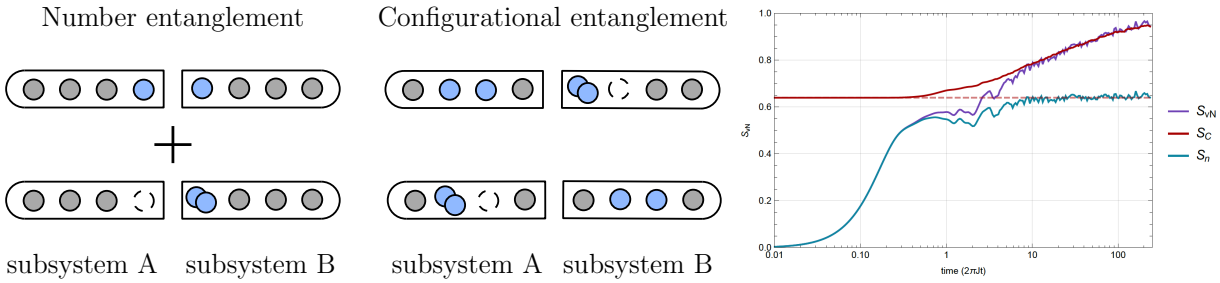


Figure 1: *Left:* The entanglement between subsystems A and B of an isolated system out of equilibrium comes from the two contributions of the number (S^n) and configurational (S^c) entanglement. The former comes from the superposition of states with different particle numbers in the subsystems, the latter from a superposition of states with different particle arrangement within the subsystems. *Right:* Total entanglement entropy as a function of time in an interacting system at strong disorder. The total entropy (purple line) is obtained as the sum of the number entropy S^n (blue line) and the configurational entropy S^c (red line). The S^c is offset by the long-time average of S^n. The qualitative behavior of the plots show that logarithmic growth of the entropy comes primarily from the configurational entropy. Reprinted from Ref. [19].

of how the entanglement arises from the various symmetry sectors. In particular, looking at systems possessing an internal global symmetry, entanglement turns out to have two different contributions, called *number* (or *fluctuation*) and *configurational* entanglement [19]. The number entanglement comes from a superposition of states having different particle numbers in the subsystems and arises from the particle motion across the boundary. The configurational entanglement is due to the superposition of states having different particle arrangement within the subsystems and requires both particle motion and interactions. These two mechanisms are shown in the left panel of Fig. 1. In the experiment [19], the time evolution of these entropies has been considered and it has been shown that, in the many-body localized phase, the number entropy grows quickly and soon saturates, irrespectively from the strength of the interaction. Conversely, the configurational entropy moves up very slowly, logarithmically in time, but only after a time delay, whose precise value depends on the interaction strength and gets larger as the interaction decreases. This behavior is shown in the right panel of Fig. 1, that is taken from Ref. [19]. These findings explain former theoretical results for the total entanglement entropy [36, 37].

At the same time, two different theoretical frameworks have been developed indipendently by Xavier, Alcaraz and Sierra [34] and Goldstein and Sela [35, 38, 39] to address the problem of extracting the *symmetry resolved* contributions for different entanglement measures. Both these approaches, applied in the context of one-dimensional critical quantum systems, showed that in the scaling limit these contributions generally obey entanglement *equipartition*, which means that they are independent of the symmetry sector. The analytical evaluation of the contributions from the different symmetry sectors to the total entanglement relies on the fact that, in a system with a globally conserved charge, the reduced density matrix for a subsystem is block diagonal.

In this Thesis, we focus on the case of a bipartite system $A \cup B$ possessing an internal $U(1)$ symmetry generated by a charge $Q = Q_A \otimes \mathbb{I}_B + \mathbb{I}_A \otimes Q_B$, which is also treated in Refs. [34, 35, 38] and will be examined in more detail in Sect. 2.2. For such system, the reduced density matrix ρ_A is characterized by a block diagonal form as shown in Fig.2, where each block

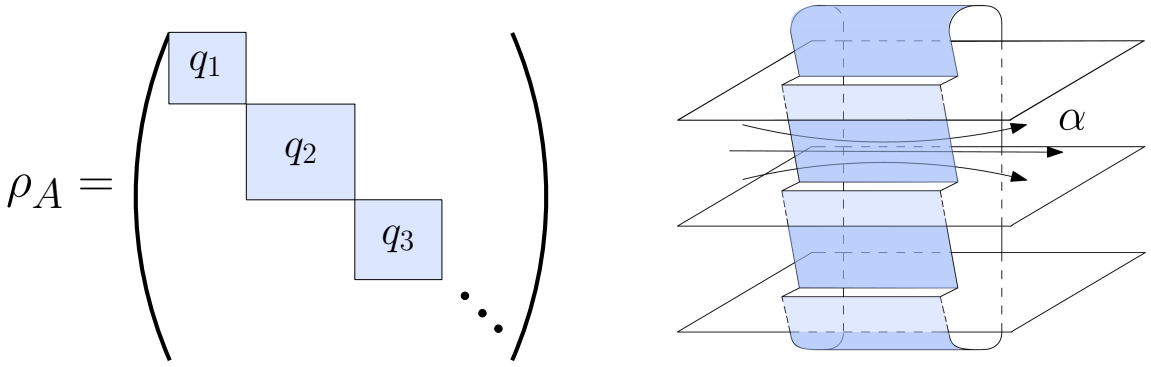


Figure 2: *Left:* Block structure of the reduced density matrix. Each block is labeled by a different eigenvalue q of Q_A. *Right:* Example of a $n = 3$ sheeted Riemann surface pierced by an Aharonov-Bohm flux α.

corresponds to an eigenvalue q of Q_A. Thus, it admits the following decomposition

$$\rho_A = \oplus_q [p(q)\rho_A(q)], \tag{0.0.8}$$

where $p(q)$ is the probability of finding q as outcome of a measure of Q_A. Each block of the reduced density matrix is normalised so that $\mathrm{Tr}\rho_A(q) = 1$. Using the block decomposition in Eq. (0.0.8), the von Neumann entropy of the reduced density matrix ρ_A can be written as the sum of diagonalized blocks as follows

$$\begin{aligned} S &= -\sum_i [\rho_A]_{ii} \log[\rho_A]_{ii} = -\sum_q \sum_i p(q)[\rho_A(q)]_{ii} \log\left(p(q)[\rho_A(q)]_{ii}\right) \\ &= -\sum_q p(q) \log p(q) \underbrace{\sum_i [\rho_A(q)]_{ii}}_{=1} - \sum_q p(q) \underbrace{\sum_i \left([\rho_A(q)]_{ii} \log[\rho_A(q)]_{ii}\right)}_{\equiv -S(q)} \\ &= -\sum_q p(q) \log p(q) + \sum_q p(q) S(q) \equiv S^n + S^c. \end{aligned} \tag{0.0.9}$$

The two contributions S^n and S^c are the previously introduced number and configurational entropy. In the last line of Eq. (0.0.9) we also introduced the *symmetry resolved entanglement entropy* $S(q)$ as the entropy corresponding to the block $\rho_A(q)$, and in analogy one can define the *symmetry resolved Rény entropies* $S_n(q)$

$$S(q) \equiv -\mathrm{Tr}[\rho_A(q) \log(\rho_A(q))], \qquad S_n(q) \equiv \frac{1}{1-n} \log \mathrm{Tr}[\rho_A(q)^n]. \tag{0.0.10}$$

The analytical evaluation of these quantities is one of the main goal of this Thesis. Unfortunately their definitions require the knowledge of the resolution of the spectrum of ρ_A in Q_A, that is generally not directly achievable.

An alternative approach, developed in Refs. [34, 35] consists in the definition of the so-called *charged moments* $Z_n(\alpha)$, which can be interpreted as the moments of ρ_A where twisted boundary conditions are imposed along the cuts of the Riemann surface.

In Ref. [35] the charged moments find a geometrical interpretation in the framework of the replica trick as partition function of a n-sheeted Riemann surface pierced by an Aharonov-Bohm flux such that the total phase accumulated by the field upon going through the entire

surface is α. The relation between twisted boundary conditions and flux insertion was previously explored, for instance, in the context of free field theories [40, 41, 42, 43]. Moreover, similar quantities have also been introduced in the holographic setting [44, 45, 46] and in the study of entanglement in mixed states [38, 47, 48].

In the case of a $1+1$-dimensional conformal field theory, the charged moments can be rewritten in terms of correlator of properly defined composite twist fields $\mathcal{T}_{n,\alpha}, \tilde{\mathcal{T}}_{n,\alpha}$ implementing twisted boundary conditions, as shown in Fig. 2. Once the charged moments are obtained, their Fourier transform gives the symmetry resolved partition functions $\mathcal{Z}_n(q)$. Then, the symmetry resolved entanglement and Rényi entropies are expressed accordingly

$$S_n(q) = \frac{1}{1-n} \ln \left[\frac{\mathcal{Z}_n(q)}{\mathcal{Z}_1(q)^n} \right] \qquad S(q) = -\partial_n \left[\frac{\mathcal{Z}_n(q)}{\mathcal{Z}_1(q)^n} \right]_{n=1} . \tag{0.0.11}$$

The study of *the symmetry resolution of entanglement* became a very active research area over the last years and has been applied in various field theoretical contexts such as conformal field theories [35, 34, 2, 49, 50, 51, 52], free lattice models [1, 53, 54, 55], integrable systems [56, 57, 58, 59, 60, 61], free quantum field theories [62], disordered systems [63], nontrivial topological phases [64, 65, 66], out-of-equilibrium quantum many-body systems [39, 3, 5, 67], non-complementary subsystems [38, 4, 68] and holography [69].

Structure of the Thesis.

This Thesis is devoted to the study of the symmetry resolution of the entanglement measures in free fermionic systems. It is organised as follows:

Part I: Preliminary notions

- In Chap. 1 we give an overview of the main definitions and concepts related to the entanglement and its measures in quantum mechanics and quantum field theory. Then, we specialize to the case of conformal field theories, to derive expressions of the entanglement entropy and negativity in all the cases that will be examined in the second part of the Thesis. We finally illustrate the main free-fermionic techniques that will be used to perform the analytical as well as numerical lattice calculations.

Part II: Results

- In Chap.2, based on Ref. [1], we consider a 1-dimensional system of free fermions hopping on a lattice, in which the conserved $U(1)$ charge is the total particle number. We evaluate the symmetry resolved Rényi and entanglement entropies determining exactly all the non-universal constants and logarithmic corrections to the scaling, thanks to the so-called Fisher-Hartwig conjecture.

- In Chap.3, based on Ref. [2], we study the symmetry resolved entanglement entropies in 1-dimensional systems in presence of boundaries, considering the cases of an interval starting from the boundary and disconnected from it. We evaluate the charged and symmetry resolved entropies for conformal invariant theories and a semi-infinite chain of free fermions, finding entanglement equipartition. Using a generalization of the lattice calculations performed in Chap.2, we also evaluate the first term breaking equipartition for the free fermionic chain.

- In Chap.4, based on Ref. [4], we study the symmetry resolution of the entanglement negativity in free fermionic systems, which admits a decomposition in terms of the charge imbalance between the two subsystems. We use conformal field theory to derive the universal behavior of the charge imbalance resolved negativity for a free Dirac field at finite temperature and size. For the lattice version of the Dirac filed, we also determine exactly the model-dependent terms using the Fisher-Hartwig conjecture. We find that at leading order the charge imbalance resolved negativity verifies equipartition. For the lattice model, we also evaluate the first corrections to this equipartition.

- In Chap.5, based on Refs. [3, 5], we study the time evolution of the symmetry resolved entanglement entropy and a suitably defined symmetry resolved mutual information in a system of free fermions after a quench. In the context of free fermions and conformal field theories, we are able to provide analytical results for the time-dependent charged and resolved entropies, and shed light on two new physical phenomena. First, the symmetry resolved Rényi entropies start evolving with a calculable time delay that depends on the charge sector. Second, there is an effective equipartition of the entanglement in the limit of large subsystem size. For free fermions, we also find that effective equipartition is verified by the mutual information. We expect that these phenomena occur in more general quantum systems, as they can be understood from the quasiparticle picture for the spreading of entanglement.

- In Appendix A, we give an overview of conformal field theory, reporting the main concepts and formulas that are needed for a more complete understanding of the previous Chapters.

Part I

Preliminary notions

Chapter 1

Entanglement

1.1 Entanglement in Quantum mechanics

1.1.1 Pure and mixed states

In physics, the state of a physical system (classical or quantum), provides a complete description of the system at any time [70].

The mathematical formulation of this concept is encoded in the postulates of Quantum Mechanics (QM) [71, 72]: a state of a quantum system is a *ray* in a complex Hilbert space $\mathcal{H}$, i.e., an equivalence class of vectors that differ by a phase multiplication factor. Adopting the Dirac notation of kets, this means that $|\psi\rangle$ and $e^{i\alpha}|\psi\rangle$ are the same physical state. Let us consider a (finite) n-dimensional Hilbert space, with $\{|u_i\rangle\}_{i=1}^{n}$ the associated complete orthonormal basis. A generic state ψ can be written as

$$|\psi\rangle = \sum_{k=1}^{n} c_k |u_k\rangle. \tag{1.1.1}$$

One can choose such vectors to have norm one, to recover the interpretation of the square moduli of their components as probabilities, that is $\sum_{i=1}^{n} |c_i|^2 = 1$. These so called *pure states*, contain all the information about the whole quantum system.

However, in most of the physical realizations the system considered has interactions with an external environment, whose state is not known. Because of this lack of information, it cannot be anymore described by a single state vector, and the notion of *mixed states* has to be introduced. A mixed state is a statistical mixture of pure states, i.e., it is described by pairs of pure states and associated probabilities $\{(p_1, |\psi_1\rangle), \cdots, (p_k, |\psi_k\rangle)\}$, that verify the condition

$$\sum_k p_k = 1. \tag{1.1.2}$$

A mixed state must not be confused with the superposition of states given by Eq.(1.1.1).

In order to include also these more general situations, the state of the system can be repre-

sented by the *density operator* operator, defined as

$$\begin{aligned} \rho: \quad \mathcal{H} \quad &\to \quad \mathcal{H} \\ \rho = \sum_k p_k |\psi_k\rangle\langle\psi_k|. \end{aligned} \tag{1.1.3}$$

The representation of this operator on a given basis is referred as *density matrix*. If the state is pure, one of the set of probabilities is $p_j = 1$, and the others are $p_k = 0$ for $k \neq j$, because of Eq.(1.1.2). Then the associated density matrix is the projector on the state known with probability one, that is

$$\rho = |\psi_j\rangle\langle\psi_j|. \tag{1.1.4}$$

The matrix elements in this case are simply given by

$$\rho_{ij} = \langle u_i|\rho|u_j\rangle = \langle u_i|\psi\rangle\langle\psi|u_j\rangle = c_i^* c_j. \tag{1.1.5}$$

For a generic mixed state, instead, introducing the coefficients $c_j^{(k)} = \langle u_j|\psi_k\rangle$, the matrix elements are given by

$$\rho_{ij} = \langle u_j|\rho|u_i\rangle = \sum_k p_k c_j^{(k)} c_i^{(k)*}. \tag{1.1.6}$$

With these definitions, one can prove the following theorem.

Theorem 1.1.1. *The density matrix has the following properties:*

i) ρ *is normalized:* $Tr(\rho) = 1$,

ii) ρ *is self adjoint:* $\rho = \rho^\dagger$,

iii) ρ *is non-negative:* $\rho_{ii} \geq 0$.

Proof: The first property can be easily shown as follows

$$\mathrm{Tr}(\rho) = \mathrm{Tr}\left(\sum_k p_k |\psi_k\rangle\langle\psi_k|\right) = \sum_n \sum_k p_k \langle u_n|\psi_k\rangle\langle\psi_k|u_n\rangle = \sum_{nk} p_k |c_n^{(k)}|^2 = 1.$$

The second property follows from the definition of ρ, since the probabilities p_k are real numbers. Finally for the third property

$$\rho_{nn} = \sum_k p_k |c_n^{(k)}|^2 \geq 0, \quad \forall n.$$

□

The density operator can be used to evaluate the expectation values of an operator $\mathbf{A}$ as

$$\langle \mathbf{A} \rangle = \mathrm{Tr}[\rho \mathbf{A}]. \tag{1.1.7}$$

In fact, if the state is pure one has

$$\begin{aligned} \langle \mathbf{A} \rangle = \langle\psi|\mathbf{A}|\psi\rangle = \sum_{ij} c_i^* c_j \langle u_i|\mathbf{A}|u_j\rangle = \sum_{ij} \langle u_i|\rho|u_j\rangle\langle u_j|\mathbf{A}|u_i\rangle = \\ = \sum_i \langle u_i|\rho\mathbf{A}|u_i\rangle = \mathrm{Tr}[\rho\mathbf{A}]. \end{aligned} \tag{1.1.8}$$

If the state is mixed, instead

$$\begin{aligned}\langle \mathbf{A} \rangle &= \sum_k p_k \langle \psi_k | \mathbf{A} | \psi_k \rangle = \sum_{ij} \sum_k p_k c_i^{(k)*} c_j^{(k)} \langle u_i | \mathbf{A} | u_j \rangle = \\ &= \sum_{ij} \langle u_j | \rho | u_i \rangle \langle u_i | \mathbf{A} | u_j \rangle = \sum_j \langle u_j | \rho \mathbf{A} | u_J \rangle = \mathrm{Tr}[\rho \mathbf{A}].\end{aligned} \tag{1.1.9}$$

The density matrix formalism turns out to be particularly useful in the study of bipartite systems, as we are going to see in the next section.

1.1.2 Bipartite systems

Let us consider a finite dimensional quantum system, divided into two complementary subsystems A and B. The associated finite-dimensional Hilbert space $\mathcal{H}_{AB}$ is given by the Kronecker product of the individual Hilbert spaces $\mathcal{H}_A \otimes \mathcal{H}_B$ associated to the two subsystems. Let $n_A = \dim \mathcal{H}_A$ and $n_B = \dim \mathcal{H}_B$, so that we can identify the orthonormal basis $\{|\psi_j\rangle_A\}_{j=1}^{n_A}$ and $\{|\phi_j\rangle_B\}_{j=1}^{n_B}$. Then, the whole system will be in a pure state $|\Psi\rangle \in \mathcal{H}_{AB}$ of the form

$$|\Psi\rangle = \sum_{ij} c_{ij} |\psi_i\rangle_A \otimes |\phi_j\rangle_B, \tag{1.1.10}$$

with $\sum_{ij} |c_{ij}|^2 = 1$. The associated density matrix will be denoted as ρ.

In typical situations, one is interested in performing a measure of an observable defined only in one of the subsystems, say A, having the form $\mathbf{O} = \mathbf{O_A} \otimes \mathbb{I}$. To this purpose, it is useful to introduce the so called *reduced density operator* ρ_A, which acts nontrivially only on the subsystem of interest and is defined as

$$\rho_A = \mathrm{Tr}_B \rho = \sum_{j=1}^{n_B} \left(\mathbb{I}_A \otimes {}_B\langle \phi_j | \right) \rho \left(\mathbb{I}_A \otimes |\phi_j\rangle_B \right), \tag{1.1.11}$$

where Tr_B denotes the operation of partial trace over the degrees of freedom of subsystem B. Similarly, one can define the reduced density operator ρ_B by tracing over the degrees of freedom of A. Inserting the expression of ρ in Eq. (1.1.11), one obtains

$$\begin{aligned}\rho_A &= \sum_{m=1}^{n_B} \left(\mathbb{I}_A \otimes {}_B\langle \phi_m | \right) \sum_{ijkl} c_{ik} c_{jl}^* (|\psi_i\rangle_A \otimes |\phi_k\rangle_B)({}_A\langle \psi_j | \otimes {}_B\langle \phi_l |) \left(\mathbb{I}_A \otimes |\phi_m\rangle_B \right) = \\ &= \sum_{ij} \left(\sum_m c_{im} c_{jm}^* \right) |\psi_i\rangle_A \, {}_A\langle \psi_j |.\end{aligned} \tag{1.1.12}$$

The *reduced density matrix* (RDM) ρ_A is defined as the matrix with elements

$$\langle \psi_i | \, \rho_A \, | \psi_j \rangle \equiv \sum_m c_{im} c_{jm}^*. \tag{1.1.13}$$

The definition of Eq. (1.1.13) can be used to show that the expectation values of the operators defined in subsystem A can be evaluated as

$$\langle \mathbf{O} \rangle = \mathrm{Tr}_A [\rho_A \mathbf{O}]. \tag{1.1.14}$$

Let us prove this relation,

$$\langle \mathbf{O} \rangle = \langle \Psi | \mathbf{O_A} \otimes \mathbb{I}_B | \Psi \rangle = \sum_{ijkl} c_{ik} c^*_{jl} \; {}_A\langle \psi_j | \mathbf{O_A} | \psi_i \rangle_A \; {}_B\langle \phi_l | \mathbb{I}_B | \phi_k \rangle_B = \sum_{ij} \left(\sum_k c_{ik} c^*_{jk} \right) \; {}_A\langle \psi_j | \mathbf{O_A} | \psi_i \rangle_A =$$
$$= \sum_{ij} \; {}_A\langle \psi_i | \rho_A | \psi_j \rangle_A \; {}_A\langle \psi_j | \mathbf{O_A} | \psi_i \rangle_A = \sum_i \; {}_A\langle \psi_i | \rho_A \mathbf{O_A} | \psi_i \rangle_A = \mathrm{Tr}_A[\rho_A \mathbf{O_A}].$$

In the next section, we are going to see the simplest example of bipartite state, using the representation in term of qbits.

1.1.3 An example: the Qbit

The elementary unit of quantum information is represented by the *qbit*. This is the quantum analog of the *bit*, a binary digit, characterized as 0 or 1, that is used to represent information in classical computers. In quantum mechanics, thanks to the superposition principle, it is possible to generalise this object to encode the information in the quantum state of a qbit.

The qbit is a quantum system, described by a 2-dimensional Hilbert space $\mathcal{H}^{(2)} = \mathbb{C}^2$ generated by the orthonormal basis vectors $\{|0\rangle, |1\rangle\}$, whose state can take any value of the form

$$|\psi\rangle = a|0\rangle + b|1\rangle, \tag{1.1.15}$$

where a, b are complex numbers satisfying the condition $|a|^2 + |b|^2 = 1$. The basis formed by the vectors $|0\rangle$ and $|1\rangle$ is called *computational basis*. A physical realization of a two level quantum system is an object with spin 1/2, like for example an electron. In this case, $|0\rangle$ and $|1\rangle$, correspond to the spin up $|\uparrow\rangle$ and spin down $|\downarrow\rangle$ states along the z-axis.

The simplest example of bipartite system is the one of two qbits, in which each subsystem is made by a single qbit. The space of the system will be 4-dimensional Hilbert space $\mathcal{H}^{(4)} = \mathbb{C}^4 \simeq \mathbb{C}^2 \otimes \mathbb{C}^2$, with basis vectors

$$|00\rangle \equiv |0\rangle \otimes |0\rangle = \begin{pmatrix} 1 \\ 0 \\ 0 \\ 0 \end{pmatrix}, \qquad |01\rangle \equiv |0\rangle \otimes |1\rangle = \begin{pmatrix} 0 \\ 1 \\ 0 \\ 0 \end{pmatrix},$$
$$|10\rangle \equiv |1\rangle \otimes |0\rangle = \begin{pmatrix} 0 \\ 0 \\ 1 \\ 0 \end{pmatrix}, \qquad |11\rangle \equiv |1\rangle \otimes |1\rangle = \begin{pmatrix} 0 \\ 0 \\ 0 \\ 1 \end{pmatrix}.$$

Then a generic 2-qbit state is a linear combination of the form

$$|\Psi\rangle = c_{00}|00\rangle + c_{01}|01\rangle + c_{10}|10\rangle + c_{11}|11\rangle. \tag{1.1.16}$$

This formalism can be used to see explicitly a simple application of the density matrix formalism introduced in the previous section. Let us consider the following example.

Example: Let us take the state $|\Psi^+\rangle = \frac{1}{\sqrt{2}}(|00\rangle + |11\rangle)$. The associated density matrix is

$$\rho = \frac{1}{2}\left(|00\rangle + |11\rangle\right)\left(\langle 00| + \langle 11|\right) = \frac{1}{2}\left(|00\rangle\langle 00| + |00\rangle\langle 11| + |11\rangle\langle 00| + |11\rangle\langle 11|\right) \tag{1.1.17}$$

The RDM ρ_1 is obtained taking the partial trace over the degrees of freedom of the second subsystem,

$$\begin{aligned}\rho_1 = \mathrm{Tr}_2\rho = \frac{1}{2}\left[(\mathbb{I}_1 \otimes \langle 0|)\,\rho\,(\mathbb{I}_1 \otimes |0\rangle) + (\mathbb{I}_1 \otimes \langle 1|)\,\rho\,(\mathbb{I}_1 \otimes |1\rangle)\right] = \\ = \frac{1}{2}\left(|0\rangle\langle 0| + |1\rangle\langle 1|\right).\end{aligned} \tag{1.1.18}$$

The state $|\Psi^+\rangle$ in the example is one out of the set of the so called *Bell states*, which form a basis of the Hilbert space $\mathcal{H}^{(4)}$,

$$\begin{aligned}|\Psi^\pm\rangle &= \frac{1}{\sqrt{2}}\left(|00\rangle \pm |11\rangle\right), \\ |\Phi^\pm\rangle &= \frac{1}{\sqrt{2}}\left(|01\rangle \pm |10\rangle\right).\end{aligned} \tag{1.1.19}$$

1.1.4 Definition of entanglement

Let us consider a bipartite system, divided into two complementary subsystems A and B. A quantitative definition of entangled pure state is the following.

Definition 1.1.1. A pure state $|\Psi\rangle \in \mathcal{H}_{AB}$ is said to be *separable* if and only if it can be written as Kronecker product of pure states $|\psi\rangle_A \in \mathcal{H}_A$ and $|\phi\rangle_B \in \mathcal{H}_B$, that is,

$$|\Psi\rangle = |\psi\rangle_A \otimes |\phi\rangle_B \tag{1.1.20}$$

otherwise it is said to be *entangled*.

Let us consider a generic two-particle state of the form (1.1.16). This state is not necessarily separable. As a check, this should be compared with a separable state of the form (1.1.20). Expressing in the computational basis the two states $|\psi\rangle_A = \sum_{j=0,1} a_j|j\rangle$ and $|\phi\rangle_B = \sum_{j=0,1} b_j|j\rangle$, the tensor product gives

$$|\psi\rangle_A \otimes |\phi\rangle_B = a_0b_0|00\rangle + a_0b_1|01\rangle + a_1b_0|10\rangle + a_1b_1|11\rangle. \tag{1.1.21}$$

Then, a state of the form given by Eq.(1.1.16) is separable if its coefficients can be equated with those in Eq.(1.1.21). It is easy to see that a sufficient condition for separability is $c_{00}c_{11} = c_{01}c_{10}$.

Example: A typical example of entangled pure states is provided by the *Bell states* in Eq.(1.1.19). In order to verify that they are entangled, let us consider the case of $|\Phi^+\rangle$. To express it as a tensor product of states, it is necessary to solve the system

$$a_0b_0 = a_1b_1 = 0, \qquad\qquad a_0b_1 = a_1b_0 = \frac{1}{\sqrt{2}},$$

but it is immediate to observe that it has no nontrivial solution. The same reasoning applies to the other Bell states.

The definition of separability can be generalized also to the case of mixed states.

Definition 1.1.2. A mixed state $\rho : \mathcal{H} \to \mathcal{H}$ is said to be *separable* if it can be written as

$$\rho = \sum_k p_k \rho_A^{(k)} \otimes \rho_B^{(k)} \tag{1.1.22}$$

where $\rho_A^{(k)}$ and $\rho_B^{(k)}$ are density matrices on $\mathcal{H}_A$ and $\mathcal{H}_B$ respectively, otherwise it is said to be *entangled*.

From this definition, it follows that the separability of ρ depends on the choice of the bipartition. It is also important to observe that the p_k in Eq. (1.1.22) represent classical probabilities, so the separable states are only classically correlated, that is, they do not contain any amount of entanglement. Then, while superposition implies entanglement in pure states, this does not generalize to mixed states.

1.1.5 Separability criteria

In general, the problem of deciding whether the state is separable or entangled is nontrivial. For bipartite pure states, an effective procedure for detecting entanglement is provided by the so called *Schmidt decomposition*. The entanglement detection and measure for mixed states is much more difficult than in pure states. To this aim, a criterion was formulated by Peres [73] and Horodecki [74], that is based on the so called *Positive Partial Transposition Criterion (PPT)*.

Schmidt decomposition

Let us formulate the following theorem, that holds for bipartite pure states.

Theorem 1.1.2 (Schmidt decomposition)**.** *Let us take a pure state $|\Psi\rangle \in \mathcal{H}_{AB} = \mathcal{H}_A \otimes \mathcal{H}_B$, with $dim(\mathcal{H}_A) = d_A$, $dim(\mathcal{H}_B) = d_B$, and assume $d_A < d_B$. Then, there exist orthonormal vector basis*

$$\{|\psi^{(i)}\rangle_A\}, \quad i = 1, \cdots, d_A, \qquad\qquad \{|\phi^{(j)}\rangle_B\}, \quad j = 1, \cdots, d_B, \tag{1.1.23}$$

such that $|\Psi\rangle$ can be written as

$$|\Psi\rangle = \sum_{k=1}^{s<d_A} \sqrt{\lambda_k} |\psi^{(k)}\rangle_A \otimes |\phi^{(k)}\rangle_B, \tag{1.1.24}$$

with $\lambda_k \geq 0$ and $\sum_i \lambda_i = 1$. The numbers $\sqrt{\lambda_k}$ are called Schmidt numbers.

Proof: Let us consider a generic vector of the form

$$|\Psi\rangle = \sum_{i=1}^{d_A} \sum_{j=1}^{d_B} c_{ij} |\tilde{\psi}^{(i)}\rangle_A \otimes |\tilde{\phi}^{(j)}\rangle_B. \tag{1.1.25}$$

The corresponding density matrix is

$$\rho = |\Psi\rangle\langle\Psi| = \sum_{ijlm} c_{ij} c^*_{ml} |\tilde{\psi}^{(i)}\rangle_A \, {}_A\langle\tilde{\psi}^{(l)}| \otimes |\tilde{\phi}^{(j)}\rangle_B \, {}_B\langle\tilde{\phi}^{(m)}|. \tag{1.1.26}$$

So the RDM of subsystem A is

$$\begin{aligned} \rho_A = \mathrm{Tr}_B[\rho] &= \sum_n {}_B\langle\tilde{\phi}^{(n)}|\rho|\tilde{\phi}^{(n)}\rangle_B = \sum_{iln} c_{in} c^*_{nl} |\tilde{\psi}^{(i)}\rangle_A \, {}_A\langle\tilde{\psi}^{(l)}| \\ &= \sum_{il} \left(\sum_n c_{in} c^*_{ln} \right) |\tilde{\psi}^{(i)}\rangle_A \, {}_A\langle\tilde{\psi}^{(l)}|. \end{aligned} \tag{1.1.27}$$

The term in the parenthesis can be seen as elements $\Lambda_{il} = \sum_n c_{in} c^*_{nl}$ of an hermitian matrix $\Lambda = \Lambda^\dagger$. The matrix can be always diagonalized as

$$\Lambda_{il} = \sum_k U_{ik} \lambda_k U^\dagger_{kl}. \tag{1.1.28}$$

Let us introduce the vectors

$$|\psi^{(k)}\rangle_A = U_{ik}|\tilde{\psi}^{(i)}\rangle_A, \quad \rightarrow \quad |\tilde{\psi}^{(i)}\rangle_A = U^*_{ki}|\psi^{(k)}\rangle_A \tag{1.1.29}$$

so that the RDM becomes

$$\rho_A = \sum_{k=1}^{s<d_A} \lambda_k |\psi^{(k)}\rangle_A \, {}_A\langle\psi^{(k)}|. \tag{1.1.30}$$

Inserting Eq. (1.1.29) into Eq. (1.1.25) one gets

$$|\Psi\rangle = \sum_k |\psi^{(k)}\rangle_A \otimes \left(\sum_{ij} c_{ij} U^*_{ik} |\tilde{\phi}^{(j)}\rangle_B\right) \equiv \sum_k |\psi^{(k)}\rangle_A \otimes |\chi^{(k)}\rangle_B \tag{1.1.31}$$

where $|\chi^{(k)}\rangle_B = \sum_{ij} c_{ij} U^*_{ik} |\tilde{\phi}^{(j)}\rangle$, so that the RDM can be also written as

$$\rho_A = \sum_{kl} |\psi^{(k)}\rangle_A \, {}_A\langle\psi^{(k)}| \, {}_B\langle\chi^{(k)}|\chi^{(k)}\rangle_B. \tag{1.1.32}$$

Comparing Eq. (1.1.30) and Eq. (1.1.32), one gets ${}_B\langle\chi^{(k)}|\chi^{(k)}\rangle_B = \delta_{kl}\lambda_k$. Finally, defining

$$|\phi^{(k)}\rangle_B \equiv \frac{1}{\sqrt{\lambda_k}} |\chi^{(k)}\rangle_B \quad \rightarrow \quad |\chi^{(k)}\rangle_B \equiv \sqrt{\lambda_k} |\phi^{(k)}\rangle_B, \tag{1.1.33}$$

the pure state $|\Psi\rangle$ becomes

$$|\Psi\rangle = \sum_{k=1}^{s<d_A} \sqrt{\lambda_k} |\psi^{(k)}\rangle_A \otimes |\phi^{(k)}\rangle_B. \tag{1.1.34}$$

□

Thanks to this theorem, according to the value of the number s, called *Schmidt number*, it is possible to say if the state $|\Psi\rangle$ is separable or not. In particular, it is separable for $s = 1$, and entangled for $s > 1$.

Let us now take the partial trace of $|\Psi\rangle$ to obtain the RDM

$$\begin{aligned} \rho_A &= \mathrm{Tr}_B \left(|\Psi\rangle\langle\Psi|\right) = \sum_k \lambda_k |\psi^{(k)}\rangle_A \, {}_A\langle\psi^{(k)}| \\ \rho_B &= \mathrm{Tr}_A \left(|\Psi\rangle\langle\Psi|\right) = \sum_k \lambda_k |\phi^{(k)}\rangle_B \, {}_B\langle\phi^{(k)}|. \end{aligned} \tag{1.1.35}$$

This means that the two RDM have the same nonzero eigenvalues, whose number is equal to the Schmidt number.

It is important to observe that the weights λ_k in the RDM above are related to the quantum coefficients of the state $|\Psi\rangle$ of the total system. If follows by definition that if the total system is entangled its RDM is mixed. An explicit example of this fact is already given in Sect. 1.1.3. In fact in this case, the density matrix corresponds to a Bell state, that is entangled, and the corresponding RDM in Eq. (1.1.18) is mixed.

Peres-Horodecki Criterion

The PPT criterion for mixed states provides a necessary condition for separability. It is based on the operation of partial transposition applied to the density matrix, and is defined as follows. Let us consider a subsystem A, divided itself in two subsystems A_1 and A_2, and denote their basis with latin letters $\{|m\rangle\}$ and greek letters $\{|\mu\}$ respectively. The density matrix elements in this basis can be writtes as $\rho_{m\mu,n\nu} \equiv \langle m,\mu|\rho|n,\nu\rangle$. One can introduce the partial transpose density matrix, obtained by transposing only the part of the operator in a given subsystem. For example, taking the partial transpose with respect to subsystem A_1, the element of the partial transposed density matrix are

$$\rho^{T_1}_{m\mu,n\nu} \equiv \rho_{n\mu,m\nu} \tag{1.1.36}$$

where the superscript T_1 indicates the partial transpose with respect to the first subsystem. One can observe that the latin indices have been switched, but not the greek ones. The transformation is not unitary, but ρ^{T_1} is still hermitian.

Theorem 1.1.3 (Peres-Horodecki criterion:)**.** *Let us consider a mixed quantum state ρ_A which is separable with respect to a bipartition. Then its partial transpose with respect to the given bipartition is positive*

Proof: Let us suppose that the state of the system A is separable with respect to a given bipartition, that is

$$\rho_A = \sum_k p_k \rho^{(k)}_{A_1} \otimes \rho^{(k)}_{A_2}, \tag{1.1.37}$$

then its partial transpose with respect to subsystem A_1 is

$$\rho^{T_1} = \sum_k p_k \left(\rho^{(k)}_{A_1}\right)^{T_1} \otimes \rho^{(k)}_{A_2}. \tag{1.1.38}$$

Since the transposition map preserves the eigenvalues, the specrtum of $\rho^{T_1}_{A_1}$ is the same of ρ_{A_1}, so that $\rho^{T_1}_{A_1}$ is still positive semidefinite. It follows that none of the eigenvalues of ρ^{T_1} is negative. □

This theorem implies that necessary condition for separability of a state is that its partial transpose has only non-negative eigenvalues. It was proven in Ref. [74] that for low dimensional systems this condition is also sufficient to ensure the separability. In particular, a state defined on bipartite Hilbert spaces $\mathcal{H} = \mathbb{C}^2 \otimes \mathbb{C}^2$ or $\mathcal{H} = \mathbb{C}^2 \otimes \mathbb{C}^3$ is separable if and only if its partial transpose is a positive operator.

1.1.6 Operational definition of entanglement

A definition of entanglement can be achieved not only specifying what entanglement is, but also how it can be actually used [75, 76]. In this operational point of view, the characterization of entanglement is related to the possible operations that can be performed on the system.

In particular, it is useful to identify a class of operation under which the entanglement between two subsystems cannot be created or increased. Among them, a special example is provided by *local operations* and *classical communication* (LOCC), which are defined as follows. Let us consider a quantum information experiment, in which operations are performed on a system whose subparts are distributed in two distantly separated laboratories. In order to avoid the disturbance induced by communication over long distance, only local operations (LO) are

performed in the well controlled environment of each laboratory. Moreover, the quantum actions on each subsystem can be coordinated via classical communication (CC). In this context, classical correlations can be defined as the ones that can be created by LOCC, while quantum correlations are the ones that are already present in the system, and cannot be generated by acting locally on the two subsytems. The mathematical definition of LOCC is nontrivial [77], but is possible to show that they belong to a more general class of operations, called *local operations*, that act separately on the two subsystems and then do not alter the amount of entanglement between them [78].

1.2 Entanglement measures

In quantum information, one is interested not only in the definition of entanglement, but also in its quantification. In other words, one would like to be able to compare the entanglement content of different quantum states.

To this purpose, a possibility could be to adopt the operational approach in terms of LOCC to provide an ordering of the states [75, 76, 79]. As already discussed, the entanglement of states does not increase under LOCC transformations. Moreover, it is possible to individuate maximally entangled states, from which any other state can be obtained through LOCC only. These considerations suggest that one could impose some form of ordering, saying that the state ρ is more entangled than a state σ if the transformation $\rho \to \sigma$ can be performed using LOCC operation. Unfortunately, LOCC manipulations can only induce a partial order in the set of the quantum states [80].

The problem can be solved by adopting an axiomatic approach, that consists in the definition of suitable real valued functions that verify some natural properties, and use them to quantify the entanglement content in a given state.

There is no universal agreement about all the postulates that a function should satisfy in order to be a good entanglement measure, however it is possible to recognize some of them which are the most common.

Definition 1.2.1. A map $E(\rho) : \rho \to E(\rho) \in \mathbb{R}^+$ from the space of density matrices into positive real numbers is an entanglement measure if it satisfies the following postulates:

1. E is not increasing under LOCC.
2. E is convex, that is, $E(\sum_i p_i \rho_i) \leq \sum_i p_i E(\rho_i)$.
3. $0 \leq E(\rho) \leq 1$ for all density operators ρ, and $E(\rho) = 0$ if and only if ρ is separable.
4. E is additive under tensor product, that is $E\left(\otimes_i \rho_i\right) = \sum_i E(\rho_i)$.

This procedure leads to the definition of most of the entanglement measures.

1.2.1 von Neumann and Rényi Entropies

In classical information theory, the amount of knowledge or uncertainty contained in a system is quantified by the so called *Shannon Entropy* [81]. Given a probability distribution $p_1, \cdots, p_N$ of a certain random variable X, the Shannon entropy is a map from such distribution to a real number, defined as

$$H[X] \equiv S(p_1, \cdots, p_N) = -\sum_{i=1}^{N} p_i \log p_i. \tag{1.2.1}$$

A more general class of entanglement measures is represented by the so called *Rényi Entropies*, labeled by the index n,with $n \geq 0$ and $n \neq 1$, and defined as

$$H_n[X] \equiv S_n(p_1, \cdots, p_N) = \frac{1}{1-n} \log \left(\sum_{i=1}^{N} p_i^n \right). \tag{1.2.2}$$

In the case of a quantum system, the probability distribution is replaced by the density operator. In particular, the definitions above can be adapted to quantify the entanglement in bipartite pure states. Let us consider a quantum system in a pure state $\rho = |\Psi\rangle\langle\Psi|$, divided in two complementary subsystems A and B. We are interested in quantifying the amount of entanglement between the two parts, so we introduce the RDM of subsystem A, obtained as $\rho_A = \mathrm{Tr}_B \rho$, and define *entanglement entropy* (EE) as the von Neumann entropy associated to ρ_A,

$$S \equiv S(\rho_A) = -\mathrm{Tr}\left(\rho_A \log \rho_A\right). \tag{1.2.3}$$

When necessary, to specify the subsystem X the notation $S^X \equiv S(\rho_X)$ will be adopted. In terms of the eigenvaules of the RDM in Eq. (1.1.35), the EE is expressed as

$$S = -\sum_i \lambda_i \log \lambda_i. \tag{1.2.4}$$

Since the nonzero eigenvalues λ_i of ρ_A are also eigenvalues of ρ_B, it follows that $S(\rho_A) = S(\rho_B)$. The entanglement entropy is a good measure of entanglement, since it satisfies the requirements of Def. 1.2.1. In addition, it satisfies the following property

5. Subadditivity: $S(\rho) \leq S(\rho_A) + S(\rho_B)$.

As in the classical case, one can introduce a larger class of entropies, the so called *Rényi entropies* (REs),

$$S_n \equiv S_n(\rho_A) = \frac{1}{1-n} \log \mathrm{Tr}(\rho_A)^n, \tag{1.2.5}$$

whose limit for $n \to 1$ gives the EE. The knowledge of the REs for all $n > 0$ gives access to the full spectrum of ρ_A [82].

The EE, and more generally the REs, quantify the entanglement between a subsystem A and its complement. This is independent of the topology of A. For example, when A consists of two or more disconnected subsets, they are still a measure of entanglement between A and the remainder. However, they do not quantify the entanglement between two subsets of A. In fact, the state of the subsystem A alone is generally mixed, and it is not possible to distinguish entanglement form classical correlations. The EE and REs can be used to construct a measure of the total correlations between the subsets, as we will see in the next section.

1.2.2 Mutual information

Let us consider two random variables X and Y, and let $p(x, y)$ be their joint probability distribution. It is then straightforward to define the *joint entropy* of X and Y as

$$H(X, Y) \equiv -\sum_{x,y} p(x, y) \log p(x, y), \tag{1.2.6}$$

which measures the total uncertainty about the pair (X, Y). Let us now suppose to know the value of Y, so that the uncertainty about (X, Y) is due to the lack of information about X. The amount of such uncertainty is given by the *conditional entropy* of X given Y, that is

$$H(X|Y) \equiv H(X, Y) - H(Y). \tag{1.2.7}$$

It is also possible to quantify the amount of information that X and Y have in common, introducing the so called *mutual information*

$$H(X : Y) \equiv H(X) + H(Y) - H(XY). \tag{1.2.8}$$

As for the Shannon entropy, we can define the quantum analog of the quantities above. In particular, we will be interested in the evaluation of the mutual information (MI) between two complementary parts A_1 and A_2 of a quantum system $A = A_1 \cup A_2$, denoted as

$$I^{A_1:A_2} \equiv I^{A_1:A_2}(\rho_A) = S^{A_1} + S^{A_2} - S^{A_1 \cup A_2}. \tag{1.2.9}$$

This quantity is a very useful measure of the correlations between A_1 and A_2 [29]. This definition can be easily generalised to a *Rényi mutual information* (RMI)

$$I_n^{A_1:A_2} \equiv S_n^{A_1} + S_n^{A_2} - S_n^{A_1 \cup A_2} = \frac{1}{1-n} \log \left(\frac{\mathrm{Tr}\rho_{A_1 \cup A_2}^n}{\mathrm{Tr}\rho_{A_1}^n \mathrm{Tr}\rho_{A_2}^n} \right). \tag{1.2.10}$$

However, as a very important difference compared to the MI in Eq. (1.2.9), the RMI is not a measure of the correlations, since it can be even negative for some states [30].

1.2.3 Negativity

Let us consider a system A divided into two subsystems A_1 and A_2, such that $A = A_1 \cup A_2$. The focus is the study of entanglement between these two parts, where the density matrix ρ_A is a mixed state (for example, when $\rho_A = \mathrm{Tr}_B \rho$ is the RDM of a larger pure system, or when it is a mixed density matrix, e. g. thermal, for an entire system). Let us denote with $|e_j^{(1)}\rangle$ and $|e_k^{(2)}\rangle$ the orthonormal basis in the Hilbert spaces $\mathcal{H}_1$ and $\mathcal{H}_2$ corresponding to the regions A_1 and A_2 respectively, then the density matrix ρ_A can be written as

$$\rho_A = \sum_{ijkl} \langle e_i^{(1)}, e_j^{(2)} | \rho_A | e_k^{(1)}, e_l^{(2)} \rangle | e_i^{(1)}, e_j^{(2)} \rangle \langle e_k^{(1)}, e_l^{(2)} |, \tag{1.2.11}$$

The partial transpose of a density matrix for the subsystem A_2 is defined by exchanging the matrix elements in the subsystem A_2, i.e.

$$\rho_A^{T_2} \equiv \sum_{ijkl} \langle e_i^{(1)}, e_l^{(2)} | \rho_A | e_k^{(1)}, e_j^{(2)} \rangle | e_i^{(1)}, e_j^{(2)} \rangle \langle e_k^{(1)}, e_l^{(2)} |, \tag{1.2.12}$$

that is equivalent to the following transformation in the operator basis

$$\left(|e_i^{(1)}, e_j^{(2)}\rangle \langle e_k^{(1)}, e_l^{(2)}| \right)^{T_2} \equiv |e_i^{(1)}, e_l^{(2)}\rangle \langle e_k^{(1)}, e_j^{(2)}| \,. \tag{1.2.13}$$

This operation can be used to define a suitable measure of the bipartite entanglement for a general mixed state, the so called *entanglement negativity* (EN) [32]

$$\mathcal{N} \equiv \frac{\mathrm{Tr}|\rho_A^{T_2}| - 1}{2}, \tag{1.2.14}$$

where $\mathrm{Tr}|O| := \mathrm{Tr}\sqrt{O^\dagger O}$ denotes the trace norm of the operator O. This quantity is entanglement monotone, and so it can be used as good quantifier of entanglement in composite systems.

Another useful quantity that can be introduce is the *logarithmic negativity* (LN)

$$\mathcal{E} \equiv \log \mathrm{Tr}|\rho_A^{T_2}|, \tag{1.2.15}$$

whose advantage with respect to $\mathcal{N}$ is that it scales and behaves more similarly to the Rényi entropies (indeed for pure states $\mathcal{E} = S_{1/2}$ [32]). The LN $\mathcal{E}$ is also entanglement monotone [75, 32].

In terms of its eigenvalues λ_i, the trace norm of $\rho_A^{T_2}$ can be written as

$$\mathrm{Tr}|\rho_A^{T_2}| = \sum_i |\lambda_i| = \sum_{\lambda_i>0} |\lambda_i| + \sum_{\lambda_i<0} |\lambda_i| = 1 + 2\sum_{\lambda_i<0} |\lambda_i|, \tag{1.2.16}$$

where in the last equality we used the normalisation $\sum_i \lambda_i = 1$. This expression makes evident that the EN measures how much the eigenvalues of the partial transpose of the density matrix are negative, a property which is the reason for the name negativity, and therefore it can be regarded as a quantitative version of Peres' criterion for separability [73]. Moreover, for non-entangled states there are no negative eigenvalues, so $\mathrm{Tr}|\rho_A^{T_2}| = 1$ and the negativity vanishes.

It is also useful to define the moments of the partial transpose, the so-called *Rényi negativities* (RNs) as

$$R_n = \mathrm{Tr}(\rho_A^{T_2})^n. \tag{1.2.17}$$

The moments R_n with integer $n \geq 2$ can also be measured in experiments [83, 84, 85], but they are not entanglement monotones. The EN and RNs have been used to characterise mixed states in various quantum systems such as in harmonic oscillator chains [86, 87, 88, 89, 90, 91, 92, 93, 94], quantum spin models [95, 96, 97, 98, 99, 100, 101, 102, 103, 104, 105, 106, 107, 106, 108], $(1+1)$-dimensonal conformal and integrable field theories [109, 110, 111, 112, 113, 114, 115, 116, 117, 118], topologically ordered phases of matter in $(2+1)$-dimensions [119, 120, 121, 122, 123], out-of-equilibrium settings [84, 124, 125, 126, 127, 128, 129, 130, 131, 132], holographic theories [133, 134, 135, 136, 137, 138].

1.3 Replica approach

The evaluation of the entanglement entropy or negativity for a statistical model with a finite number of degrees of freedom can be performed by the construction of the RDM or its partial transpose respectively, exact or numerical. Then, from the knowledge of their eigenvalues λ_i one can evaluate the entanglement entropy using Eq. (1.2.4) or the negativity using Eq. (1.2.16).

However, the calculation of the full RDM for a general interacting Quantum Field Theory (QFT) can be a challenging task and the procedure described above can be not applicable. This motivates the introduction of another approach, which is reminiscent of the "replica trick" in disordered systems and whose initial application was introduced by Holzhey, Larsen and Wilczek [27]. It was subsequently developed in by Calabrese and Cardy for the evaluation of both EE [25, 26] and EN [109, 110, 112].

1.3.1 Replicas and entanglement entropy

Let us start considering a lattice model, by observing that the eigenvalues of the RDM λ_i all belong to the interval $[0, 1]$ and are such that $\sum_i \lambda_i = 1$. This implies that, for each $n \geq 1$ also not

integer, the sum $\mathrm{Tr}\rho_A^n = \sum_i \lambda_i^n$ is absolutely convergent and analytic in the region. In particular, if the entropy $S_A = -\sum_i \lambda_i \ln \lambda_i$ is finite, the limit $n \to 1^+$ of its first derivative converges to this value. So whenever it is possible to evaluate $\mathrm{Tr}\rho_A^n$ for every $n \geq 1$, the entanglement entropy can be obtained as

$$S = -\lim_{n\to 1} \frac{\partial}{\partial n} \mathrm{Tr}\rho_A^n = \lim_{n\to 1} S_n. \tag{1.3.1}$$

The quantities $\mathrm{Tr}\rho_A^n$, which represent the moments of the RDM, can be evaluated using the replica trick, that consists in the evaluation of $\mathrm{Tr}\rho_A^n$ for integer n and the subsequent analytical continuation to a general complex value. The calculation of these quantities is found to be equivalent to that of a partition function on a n-sheeted Riemann surface, that is can be analytically performed in QFT. Then, the possibility to obtain the EE as limit for $n \to 1^+$ depends on the existence and uniqueness of a proper analytic continuation.

1.3.2 Replicas and entanglement negativity

The replica trick for the negativity can be formulated in terms of traces of integer powers of the partial transpose, that is, the RN in Eq. (1.2.17). A crucial point is that, because of the non-positiveness of the spectrum of ρ^{T_2} , the RN define two separate sequences according to the parity on n. Denoting the even $n = 2m$ as n_e and the odd $n = 2m + 1$ as n_o, the traces of integer powers of ρ^{T_2} are given by

$$\mathrm{Tr}\left(\rho^{T_2}\right)^{n_e} = \sum_i \lambda_i^{n_e} = \sum_{\lambda_i>0} |\lambda_i|^{n_e} + \sum_{\lambda_i<0} |\lambda_i|^{n_e}, \tag{1.3.2}$$

$$\mathrm{Tr}\left(\rho^{T_2}\right)^{n_o} = \sum_i \lambda_i^{n_o} = \sum_{\lambda_i>0} |\lambda_i|^{n_o} - \sum_{\lambda_i<0} |\lambda_i|^{n_o}. \tag{1.3.3}$$

One can observe that, setting $n_e = 1$ in Eq. (1.3.2) gives formally the desired quantity $\mathrm{Tr}|\rho^{T_2}|$, while setting $n_o = 1$ in Eq. (1.3.3) gives the normalization $\mathrm{Tr}\rho^{T_2} = 1$. Then the natural way to exploit the replica trick is to obtain the EN by considering the analytic continuation of the even sequence of R_{n_e} at $n_e \to 1$ [109, 110] (which is different from $R_1 = 1$), that is

$$\mathcal{E} = \lim_{n_e\to 1} \log \mathrm{Tr}\left(\rho^{T_2}\right)^{n_e} \tag{1.3.4}$$

Let us illustrate as check the case of a bipartite pure state, for which the EN is known [32]. The state $|\Psi\rangle$ of the whole system acting on the Hilbert space $\mathcal{H} = \mathcal{H}_1 \otimes \mathcal{H}_2$, admits Schmidt decomposition

$$|\Psi\rangle = \sum_j c_j \, |e_j^{(1)}, e_j^{(2)}\rangle \,, \tag{1.3.5}$$

where $|e_k^{(1)}\rangle$ and $\langle e_j^{(2)}|$ are two basis of $\mathcal{H}_1$ and $\mathcal{H}_2$, and the coefficients $c_j \in [0, 1]$. The density matrix of the system is then

$$\rho = \sum_{j,k} |e_j^{(1)}, e_j^{(2)}\rangle \, \langle e_k^{(1)}, e_k^{(2)}| \,, \tag{1.3.6}$$

and taking the partial transpose with respect to, for example, the subsystem A_2, one gets

$$\rho^{T_2} = \sum_{j,k} c_j c_k \, |e_j^{(1)}, e_k^{(2)}\rangle \, \langle e_k^{(1)}, e_j^{(2)}| \,. \tag{1.3.7}$$

It can be shown that the the trace of the n-th power of the partial transpose gives

$$\mathrm{Tr}\left(\rho^{T_2}\right)^n = \begin{cases} \sum_r c_r^{2n_o} = \mathrm{Tr}\rho_2^{n_o}, & \text{if } n = n_o \text{ odd} \\ [\sum_r c_r^{n_e}]^2 = \left[\mathrm{Tr}\rho_2^{n_e/2}\right]^2, & \text{if } n = n_e \text{ even} \end{cases} \tag{1.3.8}$$

where $\rho_2 \equiv \rho_{A_2} = \mathrm{Tr}_{A_1}\rho$.

Proof: Let us write explicitly the n-th power of the partial transpose density matrix,

$$\begin{aligned} \left(\rho^{T_2}\right)^n &= \sum_{j_1,\cdots j_n} c_{j_1}c_{k_1}\cdots c_{j_n}c_{k_n} \left|e^{(2)}_{k_1}, e^{(1)}_{j_1}\right\rangle \left\langle e^{(2)}_{j_1}, e^{(1)}_{k_1}\right| e^{(2)}_{k_2}, e^{(1)}_{j_2}\right\rangle \left\langle e^{(2)}_{j_2}, e^{(1)}_{k_2}\right| \cdots \left|e^{(2)}_{k_n}, e^{(1)}_{j_n}\right\rangle \left\langle e^{(2)}_{j_n}, e^{(1)}_{k_n}\right| \\ &= \sum_{j_1,\cdots j_n} c_{j_1}c_{k_1}\cdots c_{j_n}c_{k_n} \left|e^{(2)}_{k_1}, e^{(1)}_{j_1}\right\rangle \delta_{j_1,k_2}\delta_{k_1,j_2}\cdots\delta_{j_{n-1},k_n}\delta_{k_{n-1},j_n} \left\langle e^{(2)}_{j_n}, e^{(1)}_{k_n}\right| . \end{aligned}$$

The result of the product of delta functions depends on the parity of n as follows

$$\mathrm{Tr}\left(\rho^{T_2}\right)^n = \begin{cases} \sum_{k_1,j_1} c_{j_1}^{n_o} c_{k_1}^{n_o} \left|e^{(2)}_{k_1}, e^{(1)}_{j_1}\right\rangle \left\langle e^{(2)}_{j_1}, e^{(1)}_{k_1}\right|, & \text{if } n = n_o \text{ odd} \\ \sum_{k_1,j_1} c_{k_1}^{n_e} c_{j_1}^{n_e} \left|e^{(2)}_{k_1}, e^{(1)}_{j_1}\right\rangle \left\langle e^{(2)}_{k_1}, e^{(1)}_{j_1}\right|, & \text{if } n = n_e \text{ even} \end{cases} \tag{1.3.9}$$

which gives back the result of Eq. (1.3.8)

□

Taking limit for $n_o \to 1$ one obtains the normalization $\mathrm{Tr}(\rho^{T_2}) = \mathrm{Tr}\rho_2 = 1$, while from the limit $n_e \to 1$ one recovers the known result that the LN for a bipartite pure state is equal to the RE of order $1/2$, that is

$$\mathcal{E} = S^{1/2}_{A_2} = 2\log \mathrm{Tr}\rho_2^{1/2}. \tag{1.3.10}$$

1.3.3 Path Integral approach for the entanglement entropy

The problem of the evaluation of the entanglement entropy in QFT, as anticipated in Sec. 1.3.1, can be turned into the calculation of a partition function on a n-sheeted Riemann surface.

Let us illustrate this method for a lattice QFT in $(1+1)$ dimensions, even if it can be generalized to higher dimensions. Let us assign a discrete variable x to the position of each lattice site, separated by spacing a, and a continuous variable to the time. We denote with $\{\hat{\phi}_x\}$ the complete set of local commuting observables defined on each site, with $\{\phi_x\}$ the eigenvalues and with $|\{\phi_x\}\rangle$ the corresponding eigenvectors. Then a complete basis of the Hilbert space of the system will be formed by the states

$$\bigotimes_x |\{\phi_x\}\rangle = |\prod_x \{\phi_x\}\rangle. \tag{1.3.11}$$

We start considering the density matrix of a system in a thermal state at inverse temperature β, whose time evolution is ruled by the Hamiltonian H

$$\rho = \frac{\mathrm{e}^{-\beta H}}{Z(\beta)}, \tag{1.3.12}$$

where the partition function $Z(\beta) = \mathrm{Tr}\mathrm{e}^{-\beta H}$accounts for the normalization of the density matrix. Its matrix elements in the basis (1.3.11) are

$$\rho\left(\{\phi_x\}|\{\phi'_{x'}\}\right) \equiv \langle\prod_x\{\phi_x\}|\rho|\prod_{x'}\{\phi'_{x'}\}\rangle = Z(\beta)^{-1}\langle\prod_x\{\phi_x\}|\mathrm{e}^{-\beta H}|\prod_{x'}\{\phi'_{x'}\}\rangle. \tag{1.3.13}$$

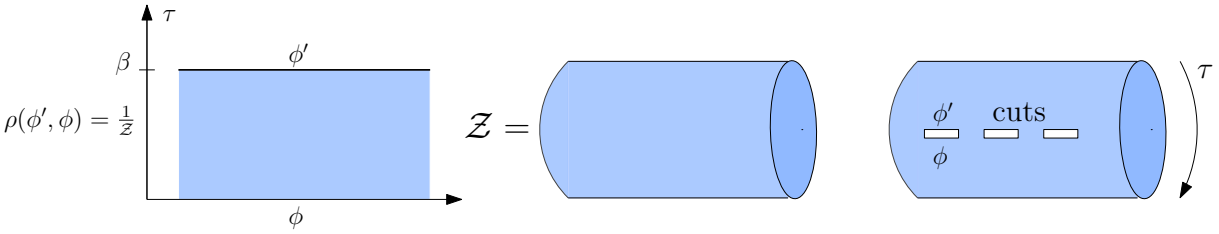


Figure 1.1: Path integral representation of the density matrix and the reduced density matrix. *Left*: Path integral representation of the density matrix $\rho(\phi|\phi')$. *Center*: Partition function $Z(\beta)$, represented by a cylinder of circumference β obtained by sewing the edges along $\tau = 0$ and $\tau = \beta$. *Right*: Reduced density matrix, obtained by sewing together the edges and leaving open cuts in correspondence of the points $x \in A$.

In the path integral formalism, the density matrix elements of the system are given by path integral on the imaginary time interval $(0, \beta)$

$$\rho\left(\{\phi_x\}|\{\phi'_{x'}\}\right) \equiv Z^{-1} \int \mathcal{D}[\phi(y,\tau)] \prod_{x'} \delta\left(\phi(y,0) - \phi'_{x'}\right) \prod_{x} \delta\left(\phi(y,\beta) - \phi_x\right) \mathrm{e}^{-S_E}, \tag{1.3.14}$$

where S_E is the euclidean action governing the evolution of the system

$$S_E = \int_0^\beta \mathrm{d}\tau L_E, \tag{1.3.15}$$

with L_E euclidean Lagrangian. The normalization factor Z, introduced so that $\mathrm{Tr}\rho = 1$, is the partition function.

According to Eq. (1.3.14), the density matrix elements can be viewed as average over all possible evolution paths of the field ϕ, with fixed conditions on the starting and ending points, and can be pictorially represented as an integration over the strip in the left panel of Fig. 1.1.

The partition function Z as a trace is obtained by setting $\{\phi_x\} = \{\phi'_{x'}\}$ and integrating over these variables. In the path integral formalism, this is equivalent to sewing together the edges along $\tau = 0$ and $\tau = \beta$ to form a cylinder of circumference β and integrating over it, as shown in the central panel of Fig. 1.1. For a subsystem A formed by all the points x lying in the set of disjoint intervals $[u_1, v_1], \cdots, [u_N, v_N]$, the trace operation is performed over the degrees of freedom of the complementary system B. In the pictorial representation, this has the effect of sewing together the edges along $\tau = 0$ only in correspondence of the points $x \in B$ and leaving open cuts for those in every interval $[u_i, v_i] \in A$, as shown in the right panel of Fig. 1.1. Then the trace of $\mathrm{Tr}\rho_A^n$ for any positive integer n can be obtained by taking n copies of the construction above, labeled by an integer j with $1 \leq j \leq n$, and sewing them cyclically along the cuts corresponding to $x \in A$ so that

$$\begin{aligned} \phi_j(x, \tau = \beta^-) &= \phi_{j+1}(x, \tau = 0^+), \\ \phi_n(x, \tau = \beta^-) &= \phi_1(x, \tau = 0^+), \qquad \forall x \in A. \end{aligned}$$

This defines an n-sheeted Riemann surface, as the one shown in Fig.1.2. Denoting with Z_n the partition function on this surface, we have that:

$$\mathrm{Tr}\rho_A^n = \frac{Z_n}{Z^n}. \tag{1.3.16}$$

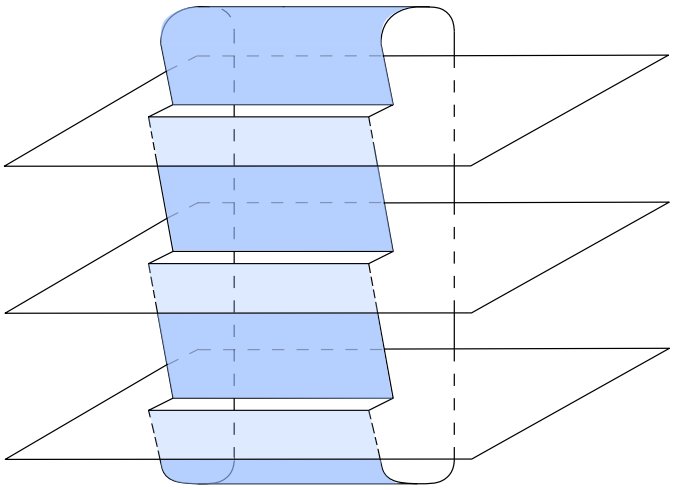


Figure 1.2: Representation of the Riemann surface $\mathcal{R}_{3,1}$ for $n = 3$ and $N = 1$.

When the right-hand side of the equation above has an unique analytic continuation to Re $n > 1$, using Eq. (1.3.1) the EE of subsystem A can be obtained as

$$S = -\lim_{n\to 1} \frac{\partial}{\partial n} \frac{Z_n}{Z^n}. \tag{1.3.17}$$

This approach can be extended from lattice to continuous systems by taking the limit $a \to 0$ and keeping the other lengths fixed. The variable x becomes real valued and the path integral is evaluated over the fields $\phi(x, \tau)$ on an n-sheeted Riemann surface, with branch points at u_j and v_j. These Riemann surfaces can be fully characterized by the number n of the copies and the number $2N$ of branching points labelling the disjoint intervals that form the subsystem A, and will be denoted by $\mathcal{R}_{n,N}$.

1.3.4 Twist Fields

The calculation of the partition function on the n-sheeted Riemann surface is in most of the cases very difficult to perform. To overcome this problem, one can start observing that the surface considered has zero curvature everywhere except at a finite number of points, represented by the boundaries u_j, v_j between the subsystems A and B. This suggests to map the problem into the complex plane, choosing appropriate boundary conditions around the points with non zero curvature in order to implement the structure of the Riemann surface. This is possible in principle since the lagrangian density $\mathcal{L}$ does not depend explicitly on the Riemann surface $\mathcal{R}$ because of its locality.

To see how this can be done in practice, let us consider the simplest case in which the subsystem A consists in a single interval $[u_1, v_1]$, whose entanglement entropy can be evaluated via the construction of the Riemann surface $\mathcal{R}_{n,1}$ made on n sheets sewed together along the cuts made of the points $x \in [u_1, v_1], \tau = 0$. The evaluation of the associated partition function can be in principle performed on a theory in the complex plane $z = x + i\tau$ thanks to the introduction of suitable fields living at $z = v_1$ and $z = u_1$. These fields and their correlation functions are defined, on the Riemann surface, through the partition function:

$$Z_{\mathcal{R}} = \int [\mathrm{d}\varphi]_{\mathcal{R}} \exp\left[-\int_{\mathcal{R}} \mathrm{d}x\mathrm{d}\tau \mathcal{L}[\varphi](x, \tau)\right] \tag{1.3.18}$$

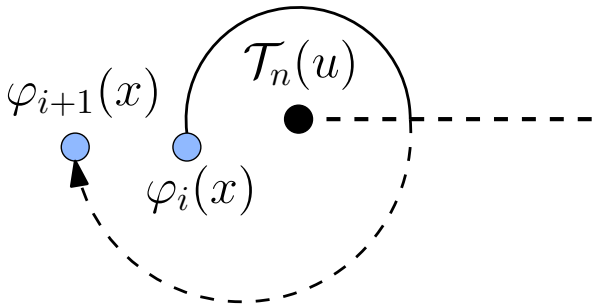


Figure 1.3: Action of the twist field $\mathcal{T}_n$ on other local fields.

where $\mathcal{L}[\varphi](x,\tau)$ is the lagrangian density. This definition however is no longer suitable in the complex plane since it compromises the locality of the theory, a requirement that is of fundamental importance in most of the results in quantum field theory, as shown in Ref. [139].

The problem can be solved implementing the complicated topology of the Riemann surface $\mathcal{R}$ on the target space where the fields live. To this purpose, let us take n independent copies of the original model, where n is the number of Riemann sheets necessary to describe the Riemann surface by coordinates on the plane, so that the multi-copy model is formally described by the following partition function

$$Z_{\mathcal{R}} = \int_{\mathcal{C}_{(u_1,v_1)}} [\mathrm{d}\varphi_1 \cdots \mathrm{d}\varphi_n] \exp\left[- \int_{\mathbb{C}} \mathrm{d}x\mathrm{d}\tau \left(\mathcal{L}[\varphi_1](x,\tau) + \cdots + \mathcal{L}[\varphi_n](x,\tau) \right) \right], \tag{1.3.19}$$

where $\mathcal{C}_{(u_1,v_1)}$ are the conditions on the fields $\varphi_1, \cdots, \varphi_n$ restricting the path integral

$$\varphi_i(x,0^+) = \varphi_{i+1}(x,0^-), \qquad x \in [u_1,v_1], \qquad i = 1, \cdots, n \tag{1.3.20}$$

with the identification $n+i \equiv i$.

The lagrangian density of the multi-copy model is then

$$\mathcal{L}^{(n)}[\varphi_1, \cdots, \varphi_n](x,\tau) = \mathcal{L}[\varphi_1](x,\tau) + \cdots + \mathcal{L}[\varphi_n](x,\tau) \tag{1.3.21}$$

and it is given by the sum of the energy densities of the n individual copies. So we have that Eq. (1.3.19) is equivalent to Eq. (1.3.18), but it also allows to define local fields at $(u_1,0)$ and $(v_1,0)$ in the multi-copy model. The fields defined in Eq. (1.3.19) are an example of a wider class of fields called *twist fields*. Twist fields can be defined in theories characterized by the presence of a global internal symmetry σ, that is, a symmetry that does not depend on the space-time degrees of freedom. In this case, the following identity holds

$$\int \mathrm{d}x\mathrm{d}\tau \mathcal{L}[\sigma\phi](x,\tau) = \int \mathrm{d}x\mathrm{d}\tau \mathcal{L}[\phi](x,\tau). \tag{1.3.22}$$

In the model with lagrangian $\mathcal{L}^{(n)}$ there is a symmetry under the exchange of copies. The twist fields defined in Eq. (1.3.19), called *branch-point twist fields*, are associated to the two opposite cyclic permutation symmetries $i \to i+1$ and $i+1 \to i$, with $(i = 1, \cdots, n, \quad \text{with} \quad n+1 \equiv 1)$. They can be denoted as $\mathcal{T}_n$ and $\tilde{\mathcal{T}}_n$, according to their actions

$$\mathcal{T}_n = \mathcal{T}_\sigma \qquad \sigma : i \to i+1 \mod n \tag{1.3.23}$$

$$\tilde{\mathcal{T}}_n = \mathcal{T}_{\sigma^{-1}} \qquad \sigma^{-1} : i+1 \to i \mod n \tag{1.3.24}$$

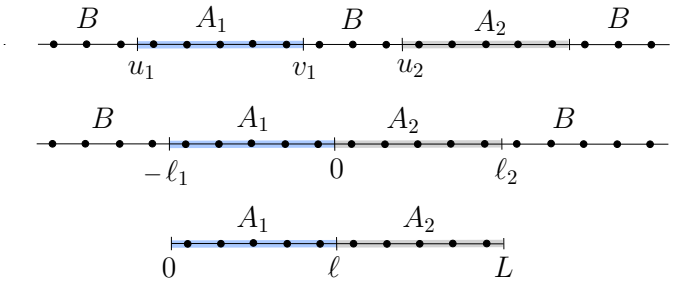


Figure 1.4: Main configurations of the $1D$ system divided into A and B. *Top*: Tripartite system made by two disjoint subsystems A_1 and A_2 with $A_1 \cup A_2 = A$ and the remainder B. *Center*: Tripartite system with adjacent intervals A_1 and A_2. *Bottom*: Two adjacent intervals which form the full system, with $B \to \emptyset$.

Their effect on a local field φ is shown in Fig. 1.3. In particular for a single interval,

$$Z_{\mathcal{R}_{n,1}} \propto \langle \mathcal{T}_n(u_1,0)\tilde{\mathcal{T}}_n(v_1,0)\rangle_{\mathcal{L}^{(n)},\mathbb{C}}. \tag{1.3.25}$$

In fact, for $x \in [u_1, v_1]$, consecutive copies are connected along the cuts $\tau = 0$ by the action of $\mathcal{T}_n(u_1,0)$, whereas for $x > v_1$, each copy is connected to itself through $\tau = 0$ because of the mutual cancellation of the conditions arising from the definition of $\mathcal{T}_n(u_1,0)$ and $\tilde{\mathcal{T}}_n(v_1,0)$.

This identification holds also for the correlation functions in the model $\mathcal{L}$ on $\mathcal{R}_{n,1}$

$$\langle \mathcal{O}(x,\tau;\text{sheet } i)\cdots\rangle_{\mathcal{L},\mathcal{R}_{n,1}} = \frac{\langle \mathcal{T}_n(u_1,0)\tilde{\mathcal{T}}_n(v_1,0)\mathcal{O}_i(x,\tau)\cdots\rangle_{\mathcal{L}^{(n)},\mathbb{C}}}{\langle \mathcal{T}_n(u_1,0)\tilde{\mathcal{T}}_n(v_1,0)\rangle_{\mathcal{L}^{(n)},\mathbb{C}}} \tag{1.3.26}$$

where $\mathcal{O}_i$ is the field in the model $\mathcal{L}^{(n)}$ coming from the i^{th} copy of $\mathcal{L}$.

The results above can be generalized to the case in which the subsystem A is made on N intervals, where Eq. (1.3.25) becomes

$$Z_{\mathcal{R}_{n,N}} \propto \langle \mathcal{T}_n(u_1,0)\tilde{\mathcal{T}}_n(v_1,0),\cdots,\mathcal{T}_n(u_N,0)\tilde{\mathcal{T}}_n(v_N,0)\rangle_{\mathcal{L}^{(n)},\mathbb{C}}. \tag{1.3.27}$$

Twist fields have found many applications in the context of 2 dimensional field theories, such as massive [139, 140, 117, 116] or integrable [141, 142, 143] ones. In particular, they play a special role in the case of 2-dimensional conformal field theories, as will be discussed in Sect. 1.4.

1.3.5 Path Integral approach for the negativity

The replica trick can be adapted to evaluate the partial transpose of the RDM, in order to obtain the EN and LN [109, 110]. Let us focus on the case of a tripartite system as the one shown in the top panel of Fig. 1.4, where $A = A_1 \cup A_2 = [u_1, v_1] \cup [u_2, v_2]$ and B its complement, even if most of the derivation can be applied to the more general case in which A_1 and A_2 are made by several disjoint intervals. The operation of partial transpose of the RDM ρ_A with respect to A_2, that consist in the exchange of the row and column indices corresponding to this interval, can be translated in the path integral formalism into the exchange of the upper and the lower edges of the cut in ρ_A corresponding A_2, as shown in the central panel of Fig. 1.5. As a consequence, in the n-sheeted Riemann surface obtained by sewing the n copies of ρ^{T_2}, the order of the row and column indices will be reversed with respect to that of a correlation of four twist field.

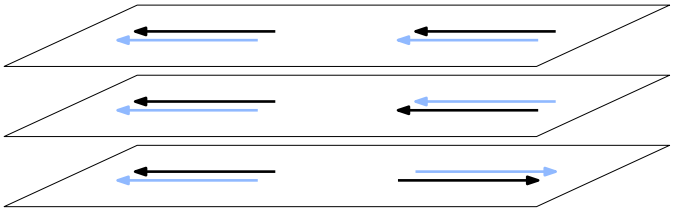


Figure 1.5: *Top*: Path integral representation of the reduced density matrix ρ_A of two disjoint intervals. *Center*: Partial transpose of ρ_A with respect to the second interval, $\rho_A^{T_2}$. *Bottom*: Reversed partial transpose $\rho_A^{C_2}$, obtained by reversing the order of row and column indices.

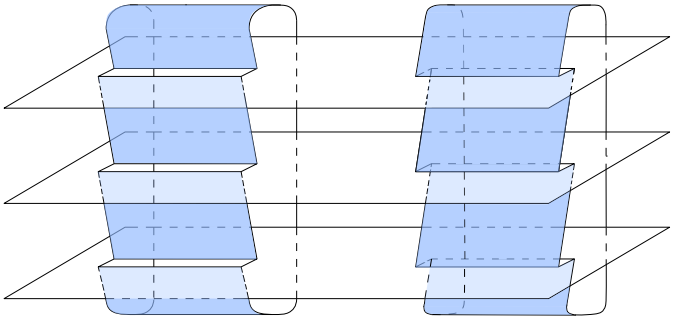


Figure 1.6: Path integral representation of $\mathrm{Tr}(\rho_A^{T_2})^n$ for $n = 3$.

This issue can be fixed by introducing the *reversed partial transpose* $\rho_A^{C_2} = C\rho_A^{T_2}C$, where the operator C reverses the order of the indices either on the lower on on the upper cut, giving the configuration shown in the bottom panel of Fig. 1.5. Since $C^2 = 1$, it follows that $\mathrm{Tr}\left(\rho_A^{T_2}\right)^n = \mathrm{Tr}\left(\rho_A^{C_2}\right)^n$, and it corresponds to the n-sheeted surface shown in Fig. 1.6, with the right order of row and column indices.

Then one can write the partition function $\mathrm{Tr}\left(\rho_A^{T_2}\right)^n$ as the following four-point function of twist fields

$$\mathrm{Tr}\left(\rho_A^{T_2}\right)^n = \mathrm{Tr}\left(\rho_A^{C_2}\right)^n = \langle \mathcal{T}_n(u_1)\tilde{\mathcal{T}}_n(v_1)\tilde{\mathcal{T}}_n(u_2)\mathcal{T}_n(v_2)\rangle. \tag{1.3.28}$$

Then the effect of the partial transposition is the exchange of two twist operator with respect to the expression of Eq. (1.3.27) for $n = 2$.

Two adjacent intervals

The case of two adjacent intervals, shown in the middle panel of Fig. 1.4, is obtained by sending $v_1 \to u_2$ so that Eq. (1.3.28) becomes

$$\mathrm{Tr}\left(\rho_A^{T_2}\right)^n = \langle \mathcal{T}_n(u_1)\tilde{\mathcal{T}}_n^2(u_2)\mathcal{T}_n(v_2)\rangle\,. \tag{1.3.29}$$

For $n = 2$ in particular, $\mathcal{T}_2^2 = 1$, so that

$$\mathrm{Tr}\left(\rho_A^{T_2}\right)^2 = \langle \mathcal{T}_2(u_1)\mathcal{T}_2(v_2)\rangle = \mathrm{Tr}\rho^2_{A_1\cup A_2}, \tag{1.3.30}$$

and for $n = 3$, one has $\tilde{\mathcal{T}}_3^2 = \mathcal{T}_3$, so that

$$\mathrm{Tr}\left(\rho_A^{T_2}\right)^3 = \langle \mathcal{T}_3(u_1)\mathcal{T}_3(u_2)\mathcal{T}_2(v_2)\rangle\,. \tag{1.3.31}$$

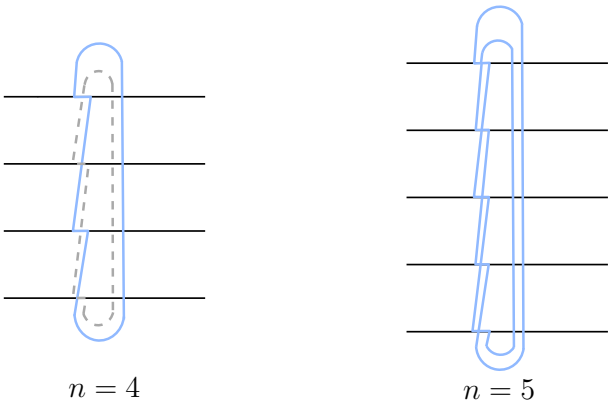


Figure 1.7: Riemann surface corresponding to Eq. (1.3.32). *Left*: For $n = 4$ even, the surface decouples in two independent parts, each with half of the sheets. *Right*: For $n = 5$ odd, the net effect is just a reshuffling of the sheets.

Single interval

It is also interesting to consider the case of a pure state shown in the bottom panel of Fig. 1.4, that can be obtained by sending $u_2 \to v_1$ and $v_2 \to u_1$, so that $B \to \emptyset$ and Eq. (1.3.28) becomes

$$\mathrm{Tr}\left(\rho_A^{T_2}\right)^n = \langle \mathcal{T}_n^2(u_2)\tilde{\mathcal{T}}_n^2(v_2)\rangle\,. \tag{1.3.32}$$

The twist field $\mathcal{T}_n^2$ connects the j-th sheet with the $(j+2)$-th, so according to the parity of n one can have two different situations, as shown in Fig. For $n = n_e$ even, the Riemann surface decouples into two $(n_e/2)$-sheeted Riemann surfaces, each corresponding to a certain parity of the sheets, while for $n = n_o$ odd it remains an n_o-sheeted Riemann surface with a reshuffled sequence of the sheets. Then, Eq. (1.3.32) gives

$$\begin{aligned}
\mathrm{Tr}\left(\rho_A^{T_2}\right)^{n_e} &= \left(\langle \mathcal{T}_{n_e/2}(u_2)\tilde{\mathcal{T}}_{n_e/2}(v_2)\rangle\right)^2 = \left(\mathrm{Tr}\rho_{A_2}^{n_e/2}\right)^2,\\
\mathrm{Tr}\left(\rho_A^{T_2}\right)^{n_o} &= \langle \mathcal{T}_{n_o}(u_2)\tilde{\mathcal{T}}_{n_o}(v_2)\rangle = \mathrm{Tr}\rho_{A_2}^{n_o},
\end{aligned} \tag{1.3.33}$$

that is the same expression found in Eq. (1.3.8).

1.4 Entanglement Entropy and Conformal Field theory

There are systems in nature that are characterized by scale invariance, that is, they show features that remain unchanged if scales of lenght, energy or other variables are multiplied by a common factor. This is the case, for example, of statistical systems that undergo a second order phase transition. When approaching a critical point, the size of fluctuations of the order parameter (or the correlation lenght ξ) diverges, allowing a description in terms of effective field theory: the microscopic details of the system turn out to be unimportant, and its behavior close to the critical point depend only on basic properties like the symmetry of the system or the spatial dimension. This observation leads to the key idea of *universality*, according to which different physical systems can be classified into universality classes, according to their critical behaviour [21, 144].

In 1970, Polyakov proposed the hypotesis that critical fluctuations show not only scale invariance, but also conformal invariance. While the former requires the invariance of the system under a uniform length rescaling, the latter also permits a non-uniform, local rescaling, and only requires that angles are kept unchanged [145].

Under renormalization group transformations, models belonging to the same universality class are characterized by the same fixed point Hamiltonian, that is invariant under rotations. Such continuum models turn out to be invariant under translations, rotations, and scalings, and can be described by conformal field theory (CFT). Each universality class is characterized by its corresponding central charge c, a number that is related the degrees of freedom of the theory. The formal treatment of CFT can be found in Appendix A.

A remarkable feature of EE and EN is that they can be used to capture the universal behavior of a theory. In particular, it has been found that the EE of a subsystem of length ℓ in a very large system in the ground state of a $1+1$ dimensional unitary CFT diverges logarithmically for large subsystem size ℓ with a coefficient $c/3$ which is universal, according to the Cardy-Calabrese formula [25, 26]

$$S(\ell) = \frac{c}{3}\log\frac{\ell}{a} + cnst. \tag{1.4.1}$$

The constant c is the central charge of the CFT and a is a short distance cut-off. This implies that, up to non-universal corrections, all CFTs which have the same central charge also have the same value as the entanglement entropy . For this reason, the EE expresses universal features of the underlying model. The formula (1.4.1) can be generalized to the cases of finite size systems [27, 25], systems near criticality [25, 139], excited states [146, 147], non-unitary CFTs [143, 148], and other measures of entanglement such as the LN in critical [109, 111, 124] and near-critical systems [149]. So the evaluation of the EE and the LN allows determining the constant c and then can be used for the classification of critical points. In discrete models whose continuous limit is described by a CFT, a numerical computation of the EE is the most efficient way of classifying their universality class. Such computations have a long history and are still a popular approach to classify critical points.

1.4.1 Entanglement entropy in CFT: single interval

Let us consider a single interval $[u, v]$ of lenght $\ell = u - v$ with no boundaries, in an infinitely long one dimensional system at finite temperature. The whole Riemann surface $\mathcal{R}_{n,1}$ can be mapped into the complex plane $\mathbb{C}$ applying to the complex coordinates $w = x + i\tau$ and $\bar{w} = x - i\tau$ the conformal transformation $w \to \zeta = (w-u)/(w-v)$, that maps the branch points to $(0;\infty)$, and then the uniformizing mapping $\zeta \to z = \zeta^{1/n} = ((w-u)/(w-v))^{1/n}$, as it is shown in Fig. 1.8. This results in the conformal mapping:

$$z = \zeta^{1/n} = \left(\frac{w-u}{w-v}\right)^{1/n}, \qquad z, \zeta \in \mathbb{C}, \quad w \in \mathcal{R}_{n,1}. \tag{1.4.2}$$

The holomorphic component of the stress tensor $T(w)$ is then related to the transformed stress tensor $T(z)$ by the relation [150]

$$T(w) = \left(\frac{dz}{dw}\right)^2 T(z) + \frac{c}{12}\{z, w\}, \tag{1.4.3}$$

where $\{w, z\} = (z'''z' - \frac{3}{2}z''^2)/z'^2$ is the Schwarzian derivative (see Appendix A.4.2 for more details). Taking the expectation value of this expression and using the fact that $\langle T(z)\rangle_{\mathbb{C}} = 0$ by

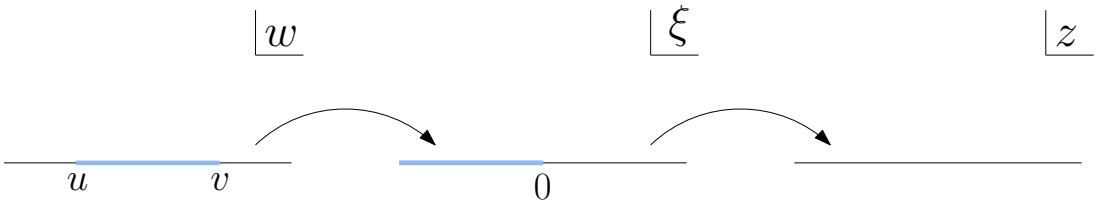


Figure 1.8: The conformal transformation of Eq. (1.4.2) is the composition of $w \to \zeta$, that maps the branch points (u, v) to $(0, \infty)$, and the uniformizing mapping $\zeta \to z$.

rotational and translational invariance, one gets

$$\langle T(w)\rangle_{\mathcal{R}_{n,1}} = \frac{c}{12}\{z, w\} = \frac{c}{24}\left(1 - \frac{1}{n^2}\right)\frac{(v-u)^2}{(w-u)^2(w-v)^2}. \tag{1.4.4}$$

Using Eq. (1.3.26) that refers to a generic operator, we can write the expectation value of the stress tensor on the Riemann surface $\mathcal{R}_{n,N}$ as

$$\langle T(w)\rangle_{\mathcal{R}_{n,1}} = \frac{\langle \mathcal{T}_n(u_1,0)\tilde{\mathcal{T}}_n(v_1,0)T_j(z)\rangle_{\mathcal{L}^{(n)},\mathbb{C}}}{\langle \mathcal{T}_n(u_1,0)\tilde{\mathcal{T}}_n(v_1,0)\rangle_{\mathcal{L}^{(n)},\mathbb{C}}}, \tag{1.4.5}$$

where the index j labels the copies in the multi-copy model.

Since the right hand side of Eq. (1.4.4) is independent on the label j, the stress tensor has the same value in each copy. Moreover, from Eq. (1.3.21) the energy density of the multi-copy model is the sum of the energy densities of the copies, so it can be obtained by a simple multiplication by n

$$\frac{\langle \mathcal{T}_n(u_1,0)\tilde{\mathcal{T}}_n(v_1,0)T^{(n)}(z)\rangle_{\mathcal{L}^{(n)},\mathbb{C}}}{\langle \mathcal{T}_n(u_1,0)\tilde{\mathcal{T}}_n(v_1,0)\rangle_{\mathcal{L}^{(n)},\mathbb{C}}} = \frac{c}{24}\left(n - \frac{1}{n}\right)\frac{(v-u)^2}{(w-u)^2(w-v)^2}. \tag{1.4.6}$$

From the comparison of this expression with the holomorphic Ward identity for the energy momentum tensor (see Eq. (A.5.4) in Appendix A)

$$\begin{aligned}\langle \mathcal{T}_n(u_1,0)\tilde{\mathcal{T}}_n(v_1,0)T^{(n)}(z)\rangle_{\mathcal{L}^{(n)},\mathbb{C}} = \\ \left(\frac{1}{w-u}\frac{\partial}{\partial u} + \frac{\Delta_{\mathcal{T}_n}}{(w-u)^2} + \frac{1}{w-v}\frac{\partial}{\partial v} + \frac{\Delta_{\tilde{\mathcal{T}}_n}}{(w-v)^2}\right)\langle \mathcal{T}_n(u_1,0)\tilde{\mathcal{T}}_n(v_1,0)\rangle_{\mathcal{L}^{(n)},\mathbb{C}}\end{aligned} \tag{1.4.7}$$

and the fact that in conformal field theory the two point functions are specified by the holomorphic and antiholomorphic dimensions by the relation

$$\langle \mathcal{T}_n(u_1,0)\tilde{\mathcal{T}}_n(v_1,0)\rangle_{\mathcal{L}^{(n)},\mathbb{C}} = \frac{1}{|u-v|^{2d_n}} \tag{1.4.8}$$

one can finally get the expression of the scaling dimensions of the twist fields $\mathcal{T}_n$ and $\tilde{\mathcal{T}}_n$, that are the same $d_n = \tilde{d}_n$ and equal to

$$d_n = \frac{c}{12}\left(n - \frac{1}{n}\right). \tag{1.4.9}$$

So *the renormalized $Z_n(A)/Z^n \propto Tr\rho_A^n$ behaves under scale and conformal transformations, apart from a possible overall constant, as the two-point function of a primary operator with scaling dimension d_n.* In particular, this means that

$$\mathrm{Tr}\rho_A^n = c_n \left(\frac{v-u}{a}\right)^{-\frac{c}{6}\left(n-\frac{1}{n}\right)}, \tag{1.4.10}$$

where the parametrer a has been inserted in order to make the final result dimensionless, and the c_n are model dependent multiplicative factors that cannot be evaluated with this method, except for c_1 that must be unity because of the normalization of the RDM

$$\mathrm{Tr}\rho_A = \lim_{n\to 1} \mathrm{Tr}\rho_A^n = \lim_{n\to 1} c_n \left(\frac{v-u}{a}\right)^{-\frac{c}{6}\left(n-\frac{1}{n}\right)} = c_1 = 1. \tag{1.4.11}$$

From (1.4.10) one can easily obtain the expression of the RE

$$\begin{aligned} S_n &= \frac{1}{1-n}\ln \mathrm{Tr}\rho_A^n = \frac{1}{1-n}\ln\left[c_n\left(\frac{v-u}{a}\right)^{-\frac{c}{6}\left(n-\frac{1}{n}\right)}\right] \\ &= \frac{c}{6}\left(1+\frac{1}{n}\right)\ln\frac{\ell}{a} + c_n', \end{aligned} \tag{1.4.12}$$

where

$$c_n' = \frac{\log c_n}{1-n}. \tag{1.4.13}$$

The EE is finally obtained by taking the limit $n \to 1^+$

$$S = \lim_{n\to 1^+} = \frac{c}{3}\ln\frac{\ell}{a} + c_1'. \tag{1.4.14}$$

Finite size or temperature

The $\mathrm{Tr}\rho_A^n$ behaves under conformal transformations as a two-point function of primary operators $\mathcal{T}$, so for a conformal mapping $z \mapsto w(z)$, it verifies (see Eq. (A.1.18))

$$\langle \mathcal{T}_n(z_1,\bar{z}_1)\tilde{\mathcal{T}}_n(z_2,\bar{z}_2)\rangle = |w'(z_1)w'(z_2)|^{d_n}\langle \mathcal{T}_n(w_1,\bar{w}_1)\tilde{\mathcal{T}}_n(w_2,\bar{w}_2)\rangle\,. \tag{1.4.15}$$

This property can be used to evaluate the partition functions for different geometries of the Riemann surface.

Let us consider a system at finite temperature, for which the thermal trace is obtained by taking the first line of each sheet and sewing it to the last one, producing n cylinders of circumference $\beta = 1/T$, and connecting them along the cut. The conformal mapping which that maps each sheet in the plane w into an infinitely long cylinder of circumference β is

$$w \to z(w) = \frac{\beta}{2\pi}\log w, \qquad\qquad w(z) = \mathrm{e}^{\frac{2\pi}{\beta}}. \tag{1.4.16}$$

Then, Eq. (1.4.15) becomes

$$\begin{aligned} \mathrm{Tr}\rho_A^n &= \langle \mathcal{T}_n(u)\tilde{\mathcal{T}}_n(v)\rangle_{cylinder} = \left|\mathrm{e}^{\frac{2\pi u}{\beta}}\mathrm{e}^{\frac{2\pi v}{\beta}}\left(\frac{2\pi}{\beta}\right)^2\right|^{\frac{c}{12}\left(n-\frac{1}{n}\right)} c_n\left(\frac{\mathrm{e}^{\frac{2\pi u}{\beta}}-\mathrm{e}^{\frac{2\pi v}{\beta}}}{a}\right)^{-\frac{c}{6}\left(n-\frac{1}{n}\right)} \\ &= c_n\left[\frac{\beta}{2\pi}\frac{\mathrm{e}^{\frac{\pi(u-v)}{\beta}}-\mathrm{e}^{\frac{\pi(v-u)}{\beta}}}{a}\right]^{-\frac{c}{6}\left(n-\frac{1}{n}\right)} = c_n\frac{\beta}{a\pi}\sinh\left(\frac{\pi|u-v|}{\beta}\right)^{-\frac{c}{6}\left(n-\frac{1}{n}\right)}. \end{aligned}$$

From this formula it is straightforward to derive the RE

$$S_n = \frac{c}{6}\left(\frac{n+1}{n}\right)\log\left[\frac{\beta}{a\pi}\sinh\left(\frac{\pi\ell}{\beta}\right)\right] + c_n', \tag{1.4.17}$$

and the EE

$$S = \frac{c}{3}\log\left[\frac{\beta}{a\pi}\sinh\left(\frac{\pi\ell}{\beta}\right)\right] + c_1'. \tag{1.4.18}$$

It is interesting to study the high and low temperature behavior of the EE. For the high temperature regime, $\beta \ll \ell$ so that $\sinh\frac{\pi\ell}{\beta} \approx \mathrm{e}^{\frac{\pi\ell}{\beta}}/2$, and consequently

$$S \approx \frac{c}{6}\frac{\pi\ell}{\beta} + c_1', \tag{1.4.19}$$

that means that the entropy is only thermal, being extensive, and proportional to temperature. In the low temperature limit $\beta \to \infty$, one has $\sinh\frac{\pi\ell}{\beta} \approx \frac{\pi\ell}{\beta}$, and it is possible to recover the formula of the EE at zero temperature

$$S \approx \frac{c}{3}\log\frac{\ell}{a} + c_1'. \tag{1.4.20}$$

This result can be used to derive the EE of a system of finite size L and periodic boundary conditions, at zero temperature. This can be obtained by orienting the branch cut perpendicular to the axis of the cylinder, and taking the substitution $\beta \to L$. The transformation in this case is

$$z \to z(w) = \frac{L}{2\pi\mathrm{i}}\log w, \qquad\qquad w(z) = \mathrm{e}^{\frac{2\pi\mathrm{i}z}{L}}, \tag{1.4.21}$$

and the steps of the calculation are the same of the previous case (with the presence of an i factor, that turns the hyperbolic sine into a sine),

$$\mathrm{Tr}\rho_A^n = c_n\left(\frac{L}{\pi a}\sin\frac{\pi\ell}{L}\right)^{-\frac{c}{6}\left(n-\frac{1}{n}\right)} \quad \Rightarrow \quad S = \frac{c}{3}\log\left(\frac{L}{\pi a}\sin\frac{\pi\ell}{L}\right). \tag{1.4.22}$$

The expression obtained is symmetric under $\ell \leftrightarrow L-\ell$, and is maximal for $\ell = L/2$. It is very useful for the test of numerical data that are mainly done in finite size.

Finite temperature and finite size

In the case of a finite system at finite temperature, periodic boundary conditions have to be imposed both on space and imaginary time axes, and this results in the calculation of a two-point function of twist field operators on a torus. In this case, the correlations depend not only on the scaling dimensions, but also on the full operator content of the theory [144], and consequently the results for the EE will depend on the universality class. Moreover, is no longer possible to use a uniformizing transformation from the torus to the plane, which are topologically different (having the torus genus $g = 1$). Using the replica trick, the n tori are joined together along the entangling interval to form a genus n Riemann surface.

In this section the focus will be on free fermionic theories, since they are the models that will be used as reference in the calculations of the second part of the Thesis. For free theories, the calculation of the REs have been performed both on the torus [151, 152, 153] and for higher

genus Riemann surfaces [154]. Since there are two periods, a fermion field ψ on a torus with periods normalized to 1 and $z = i\beta/L$, can be defined according to four types of boundary conditions, or "spin structures" $\nu = (\nu_1, \nu_2)$, obtained by choosing periodic or antiperiodic conditions in the two directions

$$\psi(z+1) = e^{2\pi i \nu_1}\psi(z), \qquad \psi(z+\tau) = e^{2\pi i \nu_2}\psi(z), \tag{1.4.23}$$

where ν_1 and ν_2 can take values 0 and 1/2. The 4 possible conditions can be indicated as Ramond (R) if periodic, and Neveu-Schwarz (NS) if antiperiodic, and will denoted as

$$\begin{array}{ll} \nu = (0,0) \equiv 1 & (R,R) \\ \nu = (0,\frac{1}{2}) \equiv 2 & (R,NS) \\ \nu = (\frac{1}{2},\frac{1}{2}) \equiv 3 & (NS,NS) \\ \nu = (\frac{1}{2},0) \equiv 4 & (NS,R) \end{array} \tag{1.4.24}$$

Let us now discuss the evaluation of the replica partition function for a single interval [154]. It can be performed following two different approaches: using the higher genus partition function on the replica surface, or using the twist field operators on the torus. Since there are four possible spin structures on the single torus, the full partition function on the genus-n replica surface is obtained as sum over all the possible 2^{2n} spin structures of this surface, denoted as $\vec{\nu}_1 = (\nu_1^{(1)}, \cdots, \nu_1^{(n)})$ and $\vec{\nu}_2 = (\nu_2^{(1)}, \cdots, \nu_2^{(n)})$. Since there are more spin structures in the genus n surface than in the torus, in order to compare higher genus calculations with twist fields calculations it is necessary to fix "diagonal" higher genus spin structures that obey the replica symmetry, that are of the type $\vec{\nu}_1^{diag} = (\nu_1, \cdots, \nu_1)$ and $\vec{\nu}_2^{diag} = (\nu_2, \cdots, \nu_2)$, where (ν_1, ν_2) is the spin structure of the original torus.

Before giving the results obtained for the partition function for both the approaches, let us introduce the Jacobi θ-functions, which are elliptic functions of two complex variables that represent the two directions on the torus. For each spin structure ν, the Jacobi functions $\theta_\nu(z|\tau)$ are given by

$$\begin{aligned} \theta_1(z|\tau) &= \theta\begin{bmatrix} 0 \\ 0 \end{bmatrix}(z|\tau) = -i\sum_{r=-\infty}^{\infty}(-1)^r y^{r+1/2} q^{(r+1/2)^2/2}, \\ \theta_2(z|\tau) &= \theta\begin{bmatrix} 0 \\ 1/2 \end{bmatrix}(z|\tau) = -i\sum_{r=-\infty}^{\infty} y^{r+1/2} q^{(r+1/2)^2/2}, \\ \theta_3(z|\tau) &= \theta\begin{bmatrix} 1/2 \\ 1/2 \end{bmatrix}(z|\tau) = -i\sum_{r=-\infty}^{\infty} y^{r} q^{r^2/2}, \\ \theta_4(z|\tau) &= \theta\begin{bmatrix} 1/2 \\ 0 \end{bmatrix}(z|\tau) = -i\sum_{r=-\infty}^{\infty}(-1)^r y^{r} q^{r^2/2}, \end{aligned} \tag{1.4.25}$$

where $q = e^{2\pi i\tau}$ and $y = e^{2\pi i z}$.

For the higher genus calculations, let us just report the final results of the calculations. One needs to introduce the period matrix of the Riemann surface, that depends on the parameters τ and $z_{12} = \ell/L$. It can be defined starting from the so-called cut abelian differentials $\omega_k(z, z_{12}, \tau)$ [155, 156], which are defined as doubly-periodic holomorphic functions on the torus, and then have the appropriate monodromy around the branch points,

$$\omega_k(z, z_{12}, \tau) = \frac{\theta_1(z|\tau)}{\theta_1\left(z + \frac{k}{n} z_{12}|\tau\right)^{1-\frac{k}{n}} \theta_1\left(z - (1-\frac{k}{n}) z_{12}|\tau\right)^{\frac{k}{n}}}. \tag{1.4.26}$$

The period matrix is

$$\Omega_{ab} = \frac{1}{n}\sum_{k=0}^{n-1} \mathrm{e}^{2\pi \mathrm{i} k(a-b)} \frac{B_k}{A_k}, \tag{1.4.27}$$

where A_k, B_k are obtained as integrals over the two periods, for $k = 0, \cdots, n-1$

$$A_k = \int_0^1 \omega_k \mathrm{d}z, \qquad\qquad B_k = \int_0^\tau \omega_k \mathrm{d}z. \tag{1.4.28}$$

The genus-n fermion partition function is [157, 154]

$$Z_n^{higher-genus} \begin{bmatrix} \vec{\nu}_1 \\ \vec{\nu}_2 \end{bmatrix} (\Omega) = \left| 2^g \left(\frac{\epsilon \partial_n \theta_1(0|\tau)}{\theta_1(z_{12}|\tau)} \right)^{\frac{1}{6}\left(n-\frac{1}{n}\right)} \frac{1}{\eta(\tau)^{2n} \prod_{k=0}^{n-1} A_k} \left(\Theta^{(n)}(0|\Omega) \begin{bmatrix} \vec{\nu}_1 \\ \vec{\nu}_2 \end{bmatrix} \right)^2 \right|, \tag{1.4.29}$$

where $\epsilon = a/L$ is a UV-cutoff to resolve the coincident points (since the theta function behaves as $\theta(z|\tau) \sim z$ as $z \to 0$). The function Θ is the Riemann-Siegel function with characteristic (ν_1, ν_2), a generalization of the Jacobi thetas having as arguments a matrix A and a vector $\vec{s}$ with the same dimension

$$\Theta(\vec{s}|A) \begin{bmatrix} \vec{\nu}_1 \\ \vec{\nu}_2 \end{bmatrix} = \sum_{\vec{m}\in\mathbb{Z}^n} \mathrm{e}^{\mathrm{i}\pi(\vec{m}+\vec{\nu}_1)^T \cdot A \cdot (\vec{m}+\vec{\nu}_1) + 2\pi \mathrm{i}(\vec{m}+\vec{\nu}_1)\cdot(\vec{s}+\vec{\nu}_2)}, \tag{1.4.30}$$

and function η is the Dedekin η-function

$$\eta(\tau) = q^{1/24} \prod_{n=1}^{\infty} (1-q^n). \tag{1.4.31}$$

In the twist-fields approach, the partition function can be obtained by computing two-point functions of twist operators on a single torus. For a fixed fermion spin structure ν and for the Dirac fermion, the result is [152, 158, 159]

$$Z_n^{twist-field} \left| \left(\frac{\epsilon \partial_z \theta_1(0|\tau)}{\theta_1(z_{12}|\tau)} \right) \right|^{\frac{1}{6}\left(n-\frac{1}{n}\right)} \prod_{k=0}^{n-1} \left| \frac{\theta_\nu(\frac{k}{n} z_{12}|\tau)}{\eta(\tau)} \right|^2. \tag{1.4.32}$$

The comparison between Eq. (1.4.29) and Eq. (1.4.32) leads to the conjecture

$$\frac{\Theta^{(n)}(0|\Omega) \begin{bmatrix} \vec{\nu}_1^{\,diag} \\ \vec{\nu}_2^{\,diag} \end{bmatrix}}{\sqrt{\prod_{k=1}^{n-1} A_k}} = \prod_{k=-\frac{n-1}{2}}^{\frac{n-1}{2}} \theta_\nu \left(\frac{k}{n} z_{12} | \tau \right). \tag{1.4.33}$$

This identity was proven for $n = 2$ [160]. Several common properties and the matching of certain zeros on both sides were proven for $n > 2$ [160].

Let us now report the results for the EE. From the expression of the twist field partition function, it follows that the n^{th} RE for a given spin structure is [161]

$$S_n = \frac{1}{1-n} \log \mathrm{Tr} \rho_A^n = \frac{1}{1-n} \log \frac{Z_n}{Z_1^n} = S_{n,0} + S_{n,1}^{(\nu)}, \tag{1.4.34}$$

and it is given by the sum between the universal term

$$S_{n,0} = -\frac{1}{6}\left(1 + \frac{1}{n}\right) \log \left| \frac{\epsilon \partial_z \theta_1(0|\tau)}{\theta_1(z_{12}|\tau)} \right|, \tag{1.4.35}$$

and the spin structure-dependent term

$$S_{n,1}^{(\nu)} = \frac{2}{1-n} \sum_{k=-\frac{n-1}{2}}^{\frac{n-1}{2}} \log \left| \frac{\theta_\nu\left(\frac{k}{n} z_{12}|\tau\right)}{\theta_\nu(0|\tau)} \right|. \tag{1.4.36}$$

Let us choose the sector $\nu = 3$, to check that S_n gives back the known results of the previous sections in the limits $\beta \to \infty$ and $L \to \infty$. Using the expansion of θ_1 around $\beta = \infty$

$$\theta_1(z|\tau) \sim 2\mathrm{e}^{-\frac{\pi\beta}{4L}} \sin \pi z + \mathcal{O}\left(\mathrm{e}^{-\frac{2\pi\beta}{L}}\right), \tag{1.4.37}$$

so the first term becomes

$$S_{n,0}(\beta \to \infty) = -\frac{1}{6}\left(1+\frac{1}{n}\right) \log \left| \frac{a}{L} \frac{2\pi \mathrm{e}^{-\frac{\pi\beta}{4L}}}{2\mathrm{e}^{-\frac{\pi\beta}{4L}} \sin \frac{\pi\ell}{L}} \right| = \frac{1}{6}\left(1+\frac{1}{n}\right) \log \left| \frac{L}{a\pi} \sin \frac{\pi\ell}{L} \right|, \tag{1.4.38}$$

while the second term vanishes. So in the limit $n \to 1$ one recovers the result of Eq. (1.4.22).

Let us now study the limit $L \to \infty$, that is equivalent to the limit $\tau \to 0$. One can use the modular transformation rules for the θ-function

$$\theta_1(z|\tau) = -(-\mathrm{i}\tau)^{-1/2} \mathrm{e}^{-\frac{\pi \mathrm{i} z^2}{\tau}} \theta_1(z/\theta| - 1/\tau), \tag{1.4.39}$$

and the asymptotic form of θ_1 in the limit of small τ

$$\theta_1(z/\theta| - 1/\tau) = -2\mathrm{i}\mathrm{e}^{-\frac{\pi L}{4\beta}} \sinh \frac{\pi z L}{\beta} + \mathcal{O}^{\frac{3\pi L}{\beta}(z-3/4)}. \tag{1.4.40}$$

The result for the first part is

$$\begin{aligned} S_{n,0}(L \to \infty) &= -\frac{1}{6}\left(1+\frac{1}{n}\right) \log \left| \frac{a}{L} \frac{\pi L}{\beta} \frac{\mathrm{e}^{\pi \mathrm{i} \left(\frac{\ell}{L}\right)^2 \frac{L}{\mathrm{i}\beta}}}{\sinh\left(\frac{\pi\ell}{\beta}\right)} \right| \\ &= \frac{1}{6}\left(1+\frac{1}{n}\right) \left[-\frac{\pi\ell^2}{L\beta} + \log \left| \frac{\beta}{\pi a} \sinh\left(\frac{\pi\ell}{\beta}\right) \right| \right], \end{aligned} \tag{1.4.41}$$

and for the second part

$$S_{n,1}(L \to \infty) = \frac{1}{6}\left(1+\frac{1}{n}\right) \frac{\pi\ell^2}{L\beta} - \frac{2}{1-n} \sum_{j=1}^{\infty} \frac{(-1)^j}{j} \frac{1}{\sinh\left(\frac{\pi j}{\beta}\right)} \left[\frac{\sinh\left(\frac{\pi\ell j}{\beta}\right)}{\sinh\left(\frac{\pi\ell j}{n\beta}\right)} - n \right]. \tag{1.4.42}$$

So one can see that the first terms of the two parts cancel each other, the total RE gives the result of Eq. (1.4.17) plus a correction term

$$S_n(L \to \infty) = \frac{1}{6}\left(1+\frac{1}{n}\right) \log \left| \frac{\beta}{\pi a} \sinh\left(\frac{\pi\ell}{\beta}\right) \right| - \frac{2}{1-n} \sum_{j=1}^{\infty} \frac{(-1)^j}{j} \frac{1}{\sinh\left(\frac{\pi j}{\beta}\right)} \left[\frac{\sinh\left(\frac{\pi\ell j}{\beta}\right)}{\sinh\left(\frac{\pi\ell j}{n\beta}\right)} - n \right]. \tag{1.4.43}$$

1.4.2 Systems with boundaries

In most of the real experiments as well as in numerical simulations, physical systems are characterized by the presence of boundaries. From the point of view of analytical calculations, these situations can be treated in the formalism of Boundary Conformal Field Theory (BCFT).

Let us consider a 1-dimensional system in a semi-infinite line $[0,\infty)$, and a finite interval $A=[0,\ell]$ starting from the boundary. The n-sheeted Riemann surface $\tilde{\mathcal{R}}_{n,1}$ can be constructed by taking n copies of the half plane $x\geq 0$, and sewing them together in $0\leq x\leq \ell$, at $\tau=0$.

Let us start considering a system at zero temperature. The upper-half plane (UHP) can be parametrized by the complex variable $w=\tau+\mathrm{i}x$. The n-sheeted Riemann surface can be mapped to the unit disk $\mathcal{D}:|z|<1$ using the uniformizing transformation

$$z=\left[\frac{(w-\mathrm{i}\ell)}{(w+\mathrm{i}\ell)}\right]. \tag{1.4.44}$$

The corresponding transformation of the stress tensor is

$$\langle T(w)\rangle_{\tilde{R}_n,1}=\sum_j\left(\frac{\mathrm{d}z}{\mathrm{d}w}\right)^2\langle T_j(z)\rangle_{\mathcal{D}}+\frac{nc}{12}\{z,w\}, \tag{1.4.45}$$

and using the fact that $\langle T(z)\rangle=0$ by rotational invariance

$$\langle T(w)\rangle_{\tilde{R}_n,1}=\frac{c}{24}\left(n-\frac{1}{n}\right)\frac{2\ell^2}{(w-\ell)^2(w+\ell)^2}. \tag{1.4.46}$$

In presence of a boundary, the analogous of Eq. (1.4.5) is

$$\langle T(w)\rangle_{\tilde{R}_n,1}=\frac{\langle T(w)\mathcal{T}_n(\mathrm{i}\ell)\rangle_{\mathrm{UHP}}}{\langle\mathcal{T}_n(\mathrm{i}\ell)\rangle_{\mathrm{UHP}}}, \tag{1.4.47}$$

with $\langle\mathcal{T}_n(\mathrm{i}\ell)\rangle_{\mathrm{UHP}}=2\ell^{-d_n}$. So one gets the following relation

$$\langle T(w)\rangle_{\tilde{R}_n,1}=\frac{c}{24}\left(n-\frac{1}{n}\right)\frac{2\ell^2}{(w-\ell)^2(w+\ell)^2}, \tag{1.4.48}$$

that, compared with the conformal Ward identity for BCFT [162], gives the scaling dimension

$$d_n=\frac{c}{12}\left(n-\frac{1}{n}\right). \tag{1.4.49}$$

Then it follows that

$$\mathrm{Tr}\rho_A^n=\langle\mathcal{T}_n(\ell)\rangle\sim\frac{\tilde{c}_n}{(2\ell)^{d_n}}=\tilde{c}_n\left(\frac{2\ell}{a}\right)^{-\frac{c}{12}\left(n-\frac{1}{n}\right)}, \tag{1.4.50}$$

where the constants $\tilde{c}_n$ are different from those c_n of the periodic case. So, the scaling of the REs for the interval $A=[0,\ell]$ is [25, 26]:

$$S_n=\frac{c}{12}\left(1+\frac{1}{n}\right)\log 2\ell+\tilde{c}_n', \tag{1.4.51}$$

where the non universal constants $\tilde{c}'_n$ are related to the c'_n in Eq. (1.4.13) by the universal relation [25, 163]

$$\tilde{c}'_n - \frac{c'_n}{2} = \log g, \tag{1.4.52}$$

and $\log g$ is the boundary entropy [164, 165]. For the tight-binding chain with OBC that will be considered in Chap. 3, one has $g = 1$ [164]. Finally, the EE is

$$S = \frac{c}{6}\log(2\ell) + \tilde{c}'_1, \qquad \text{with} \quad \tilde{c}_1 = -\frac{\partial}{\partial n}\tilde{c}_n. \tag{1.4.53}$$

Also in this case, it is possible to use the transformation properties of correlation functions under conformal mapping to evaluate the EE in different cases.

Let us consider a system of finite size L. In this case, the complex z-plane is a strip of width L, that can be obtained from the UHP w via the conformal mapping $z = \frac{L}{\pi}\log w$, so that

$$\langle \mathcal{T}_n(\ell)\rangle_{strip} = \left|w'(\ell)\right|^{d_n} \langle \mathcal{T}_n(w(\ell))\rangle_{\text{UHP}}\,. \tag{1.4.54}$$

In BCFT, the one-point function of a scalar primary field with scaling dimension d_Φ in the UHP is [162]

$$\langle \Phi(w)\rangle_{\text{UHP}} = \frac{A^b_\Phi}{[2\text{Im}(w)]^{d_\Phi}}, \tag{1.4.55}$$

where the normalisation factor A^b_Φ is a non-universal amplitude. So in our case

$$\text{Tr}\rho_A^n = \langle \mathcal{T}_n(\ell)\rangle_{strip} = \left[\frac{\pi}{L}\frac{\tilde{c}_n}{2\text{Im}\left(\mathrm{e}^{\frac{\mathrm{i}\pi\ell}{L}}\right)}\right]^{d_n} = \left(\frac{\pi}{2L}\frac{\tilde{c}_n}{\sin(\pi\ell/L)}\right)^{\frac{c}{12}\left(n-\frac{1}{n}\right)} \tag{1.4.56}$$

and the EE is

$$S = \frac{c}{6}\log\left[\frac{2L}{\pi}\sin\left(\frac{\pi\ell}{L}\right)\right] + \tilde{c}'_1. \tag{1.4.57}$$

In the case of a system of finite temperature β, the z-plane is a half-cylinder with the axis parallel to the segment ℓ, and it can be obtained from the unit disk $\mathcal{D}$ where $w = \mathrm{e}^{\mathrm{i}2\pi z/\beta}$. The one-point function on the unit disk, can be obtained from that on the UHP via Mobius transformation, and introducing the parametrization $w = \rho\mathrm{e}^{\mathrm{i}\theta}$, it can be shown to be equal to

$$\langle T_n(\rho)\rangle_{\mathcal{D}} = \frac{\tilde{c}_n}{(1-\rho)^{d_n}}. \tag{1.4.58}$$

So, the expectation value of $\mathcal{T}_n$ on the half-cylinder is

$$\langle \mathcal{T}_n(\mathrm{i}\ell)\rangle_{half-cyl} = \tilde{c}_n\left[\frac{2\pi}{\beta}\frac{\mathrm{e}^{-2\pi\ell/\beta}}{1-\mathrm{e}^{-4\pi\ell/\beta}}\right]^{d_n} = \tilde{c}_n\left(\frac{\pi}{\beta}\frac{1}{\sinh(2\pi\ell/\beta)}\right), \tag{1.4.59}$$

and the entanglement entropy is

$$S = \frac{c}{6}\log\left[\frac{\pi}{\beta}\sinh\left(\frac{2\pi\ell}{\beta}\right)\right] + \tilde{c}'_1. \tag{1.4.60}$$

1.4.3 Disjoint intervals

Let us consider a system $A = \bigcup_{i=1}^{N} A_i$ that consists of $N \geq 2$ disjoint intervals in an infinite line. The intervals are denoted as $A_i = [u_i, v_i]$, with $i = 1, \cdots, N$, ordered as $u_1 < v_1 < \cdots < u_N < v_N$. The $\mathrm{Tr}\rho_A^n$ is given by the $2N$-point function of twist fields

$$\mathrm{Tr}\rho_A^n = \left\langle \prod_{i=1}^{N} \mathcal{T}_n(u_i)\tilde{\mathcal{T}}_n(v_i) \right\rangle. \tag{1.4.61}$$

For four and higher point correlation functions of primary fields, global conformal invariance does not completely fixes the twist fields correlation functions, since it is possible to define different invariant ratios in terms of the points u_i and v_i. For example, let us consider the conformal map [166]

$$w_N(z) = \frac{(u_1 - z)(u_N - z)}{(u_1 - u_N)(z - v_N)}, \tag{1.4.62}$$

which sends $u_1 \to 0, u_N \to 1$ and $v_N \to \infty$. Each of the remaining $2N - 3$ points can be sent to the harmonic ratios $x_1 = w_N(v_1), x_2 = w_N(u_2), \cdots, x_{2N-3} = w_N(v_{N-1})$, which are invariant under $SL(2, \mathbb{C})$ tranformations. The ordering $0 < x_1 < x_2 < \cdots < x_{2N-3}$ of the ratios in preserved by the map in Eq. (1.4.62). Global conformal invariance gives the following expression of the $2N$-point function in Eq. (1.4.61)

$$\mathrm{Tr}\rho_A^n = c_n^N \left| \frac{\prod_{i<j}(u_j - u_i)(v_j - v_i)}{\prod_{i,j}(v_j - u_i)} \right|^{2d_n} \mathcal{F}_{N,n}(\mathbf{x}), \tag{1.4.63}$$

where $i, j = 1, \cdots, N$ and $\mathbf{x}$ is the vector with elements $x_1, \cdots, x_{2N-3}$. The function $\mathcal{F}_{N,n}(\mathbf{x})$ encodes the full operator content of the model, and therefore it must be computed case by case. The normalization $\mathrm{Tr}\rho_A = 1$ gives $\mathcal{F}_{N,1} = 1$.

Let us focus on the case of a subsystem $A = A_1 \cup A_2$ made of $N = 2$ disjoint intervals. The moments $\mathrm{Tr}\rho_A^n$ are given by the four-point function $\langle \mathcal{T}_n(u_1)\tilde{\mathcal{T}}_n(v_1)\mathcal{T}_n(u_2)\tilde{\mathcal{T}}_n(v_2)\rangle$, that is given by Eq. (1.4.63) for $n = 2$

$$\mathrm{Tr}\rho_A^n = c_n^2 \left(\frac{(u_2 - u_1)(v_2 - v_1)}{(v_1 - u_1)(v_2 - u_2)(v_2 - u_1)(v_1 - u_2)} \right)^{2d_n} \mathcal{F}_{2,n}(x), \tag{1.4.64}$$

where x is the four-point ratio

$$x = \frac{(u_1 - v_1)(u_2 - v_2)}{(u_1 - u_2)(v_1 - v_2)} \in (0, 1). \tag{1.4.65}$$

The function $\mathcal{F}_{2,n}(x)$ has been studied in several works [40, 167, 168, 169, 170, 171, 172, 173, 174]. For the CFT describing the free compactified boson on a circle of radius R, its exact form is [175]

$$\mathcal{F}_{2,n}(x) = \frac{\Theta(0|\eta\Gamma)\Theta(0|\Gamma/\eta)}{[\Theta(0|\Gamma)]^2}, \tag{1.4.66}$$

where $\eta = 2R^2$ and Γ is an $(n-1) \times (n-1)$ matrix whose elements are

$$\begin{aligned} \Gamma_{r,s} &= \frac{2\mathrm{i}}{n} \sum_{k=1}^{n-1} \sin\left(\pi \frac{k}{n}\right) \beta_{k/n} \cos\left[2\pi \frac{k}{n}(r-s)\right], \\ \beta_y &= \frac{{}_2F_1(y, 1-y; 1; 1-x)}{{}_2F_1(y, 1-y; 1; x)}, \end{aligned} \tag{1.4.67}$$

with ${}_2F_1$ hypergeometric function. The $\Theta(0|\Gamma)$ is the Riemann-Siegel function

$$\Theta(0|\Gamma) = \sum_{m\in\mathbb{Z}^{n-1}} e^{i\pi m^T\cdot\Gamma\cdot m}. \tag{1.4.68}$$

For $\eta = 1/2$, the free bosonic theory correponds to the scaling limit of the XX spin chain, the so called Dirac point. In this case [175, 168]

$$\mathcal{F}^{Dirac}_{2,n}(x) = \frac{1}{2^{n-1}|\Theta(0|\tau)|^2}\sum_{\epsilon,\delta}\left|\Theta(0|\tau)\begin{bmatrix}\epsilon\\ \delta\end{bmatrix}\right|^2, \tag{1.4.69}$$

where $\Theta(0|\tau)\begin{bmatrix}\epsilon\\ \delta\end{bmatrix}$ is the Riemann-Siegel function with characteristic (ϵ,δ) given in Eq. (1.4.30).

1.4.4 Entanglement negativity in conformal field theory

Let us now illustrate the explicit calculation of the EN in CFT, where global conformal invariance can be used to determine the expressions of $\mathrm{Tr}(\rho_A^{T_2})^n$.

Single interval

Let us start considering the case of a single interval, that is the configuration shown in the bottom panel of Fig. 1.4, and it is obtained by sending $B\to\emptyset$. Then, A_2 is a single interval embedded in an infinite system and the reduced density matrix describes a pure system, and one can use Eq. (1.3.33) and Eq. (1.4.10) to get

$$\mathrm{Tr}\left(\rho_A^{T_2}\right)^{n_e} = (\langle\mathcal{T}_{n_e/2}(u_2)\tilde{\mathcal{T}}_{n_0}(v_2)\rangle)^2 = \left(\mathrm{Tr}\rho_{A_2}^{n_e/2}\right)^2 = c^2_{n_e/2}\left(\frac{\ell}{a}\right)^{-\frac{c}{3}\left(\frac{n_e}{2}-\frac{2}{n_e}\right)}, \tag{1.4.70}$$

and

$$\mathrm{Tr}\left(\rho_A^{T_2}\right)^{n_o} = \langle\mathcal{T}_{n_o}(u_2)\tilde{\mathcal{T}}_{n_o}(v_2)\rangle = \mathrm{Tr}\rho_{A_2}^{n_o} = c_{n_o}\left(\frac{\ell}{a}\right)^{-\frac{c}{6}\left(n_o-\frac{1}{n_o}\right)}, \tag{1.4.71}$$

where $\ell = u_2 - v_2$ and the non-universal constants n_e and n_o are the same appearing in the EE. From the above equations, it is possible to deduce the scaling dimensions of the twist operators. For $n = n_e$ even, the fields $\mathcal{T}^2_{n_e}$ and $\tilde{\mathcal{T}}^2_{n_e}$ have dimensions

$$d_{\mathcal{T}^2_{n_e}} = d_{\tilde{\mathcal{T}}^2_{n_e}} = \frac{c}{6}\left(\frac{n_e}{2}-\frac{2}{n_e}\right). \tag{1.4.72}$$

For $n = n_o$, instead the dimensions of $\mathcal{T}^2_{n_o}$ and $\tilde{\mathcal{T}}^2_{n_o}$ are

$$d_{\mathcal{T}^2_{n_o}} = d_{\tilde{\mathcal{T}}^2_{n_o}} = \frac{c}{12}\left(n_o-\frac{1}{n_o}\right), \tag{1.4.73}$$

that is, they are equal to the dimension of $\mathcal{T}_{n_o}$. Then, the analytic continuation $n_e\to 1$ from the even branch gives

$$||\rho_A^{T_2}|| = \lim_{n_e\to 1}\mathrm{Tr}\left(\rho_A^{T_2}\right)^{n_e} = c^2_{1/2}\left(\frac{\ell}{a}\right)^{c/2}, \tag{1.4.74}$$

so that one finally gets the negativity

$$\mathcal{E} = \frac{c}{2}\log\frac{\ell}{a} + 2\log c_{1/2}. \tag{1.4.75}$$

So, one recovers the result that for pure states the logarithmic negativity is equal to the Rény entropy for $n = 1/2$. The limit $n_o \to 1$ gives instead the normalization $\mathrm{Tr}\rho_A^{T_2} = 1$.

Two adjacent intervals

Let us now consider the case of two adjacent intarvals A_1 and A_2, which is illustrated in the middle panel of Fig. 1.4. This configuration is obtained by sending $v_1 \to u_2$ into Eq. (1.3.28),

$$\mathrm{Tr}(\rho_A^{T_2})^n = \langle \mathcal{T}_n(-\ell_1)\tilde{\mathcal{T}}_n^2(0)\mathcal{T}_n(\ell_2)\rangle \tag{1.4.76}$$

The two other extrema are chosen such that $u_1 = -\ell_1$ and $v_2 = \ell_2$. Using the conditions imposed by conformal symmetry on three-point functions (see Eq. (A.1.23) in Appendix A), one gets the following expression

$$\mathrm{Tr}(\rho_A^{T_2})^n = \langle \mathcal{T}_n(-\ell_1)\tilde{\mathcal{T}}_n^2(0)\mathcal{T}_n(\ell_2)\rangle = c_n^2 \frac{C_{\mathcal{T}_n\tilde{\mathcal{T}}_n^2\mathcal{T}_n}}{(\ell_1\ell_2)^{d_{\mathcal{T}_n^2}}(\ell_1+\ell_2)^{2d_{\mathcal{T}_n}-d_{\mathcal{T}_n^2}}}. \tag{1.4.77}$$

that is normalized such that the structure constant $C_{\mathcal{T}_n\tilde{\mathcal{T}}_n^2\mathcal{T}_n}$ is universal.

Let us study this expression for $n = n_e$ even, in order to derive the logarithmic negativity via analytic continuation. Using the scaling dimension in Eq. (1.4.72), one gets

$$\mathrm{Tr}\left(\rho_A^{T_2}\right)^{n_e} \propto (\ell_1\ell_2)^{-\frac{c}{6}\left(\frac{n_e}{2}-\frac{2}{n_e}\right)}(\ell_1+\ell_2)^{-\frac{c}{6}\left(\frac{n_e}{2}+\frac{1}{n_e}\right)}, \tag{1.4.78}$$

so that the analytic continuation $n_e \to 1$ gives

$$||\rho_A^{T_2}|| \propto \left(\frac{\ell_1\ell_2}{\ell_1+\ell_2}\right)^{\frac{c}{4}}, \tag{1.4.79}$$

and finally the logarithmic negativity is

$$\mathcal{E} = \left(\frac{c}{4}\log\frac{\ell_1\ell_2}{\ell_1+\ell_2}\right). \tag{1.4.80}$$

Similarly for $n = n_o$ odd, one gets

$$\left(\rho_A^{T_2}\right)^{n_o} \propto (\ell_1\ell_2(\ell_1+\ell_2))^{-\frac{c}{12}\left(n_o-\frac{1}{n_o}\right)} \tag{1.4.81}$$

that for $n_o \to 1$ gives the normalization $\mathrm{Tr}\rho_A^{T_2}$, as expected.

For $n = 2$, Eq. (1.4.79) gives

$$\mathrm{Tr}\left(\rho_A^{T_2}\right)^2 = c_2^2 C_{\mathcal{T}_n\tilde{\mathcal{T}}_n^2\mathcal{T}_n}(\ell_1+\ell_2)^{-\frac{c}{4}} \tag{1.4.82}$$

while from Eq. (1.4.10) one gets

$$\mathrm{Tr}(\rho_{a_1\cup A_2}^2) = c_2(\ell_1+\ell_2)^{-\frac{c}{6}\left(2-\frac{1}{2}\right)} = c_2(\ell_1+\ell_2)^{-\frac{c}{4}} \tag{1.4.83}$$

The two expressions above are equal, as predicted by Eq. (1.3.30), if $C_{\mathcal{T}_n\tilde{\mathcal{T}}_n^2\mathcal{T}_n} = c_2^{-1}$.

Finite systems

The previous results can be used to study the case of a system with finite lenght L and periodic boundary conditions. As already seen in the case of the EE, this can be done via conformal mapping from the cylinder to the plane, that for this case leads to the substitution

$$\ell_i \quad \to \frac{L}{\pi} \sin\left(\frac{\pi \ell_i}{L}\right). \tag{1.4.84}$$

For the case of the single interval, the generalizations of Eq. (1.4.70) and Eq. (1.4.71) are

$$\begin{aligned} \mathrm{Tr}\left(\rho_A^{T_2}\right)^{n_e} &= c_{n_e/2}^2 \left(\frac{L}{\pi a}\sin\frac{\pi\ell}{L}\right)^{-\frac{c}{3}\left(\frac{n_e}{2}-\frac{2}{n_e}\right)} \\ \mathrm{Tr}\left(\rho_A^{T_2}\right)^{n_o} &= c_{n_o} \left(\frac{L}{\pi a}\sin\frac{\pi\ell}{L}\right)^{-\frac{c}{6}\left(n_o-\frac{1}{n_o}\right)} \end{aligned} \tag{1.4.85}$$

and the logarithmic negativity is

$$\mathcal{E} = \frac{c}{2}\log\left(\frac{L}{\pi a}\sin\frac{\pi\ell}{L}\right) + 2\log c_{1/2}. \tag{1.4.86}$$

For the case of two adjacent intervals, Eq. (1.4.78) and Eq. (1.4.81) can be generalised as

$$\begin{aligned} \mathrm{Tr}\left(\rho_A^{T_2}\right)^{n_e} &\propto \left[\frac{L^2}{\pi^2}\sin\left(\frac{\pi\ell_1}{L}\right)\sin\left(\frac{\pi\ell_2}{L}\right)\right]^{-\frac{c}{6}\left(\frac{n_e}{2}-\frac{2}{n_e}\right)} \left[\frac{L}{\pi}\sin\left(\frac{\pi(\ell_1+\ell_2)}{L}\right)\right]^{-\frac{c}{6}\left(\frac{n_e}{2}+\frac{1}{n_e}\right)}, \\ \mathrm{Tr}\left(\rho_A^{T_2}\right)^{n_o} &\propto \left[\frac{L^3}{\pi^3}\sin\left(\frac{\pi\ell_1}{L}\right)\sin\left(\frac{\pi\ell_2}{L}\right)\sin\left(\frac{\pi(\ell_1+\ell_2)}{L}\right)\right]^{-\frac{c}{12}\left(n_o-\frac{1}{n_o}\right)}. \end{aligned} \tag{1.4.87}$$

Finally, the LN is

$$\mathcal{E} = \frac{c}{4}\log\left[\frac{L}{\pi}\frac{\sin\left(\frac{\pi\ell_1}{L}\right)\sin\left(\frac{\pi\ell_2}{L}\right)}{\sin\left(\frac{\pi(\ell_1+\ell_2)}{L}\right)}\right] + \mathrm{cnst}. \tag{1.4.88}$$

1.5 Entanglement spreading in integrable systems out of equilibrium

Understanding the dynamics of entanglement in out-of-equilibrium quantum many-body systems is a prominent challenge in many problems of contemporary physics, such as the equilibration and thermalisation of isolated many-body systems [176, 177, 178, 179, 180], the emergence of thermodynamics in quantum systems [181, 182, 183, 184] or the effectiveness of classical computers to simulate quantum dynamics [185, 186, 187, 188, 189]. The last decade witnessed an intense theoretical effort aimed at better understanding the dynamics of quantum many-body systems after a *quantum quench*, the simplest and most broadly studied protocol to drive a quantum system out of equilibrium [190, 191]. In integrable systems, the entanglement dynamics after a quench is well described and understood in terms of the *quasiparticle picture* [192, 193, 127, 194]. These intense theoretical progress moved together with groundbreaking cold-atom and ion-trap experiments. Most notably, it has been possible to measure the many-body entanglement of non-equilibrium states [18, 19, 195, 84].

1.5.1 Dynamics of a system after a quench

Let us consider an isolated many-body quantum system, prepared at time $t < 0$ in a pure state $|\psi_0\rangle$ which is the ground state of some hamiltonian $H(\lambda_0)$ depending on a parameter λ_0 (that represents, for example, an external magnetic field). At time $t = 0$ the parameter λ_0 is abruptly changed to $\lambda_0 \to \lambda$, so that at later times $t > 0$ the system evolves *unitarily* under the action of the Hamiltonian $H(\lambda)$,

$$|\psi(t)\rangle = \mathrm{e}^{-\mathrm{i}H(\lambda)t}\,|\psi_0\rangle\,, \tag{1.5.1}$$

where $\hbar = 1$. This protocol is the so called quantum quench.

Thanks to many theoretical and experimental studies, it is nowadays known that for large times and in the thermodynamic limit, the expectation values of many observables relax to stationary values [180, 181, 194]. Moreover, even if the dynamics determining the evolution is unitary and the initial state is pure, the stationary values of some observables after a quench are described by statistical ensembles. So, it is then crucial to understand how the reversibility of the unitary dynamics can be reconciled with the irreversibility of statistical mechanics.

The key tool to explain the equilibration of a closed quantum system to a statistical ensemble is the RDM. Given a spatial bipartition of the system into two complementary parts, let us denote as $\rho(t) = |\psi(t)\rangle\langle\psi(t)|$ the time-dependent density matrix of the whole system, and as $\rho_A(t) = \mathrm{Tr}_B\rho(t)$ the reduced density matrix of subsystem A.

An isolated infinite system after a quench is said to relax to a stationary state, if *for all* finite subsystems A, the limit of the RDM $\rho_A(t)$ for infinite time exists, i.e.,

$$\exists \lim_{t\to\infty} \rho_A(t) \equiv \rho_A(\infty). \tag{1.5.2}$$

It is important to observe that the thermodynamic limit must be taken before the infinite time one. Moreover, since the subsystem A can be placed in an arbitrary position and it has an arbitrary (finite) dimension, a third limit of a very large subsystem A can also be taken, but only after the other two. This allow to extend the validity of Eq. (1.5.2) to the whole system.

Let us now clarify in which sense the stationary state $\rho_A(\infty)$ can be described by a statistical ensemble. Given a statistical ensemble E, let ρ_E be the corresponding density matrix for the whole system. It is important to stress that ρ_E is a mixed state, and must not be confused with the density matrix ρ of the whole system, that is instead a pure state. The reduced density matrix of A is $\rho_{A,E} = \mathrm{Tr}_B\rho_E$. Then, the stationary state is said to be described by the statistical ensemble E if, *for any* finite subsystem A,

$$\rho_A(\infty) = \rho_{A,E}, \qquad \forall A \quad \text{finite}. \tag{1.5.3}$$

An example of statistical ensemble is the canonical or Gibbs ensemble, described by the thermal density matrix

$$\rho_{Gibbs} = \frac{\mathrm{e}^{-\beta H}}{Z}, \qquad Z = \mathrm{Tr}(\mathrm{e}^{-\beta H}). \tag{1.5.4}$$

A non-equilibrium quantum system is said to *thermalise* after a quantum quench when it relaxes to the Gibbs distribution. The inverse temperature β is then fixed by the conservation of energy

$$\mathrm{Tr}[H\rho_E] = \langle\psi_0|\,H\,|\psi_0\rangle\,. \tag{1.5.5}$$

While in general all non-integrable systems are expected to relax to a thermal state, (with some exceptions represented by chaotic ones), the situation is different for integrable models,

for which the dynamics and the relaxation are constrained by the presence of conservation laws. Integrable models are characterised by an infinite number of integrals of motion in involution $[I_m, I_n] = 0$, so that the system for large times is described by a generalised Gibbs ensemble (GGE)

$$\rho_{GGE} = \frac{\mathrm{e}^{-\sum_n \lambda_n I_n}}{Z}, \qquad Z = \mathrm{Tr}\mathrm{e}^{-\sum_n \lambda_n I_n}. \tag{1.5.6}$$

However, not all the integrals of motion that commute with the Hamiltonian contribute in the GGE density matrix. Without entering in details, the only integrals of motion that appear in the GGE are those which are *local*, i.e., they can be written as integrals of a local density, and the *quasi-local* ones [196]. This is justified by the fact that one is interested in the evaluation of the expectation values of local observables. The Lagrange multipliers λ_n are also in this case fixed by the constraints given by the conservation relations

$$\mathrm{Tr}[I_n \rho_{GGE}] = \langle \psi_0 | \, I_n \, | \psi_0 \rangle \, . \tag{1.5.7}$$

Let us apply the previous notions to the study of entanglement. From Eq. (1.5.3) it follows that, when an isolated system relaxes towards a statistical ensemble E, the stationary value of the entanglement entropy is

$$S^A(\infty) = -\mathrm{Tr}[\rho_A(\infty) \log \rho_A(\infty)] = -\mathrm{Tr}[\rho_{A,E} \log \rho_{A,E}] = S^A_E. \tag{1.5.8}$$

So the stationary entanglement entropy is equal to the entropy of the statistical ensemble, which is a thermodynamic quantity.

The identification suggests that *thermodynamic entropy of the statistical ensemble is the entanglement entropy accumulated during the time evolution*. So the study of the entanglement dynamics gives also information about the emergence of thermodynamics in isolated systems.

1.5.2 CFT approach to global quantum quenches

Many insights into the quench dynamics of many-body systems can be obtained thanks to the study of $(1+1)$ dimensional CFTs [192, 190, 191, 197, 198].

Let us consider a one-dimensional quantum stystem prepared at $t = 0$ in a pure state $|\psi_0\rangle$, which is the ground state of a gapped hamiltonian H_0. At time $t > 0$, the system is let evolve unitarily under the action of a different hamiltonian H, so that the corresponding time evolved state is $\mathrm{e}^{-\mathrm{i}Ht} |\psi_0\rangle$. The interest is in the study of the time evolution of correlation functions, i.e., the expectation values of products of local operators $\Phi_i(x_i)$

$$\langle \psi_0 | \, \mathrm{e}^{\mathrm{i}Ht} \Phi_1(x_1) \Phi_2(x_2) \cdots \Phi_n(x_n) \mathrm{e}^{-\mathrm{i}Ht} \, | \psi_0 \rangle \, . \tag{1.5.9}$$

Since CFT is generally formulated in euclidean space, this expression can be rewritten in term of imaginary time evolution

$$\langle \psi_0 | \, \mathrm{e}^{-H\tau_2} \Phi_1(x_1) \Phi_2(x_2) \cdots \Phi_n(x_n) \mathrm{e}^{-H\tau_1} \, | \psi_0 \rangle \, , \tag{1.5.10}$$

that represents the correlation function in an infinite euclidean strip of width $\tau_1 + \tau_2$. The time evolution in Eq. (1.5.9) is recovered by taking the analytical continuations $\tau_1 \to \mathrm{i}t$ and $\tau_2 \to -\mathrm{i}t$, but in this way one would obtain a strip of zero total width.

For a critical system, whose time evolution is governed by a $(1+1)$-dimensional CFT, this problem can be solved by applying the theory of boundary critical phenomena. In fact, according to the renormalization group (RG) theory, when the system is close to a quantum critical

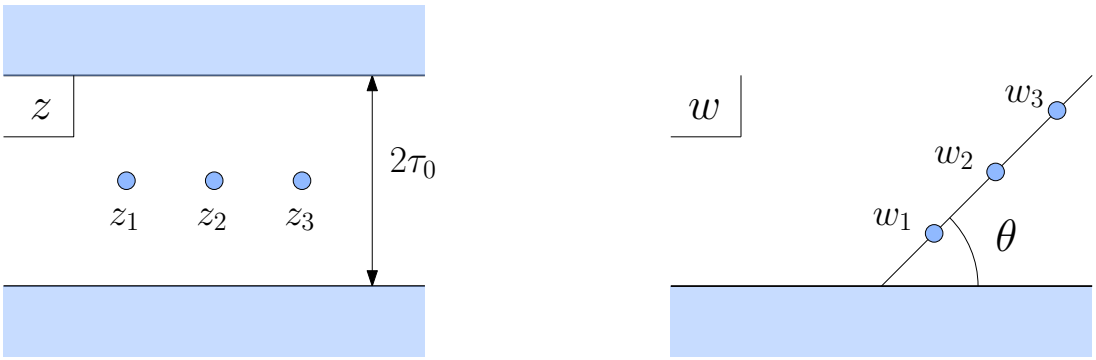


Figure 1.9: *Left*: Space-imaginary time region in Eq (1.5.11).*Right*: Conformal mapping of the strip geometry to the UHP.

points its bulk properties can be described by a bulk RG fixed point, and the boundary conditions flow to number of possible boundary fixed points. Then, the boundary conditions $|\psi_0\rangle$ at $\tau = \tau_1$ and τ_2 can be replaced with the conformal invariant boundary conditions $|\psi_0^*\rangle$ at $\tau = -\tau_0 + \tau_1$ and $\tau = \tau_0 + \tau_2$, where τ_0 is the so called extrapolation lenght. This lenght can be interpreted as a measure of how much the conformal invariant boundary state differs from the original one, and the above argument can also be rephrased by assuming that the initial state is of the form $|\psi_0\rangle \propto \mathrm{e}^{-\tau_0 H}|\psi_0^*\rangle$. Then, by translating the imaginary time by $\tau_0 + \tau_1$ for convenience, one can consider the following correlation function in the euclidean strip $\tau \in [0, 2\tau_0]$

$$\langle\psi_0^*|\,\Phi_1(x_1,\tau)\Phi_2(x_2,\tau)\cdots\Phi_n(x_n,\tau)\,|\psi_0^*\rangle\,, \tag{1.5.11}$$

as shown in the left panel of Fig. 1.9. The time τ has to be considered real during the calculations, and analytically continued to $\tau \to \tau_0 + it$ only in the end. With these prescriptions, it is now possible to perform the evaluation of the correlation functions.

1.5.3 Correlation functions following a global quench

Let us parametrize the strip geometry of Eq. (1.5.11) with the complex number $z = r + \mathrm{i}\tau$, where $0 < \mathrm{Im} z < 2\tau_0$. As already seen in Sect. 1.4.2, this geometry can be mapped to the UHP $\mathrm{Im} w > 0$ via the conformal transformation $z(w) = 2\tau_0/\pi \log z$, as shown in Fig. 1.9, and the correlation functions in the strip and in the UHP are related as in Eq. (1.4.54), that is

$$\langle\prod_i \Phi_i(z_i)\rangle_{strip} = \prod_i z'(w_i)^{-d_{\Phi_i}/2}\overline{z'(w_i)}^{-d_{\Phi_i}/2}\langle\prod_i \Phi_i(w_i)\rangle_{\mathrm{UHP}}, \tag{1.5.12}$$

where d_{Φ_i} is the scaling dimension of the field Φ_i.

The one-point function of a scalar primary field in the UHP is given in Eq. (1.4.55), so in analogy with Eq. (1.4.56) one gets

$$\langle\Phi(z)\rangle_{strip} = |z'(w)|^{-d_\Phi} = A_\Phi^b\left[\frac{\pi}{4\tau_0}\frac{1}{\sin(\pi\tau/(2\tau_0))}\right]^{d_\Phi}. \tag{1.5.13}$$

Then the analytic continuation to real time $\tau = \tau_0 + it$ gives

$$\langle\Phi(t)\rangle = A_\Phi^b\left[\frac{\pi}{4\tau_0}\frac{1}{\cosh(\pi\tau/(2\tau_0))}\right]^{d_\Phi} \simeq A_\Phi^b\left(\frac{\pi}{2\tau_0}\right)^{d_\Phi}\mathrm{e}^{-\frac{\pi t d_\Phi}{2\tau_0}}. \tag{1.5.14}$$

This result tells us that that any primary field decays to zero exponentially in time. The relaxation time is non-universal and equal to $t_\Phi^{rel} = 2\tau_0/\pi d_\Phi$. An important exception to this behavior is the local energy density that is found to be constain in time, as expected for a energy conserving dynamics.

Let us now consider the time evolution of two-point functions of primary operators, placed in the points $z_1 = 0 + i\tau$ and $z_2 = \ell + i\tau$ of the strip. Their correlation function can be obtained from that in the UHP, which is

$$\langle \Phi(w_1)\Phi(w_2)\rangle_{\rm UHP} = \left(\frac{|w_1-\bar w_2||w_2-\bar w_1|}{|w_1-w_2||\bar w_1-\bar w_2||w_1-\bar w_1||z_2-\bar w_2|}\right)^{d_\Phi} \mathcal{F}(\eta), \tag{1.5.15}$$

where η is the four-point ratio. After some algebra and taking the analytic continuation $\tau = \tau_0 + it$, one gets

$$\langle \Phi(\ell,t)\Phi(0,t)\rangle_{strip} \simeq \left(\frac{\pi}{2\tau_0}\right)^{2d_\Phi} \left(\frac{e^{\pi\ell/2\tau_0}+e^{-\pi\ell/2\tau_0}+2\cosh(\pi t/\tau_0)}{(e^{\pi\ell/4\tau_0}-e^{-\pi\ell/4\tau_0})^2}\cosh^2(\pi t/2\tau_0)\right)^{d_\Phi} \mathcal{F}(\eta). \tag{1.5.16}$$

The four point ratio η, after the conformal mapping to the strip and in the limit of ℓ/τ_0 and t/τ_0 large, is given by

$$\eta \sim \frac{e^{\pi t/\tau_0}}{e^{\pi\ell/2\tau_0}+e^{\pi t/\tau_0}}. \tag{1.5.17}$$

For $t < \ell/2$, it is possible to neglect the term $e^{\pi t/\tau_0}$ in the denominator, so that the ratio η vanishes as $\eta \sim e^{\pi(t-\ell/2)/\tau_0}$, while for $t > \ell/2$ the term $e^{\pi\ell/2\tau_0}$ can be neglected and $\eta \sim 1$. So, even if the function $\mathcal{F}(\eta)$ is generally not known, it is sufficient to know its behavior for $\eta \sim 0$, that is close to the surface, and $\eta \sim 1$, that is in the bulk. In particular, for $\eta \ll 1$ the short distance expansion gives

$$\mathcal{F}(\eta) \simeq (A_\Phi^b)^2 \eta^{d_b}, \tag{1.5.18}$$

where d_b is the scaling dimension of the leading boundary operator coupled with Φ, while in the bulk $\mathcal{F}(1) = 1$ [191, 198]. Expanding also the prefactor of $\mathcal{F}(\eta)$ in Eq. (1.5.16) for $t, \ell \gg \tau_0$, one finally gets

$$\langle \Phi(\ell,t)\Phi(0,t)\rangle \simeq \left(\frac{\pi}{2\tau_0}\right)^{2d} \times \begin{cases} e^{-d_\Phi \pi\ell/2\tau_0}, & \text{for } t > \ell/2 \\ (A_\Phi^b)^2 e^{-d_\Phi \pi t/\tau_0} e^{\pi d_\Phi^b (t-\ell/2)/\tau_0}, & \text{for } t < \ell/2 \end{cases} \tag{1.5.19}$$

The results of this section can be used to determine the time evolution of the entanglement entropy after a quench.

1.5.4 Evolution of the entanglement entropy after a global quench

Let us consider the case of a system A consisting in a single interval of lenght ℓ, and embedded in an infinite system. As already seen for the equilibrium case, the $\mathrm{Tr}\rho_A^n$ is equivalent to the two-point function of twist fields of dimension d_n given by Eq. (1.4.9). So from Eq.(1.5.16), the limit of $\ell, t \gg \tau_0$ gives

$$\mathrm{Tr}\rho_A^n(t) \simeq c_n \left[\frac{\pi^2}{4\tau_0^2}\frac{\cosh\left(\frac{\pi\ell}{2\tau_0}\right)+\cosh\left(\frac{\pi v t}{\tau_0}\right)}{2\sinh^2\left(\frac{\pi\ell}{4\tau_0}\right)\cosh^2\left(\frac{\pi v t}{2\tau_0}\right)}\right]^{d_n}. \tag{1.5.20}$$

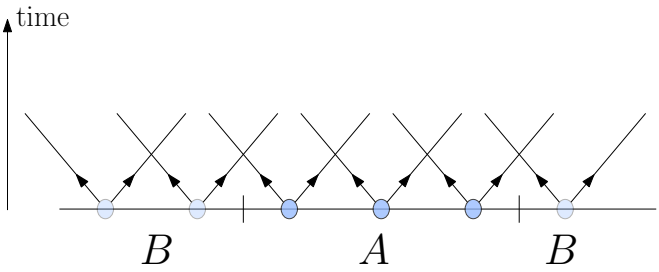


Figure 1.10: Illustration of the quasiparticle picture for the entanglement spreading in a one-dimensional integrable system. The arrows indicate the propagation of the quasiparticles with the largest velocity v_M.

The EE is then obtained from analytic continuation for real n, differentiating respect to n and in the limit for $n \to 1$,

$$S(t) \simeq \frac{c}{3} \log \tau_0 + \begin{cases} \frac{\pi c t}{6\tau_0}, & \text{for } t < \ell/2 \\ \frac{\pi c \ell}{12\tau_0}, & \text{for } t > \ell/2 \end{cases} \tag{1.5.21}$$

This result shows that the entropy $S(t)$ has an initial linear growth in time, and then saturates at $t = \ell/2$. The cusp between these two regimes is not sharp, but rounded around a region $|t - \ell/2| \sim \tau_0$.

1.5.5 Quasiparticle picture

The qualitative, but also many of the quantitative features of the entanglement dynamics presented in the previous paragraphs can be understood in terms of the quasiparticle picture for the entanglement evolution. This is a very powerful framework leading to analytic predictions for the time evolution of the EE that are valid for an arbitrary integrable model, and provides exact results in the space-time scaling limit $t, \ell \to \infty$ with t/l finite.

Quasiparticle picture for entanglement

Let us consider a many-body quantum system prepared in an initial state $|\psi_0\rangle$ with an extensive energy on top of the ground state of the Hamiltonian H which governs its time evolution. The initial state can be regarded as a source of quasiparticle excitations, which are assumed to be produced in independent pairs with opposite momenta k and $-k$. (The assumption can be weakened in free models, see e.g. [199, 200, 201], it is instead fundamental for interacting integrable systems [202].) This situation is illustrated in Fig. 1.10.

Let us first suppose that the quasiparticles are all of the same species, so that they can be characterised only by their momentum k. After being produced, each particle moves ballistically with velocity $v(k)$. The key assumption of this description is that the quasiparticles emitted from different points are incoherent, while those emitted from the same point are entangled and as they move far from each other they spread the entanglement and the correlations through the system. In particular, the entanglement of a subsystem A with its complement after a time t is proportional to the total number of entangled pairs shared by the two parts at that time. Hence, just by counting these pairs, when the subsystem A is an interval of length ℓ

embedded in an infinite system, the entanglement entropy evolves as [192]

$$S(t) = 2t \int_{2v(k)t<\ell} \mathrm{d}k\, v(k)s(k) + \ell \int_{2v(k)t>\ell} \mathrm{d}k\, s(k), \tag{1.5.22}$$

where the function $s(k)$ depends on the rate of production of the quasiparticles with momentum $\pm k$ and their contribution to the entanglement entropy. The velocity $v(k)$ has a maximum value v_M, whose existence, for spin chains, is guaranteed by the Lieb-Robinson bound [203]. Hence, the two terms of Eq. (1.5.22) give two different regimes as the entropy evolves in time. For times $t \leqslant \ell/(2v_M)$ the domain of integration of the second integral vanishes, and the entropy grows linearly in time. For larger times, the entanglement growth slows down and for $t \gg \ell/2v_M$ the second integral dominates and the entropy is finally extensive in the subsystem length.

In the presence of different species of independent quasiparticles the result can be generalised by summing over them [193],

$$S(t) = \sum_m \left[2t \int_{2v_m(k)t<\ell} \mathrm{d}k\, v_m(k)s_m(k) + \ell \int_{2v_m(k)t>\ell} \mathrm{d}k\, s_m(k) \right]. \tag{1.5.23}$$

By properly characterising the functions $v_m(k)$ and $s_m(k)$, Eq. (1.5.23) can be applied to all integrable systems [193, 127, 194]. It is important to stress that while the generalisation to the Rényi entropies is very easy for free models (in Eq. (1.5.22) it is enough to replace $s(k)$ with an appropriate $s_n(k)$, see [204] and below), it is still an open problem for interacting integrable models [204, 205, 206, 207, 208].

Quasiparticle picture for mutual information

Let us consider the case in which the subsystem A of length ℓ is formed by two disjoint intervals A_1 and A_2 of respective lengths ℓ_1 and ℓ_2 that are separated by a distance d. Without loss of generality one can consider $\ell_1 \leqslant \ell_2$. Since the total mutual information is a combination of entanglement entropies for which the quasiparticle picture holds, it is natural that it must be related to the number of entangled pairs that, once emitted from the same point, are shared by the two subsystem at subsequent times.

This counting of quasiparticles is straightforward, but we report here for completeness. Let us first assume that the quasiparticles possess a single velocity v. It follows that for short times $t \leqslant d/(2v)$ there are no entangled quasiparticles shared by the two intervals and the mutual information is zero. It then increases linearly for $d/(2v) \leqslant t \leqslant (d+\ell_1)/(2v)$. There is a plateau for $(d+\ell_1)/(2v) \leqslant t \leqslant (d+\ell_2)/(2v)$, after which it decreases linearly in time up to $t = (d+\ell)/2v$. There are no longer any quasiparticles shared between the subsystems for larger times, so that the mutual information vanishes for $t \geqslant (d+\ell)/2v$. Tthis behaviour is illustrated in Fig. 1.11. Accordingly, the resulting dynamics of the mutual information is proportional to $[\max(d, 2vt) + \max(d+\ell, 2vt) - \max(d+\ell_1, 2vt) - \max(d+\ell_2, 2vt)]$[112, 209].

In the presence of a non-trivial dispersion (and hence different velocities $v(k)$), it is enough to integrate over k to get [193, 127]

$$I_1^{A_1:A_2} = \int \mathrm{d}k\, s(k)[\max(d, 2v(k)t) + \max(d+\ell, 2v(k)t) - \max(d+\ell_1, 2v(k)t) - \max(d+\ell_2, 2v(k)t)]. \tag{1.5.24}$$

where $s(k)$ for free fermions is given by

$$s(k) = \frac{1}{2\pi}(-n_k \log n_k - (1-n_k)\log(1-n_k)). \tag{1.5.25}$$

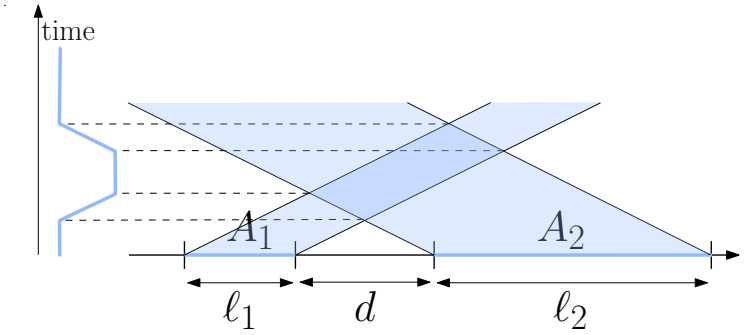


Figure 1.11: Illustration of the entanglement and mutual information dynamics of two disjoint subsystems. On the left we report the shape of the mutual information with a single velocity of quasiparticles. In the main plot, the dark blue area counts the quasiparticles shared between the two disjoint sets.

1.6 Free fermions on the lattice

The lattice model that will be used as reference for the evaluation of the entanglement entropy is the *hopping hamiltonian*, a simple lattice model that describes, for example, electrons hopping in a 1-dimensional lattice

$$H = -\sum_{j=0}^{L-1} \left(c_j^\dagger c_{j+1} + c_{j+1}^\dagger c_j \right) + 2h \sum_{j=0}^{L-1} c_j^\dagger c_j, \tag{1.6.1}$$

where h is the chemical potential and c_i are fermionic spinless degrees of freedom, satisfying the anti-commutation relations

$$\{c_i^\dagger, c_j\} = \delta_{ij}, \qquad \{c_i, c_j\} = 0. \tag{1.6.2}$$

One can observe that the number of particles is conserved, i.e., $[H, c_j^\dagger c_j] = 0$.

The model described by Eq. (1.6.1) can be also obtained from the XX model, which corresponds to a chain of L spins 1/2 in a magnetic field with nearest neighbour interaction

$$\mathcal{H}_{XX} = -\frac{1}{2} \sum_{j=0}^{L-1} (\sigma_j^x \sigma_{j+1}^x + \sigma_j^y \sigma_{j+1}^y) + h \sum_{j=1}^{L-1} \sigma_j^z, \tag{1.6.3}$$

where σ_j^α, with $\alpha = x, y, z$, are the Pauli matrices at site i and $h > 0$ is the magnetic field, and is assumed to be oriented in the positive Z-direction. The mapping between the two models is provided by the *Jordan-Wigner transformations*, which establish the following relation between the fermionic operators and the Pauli matrices

$$c_j = \left(\prod_{l=1}^{j-1} \sigma_l^z \right) \frac{\sigma_j^x - \mathrm{i}\sigma_j^y}{2}. \tag{1.6.4}$$

The hamiltonian in Eq. (1.6.1) can be diagonalized via Fourier transform of the fermionic

operators

$$\begin{aligned}\tilde{c}_k &= \frac{1}{\sqrt{L}}\sum_{j=0}^{L-1} c_j e^{-i\frac{2\pi}{L}kj},\\ \tilde{c}_k^\dagger &= \frac{1}{\sqrt{L}}\sum_{j=0} e^{i\frac{2\pi}{L}kj} c_j^\dagger,\end{aligned} \tag{1.6.5}$$

where $0 \leq k \leq L-1$. It can be easily verified that the Fourier transformed operators satisfy the canonical anti-commutation relations

$$\{\tilde{c}_k^\dagger, \tilde{c}_m\} = \delta_{km}, \qquad \{\tilde{c}_k, \tilde{c}_m\} = 0. \tag{1.6.6}$$

In terms of these operators, the hamiltonian becomes

$$\mathcal{H} = \sum_{k=0}^{L-1}\left(2h - 2\cos\frac{2\pi k}{L}\right)\tilde{c}_k^\dagger \tilde{c}_k, \tag{1.6.7}$$

so the single particle dispersion relation is then given by

$$\varepsilon_k = 2h - 2\cos\frac{2\pi k}{L}. \tag{1.6.8}$$

The occupation of the k-th mode is favoured or not according to the fact that the corresponding ε_k is negative or positive, that is, it lowers or increases the energy of the total system. Accordingly, different situations can occur. If $h > 1$, one has that $\varepsilon_k \geq 0$ for all the modes k, so the ground state of the system corresponds to the state with no excitations, and is annihilated by all the operators $\tilde{c}_k$

$$\tilde{c}_k |GS\rangle = 0, \qquad \forall k. \tag{1.6.9}$$

If $0 \leq h < 1$, instead, the ground state is populated only in the energy levels such that $\varepsilon_k < 0$, so that it can be characterized as follows

$$\begin{aligned}\tilde{c}_k |GS\rangle &= 0, \quad \text{if} \quad \varepsilon_k > 0\\ \tilde{c}_k^\dagger |GS\rangle &= 0, \quad \text{if} \quad \varepsilon_k < 0.\end{aligned} \tag{1.6.10}$$

The maximum value k_c of the number k is determined by the chemical potential, and verifies the condition

$$h - \cos\frac{2\pi k_c}{L} = 0 \quad \rightarrow \quad k_c = \left\lfloor \frac{L}{2\pi}\arccos h \right\rfloor \tag{1.6.11}$$

where the brackets $\lfloor\cdot\rfloor$ denote the floor function, in order to express k as a natural number.

The Fermi momentum can be defined as the one corresponding to the number k_c, that is

$$k_F = \frac{2\pi k_c}{L} = \arccos h. \tag{1.6.12}$$

From the Fermi momentum one can also define the filling fraction ν as $\nu = k_F/\pi$. The particular case $h = 0$, corresponding to the values $k_F = \arccos 0 = \pi/2$ and $\nu = 1/2$, is referred as $halffilling$.

One can also calculate the correlation matrix of the system in the ground state [210]. Let us suppose that the system of interest is a block of ℓ consecutive sites, then its correlation matrix is

defined as $[C]_{mn} = \langle c_m^\dagger c_n \rangle$, with $m, n = 0, \cdots, \ell - 1$. Given the simple structure of the ground state, it can be easily derived starting from the matrix elements

$$\langle \tilde{c}_k^\dagger \tilde{c}_{k'} \rangle = \begin{cases} \delta_{kk'}, & \text{if } \varepsilon_k < 0 \\ 0, & \text{if } \varepsilon_k > 0. \end{cases} \tag{1.6.13}$$

Going back in the Fourier transform one obtains

$$\begin{aligned} \langle c_m^\dagger c_n \rangle &= \left\langle \sum_{k,k'} \frac{1}{L} \mathrm{e}^{-\frac{2\pi \mathrm{i}}{L}(km - k'n)} \tilde{c}_k^\dagger \tilde{c}_{k'} \right\rangle = \sum_{k,k'} \frac{1}{L} \mathrm{e}^{-\frac{2\pi \mathrm{i}}{L}(km - k'n)} \langle \tilde{c}_k^\dagger \tilde{c}_{k'} \rangle = \\ &= \sum_{|k|<k_c} \frac{1}{L} \mathrm{e}^{-\frac{2\pi \mathrm{i} k}{L}(m-n)} = \sum_{k=0}^{k_c} \frac{1}{L} \left(\mathrm{e}^{-\frac{2\pi \mathrm{i} k(m-n)}{L}} + \mathrm{e}^{\frac{2\pi \mathrm{i} k(m-n)}{L}} \right) = \\ &= \frac{2}{L} \sum_{k}^{k_c} \cos\left[\frac{2\pi k}{L} (m-n) \right]. \end{aligned} \tag{1.6.14}$$

In the thermodynamic limit the sum can be evaluated as an integral, and it gives

$$[C]_{mn} = \langle c_m^\dagger c_n \rangle = \frac{1}{\pi} \frac{\sin\left(\frac{2\pi}{L} k_c (m-n)\right)}{(m-n)} = \frac{1}{\pi} \frac{\sin\left(k_F (m-n)\right)}{(m-n)}. \tag{1.6.15}$$

As we are going to show in the next section, for lattice systems of free particles the eigenvalues of the correlation matrix can be related to the ones of the reduced density matrix of the system, and then can be used to evaluate the EE [211, 212, 213].

1.6.1 Correlation matrix techniques

Let us consider a lattice system of free fermions, described by the hamiltonian [211]

$$H = -\sum_{ij} h_{ij} c_i^\dagger c_j, \tag{1.6.16}$$

whose eigenstates are Slater determinants. Let us focus on a subsystem A of ℓ sites, for which one can construct the restricted correlation matrix as expectation value on such eigenstates,

$$C_{ij} = \langle c_i^\dagger c_j \rangle, \qquad i, j \in A. \tag{1.6.17}$$

Since the hamiltonian is Gaussian, due to Wick's theorem any higher order correlation function can be decomposed into the sum over all the possible permutations of two-point correlations. For example, for four-point correlation functions,

$$\langle c_j^\dagger c_k^\dagger c_l c_m \rangle = \langle c_k^\dagger c_l \rangle \langle c_j^\dagger c_m \rangle - \langle c_j^\dagger c_l \rangle \langle c_k^\dagger c_m \rangle. \tag{1.6.18}$$

In terms of the reduced density matrix ρ_A, the correlation matrix in Eq. (1.6.17) can also be evaluted as

$$C_{ij} = \mathrm{Tr}\left(\rho_A c_i^\dagger c_j \right). \tag{1.6.19}$$

Since the reduced density matrix has positive eigenvalues, it can be expressed as the exponential of a hermitian operator H_A, called entanglement hamiltonian

$$\rho_A = \mathcal{K} \mathrm{e}^{-H_A}. \tag{1.6.20}$$

In particular, since the higher order correlators can be expressed in terms of ρ_A, and because of Wick's theorem, the Hamiltonian H_A turns out to be itself quadratic

$$H_A = \sum_{ij} t_{ij} c_i^\dagger c_j. \tag{1.6.21}$$

The entanglement hamiltonian can be diagonalized introducing the fermionic operators

$$a_k = \sum_i c_i \phi_k(i), \tag{1.6.22}$$

where $\phi_k(i)$ are eigenstates of H_A with eigenvalues ε_k. Then the reduced density matrix becomes

$$\rho_A = \mathcal{K} \mathrm{e}^{-\sum_k \varepsilon_k a_k^\dagger a_k}. \tag{1.6.23}$$

Pluggiung this expression into Eq. (1.6.19) one obtains

$$\begin{aligned} C_{ij} &= \sum_{k,k'} \phi_k^*(i)\phi_{k'}(j) \mathrm{Tr}\left(\mathrm{e}^{\sum_q \varepsilon_q a_q^\dagger a_q} a_k^\dagger a_{k'}\right) = \\ &= \sum_k \phi_k^*(i)\phi_k(j) \left\langle a_k^\dagger a_k \right\rangle = \sum_k \phi_k^*(i)\phi_k(j) \frac{1}{1+\mathrm{e}^{\varepsilon_k}} \end{aligned} \tag{1.6.24}$$

This expression can be compared to the one of the entanglement hamiltonian written in the basis of the a_k, that is

$$(H_A)_{ij} = \sum_k \phi_k^*(i)\phi_k(j)\varepsilon_k \tag{1.6.25}$$

By comparing the two expressions above, it is possible to express the eigenvalues ζ_k of the correlation matrix in terms of the ε_k

$$\zeta_k = \frac{1}{1+\mathrm{e}^{\varepsilon_k}}, \tag{1.6.26}$$

or, in matrix form

$$\mathbf{H_A^T} = \log(\mathbf{C}^{-1} - \mathbb{I}) \tag{1.6.27}$$

This relation can be used to express the eigenvalues of the RDM in terms of those of the correlation matrix. The RDM in the diagonal basis is the Kronecker product of single-particle matrices,

$$\rho_A = \otimes_k \frac{\mathrm{e}^{-\varepsilon_k a_k^\dagger a_k}}{1+\mathrm{e}^{-\varepsilon_k}}. \tag{1.6.28}$$

The eigenvalues of $a_k^\dagger a_k$, are 0 and 1, which correspond to an occupied and an empty mode respectively, then the eigenvalues of ρ_A are

$$\frac{\mathrm{e}^{-\varepsilon_k}}{1+\mathrm{e}^{-\varepsilon_k}} = \zeta_k, \qquad \frac{1}{1+\mathrm{e}^{-\varepsilon_k}} = 1-\zeta_k. \tag{1.6.29}$$

So, it is finally possible to obtain the EE in terms of eigenvalues of the correlation matrix

$$S = -\mathrm{Tr}\rho_A \log \rho_A = -\sum_k [\zeta_k \log \zeta_k + (1-\zeta_k)\log(1-\zeta_k)]. \tag{1.6.30}$$

Similarly, for the REs one gets

$$S_n = \frac{1}{1-n} \log \mathrm{Tr}\rho_A^n = \frac{1}{1-n} \sum_k \log[\zeta_k^n + (1-\zeta_k)^n]. \tag{1.6.31}$$

This representation of S_n is particularly convenient for numerical computations: once computed the eigenvalues of the correlation matrix C_{ij} by standard linear algebra methods, the entropy can easily be evaluated using Eq. (1.6.31). This procedure reduces the problem of computing the RDM from an exponential to a linear problem in the system size.

Part II

Results

Chapter 2

Symmetry resolved entanglement in free fermionic systems

Summary: *In this Chapter, based on Ref. [1], we consider the symmetry resolved REs in the one dimensional tight binding model, equivalent to the spin-1/2 XX chain in a magnetic field. We exploit the generalised Fisher-Hartwig conjecture to obtain the asymptotic behaviour of the EE with a flux charge insertion at leading and subleading orders. The $o(1)$ contributions are found to exhibit a rich structure of oscillatory behaviour. We then use these results to extract the symmetry resolved entanglement, determining exactly all the non-universal constants and logarithmic corrections to the scaling that are not accessible to the field theory approach. We also discuss how our results are generalised to a one-dimensional free fermi gas.*

2.1 Introduction

The study of the symmetry resolution of entanglement in systems possessing an internal symmetry has proven to be a fundamental step for a more refined understanding of the entanglement dynamics. As shown in the experiment by Lukin et al. [19], the total entanglement of such systems is given by the sum of two different and measurable contributions, the *configurational* and *number* (or *fluctuation*) entanglement, that account for the entanglement within symmetry sectors and fluctuations thereof respectively.

The theoretical framework developed to address the problem of extracting the *symmetry resolved* contributions for different entanglement measures [35, 38, 34, 39], was based on the definition of the charged moments $Z_n(\alpha)$, evaluated via replica trick as partition functions over a multisheeted Riemann surface pierced by an appropriate Aharonov-Bohm flux [35]. It was also pointed out the *equipartition of entanglement* in the different charge sector, at leading order in the subsystem lenght [35, 38, 34].

If on one hand the field theory approach is very powerful and versatile in order to provide the scaling limit of both the charged and symmetry resolved EEs, on the other, it does not give access to non-universal model-dependent pieces which are also very important to accurately characterise critical systems. As we are going to see, for the special case of free fermions, we

can go beyond the field theory results. Indeed, we can rely on the *(generalised) Fisher-Hartwig conjecture* [214, 215, 216, 217] to compute systematic expansions of these entropies which reproduce the field theory results and provide exact expressions for the non-universal terms. In fact, this method, which has already been explored for the standard EE and RE [216, 217], can be simply generalised to the same quantities with a further flux insertion and therefore to their symmetry resolved analogue.

The chapter is organised as follows. In Section 2.2 we give a more formal and complete treatment of the topics presented in the Introduction. In particular we define carefully all the quantities we will be dealing with and present the analytic results of the field theory approach. Sections 4.2.3 and 2.4 are the core of this chapter, where we derive results for free fermions on a lattice for the charged and the symmetry resolved EEs, respectively. In Section 2.5 we show how all results derived for the lattice model can be directly adapted to a free Fermi gas. We conclude in Section 2.6 with some remarks and discussions. Some details of the calculations can be found in the appendix.

2.2 Symmetry resolution and flux insertion

Let us consider a many body quantum system with an internal $U(1)$ symmetry. Let ρ be the density matrix in a given (pure) state and Q the operator generating such symmetry. If the system is in a given representation of the charge Q, i.e., in an eigenstate of Q corresponding to a definite eigenvalue, then $[\rho, Q] = 0$.

We will be interested in a bipartition of the total system into two complementary spatial subsystems A and B, with $\rho_A = \mathrm{Tr}_B \rho$ being the RDM of the subsystem A. Usually the operator Q splits in the sum $Q = Q_A + Q_B$, meaning that Q comes from local degrees of freedom within the two subsystems. Consequently, by taking the trace over B of $[\rho, Q] = 0$, we find that $[\rho_A, Q_A] = 0$. This implies that ρ_A acquires a block diagonal form, in which each block corresponds to a different charge sector with a definite eigenvalue q of Q_A, i.e.,

$$\rho_A = \oplus_q \Pi_q \rho_A = \oplus_q \left[p(q) \rho_A(q) \right], \tag{2.2.1}$$

where Π_q is the projector on eigenspace of fixed value of q in the spectrum of Q_A. In the last equality we factorised $p(q) = \mathrm{Tr}(\Pi_q \rho_A)$, the probability of finding q as the outcome of a measurement of Q_A. Note that in this way the density matrices $\rho_A(q)$ of different blocks are normalised as $\mathrm{Tr}\rho_A(q) = 1$.

Our goal is to understand how the entanglement is distributed in the different charge sectors. Focusing on the EE as a prototypical example, Eq. (2.2.1) implies the decomposition

$$S = \sum_q p(q) S(q) - \sum_q p(q) \log p(q) \equiv S^c + S^n, \tag{2.2.2}$$

where $S(q)$ is the *symmetry resolved EE*, defined as the entropy associated to $\rho_A(q)$ in (2.2.1)

$$S(q) \equiv -\mathrm{Tr}\left[\rho_A(q) \log \rho_A(q) \right]. \tag{2.2.3}$$

The two different contributions in (2.2.2) are the *configurational* and the *number* EEs defined in the Introduction. The configurational EE $S^c \equiv \sum_q p(q) S(q)$ [218, 19], measures the total entropy due to each charge sector (weighted with their probability) and the number EE $S^n = -\sum_q p(q) \log p(q)$ [19], instead, takes into account the entropy due to the fluctuations of the value of the charge within the subsystem A.

Similarly, one defines also *symmetry resolved REs* as

$$S_n(q) \equiv \frac{1}{1-n} \log \mathrm{Tr}\left[\rho_A(q)\right]^n . \tag{2.2.4}$$

In general evaluating such symmetry resolved quantities is a highly non-trivial problem, mainly due to the non local nature of the projector Π_q. As mentioned in the Introduction, this problem has been understood from a different perspective in [35, 34]. This approach works as follows. Let us first define the (unnormalised) quantity

$$\mathcal{Z}_n(q) \equiv \mathrm{Tr}\left(\Pi_q \rho_A^n\right), \tag{2.2.5}$$

which is related to the entanglement and REs in (2.2.3) and (2.2.4) (respectively) through

$$S_n(q) = \frac{1}{1-n} \log\left[\frac{\mathcal{Z}_n(q)}{\mathcal{Z}_1(q)^n}\right] \qquad S(q) = -\partial_n \left[\frac{\mathcal{Z}_n(q)}{\mathcal{Z}_1(q)^n}\right]_{n=1} . \tag{2.2.6}$$

Also the probability $p(q)$ is read off $\mathcal{Z}_n$ as

$$p(q) = \mathcal{Z}_1(q). \tag{2.2.7}$$

The key observation of Refs. [35, 34] is that (2.2.5) is given by the following Fourier transform

$$\mathcal{Z}_n(q) = \int_{-\pi}^{\pi} \frac{\mathrm{d}\alpha}{2\pi} \mathrm{e}^{-\mathrm{i}q\alpha} \quad Z_n(\alpha), \tag{2.2.8}$$

where

$$Z_n(\alpha) \equiv \mathrm{Tr}\left(\rho_A^n \mathrm{e}^{\mathrm{i}Q_A\alpha}\right), \tag{2.2.9}$$

are the charged moments defined in the Introduction. Note that $Z_n(0) = \mathrm{Tr}\rho_A^n$. Therefore, we can access the symmetry resolved EE by studying $Z_n(\alpha)$ (which, as explained below, are much easier to compute) and after Fourier transforming.

2.2.1 Replica method and results from QFT

In Ref. [35] a geometric approach in the framework of the replica trick has been introduced and it is applicable to generic (1+1)-dimensional QFT. The main idea is to insert an appropriate conjugate Aharonov-Bohm flux through a multi-sheeted Riemann surface $\mathcal{R}_n$, such that the total phase accumulated by the field upon going through the entire surface is α. The result is that $Z_n(\alpha)$ is the partition function on such modified surface.

In QFT language, the insertion of the flux corresponds to a twisted boundary condition, which, as usually done in this context, can be implemented by the action of a local operator, acting at the boundary of the subsystem A. This operator is a modified *twist field* $\mathcal{T}_{n,\alpha}$ whose action, in operator formalism, is defined by [35]

$$\mathcal{T}_{n,\alpha}(x,\tau)\phi_i(x',\tau) = \begin{cases} \phi_{i+1}(x',\tau)\mathrm{e}^{\mathrm{i}\alpha\delta_{i,j}}\mathcal{T}_{n,\alpha}(x,\tau) & (x<x'), \\ \phi_i(x',\tau)\mathcal{T}_{n,\alpha}(x,\tau) & \text{otherwise.} \end{cases} \tag{2.2.10}$$

In this way one can further reformulate the problem in terms of a correlation function of twist fields [139]. In the simplest case of the subsystem consisting of a single interval $A = [0,\ell]$

$$Z_n(\alpha) = \langle \mathcal{T}_{n,\alpha}(\ell,0)\tilde{\mathcal{T}}_{n,\alpha}(0,0)\rangle. \tag{2.2.11}$$

where $\tilde{\mathcal{T}}$ is the antitwist field. If we now specialise to (1+1) dimensional CFT, $\mathcal{T}_{n,\alpha}$ and $\tilde{\mathcal{T}}_{n,\alpha}$ behave as primary operators with conformal dimension given by [35]

$$\Delta_{n,\alpha} = \Delta_n + \frac{\Delta_\alpha}{n}, \qquad \Delta_n = \frac{c}{24}\left(n - \frac{1}{n}\right), \tag{2.2.12}$$

meaning that the phase shift is implemented by a composite twist field that can be written as $\mathcal{T}_{n,\alpha} = \mathcal{T}_n \cdot \mathcal{V}_\alpha$. This immediately implies

$$Z_n(\alpha) = c_{n,\alpha}\ell^{-\frac{c}{6}\left(n-\frac{1}{n}\right)-2\frac{\Delta_\alpha+\bar{\Delta}_\alpha}{n}}, \tag{2.2.13}$$

where c is the central charge of the CFT and $c_{n,\alpha}$ the unknown non-universal normalisation of the composite twist-field.

The focus of Ref. [35] was a free boson compactified on a circle of radius R, i.e., a Luttinger liquid with Luttinger parameter K. In this case the operator $\mathcal{V}_\alpha$ implementing the twisted boundary conditions is a vertex operator with (holomorphic and antiholomorphic) scaling dimensions

$$\Delta_\alpha = \bar{\Delta}_\alpha = \frac{1}{2}\left(\frac{\alpha}{2\pi}\right)^2 K. \tag{2.2.14}$$

From Eq. (2.2.13), the symmetry resolved moments are found by taking the Fourier transform as in Eq. (2.2.8). At leading order for large ℓ, this reads [35]

$$\mathcal{Z}_n(q) \simeq \ell^{-\frac{c}{6}\left(n-\frac{1}{n}\right)}\sqrt{\frac{n\pi}{2K\log\ell}}\,\mathrm{e}^{\frac{n\pi^2(q-\langle Q_A\rangle)^2}{2K\log\ell}}. \tag{2.2.15}$$

Notice that we set a posteriori the average number of the charge in the subsystem $\langle Q_A\rangle$, since it is a non-universal quantity, not encoded in the CFT. For a given microscopic model, its origin can be easily traced back, e.g. as a phase shift in the bosonisation rule.

Through Eq. (2.2.6), this leads to the following result at leading order for the RE and the von Neumann EE

$$S_n(q) = S_n - \frac{1}{2}\log\left(\frac{2K}{\pi}\log\ell\right) + O(\ell^0), \qquad S(q) = S - \frac{1}{2}\log\left(\frac{2K}{\pi}\log\ell\right) + O(\ell^0). \tag{2.2.16}$$

This result has been dubbed *equipartition of entanglement* [34]: at leading order the entanglement is the same in the different charge sectors, just the probability $p(q)$ of being in a given sector varies.

2.3 Free fermions on a lattice: flux insertion and charged entropies

Eq. (2.2.16) provides the leading symmetry resolved EEs of all microscopic models with a $U(1)$ symmetry, that, at low energy, are described by a CFT. Indeed the results in Eq. (2.2.16) have been tested numerically both for free fermions [219, 35, 34] and in interacting spin chains [220, 34, 33]. In this Section, we are going to provide an analytic derivation for the special case of a chain of free fermions, whose scaling limit is indeed described by a free compact boson with $K = 1$. Our analysis will also provide the exact value of the non-universal constants, as well as the corrections to (2.2.16) for this specific model.

We consider the tight binding model in one dimension with hamiltonian

$$H = -\sum_i \left[c_i^\dagger c_{i+1} + c_{i+1}^\dagger c_i - 2h\left(c_i^\dagger c_i - \frac{1}{2}\right)\right], \tag{2.3.1}$$

where c_i are free fermionic spinless degrees of freedom, satisfying the anticommutation relations $\{c_i, c_j^\dagger\} = \delta_{ij}$ and h is the chemical potential. H is diagonal in momentum space and its ground state is a Fermi sea with Fermi momentum $k_F = \arccos|h|$. As it is clear from (2.3.1), the particle number $Q = \sum_i c_i^\dagger c_i$ is a conserved $U(1)$ charge of the model. It is also local and $Q = Q_A + Q_B$ for any spatial bipartition of the chain.

The Jordan-Wigner transformation maps the Hamiltonian (2.3.1) to the XX spin chain, as discussed in Sect. 1.6. In this case, the charge Q becomes the spin in the z direction. Depending on the boundary conditions, the sum over i in the Hamiltonians can run over a finite, semi-infinite, or infinite number of sites.

In the following we will be interested in the bipartition where the subsystem A is given by ℓ contiguous lattice sites. The corresponding RDM of the subsystem can then be written as [221, 211, 212, 213]

$$\rho_A = \det C_A \exp\Big(\sum_{i,j}\Big[\log(C_A^{-1}-1)\Big]_{ij} c_i^\dagger c_j\Big), \tag{2.3.2}$$

where the $\ell \times \ell$ matrix $(C_A)_{ij} \equiv \langle c_i^\dagger c_j\rangle$ is the correlation matrix restricted to the subsystem A, that for the ground-state of an infinite chain has elements

$$[C_A]_{i,j} = \frac{\sin k_F(i-j)}{\pi(i-j)}, \qquad i,j \in A. \tag{2.3.3}$$

Note that C_A is a Toeplitz matrix, meaning that its entries only depend on the difference $(i-j)$: this is a key point for what follows.

If one write the eigenvalues of the matrix C_A as $(1+\nu_k)/2$ (with $k \in [1,\ell]$), then simple algebra leads to the moments of ρ_A as

$$\mathrm{Tr}\rho_A^n = \prod_{i=1}^{\ell}\left[\left(\frac{1+\nu_i}{2}\right)^n + \left(\frac{1-\nu_i}{2}\right)^n\right], \tag{2.3.4}$$

and, equivalently, the REs read

$$S_n = \sum_{i=1}^{\ell} e_n(\nu_i), \qquad e_n(x) \equiv \frac{1}{1-n}\log\left[\left(\frac{1+x}{2}\right)^n + \left(\frac{1-x}{2}\right)^n\right]. \tag{2.3.5}$$

It has been first noticed in Ref. [35] that the α-dependent moments $Z_n(\alpha)$, defined in (2.2.8), can be also easily written in terms of the eigenvalues of the correlation matrix with a simple modification of the above formulas, i.e.,

$$Z_n(\alpha) = \prod_{i=1}^{\ell}\left[\left(\frac{1+\nu_i}{2}\right)^n \mathrm{e}^{\mathrm{i}\alpha} + \left(\frac{1-\nu_i}{2}\right)^n\right]. \tag{2.3.6}$$

The interpretation of this equation is straightforward: each particle carries a weight $\mathrm{e}^{\mathrm{i}\alpha}$ while the holes carry weight 1. Eq. (2.3.6) provides a very simple method for the numerical computation of $Z_n(\alpha)$. Not only: as we are going to discuss next, it is also the right starting point to get the asymptotic analytic expressions of $Z_n(\alpha)$.

Before embarking into the study of $Z_n(\alpha)$ a quick recap of its properties and limits is necessary, also to provide useful consistency checks for our calculations. First, for $n = 1$

$$Z_1(\alpha) \equiv \mathrm{Tr}\rho_A \mathrm{e}^{\mathrm{i}Q_A\alpha} = \prod_{i=1}^{\ell}\left[\left(\frac{1+\nu_i}{2}\right)\mathrm{e}^{\mathrm{i}\alpha} + \left(\frac{1-\nu_i}{2}\right)\right], \tag{2.3.7}$$

is the moment-generating function of Q_A. This quantity has been already studied in the literature [222, 223, 224, 225, 226] also because of its relation with the EE itself. We will see that it is simply related to another quantity usually introduced in this context ($D_\ell(\lambda)$ of the next subsection). The first moment is just the average number of particle in A, i.e., $\langle Q_A \rangle = \ell k_F/\pi$. Hence $Z_1(\alpha) = 1 + \mathrm{i}\alpha\langle Q_A\rangle + O(\alpha^2)$. At half-filling $Z_1(\alpha)$ further simplifies as a consequence of the fact that, by particle-hole symmetry, for each ν_i there is a ν_j such that $(1-\nu_i) = (1+\nu_j)$. Thus we have

$$Z_1(\alpha) = \mathrm{e}^{\mathrm{i}\alpha\ell/2} \prod_i \left[\left(\frac{1+\nu_i}{2}\right) \mathrm{e}^{\mathrm{i}\alpha/2} + \left(\frac{1-\nu_i}{2}\right) \mathrm{e}^{-\mathrm{i}\alpha/2} \right] = \mathrm{e}^{\mathrm{i}\alpha\ell/2} g(\alpha)\,, \tag{2.3.8}$$

with $g(\alpha)$ real and even. For general filling instead the odd cumulants are non-vanishing (the odd derivatives of $\log Z_1(\alpha)$ are non zero) and $Z_1(\alpha)$ has no particular parity or reality properties. Indeed, Eq. (2.3.8) remains true for generic n

$$Z_n(\alpha) = \mathrm{e}^{\mathrm{i}\alpha\ell/2} \prod_i \left[\left(\frac{1+\nu_i}{2}\right)^n \mathrm{e}^{\mathrm{i}\alpha/2} + \left(\frac{1-\nu_i}{2}\right)^n \mathrm{e}^{-\mathrm{i}\alpha/2} \right] = \mathrm{e}^{\mathrm{i}\alpha\ell/2} g_n(\alpha)\,, \tag{2.3.9}$$

with $g_n(\alpha)$ real and even. This symmetry of $Z_n(\alpha)$ at half-filling represents a cross check of our numerical and analytic calculations. Again, away from half-filling, $\log Z_n(\alpha)$ has all non-zero derivatives.

We notice that by Fourier transforming (2.3.6) one easily gets

$$\mathcal{Z}_n(q) = \sum_{\mathcal{S}_q} \prod_{i\in\mathcal{S}_q} \left(\frac{1+\nu_i}{2}\right)^n \prod_{j\in\bar{\mathcal{S}}_q} \left(\frac{1-\nu_j}{2}\right)^n, \tag{2.3.10}$$

where the sum is over all subset $\mathcal{S}_q$ of $\mathcal{S} = 1, \cdots, \ell$ of cardinality q and $\bar{\mathcal{S}}_q$ denotes the complementary subset. Unfortunately Eq. (2.3.10) is not a very convenient way to get $\mathcal{Z}_n(q)$, since one has to sum over $\ell!/((\ell-q)!q!)$ terms and this is impossible already for moderate values of ℓ. The most convenient way to extract $\mathcal{Z}_n(q)$ is by direct Fourier transform of $Z_n(\alpha)$.

2.3.1 Charged entropies via the generalised Fisher-Hartwig conjecture

The method that we employ takes advantage of the Toeplitz nature of the correlation matrix that can be handled with the *(generalised) Fisher-Hartwig conjecture* providing the asymptotics of determinant of Toeplitz matrices. This technique has been used already in the context of entanglement in free lattice models to derive the leading term and the corrections to EEs [216, 217, 227, 228, 229, 230, 231, 232, 233]. We are going to show that the same technology applies also to the α-dependent moments $Z_n(\alpha)$ and therefore, as a consequence of the discussion above, to their symmetry resolved equivalent $\mathcal{Z}_n(q)$.

The starting point of our analysis is to rewrite the logarithm of Eq. (2.3.6)

$$\log Z_n(\alpha) = \sum_{i=1}^{\ell} f_n(\nu_i, \alpha), \quad f_n(x,\alpha) = \log\left[\left(\frac{1+x}{2}\right)^n \mathrm{e}^{\mathrm{i}\alpha} + \left(\frac{1-x}{2}\right)^n \right], \tag{2.3.11}$$

as a contour integral

$$\log Z_n(\alpha) = \frac{1}{2\pi i} \oint \mathrm{d}\lambda\, f_n(\lambda,\alpha) \frac{\mathrm{d}\log D_\ell(\lambda)}{d\lambda}, \tag{2.3.12}$$

where the contour of integration encircles the segment $[-1,1]$. Here we defined the characteristic polynomial of C_A as the determinant

$$D_\ell = \det\left[(\lambda+1)\mathbb{I}_A - 2C_A\right], \tag{2.3.13}$$

where $\mathbb{I}_A$ is the identity matrix restricted to A. In the basis that diagonalises C_A, such determinant simply becomes $D_\ell = \prod_i(\lambda-\nu_i)$ and therefore, by residue theorem, Eq. (2.3.12) is the same as (2.3.11). Notice that $D_\ell(\lambda)$ is related to the generating function $Z_1(\alpha)$ as

$$Z_1(\alpha) = \left(\frac{1-\mathrm{e}^{\mathrm{i}\alpha}}{2}\right)^\ell D_\ell\left(i\cot\frac{\alpha}{2}\right). \tag{2.3.14}$$

In Refs. [216, 217] it has been exploited the fact that the matrix $(\lambda+1)\mathbb{I}_A - 2C_A$ has a Toeplitz form. Therefore the asymptotics for large ℓ of the determinant D_ℓ in (2.3.13) is obtained by means of the generalised Fisher-Hartwig conjecture.

The Fisher-Hartwig formula is written in terms of the *symbol* of the Toeplitz matrix, defined as the Fourier transform of g_l

$$g_l = \int_{-\pi}^{\pi}\frac{d\theta}{2\pi}e^{il\theta}g(\theta), \tag{2.3.15}$$

that in the case considered here is given by

$$g(\theta) = \begin{cases} \lambda+1, & \theta\in[-\pi,-k_F]\cup[k_F,\pi], \\ \lambda-1, & \theta\in[-k_F,k_F]. \end{cases} \tag{2.3.16}$$

In the integration domain (2.3.15) the symbol has two discontinuities, located at $\theta_1 = -k_F$ and $\theta_2 = k_F$. The Fisher-Hartwig formula relies on the possibility to express the symbol in the following form

$$g(\theta) = f(\theta)\prod_{r=1}^{R}e^{ib_r[\theta-\theta_r-\pi\,\mathrm{sgn}(\theta-\theta_r)]}(2-2\cos(\theta-\theta_r))^{a_r}, \tag{2.3.17}$$

where R is an integer, a_r, b_r, θ_r are constants and $f(\theta)$ is a smooth function with winding number zero. For the symbol $g(\theta)$ in Eq. (2.3.16), there are two discontinuities so that $R=2$, and the constants assume the values $a_{1,2}=0$, $b_2=-b_1=\beta_\lambda+m$ and $f(\theta)=f_0=(\lambda+1)e^{-2ik_Fm}e^{-2ik_F\beta_\lambda}$, where

$$\beta_\lambda = \frac{1}{2\pi i}\log\left[\frac{\lambda+1}{\lambda-1}\right], \qquad \text{with} \quad \frac{d\beta_\lambda}{d\lambda} = \frac{1}{\pi i}\frac{1}{1-\lambda^2}, \tag{2.3.18}$$

and the integer $m\in\mathbb{Z}$ labels the different inequivalent representations of the symbol. Usually one refers simply to the Fisher-Hartwig formula when there is a single representation of the symbol and to the generalised one when there are multiple representations, as it is the case for us. For a Toeplitz matrix T with a symbol of the form (2.3.16) without inequivalent representation, the Fisher-Hartwig formula provides the large ℓ behaviour

$$\det T \simeq F[f(\theta)]^\ell\left(\prod_{j=1}^{R}\ell^{a_j^2-b_j^2}\right), \qquad \text{where} \quad F[f(\theta)] = \exp\left(\frac{1}{2\pi}\int_0^{2\pi}d\theta\log f(\theta)\right). \tag{2.3.19}$$

When the symbol has several inequivalent representations, as for our case, one has to sum over all of them [214, 217], obtaining, in our specific case, the asymptotic for large ℓ

$$D_\ell(\lambda) \simeq (\lambda+1)^\ell \left(\frac{\lambda+1}{\lambda-1}\right)^{-\frac{k_F\ell}{\pi}} \sum_{m\in\mathbb{Z}} L_k^{-2(m+\beta_\lambda)^2} \mathrm{e}^{-2\mathrm{i}k_F m\ell} \left[G(m+1+\beta_\lambda)G(1-m-\beta_\lambda)\right]^2 . \tag{2.3.20}$$

For the moments $\mathrm{Tr}\rho_A^n$, i.e., $Z_n(\alpha=0)$ in (2.3.11), the leading term in the sum for D_ℓ in Eq. (2.3.20) is the one with $m=0$, first evaluated in [216]. The next to leading contributions come from the terms with $m=\pm 1$ (at the same order) as shown in [217]. The situation for $\alpha \neq 0$ is slightly more complicated. For $-\pi < \alpha < \pi$ the leading term is always the one with $m=0$. Since $Z_n(\alpha)$ is periodic in α with period 2π we will restrict ourselves to $\alpha \in [-\pi,\pi]$, having in mind that, if required, the function can be extended outside of this interval by periodicity. Concerning the subleading contributions, the terms with $m=\pm 1$ have different power laws, but one of them is always dominating, as we shall see. Anyhow, for values of α close to $\pm\pi$, also next-to-next leading terms should be taken into account in order to get reasonable results for moderately large values of ℓ. In the following we first compute the leading term and then we move to the calculations of the corrections.

Leading term $(m=0)$

For $\alpha \in [-\pi,\pi]$, the leading behaviour of Eq. (2.3.12) is given by term with $m=0$ in (2.3.20), i.e.,

$$D_\ell^{(0)}(\lambda) \equiv (\lambda+1)^\ell \left(\frac{\lambda+1}{\lambda-1}\right)^{-\frac{k_F\ell}{\pi}} L_k^{-2\beta_\lambda^2} \left[G(1+\beta_\lambda)G(1-\beta_\lambda)\right]^2 , \tag{2.3.21}$$

so that the integral (2.3.12) is $\log Z_n(\alpha) = \log Z_n^{(0)}(\alpha) + o(\ell^0)$ with

$$\log Z_n^{(0)}(\alpha) = \frac{1}{2\pi\mathrm{i}} \oint \mathrm{d}\lambda\, f_n(\lambda,\alpha) \frac{\mathrm{d}\log D_\ell^{(0)}(\lambda)}{\mathrm{d}\lambda} = a_0\ell + a_1 \log L_k + a_2, \tag{2.3.22}$$

where

$$a_0 = \frac{1}{2\pi\mathrm{i}} \oint \mathrm{d}\lambda f_n(\lambda,\alpha) \left(\frac{1-k_F/\pi}{1+\lambda} - \frac{k_F/\pi}{1-\lambda}\right), \tag{2.3.23}$$

$$a_1 = \frac{1}{2\pi\mathrm{i}} \oint \mathrm{d}\lambda f_n(\lambda,\alpha) \frac{\mathrm{d}(-2\beta_\lambda^2)}{\mathrm{d}\lambda} = \frac{2}{\pi^2} \oint \mathrm{d}\lambda f_n(\lambda,\alpha) \frac{\beta_\lambda}{1-\lambda^2}, \tag{2.3.24}$$

$$a_2 = \frac{1}{\pi\mathrm{i}} \oint \mathrm{d}\lambda f_n(\lambda,\alpha) \frac{\mathrm{d}\log[G(1+\beta_\lambda)G(1-\beta_\lambda)]}{\mathrm{d}\lambda}, \tag{2.3.25}$$

are respectively the linear, the logarithmic and the constant term (in ℓ) coming from $\log D_\ell^{(0)}$ in Eq. (2.3.21). These three integrals are explicitly calculated in Appendix 2.A with final result

$$\log Z_n^{(0)}(\alpha) = \mathrm{i}\alpha\frac{k_F\ell}{\pi} - \left[\frac{1}{6}\left(n-\frac{1}{n}\right) + \frac{2}{n}\left(\frac{\alpha}{2\pi}\right)^2\right] \log L_k + \Upsilon(n,\alpha), \tag{2.3.26}$$

where

$$\Upsilon(n,\alpha) = n\mathrm{i}\int_{-\infty}^{\infty} \mathrm{d}w [\tanh(\pi w) - \tanh(\pi n w + \mathrm{i}\alpha/2)] \log\frac{\Gamma(\frac{1}{2}+\mathrm{i}w)}{\Gamma(\frac{1}{2}-\mathrm{i}w)}, \tag{2.3.27}$$

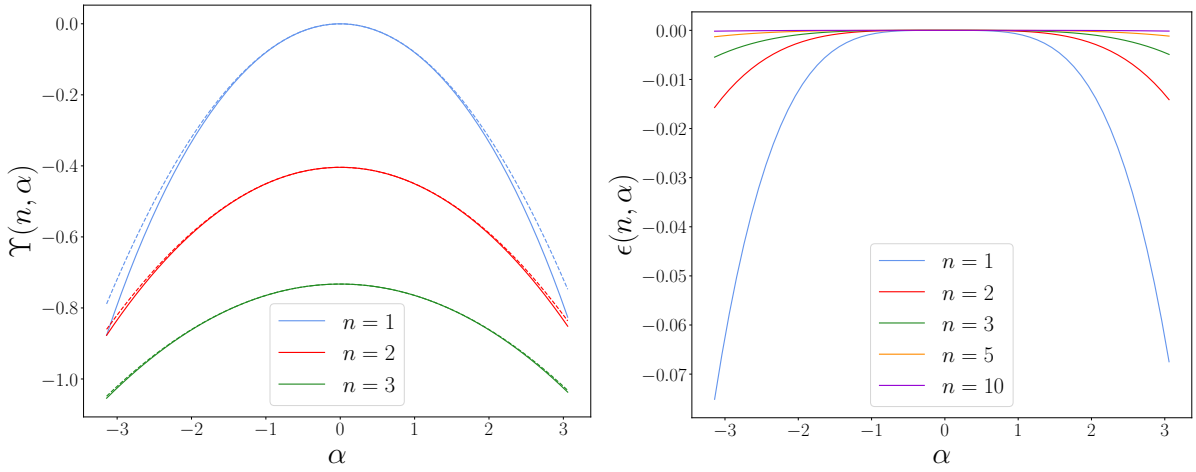


Figure 2.1: $\Upsilon(n,\alpha)$ in Eq. (2.3.27) as a function of α for $n=1,2,3$ (top to bottom in the left panel). The exact forms (full lines) are compared with the quadratic approximation $\Upsilon(n)+\gamma_2(n)\alpha^2$ (dashed lines) showing that, although very close, they are definitively different. To highlight this similarity we plot in the right panel the difference $\epsilon(n,\alpha)$, cf. Eq (2.3.28) which is tiny, but non zero.

in analogy with the definition $\Upsilon(n)$ in [216], which is recovered when $\alpha=0$. We stress that $\Upsilon(n,\alpha)$ is real for α real, even if not apparent from the formula. For future reference it is useful to write $\Upsilon(n,\alpha)$ as

$$\Upsilon(n,\alpha)=\Upsilon(n)+\gamma_2(n)\alpha^2+\epsilon(n,\alpha),\qquad \epsilon(n,\alpha)=O(\alpha^4), \tag{2.3.28}$$

where the analytic expression of $\gamma_2(n)$ is

$$\gamma_2(n)=\frac{n\mathrm{i}}{4}\int_{-\infty}^{\infty}\mathrm{d}w[\tanh^3(\pi n w)-\tanh(\pi n w)]\log\frac{\Gamma(\frac{1}{2}+\mathrm{i}w)}{\Gamma(\frac{1}{2}-\mathrm{i}w)}\,. \tag{2.3.29}$$

Eq. (2.3.26) contains several pieces of information. The linear term is just the mean number of particles in A, $\langle Q_A\rangle=k_F\ell/\pi$, as expected. Anyhow, this is the only term with an imaginary part up to order $O(1)$. We know that this is *exactly* true at half-filling ($k_F=\pi/2$), cf. Eq. (2.3.9). For generic filling, it is not true in general and we will observe in numerics tiny deviations at small ℓ in the imaginary part of $\log Z_n(\alpha)$. The term $\propto\log L_k$ provides the dimension of the modified twist field which comes out from the field theory calculation: the result agrees with the one found by CFT methods in (2.2.13) when specialised to a compact boson with $K=1$. Indeed, this result, that was already checked numerically in [35], has been also analytically calculated by means of Widom conjecture in [219]. The constant term in Eq. (2.3.26) is probably the most interesting one, first because it is a result that was not known by other means (being non-universal cannot be fixed by field theory), and second because it provides few physical consequences. It is real and even in α, a property that was guaranteed only at half filling. It is independent from k_F, as its limit for $\alpha=0$ [216]. Finally, it is very close to a parabola, but all the even terms in the series expansion are non zero, although $\epsilon(n,\alpha)$, cf. Eq. (2.3.28), is very small. In Figure 2.1 we report $\Upsilon(n,\alpha)$ as function of α for some n and compare it with the quadratic approximation $\Upsilon(n)+\gamma_2(n)\alpha^2$. The closeness of the two curves shows that the quadratic approximation will be enough for most of the applications, as we shall explicitly

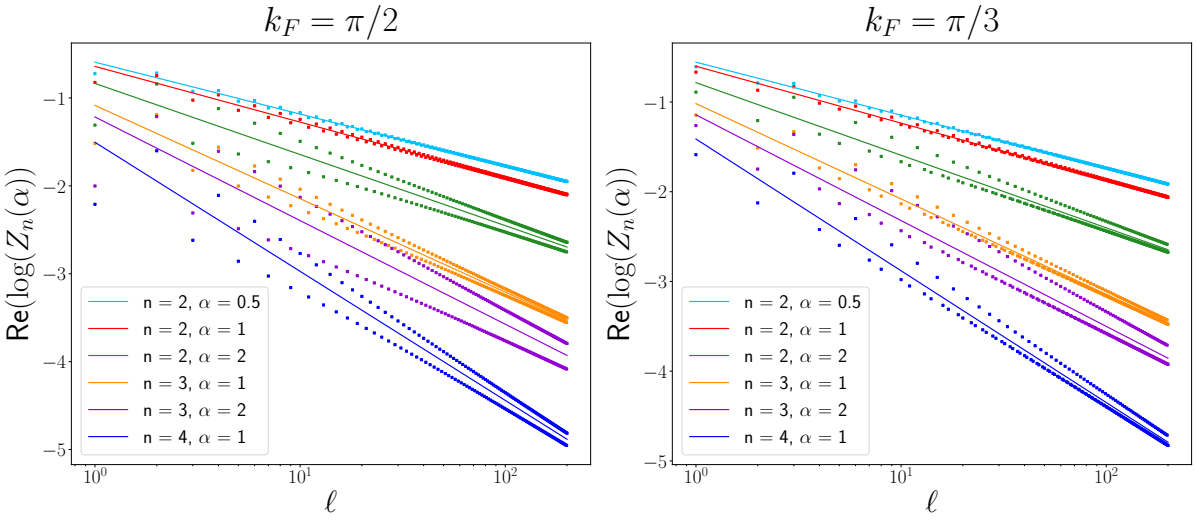


Figure 2.2: Leading scaling behaviour of the charged REs with the insertion of a flux α. The numerical results (symbols) for several values of α and n are reported as function of ℓ for the filling $k_F = \pi/2$ (left) and $k_F = \pi/3$ (right). The numerical data match well the Fisher-Hartwig prediction (cf. Eq. (2.3.26)) although large oscillating corrections to the scaling are present.

show. The accuracy of the quadratic approximation is also evident from the plot of $\epsilon(n,\alpha)$ in the right panel of Figure 2.1. On passing, this precision of the quadratic approximation of $\Upsilon(n,\alpha)$ explains, a posteriori, the quality of the symmetry resolved spectrum obtained in Ref. [35] exploiting the method of Stieltjes transform [82] which implicitly assumes this approximation.

In Figure 2.2 we report the numerical data for REs with the insertion of a flux α for several values of n and α and with fillings $k_F = \pi/2$ (left) and $k_F = \pi/3$ (right). The theoretical prediction for the leading scaling in Eq. (2.3.26) is also reported for comparison. It is evident that the analytical result correctly describes the asymptotic data, but large and oscillating corrections to the scaling are present. The amplitude of these oscillations increase with n and with α. This peculiar n dependence was already known at $\alpha = 0$ [217, 234, 235, 236, 237]. In the following subsection we will explicitly consider these oscillations and work out their analytical description.

Leading corrections $(m = \pm 1)$

The leading correction to the determinant $D_\ell(\lambda)$ comes from the terms with $m = \pm 1$ in (2.3.20) and is given by [217]

$$D_\ell(\lambda) \simeq D_\ell^{(0)}(\lambda)[1 + \Psi_\ell(\lambda)],$$
$$\Psi_\ell(\lambda) = \mathrm{e}^{-2\mathrm{i}k_F\ell} L_k^{-2(1+2\beta_\lambda)} \frac{\Gamma^2(1+\beta_\lambda)}{\Gamma^2(-\beta_\lambda)} + \mathrm{e}^{2\mathrm{i}k_F\ell} L_k^{-2(1-2\beta_\lambda)} \frac{\Gamma^2(1-\beta_\lambda)}{\Gamma^2(\beta_\lambda)}. \quad (2.3.30)$$

We define the difference

$$d_n(\alpha) \equiv \log Z_n(\alpha) - \log Z_n^{(0)}(\alpha), \quad (2.3.31)$$

that for large L_κ is

$$d_n(\alpha) \simeq \frac{1}{2\pi\mathrm{i}} \oint \mathrm{d}\lambda\, f_n(\lambda,\alpha) \frac{\mathrm{d}\log[1+\Psi_\ell(\lambda)]}{\mathrm{d}\lambda} = \frac{1}{2\pi\mathrm{i}} \oint \mathrm{d}\lambda\, f_n(\lambda,\alpha) \frac{\mathrm{d}\Psi_\ell(\lambda)}{\mathrm{d}\lambda} + \cdots. \quad (2.3.32)$$

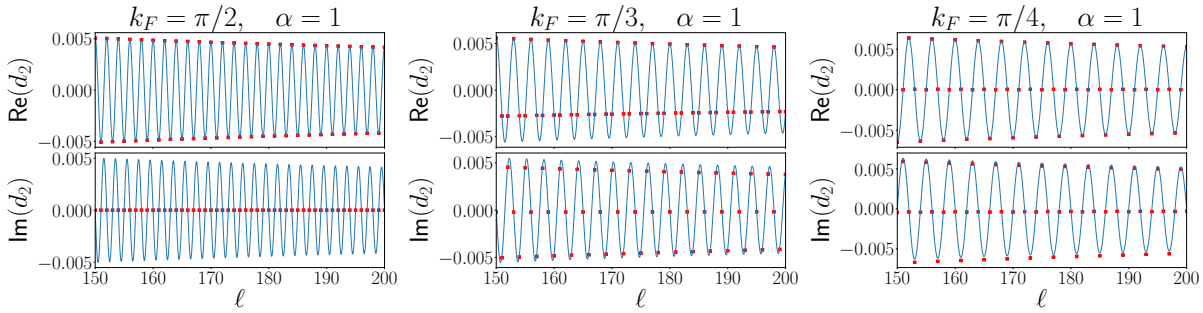


Figure 2.3: Behaviour of the leading corrections to the scaling. The difference $d_2(\ell) \equiv \log Z_2(\alpha) - \log Z_2^{(0)}(\alpha)$ is reported for $\alpha = 1$ and $k_F = \pi/2$ (left), $k_F = \pi/3$ (middle), $k_F = \pi/4$ (right) as a function of ℓ. The numerical data (symbols) perfectly match the calculated leading correction to the scaling from generalised Fisher-Hartwig conjecture in Eq. (3.3.22) both for real and imaginary part.

Changing variable to $\lambda = \tanh(\pi w)$, in the final integral we only need the discontinuities across the branch cut that for the two cases are

$$\begin{aligned}
\left[L_\kappa^{-2-4\beta}\frac{\Gamma^2(1+\beta)}{\Gamma^2(-\beta)}\right]_{\beta=-\mathrm{i}w-\frac{1}{2}} - \left[L_\kappa^{-2-4\beta}\frac{\Gamma^2(1+\beta)}{\Gamma^2(-\beta)}\right]_{\beta=-\mathrm{i}w+\frac{1}{2}} &\simeq L_\kappa^{4\mathrm{i}w}\gamma^2(w), \\
\left[L_\kappa^{-2+4\beta}\frac{\Gamma^2(1-\beta)}{\Gamma^2(\beta)}\right]_{\beta=-\mathrm{i}w-\frac{1}{2}} - \left[L_\kappa^{-2+4\beta}\frac{\Gamma^2(1-\beta)}{\Gamma^2(\beta)}\right]_{\beta=-\mathrm{i}w+\frac{1}{2}} &\simeq -L_\kappa^{-4\mathrm{i}w}\gamma^2(-w),
\end{aligned}$$

where we have dropped terms of order $O(L_k^{-4})$ compared to the leading ones and we have defined

$$\gamma(w) = \frac{\Gamma(\frac{1}{2} - \mathrm{i}w)}{\Gamma(\frac{1}{2} + \mathrm{i}w)}. \tag{2.3.33}$$

Integrating by parts and using (2.A.4) we finally get

$$\begin{aligned}
d_n(\alpha) \simeq \frac{\mathrm{i}n}{2}\int_{-\infty}^{\infty} \mathrm{d}w\,(\tanh(\pi w) - \tanh(\pi n w + \mathrm{i}\alpha/2)) \\
\times \left[\mathrm{e}^{-2\mathrm{i}k_F\ell}L_k^{4\mathrm{i}w}\gamma^2(w) - \mathrm{e}^{2\mathrm{i}k_F\ell}L_k^{-4\mathrm{i}w}\gamma^2(-w)\right].
\end{aligned} \tag{2.3.34}$$

This integral can be evaluated on the complex plane by residue theorem. For the first piece of the integral in square bracket, we should close the contour in the upper half plane, while for the second piece in the lower half plane. In principle we should sum over all residues inside the integration contour, but if we are interested in the limit of large L_k, we can limit ourself to consider the singularities closest to the real axis. For the first integral this is at $w = \mathrm{i}/(2n)(1 - \alpha/\pi)$ while for the second one it is at $w = -\mathrm{i}/(2n)(1 + \alpha/\pi)$. Summing up the two contributions corresponding to $m = 1$ and $m = -1$ respectively, we finally have

$$d_n(\alpha) = \mathrm{e}^{-2\mathrm{i}k_F\ell}L_k^{-\frac{2}{n}\left(1-\frac{\alpha}{\pi}\right)}\left[\frac{\Gamma\left(\frac{1}{2}+\frac{1}{2n}-\frac{\alpha}{2\pi n}\right)}{\Gamma\left(\frac{1}{2}-\frac{1}{2n}+\frac{\alpha}{2\pi n}\right)}\right]^2 + \mathrm{e}^{2\mathrm{i}k_F\ell}L_k^{-\frac{2}{n}\left(1+\frac{\alpha}{\pi}\right)}\left[\frac{\Gamma\left(\frac{1}{2}+\frac{1}{2n}+\frac{\alpha}{2\pi n}\right)}{\Gamma\left(\frac{1}{2}-\frac{1}{2n}-\frac{\alpha}{2\pi n}\right)}\right]^2. \tag{2.3.35}$$

Let us comment on this result. First, it is obvious that the formula is valid only for $-\pi < \alpha < \pi$, else one of the power laws would blow up as a consequence of the fact that one of the terms for

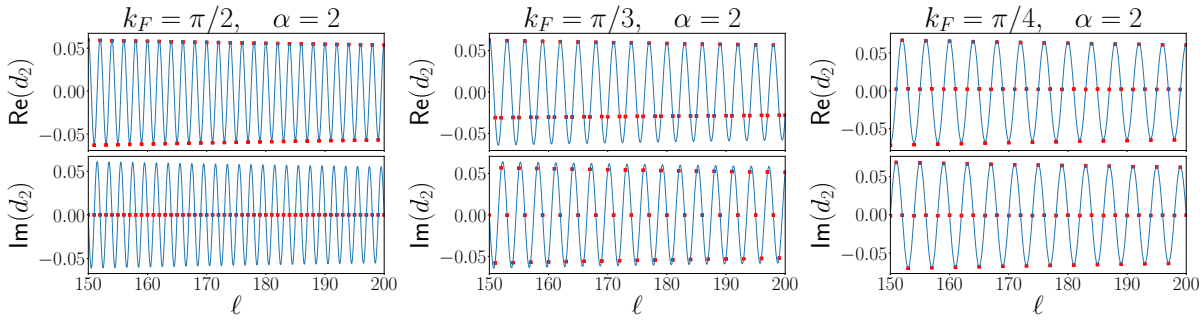


Figure 2.4: Behaviour of the leading corrections to the scaling. The difference $d_2(\ell) \equiv \log Z_2(\alpha) - \log Z_2^{(0)}(\alpha)$ is reported for $\alpha = 2$ and $k_F = \pi/2$ (left), $k_F = \pi/3$ (middle), $k_F = \pi/4$ (right) as a function of ℓ. The numerical data (symbols) perfectly match the calculated leading correction to the scaling from generalised Fisher-Hartwig conjecture in Eq. (3.3.22) both for real and imaginary part. We notice that here Eq. (3.3.22) works slightly worst compared to the case $\alpha = 1$ in Fig. 2.3.

$m = \pm 1$ becomes the leading ones. Then we see that this correction is real only for $\alpha = 0$ and at half-filling (when it should be real at all orders, cf. Eq. (2.3.9)). Away from half filling, there is generically a non-zero imaginary part. The two contributions have a different power-law decays (for $\alpha \neq 0$) and so only one of them is the leading correction depending on the sign of α. However, for α close to zero, the two powers are too close in magnitude and they should be both taken into account in order to have an accurate description of the data for moderately large values of ℓ. When α gets closer and closer to $\pm\pi$, Eq. (3.3.22) becomes accurate only for very large ℓ because the term with $m = 0$ is about of the same order of magnitude as the one with $m = \pm 1$ (depending on the sign of α). A better description of the asymptotic behaviour may be achieved using Eq. (2.3.20) without expanding as in Eq. (2.3.30). Finally, let us notice that, while in the absence of flux ($\alpha = 0$) the oscillating corrections to the scaling vanish in the limit $n \to 1$ [217], for $\alpha \neq 0$ also the von Neumann entropy presents leading oscillating corrections described by Eq. (3.3.22).

In Figures 2.3 and 2.4 we report the difference $d_2(\alpha)$ as calculated numerically for $k_F = \pi/2, \pi/3, \pi/4$ and for $\alpha = 1$ and $\alpha = 2$ as function of ℓ. The numerical data are compared with the leading prediction in Eq. (3.3.22) and the agreement is extremely good. We actually observe that this prediction works slightly worst for $\alpha = 2$ (cf. Fig. 2.4) than for $\alpha = 1$ (cf. Fig. 2.3). We indeed checked that the match becomes worst and worst when α moves close to π, when the leading term in the generalised Fisher-Hartwig changes. In principle it is possible to systematically analyse further corrections to $\log Z_n(\alpha)$ by taking into account the known expansion of $D_\ell(\lambda)$ in powers of ℓ [217], but this is very cumbersome and far beyond the scope of this paper.

2.4 Free fermions on a lattice: symmetry resolved entropies

In this section we finally move to the symmetry resolved entropies and to their analysis.

2.4.1 Q_A-resolved moments via Fourier trasform

The first step toward the symmetry resolved entropies is to calculate $\mathcal{Z}_n(q)$, the Fourier transform of $Z_n(\alpha)$ as defined in Eq. (2.2.8). We will show that we may obtain a very accurate prediction by keeping only the $m = 0$ term in (2.3.20), but with all non-universal pieces. Within this approximation the Fourier transform $\mathcal{Z}_n(q)$ is

$$\mathcal{Z}_n(q) \simeq \int_{-\pi}^{\pi} \frac{\mathrm{d}\alpha}{2\pi} \mathrm{e}^{-\mathrm{i}q\alpha} Z_n^{(0)}(\alpha) = L_k^{-\frac{1}{6}\left(n-\frac{1}{n}\right)} \int_{-\pi}^{\pi} \frac{\mathrm{d}\alpha}{2\pi} \mathrm{e}^{-\mathrm{i}\left(q-\frac{k_F}{\pi}\ell\right)\alpha - b_n\alpha^2} \mathrm{e}^{\Upsilon(n,\alpha)}, \tag{2.4.1}$$

where we defined the "bare variance"

$$b_n = \frac{2}{n}\frac{1}{4\pi^2}\log L_k. \tag{2.4.2}$$

As a first step we use Eq. (2.3.28) to rewrite $\mathcal{Z}_n(q)$ as

$$\begin{aligned}\mathcal{Z}_n(q) &\simeq \mathrm{e}^{\Upsilon(n)} L_k^{-\frac{1}{6}\left(n-\frac{1}{n}\right)} \int_{-\pi}^{\pi} \frac{\mathrm{d}\alpha}{2\pi} \mathrm{e}^{-\mathrm{i}\left(q-\frac{k_F}{\pi}\ell\right)\alpha - (b_n-\gamma_2(n))\alpha^2} \mathrm{e}^{\epsilon(n,\alpha)} \\ &= Z_n^{(0)}(0) \int_{-\pi}^{\pi} \frac{\mathrm{d}\alpha}{2\pi} \mathrm{e}^{-\mathrm{i}\left(q-\frac{k_F}{\pi}\ell\right)\alpha - b_n^R\alpha^2} g_n(\alpha),\end{aligned} \tag{2.4.3}$$

where $Z_n^{(0)}(0) = Z_n^{(0)}(\alpha = 0) = \mathrm{e}^{\Upsilon(n)} L_k^{-\frac{1}{6}\left(n-\frac{1}{n}\right)}$, we defined the "renormalised variance"

$$b_n^R \equiv b_n - \gamma_2(n)\,, \tag{2.4.4}$$

and $g_n(\alpha) \equiv \mathrm{e}^{\epsilon(n,\alpha)}$. Up to this point, we only rewrote the starting expression (2.4.1). We now proceed by treating the integral, for large subsystem size ℓ, by means of the saddle point approximation. When $\ell \gg 1$, the large parameter in (2.4.3) is b_n. Furthermore, we assume that $g_n(\alpha) = 1$, because we have shown in the previous section that the function $\epsilon(n,\alpha) \ll 1$, cf. Fig. 2.1. Within this approximation we finally get

$$\begin{aligned}\mathcal{Z}_n(q) \simeq Z_n^{(0)}(0) \int_{-\infty}^{\infty} \frac{\mathrm{d}\alpha}{2\pi} \mathrm{e}^{-\mathrm{i}\left(q-\frac{k_F}{\pi}\ell\right)\alpha - b_n^R\alpha^2} &= Z_n(0)\mathrm{e}^{-\frac{(q-\bar{q})^2}{4b_n^R}} \sqrt{\frac{1}{4\pi b_n^R}} = \\ Z_n(0)\sqrt{\frac{n\pi}{2(\log L_k - 2\pi^2 n\gamma_2(n))}}&\mathrm{e}^{-\frac{n\pi^2(q-\bar{q})^2}{2(\log L_k - 2\pi^2 n\gamma_2(n))}},\end{aligned} \tag{2.4.5}$$

where we defined $\bar{q} \equiv \langle Q_A \rangle = \ell k_F/\pi$.

Eq. (2.4.5) is one of the main results of this paper. Let us discuss its features. First, in the limit $\ell \to \infty$, we recover the CFT result (2.2.15) for $K = 1$, but with the correct normalisation of $Z_n(0)$. Although this normalisation was not previously known rigorously (at least to the best of our knowledge), it could have been easily guessed from the results in the absence of flux (i.e., $\alpha = 0$ of Ref. [216]). The mean of the gaussian term is $\bar{q}$ and it is not changed compared to the result (2.2.15). Consequently, the main new insight from Eq. (2.4.5) is the prediction for the constant term to add to $\log L_k$ (or equivalently, the multiplicative scale for L_k as in [34]). Although this non-universal constant is a correction to the leading behaviour (expanding for large L_k, it gives a term going like $(\log L_k)^{-1}$), it is very important: the $(\log L_k)^{-1}$ decay is so slow that it must be taken into account even for very large L_k in order to quantitatively describe the data, as we shall see.

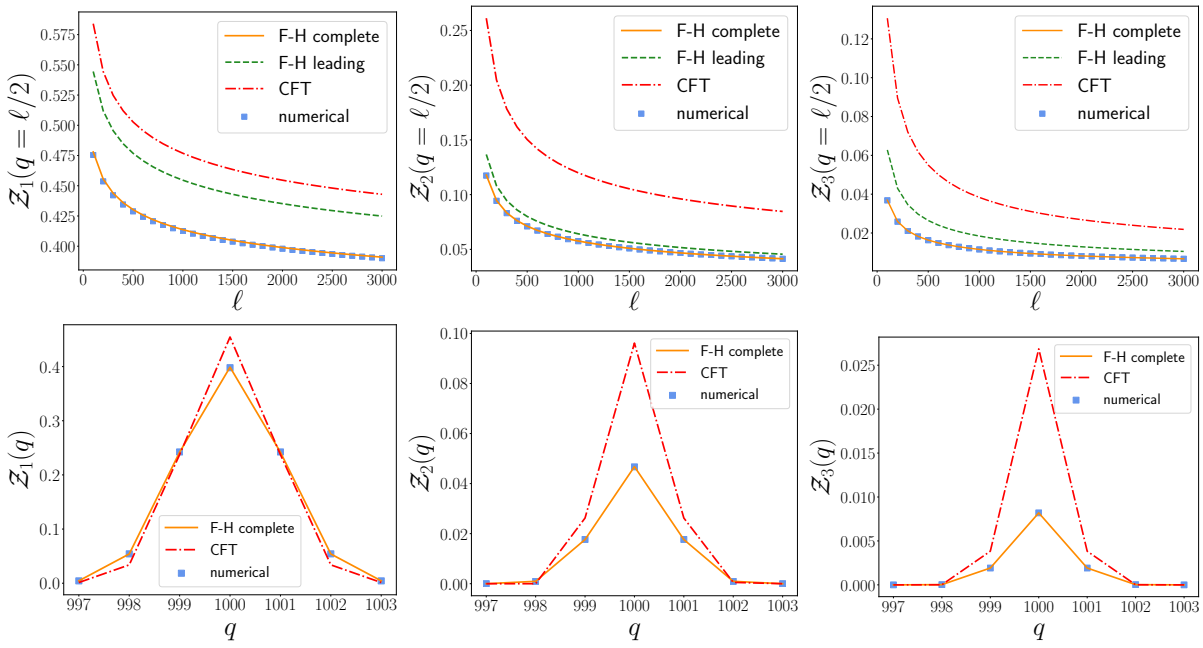


Figure 2.5: Symmetry resolved partition sums $\mathcal{Z}_n(q)$. *Top*: $\mathcal{Z}_n(q = \ell/2)$ at half filling as a function of ℓ. The numerical data for $n = 1, 2, 3$ (left to right) are compared with: i) the CFT prediction without fixing the non universal constant (dot-dashed line); ii) the leading Fisher-Hartwig prediction at $O(1)$, i.e., Eq. (2.4.5) with $\gamma_2(n) = 0$ (dotted line); iii) the complete Fisher-Hartwig result, Eq. (2.4.5) (full line). Clearly only the latter accurately describes the data, although the qualitative behaviour is the same for all curves. *Bottom*: $\mathcal{Z}_n(q)$ at half filling for $\ell = 2000$ as function of q. The numerical data for $n = 1, 2, 3$ (left to right) are compared with: i) the CFT prediction without fixing the non universal constant (dot-dashed line); ii) the complete Fisher-Hartwig result, Eq. (2.4.5) (full line).

Given the importance that the quantity $\gamma_2(n)$ in Eq. (2.3.29) has in this analysis, we report its explicit numerical value for some n: $\gamma_2(1) = -0.0799027$, $\gamma_2(2) = -0.0462208\ldots$, and $\gamma_2(3) = -0.0319926\ldots$ (in particular $\gamma_2(1) = -(1+\gamma_E)/(2\pi^2)$ with γ_E the Euler constant, as anticipated in [34]). The importance of this constant in the description of the numerical data, was understood already in [34], where the authors define $g_n = 2e^{-2\pi^2 n \gamma_2(n)}$ and provide the analytic results for $n = 1$, as well as a numerical estimate for $n = 2$, i.e., $g_2 \sim 12.39$ which is very close to the exact value that we have found $g_2 = 12.4022\ldots$.

Let us briefly discuss the terms that have been neglected in the derivation of Eq. (2.4.5). The most relevant one comes from having approximated $g_n(\alpha)$ with 1. By expanding this function in powers of α, it is immediate to realise that the series coefficient α^{2k} (with $k \geq 2$) provides a correction to the leading term of the order $(\log L_k)^{-k}$. Anyhow, these factors influence little the final result because the amplitude of the various terms is very small. Another correction comes from the extremes of integration that we pushed to $\pm\infty$ instead of $\pm\pi$. Although their effect can be taken into account as done in Ref. [34], they provide corrections which decay as $e^{-\pi^2 b_n^R}/b_n^R$, i.e., algebraically in L_k, and so negligible at this level. Also the corrections due to the terms with $m \neq 0$ in Eq. (2.3.20) decay as power laws in L_k and can be safely neglected at this stage.

In Figure 2.5 we report the numerically calculated symmetry resolved partition sums $\mathcal{Z}_n(q)$.

We compare the numerical data for $n = 1, 2, 3$ with the CFT prediction without fixing the non universal constant as in Eq. (2.2.15). The qualitative agreement is reasonable, but quantitatively far. We also report the prediction for $\mathcal{Z}_n(q)$ at order $O(\ell^0)$: the curves moves closer to the numerical data, but the match is still not perfect. Only when we use the complete Fisher-Hartwig prediction Eq. (2.4.5) (with the correct value of $\gamma_2(n)$), the data are perfectly reproduced. As anticipated, including the logarithmic corrections is fundamental to have an accurate description of the data. Also the q-dependence of $\mathcal{Z}_n(q)$ is perfectly captured by Eq. (2.4.5) as shown in the lower panels of Figure 2.5.

2.4.2 Symmetry resolved Rényi and entanglement entropy

We now use Eq. (2.4.5) to calculate the symmetry resolved REs and the Von Neumann EEs. Let us start from the former. Eq. (2.2.6) implies

$$S_n(q) = \frac{1}{1-n} \log \left[\frac{\mathcal{Z}_n(q)}{\mathcal{Z}_1(q)^n} \right] \simeq \frac{1}{1-n} \log \frac{Z_n(0)}{(Z_1(0))^n} \frac{\mathrm{e}^{-\frac{(q-\bar{q})^2}{4b_n^R}}}{\mathrm{e}^{-\frac{n(q-\bar{q})^2}{4b_1^R}}} \frac{(4\pi b_n^R)^{-1/2}}{(4\pi b_1^R)^{-n/2}} . \tag{2.4.6}$$

The first ratio in Eq. (2.4.6) just gives the total RE of order n, with the right additive constant (and indeed this is true at all orders). The other q-independent term is

$$\begin{aligned} \frac{1}{1-n} \log \frac{(4\pi b_n^R)^{-1/2}}{(4\pi b_1^R)^{-n/2}} &= -\frac{1}{2} \log \frac{2}{\pi} + \frac{\log n}{2(1-n)} + \frac{1}{1-n} \log \frac{(\log L_k - 2\pi^2 \gamma_2(1))^{n/2}}{(\log L_k - 2\pi^2 n \gamma_2(n))^{1/2}} \\ &= -\frac{1}{2} \log \left(\frac{2}{\pi} \log \delta_n L_k \right) + \frac{\log n}{2(1-n)} + \cdots . \end{aligned} \tag{2.4.7}$$

The constant δ_n has been introduced to resum partially the subleading corrections to the scaling ((i.e. we used $\log(\log(x)) + a/\log(x) = \log(\log(\mathrm{e}^a x)) + O(\log^2 x)$) and it is given by

$$\log \delta_n = -\frac{2\pi^2 n (\gamma_2(n) - \gamma_2(1))}{1-n} . \tag{2.4.8}$$

The last term is the ratio of the two Gaussian factors which is the only one depending on q. For this last contribution we have

$$\frac{1}{1-n} \log \mathrm{e}^{\frac{n(q-\bar{q})^2}{4b_1^R} - \frac{(q-\bar{q})^2}{4b_n^R}} = (q-\bar{q})^2 \pi^4 \frac{n}{1-n} (\gamma_2(1) - n\gamma_2(n)) \frac{1}{\log^2 \kappa_n L_k} + \dots , \tag{2.4.9}$$

where the constant

$$\log \kappa_n = -\pi^2 (\gamma_2(1) + n\gamma_2(n)), \tag{2.4.10}$$

has been introduced, again, to resum partially the subleading corrections.

Putting together the three pieces we have

$$S_n(q) = S_n - \frac{1}{2} \log \left(\frac{2}{\pi} \log \delta_n L_k \right) + \frac{\log n}{2(1-n)} + (q-\bar{q})^2 \pi^4 \frac{n(\gamma_2(1) - n\gamma_2(n))}{1-n} \frac{1}{\log^2 \kappa_n L_k} + \cdots . \tag{2.4.11}$$

This equation not only predicts the leading diverging behaviour for large ℓ which was already known from CFT [35, 34] (cf. Eq. (2.2.16)), but also the non-universal additive constant, as

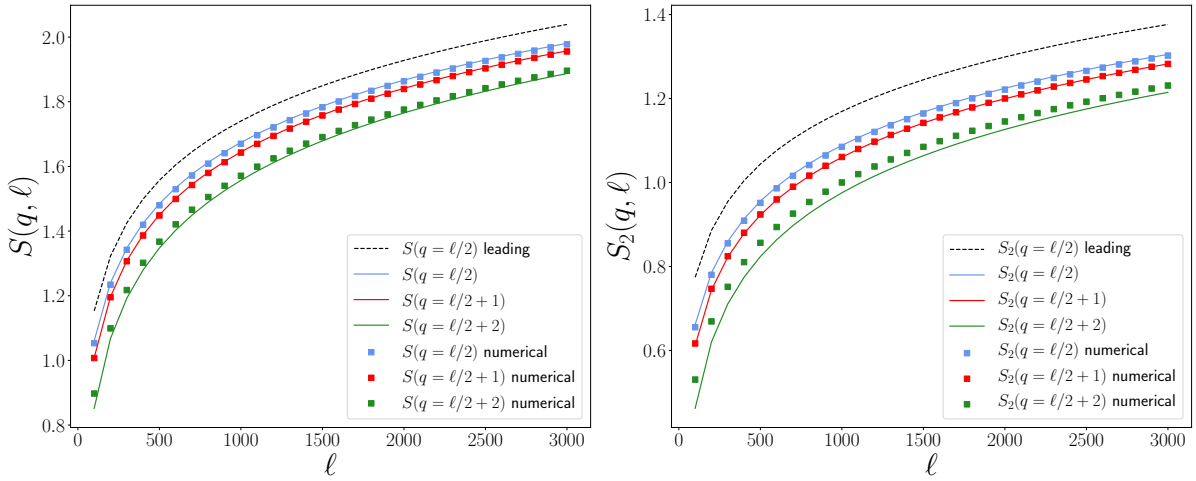


Figure 2.6: Von Neumann (left) and second Rényi (right) symmetry resolved EEs. The numerical data (symbols) for $q = \ell/2, \ell/2+1, \ell/2+2$ are compared with the theoretical predictions Eqs. (2.4.11) and (2.4.12). The figures also highlight the importance of the logarithmic corrections to the scaling which are fundamental in order to accurately describe the data for ℓ as large as 3000 and even larger. Increasing the values of $(q-\bar{q})^2$, the corrections to the scaling that we neglect become more important.

well as the some subleading corrections in $\log L_k$. The latter are not only important to correctly describe the data, but are also the leading q-dependent contributions. So while the leading and finite terms satisfy the equipartition of entanglement [34], within our approach we are able to identify the leading term that breaks this equipartition.

Taking now the limit for $n \to 1$, we get the von Neumann entropy

$$S(q) = S - \frac{1}{2}\log\left(\frac{2}{\pi}\log\delta_1 L_k\right) - \frac{1}{2} + (q-\bar{q})^2\,\pi^4\frac{(\gamma_2(1)+\gamma_2'(1))}{\log^2\kappa_1 L_k} + \cdots, \tag{2.4.12}$$

with $\log\delta_1 = 2\pi^2\gamma_2'(1)$ and $\gamma_2'(1) = 0.0545724$.

These Fisher-Hartwig calculations for the symmetry resolved entanglement are compared with the numerical data in Figure 2.6. It is evident in these figures that the results for different q are *not* on top of each other although we reported ℓ as large as 3000. Indeed their difference (that we know to go to zero as $(\log\ell)^{-2}$) can be easily misinterpreted as a different additive constant if one would proceed with a fit of the numerical data. Only the exact knowledge of the asymptotic behaviour of Eqs. (2.4.11) and (2.4.12) allow us to correctly understand the data. In the figure we also report Eqs. (2.4.11) and (2.4.12) truncated at $o(1)$ (just for $q = \bar{q}$), showing that these leading curves are far from the data and that the distance between the two barely reduces. We stress that not only the prefactor of the logarithmic corrections are important, but also the precise values of the amplitudes in Eqs. (2.4.10) and (2.4.8), as it is easy to check. Finally we observe that increasing $(q-\bar{q})$ the corrections to the scaling that we neglected become more important.

We finish the section commenting about the double log contribution in Eqs. (2.4.11) and (2.4.12). It may seem rather awkward that all the symmetry resolved contributions have a double log correction, while the total EE does not. Indeed, when calculating the total entanglement this double log cancels when summing to the fluctuation entanglement S^n as in Eq. (2.2.2).

Indeed, taking as a prototypical example the von Neumann entropy and using that the probability is $p(q) = \mathcal{Z}_1(q)$, we have

$$S^n = -\int_q \mathcal{Z}_1(q)\log\mathcal{Z}_1(q) \simeq -\int \mathrm{d}q \frac{\mathrm{e}^{-\frac{(q-\bar{q})^2}{4b_1^R}}}{\sqrt{4\pi b_1^R}} \log \frac{\mathrm{e}^{-\frac{(q-\bar{q})^2}{4b_1^R}}}{\sqrt{4\pi b_1^R}} = \frac{1}{2}(1+\log 4\pi b_1^R) =$$
$$= \frac{1}{2}\Big(1+\log\Big(\frac{2}{\pi}\log L_k - \gamma_2(1)\Big)\Big) = \frac{1}{2}+\frac{1}{2}\log\Big(\frac{2}{\pi}\log L_k\Big) + O(L_k^{-1})\,. \quad (2.4.13)$$

Note that both leading terms in S^n in the above equation cancel *exactly* with the corresponding ones in the symmetry resolved entanglement in Eq. (2.4.12). The same is true for all REs of arbitrary order.

2.5 Charged and symmetry resolved entanglement for the Fermi gas

In this section we derive the symmetry resolved EE for a one-dimensional Fermi gas using the overlap matrix approach [238, 239]. This technique has been successfully applied to the calculation of entanglement in many different circumstances [240, 238, 239, 241, 242, 243, 244, 245, 246, 247].

The system we are going to study consists of a gas of N free spinless non-relativistic one-dimensional fermions with some suitable boundary conditions in order to have a discrete energy spectrum. The many body wave functions $\Psi(x_1,...,x_N)$ is the Vandermonde determinant $\Psi(x_1,...,x_N) = \det[\phi_m(x_n)]/\sqrt{N!}$, built with the occupied single particle eigenstates with wave functions $\phi_m(x)$. The many body ground state is obtained by filling the N levels with lowest energies. Given that there is no lattice, the particle number N provides also the ultraviolet cutoff.

Our focus is again a subsystem, now taken to be a single interval A, and its entanglement with the rest of the system. The RDM ρ_A in the subsystem A is obtained as the continuous limit of Eq. (2.3.2). Therefore we can still exploit its gaussian nature. A crucial quantity is the *overlap matrix* associated to A defined as

$$\mathbb{A}_{nm} = \int_A \phi_n^*(x)\phi_m(x)\mathrm{d}x, \qquad n,m = 1,\cdots,N. \quad (2.5.1)$$

In fact, it has been shown [239, 238] that the (continuous) correlation matrix and the (discrete) overlap matrix share the same eigenvalues $(1+\nu_k)/2$ (with $k \in [1,N]$) and so, for example, the moments of the RDM may be written as

$$\mathrm{Tr}\rho_A^n = \prod_{i=1}^{N}\left[\left(\frac{1+\nu_i}{2}\right)^n + \left(\frac{1-\nu_i}{2}\right)^n\right]. \quad (2.5.2)$$

In the case of a system with periodic boundary conditions in the interval $[0,L]$, the eigenfunctions are plane waves $\phi_k(x) = \mathrm{e}^{2\pi\mathrm{i}kx/L}/\sqrt{L}$ with integer wave-numbers k. When the subsystem is also an interval, say $A = [0,\ell]$, the overlap matrix is easily calculated and reads

$$\mathbb{A}_{nm} = \frac{\sin\pi(n-m)\ell/L}{\pi(n-m)}, \qquad n,m = 1,\cdots,N. \quad (2.5.3)$$

A crucial observation made in [239] is that such matrix is identical to the lattice correlation matrix, Eq. (2.3.3), upon identifying k_F/π with ℓ/L and N with ℓ. As a consequence, this

simple replacement allows to translate all the results from the lattice to the continuous model. In particular all formulas derived for the tight binding model are valid also for the gas, where now L_k is not anymore $2\ell \sin k_F$, but

$$L_k = 2N \sin \pi \frac{\ell}{L} . \tag{2.5.4}$$

This replacement allows to show rigorously the CFT scaling in finite size for this model.

For the symmetry resolved entanglement we can straightforwardly make our predictions for the gas. First of all, the entanglement REs in the presence of a flux are

$$\begin{aligned} \log Z_n(\alpha) = \mathrm{i}\alpha \frac{\ell N}{L} - \left[\frac{1}{6}\left(n - \frac{1}{n}\right) + \frac{2}{n}\left(\frac{\alpha}{2\pi}\right)^2\right] \log\left[2N \sin\left(\pi \frac{\ell}{L}\right)\right] + \mathrm{Y}(n,\alpha) + \\ \mathrm{e}^{-\frac{2\mathrm{i}\pi\ell N}{L}} \left[2N \sin\left(\pi \frac{\ell}{L}\right)\right]^{-\frac{2}{n}\left(1-\frac{\alpha}{\pi}\right)} \left[\frac{\Gamma\left(\frac{1}{2} + \frac{1}{2n} - \frac{\alpha}{2\pi n}\right)}{\Gamma\left(\frac{1}{2} - \frac{1}{2n} + \frac{\alpha}{2\pi n}\right)}\right]^2 + \\ + \mathrm{e}^{\frac{2\mathrm{i}\pi\ell N}{L}} \left[2N \sin\left(\pi \frac{\ell}{L}\right)\right]^{-\frac{2}{n}\left(1+\frac{\alpha}{\pi}\right)} \left[\frac{\Gamma\left(\frac{1}{2} + \frac{1}{2n} + \frac{\alpha}{2\pi n}\right)}{\Gamma\left(\frac{1}{2} - \frac{1}{2n} - \frac{\alpha}{2\pi n}\right)}\right]^2 , \end{aligned} \tag{2.5.5}$$

where we only included the leading contributions at $m = 0, \pm 1$ in the generalised Fisher-Hartwig conjecture. We tested this result against exact numerical computations and, as for the lattice model, we found that it provides a very accurate description as long as α is not close to $\pm\pi$.

Similarly, for the symmetry resolved entropies the predictions for the gas are obtained simply by plugging Eq. (2.5.4) into Eqs. (2.4.11) and (2.4.12) for Rényi and von Neumann entropy respectively (with $\bar{q} = \frac{\ell N}{L}$).

2.6 Concluding remarks

In this chapter we derived exact formulas for the asymptotic behaviour of the symmetry resolved EEs in free fermion systems. First we obtained an exact expression for the charged entropies given by Eqs. (2.3.26) (asymptotic behaviour up to order $O(1)$) and (3.3.22) (leading corrections to the scaling). The leading logarithmic term in Eq. (2.3.26) perfectly matches the CFT prediction, but we also determined the non-universal $O(1)$ contribution. The $o(1)$ corrections present interesting oscillatory behaviour and a power law decay with exponents that depend on the flux α. We then moved to the truly symmetry resolved entropies given by the Fourier transform of the charged ones. The partition sums are given by Eq. (2.4.5), while Rényi and von Neumann entropy by Eqs. (2.4.11) and (2.4.12) respectively. These equations agree in the limit of large ℓ with the CFT results, but we also determine a number of non-universal constants as well as logarithmic corrections to the scaling which are fundamental for an accurate description of the numerical data. Our analysis also provide the first term in the expansion for large ℓ which depend on the symmetry sector, hence breaking the equipartition of entanglement [34]. We also related the the double logarithmic correction to the fluctuation entanglement.

2.A Appendix: Details of calculations

In this appendix we report the details of the calculation needed in Section 4.2.3.

The first integral is the linear term in ℓ

$$a_0 = \frac{1}{2\pi \mathrm{i}} \oint \mathrm{d}\lambda f_n(\lambda,\alpha) \left(\frac{1-k_F/\pi}{1+\lambda} - \frac{k_F/\pi}{1-\lambda} \right) . \tag{2.A.1}$$

While the first piece is analytic in λ (because $f_n(-1,\alpha)=0$), the second piece has a simple pole in $\lambda = 1$, leading to

$$a_0 = -\frac{k_F/\pi}{2\pi \mathrm{i}} \oint \mathrm{d}\lambda \frac{f_n(\lambda,\alpha)}{1-\lambda} = \mathrm{i}\alpha \frac{k_F}{\pi} . \tag{2.A.2}$$

The second integral is

$$a_1 = \frac{2}{\pi^2} \oint \mathrm{d}\lambda f_n(\lambda,\alpha) \frac{\beta_\lambda}{1-\lambda^2}, \tag{2.A.3}$$

The only non zero contribution to the contour integral comes from the discontinuity at the cut of β_λ,

$$\beta_{x\pm \mathrm{i}\epsilon} = -\mathrm{i}w(x) \mp \frac{1}{2}, \qquad \text{with} \qquad w(x) = \frac{1}{2\pi} \log \frac{1+x}{1-x}, \tag{2.A.4}$$

and hence we finally have

$$a_1 = \frac{2}{\pi^2} \int_{-1}^{1} \mathrm{d}\lambda \, \frac{f_n(\lambda,\alpha)}{1-\lambda^2}. \tag{2.A.5}$$

This integral may be considered as the final answer, but indeed it may be simply evaluated analytically. First one performs the change of variable

$$w = \frac{1}{2\pi} \log \frac{1+\lambda}{1-\lambda}, \qquad \lambda = \tanh(\pi w) , \quad -\infty < w < \infty, \tag{2.A.6}$$

to get

$$a_1 = \frac{2}{\pi} \int_{-\infty}^{\infty} \mathrm{d}w f_n(\tanh(\pi w),\alpha) . \tag{2.A.7}$$

At this point, integrate by part using

$$\frac{\mathrm{d}}{\mathrm{d}w} f_n(\tanh(\pi w),\alpha) = \pi n [\tanh(\pi n w + \mathrm{i}\alpha/2) - \tanh(\pi w)] , \tag{2.A.8}$$

to get

$$a_1 = \frac{2}{n} \int_{-\infty}^{\infty} \mathrm{d}w w (\tanh(\pi w) - \tanh(\pi n w + \mathrm{i}\alpha/2)) . \tag{2.A.9}$$

Consider now the difference

$$a_1 - a_1|_{\alpha=0} = \frac{2}{n} \int_{-\infty}^{\infty} \mathrm{d}w w (\tanh(\pi n w) - \tanh(\pi n w + \mathrm{i}\alpha/2)) = \frac{2}{\pi^2 n} \int_{-\infty}^{\infty} \mathrm{d}z z (\tanh(z) - \tanh(z + \mathrm{i}\alpha/2)) . \tag{2.A.10}$$

The derivative with respect to α of the last integral is

$$\frac{\mathrm{i}}{\pi^2 n} \int_{-\infty}^{\infty} \mathrm{d}z \frac{z}{\cosh(z+\mathrm{i}\alpha/2)} = -\frac{\alpha}{\pi^2 n} . \tag{2.A.11}$$

Integrating back and using the boundary condition that the difference for $\alpha = 0$ is zero by definition, we finally have

$$a_1 - a_1|_{\alpha=0} = -\frac{\alpha^2}{2\pi^2 n}\,, \tag{2.A.12}$$

that using the known value of $a_1|_{\alpha=0}$ [216] is equivalent to Eq. (2.3.26).

The last integral is

$$a_2 = \frac{1}{\pi \mathrm{i}} \oint \mathrm{d}\lambda f_n(\lambda,\alpha) \frac{\mathrm{d}\log[G(1+\beta_\lambda)G(1-\beta_\lambda)]}{\mathrm{d}\lambda}\,. \tag{2.A.13}$$

Let us first integrate by parts

$$a_2 = -\frac{1}{\pi \mathrm{i}} \oint \mathrm{d}\lambda \frac{\mathrm{d}f_n(\lambda,\alpha)}{\mathrm{d}\lambda} \log[G(1+\beta_\lambda)G(1-\beta_\lambda)]\,. \tag{2.A.14}$$

Again the only discontinuity at the cut comes from the function β_λ, so that

$$\log \frac{G(1+\beta_{x+\mathrm{i}\epsilon})G(1-\beta_{x+\mathrm{i}\epsilon})}{G(1+\beta_{x-\mathrm{i}\epsilon})G(1-\beta_{x-\mathrm{i}\epsilon})} = \log \frac{G(\frac{1}{2}-\mathrm{i}w(x))G(\frac{3}{2}+\mathrm{i}w(x))}{G(\frac{3}{2}-\mathrm{i}w(x))G(\frac{1}{2}+\mathrm{i}w(x))} = \log \frac{\Gamma(\frac{1}{2}+\mathrm{i}w(x))}{\Gamma(\frac{1}{2}-\mathrm{i}w(x))}\,, \tag{2.A.15}$$

where we used $\Gamma(z) = G(z+1)/G(z)$. We then have

$$a_2 = \frac{1}{\pi \mathrm{i}} \int_{-1}^{1} \mathrm{d}\lambda \frac{\mathrm{d}f_n(\lambda,\alpha)}{\mathrm{d}\lambda} \log \frac{\Gamma(\frac{1}{2}+\mathrm{i}w(x))}{\Gamma(\frac{1}{2}-\mathrm{i}w(x))}\,. \tag{2.A.16}$$

Changing the integration variable from λ to w as in Eq. (2.A.6) and using the derivative in Eq.(2.A.8) we finally get

$$a_2 = n\mathrm{i} \int_{-\infty}^{\infty} dw[\tanh(\pi w) - \tanh(\pi n w + \mathrm{i}\alpha/2)] \log \frac{\Gamma(\frac{1}{2}+\mathrm{i}w)}{\Gamma(\frac{1}{2}-\mathrm{i}w)}\,. \tag{2.A.17}$$

Chapter 3

Boundary effects on symmerty resolved entanglement

***Summary**: In this Chapter, based on Ref. [2] we study the symmetry resolved EEs in one-dimensional systems with boundaries. We provide some general results for conformal invariant theories and then move to a semi-infinite chain of free fermions. We consider both an interval starting from the boundary and away from it. We derive exact formulas for the charged and symmetry resolved entropies based on theorems and conjectures about the spectra of Toeplitz+Hankel matrices. En route to characterise the interval away from the boundary, we prove a general relation between the eigenvalues of Toeplitz+Hankel matrices and block Toeplitz ones. An important aspect is that the saddle-point approximation from charged to symmetry resolved entropies introduces algebraic corrections to the scaling that are much more severe than in systems without boundaries.*

3.1 Introduction

The earlier theoretical work aimed at the characterisation of the interplay between entanglement and internal symmetries of a quantum system [35, 34, 1, 49, 33, 38, 39, 62, 53, 56, 57, 55, 54, 63, 64, 66, 58, 65] have almost entirely focused on systems with periodic boundary conditions (PBC). However, there are many fundamental reasons to investigate systems with boundaries, in particular open boundary conditions (OBC). Just to quote a few: experimental solid-state systems typically have OBC; in trapped cold atoms, the vanishing of the density beyond a trapping length induces OBC in the inhomogeneous gas that can be treated with the methods of field theories in curved space [248]; in some non equilibrium situations such as a quantum quench, the initial state can be treated as a boundary state in imaginary time formalism [192]. The goal of this Chapter is to study the effects of boundary conditions, in particular open, on symmetry resolved entanglement in conformal field theories and in free fermions chains. The latter can be treated with simple exact methods.

One of the remarkable results about the REs and EE in extended quantum systems is their universal scaling behaviour in CFT when the subsystem A is an interval of length ℓ embedded in the infinite line [25, 26, 27, 28], expressed in Eq. (1.4.12) As shown in Sect. 1.4.2, the

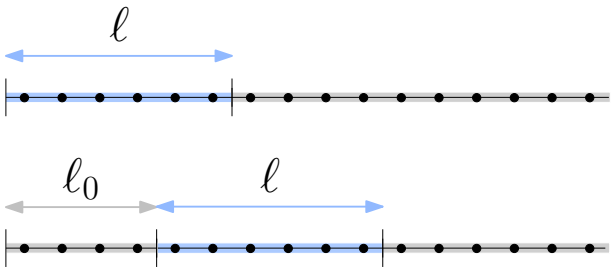


Figure 3.1: The two geometries we consider in this manuscript for a semi-infinite system. The subsystem A is always an interval of length ℓ that starts either from the boundary (top) or at distance ℓ_0 from it (bottom with $\ell_0 = 3$).

presence of a boundary strongly affects such universal behaviour. For example, for a semi-infinite boundary CFT starting (say) at $x = 0$, the scaling of the Renyi entropies for the interval $A = [0, \ell]$ (see Fig. 3.1) is given by Eq. (1.4.51) [25, 26]

In a microscopic gapless model (e.g., a spin chain) the leading corrections to the asymptotic conformal behaviour given by Eqs. (1.4.12) and (1.4.51) decay as $\ell^{-2K/n}$ [217, 234, 235, 237, 236] and $\ell^{-K/n}$ [249, 229, 235] for PBC and OBC, respectively (K is the scaling dimension of a relevant operator as we will see later on). These corrections oscillate with ℓ, except for PBC at $n = 1$.

When the subsystem A is placed at distance ℓ_0 from the boundary (i.e. $A = [\ell_0, \ell_0 + \ell]$, see Fig. 3.1), according to Eq. (1.4.64) CFT predicts the general scaling form for the EEs

$$S_n = \frac{c}{12}\left(1 + \frac{1}{n}\right) \log \frac{4\ell^2 \ell_0 (\ell + \ell_0)}{(2\ell_0 + \ell)^2} + c'_n + \frac{\log \mathcal{F}_n(x)}{1 - n}, \tag{3.1.1}$$

where $x \in [0, 1]$ is the anharmonic ratio

$$x = \frac{\ell^2}{(2\ell_0 + \ell)^2}, \tag{3.1.2}$$

and $\mathcal{F}_n(x)$ is a function depending on the full operator content of the considered boundary CFT and normalised as $\mathcal{F}_n(0) = 1$ (to recover the bulk result (1.4.12) for $\ell_0 \gg \ell$, i.e. $x \to 0$). Such a universal function should be calculated on a case by case basis, analogously to the one for two disjoint intervals in periodic systems [170, 175, 171]. Some general results for $\mathcal{F}_n(x)$ in the boundary compact boson CFT (Luttinger liquid) appeared only recently [250, 251].

In this Chapter, we consider the symmetry resolved entanglement of CFT and free fermionic systems with boundaries. In Sec. 3.2 we present our results for the symmetry resolved entanglement within boundary CFT. In Sec. 3.3 we move to free fermions on the semi-infinite line and consider a block starting from the boundary which can be analysed with a generalisation of the Fisher-Hartwig formula. In order to study the case of a block away from the boundary, we first prove in Sec. 3.4 a general relation between the spectra of certain Toeplitz+Hankel matrices (related to the case of interest) and block Toeplitz ones (related to two disjoint blocks in an infinite chain). Hence in Sec. 3.5 we calculate the charged entropy for two blocks in an infinite chain, which are then used in Sec. 3.6 to infer the results for the interval away from the boundary. We conclude in Sec. 3.7 with a summary of the results and further discussions.

3.2 Entanglement entropy, CFT, and boundaries

In this section we present our boundary CFT results for the charged and symmetry resolved entropies. We start from a 1D system in a semi-infinite line $[0;\infty)$ and a subsystem A consisting in a finite interval $[0;\ell)$ as in Fig. 3.1. From general CFT scaling, one expects the charged moments $Z_n(\alpha)$ to be

$$Z_n(\alpha) \equiv \mathrm{Tr}\left[\rho_A^n e^{\mathrm{i}Q_A\alpha}\right] = \langle \mathcal{T}_{n,\alpha}(\ell)\rangle_{\mathrm{HP}} = \tilde{c}_{n,\alpha}(2\ell)^{-\frac{c}{12}(n-\frac{1}{n})-\frac{\Delta_\alpha}{n}}, \tag{3.2.1}$$

where the subscript HP stands for the average over the (right) half plane $z = x + \mathrm{i}\tau$ with $x \in \mathbb{R}^+$ and $\tau \in \mathbb{R}$. Anyhow, it is worth to obtain such (correct) prediction from first principles by merging the boundary CFT approach to the EE [25, 26] with the insertion of the Aharonov-Bohm flux [35].

The n-sheeted Riemann surface then consists of n copies of the half plane $x \geq 0$ sewn together along $0 \leq x \leq \ell, \tau = 0$ (see Sect. 1.4.2). Once again, the flux between the j-th and $(j+1)$-th replicas can be implemented by the definition of local composite twist fields $\mathcal{T}_{n,\alpha} = \mathcal{T}_n\mathcal{V}_\alpha$ at the end-point of the region A, where $\mathcal{V}_\alpha$ is responsible for the Aharonov-Bohm flux and $\mathcal{T}_n$ generates the Riemann geometry. The scaling dimension of the composite twist field is obtained by evaluating the expectation value of the total stress-energy tensor $T(w) = \sum_{j=1}^n T_j(w)$ in the Riemann geometry $\mathcal{R}_n$ with inserted flux α. First, the transformation

$$z = \left(\frac{\ell - w}{\ell + w}\right)^{1/n}, \tag{3.2.2}$$

maps the whole Riemann surface into the unit disc $\mathcal{D} = \{|z| < 1\}$ with the flux α. Thus we have

$$\langle T(w)\rangle_{\mathcal{R}_{n,\alpha}} = \sum_j \left(\frac{\mathrm{d}z}{\mathrm{d}w}\right)^2 \langle T_j(z)\rangle_{\mathcal{D},\alpha} + \frac{nc}{12}\{z,w\}, \tag{3.2.3}$$

where the Schwartzian derivative is given in this case by

$$\frac{c}{12}\{z,w\} = \frac{c}{24}\left(1 - \frac{1}{n^2}\right)\frac{(2\ell)^2}{(w-\ell)^2(w+\ell)^2}. \tag{3.2.4}$$

In Eq. (3.2.3) we added the subscript α to stress that the expectation values are taken in the presence of a flux. Notice that $\langle T_j(z)\rangle_{\mathcal{D},\alpha}$ is non-zero for $\alpha \neq 0$. To calculate it, let us start by noticing that the transformation (3.2.2) maps the subsystem A (say on the first sheet) into $[0,1]$ and the branch point into the origin. Hence, a closed path encircling the branch point n times is mapped into a single-winding orbit around the origin so that

$$\langle T_j(z)\rangle_{\mathcal{D},\alpha} = \frac{\langle T_j(z)\mathcal{V}_\alpha(0)\rangle_{\mathcal{D}}}{\langle \mathcal{V}_\alpha(0)\rangle_{\mathcal{D}}}, \tag{3.2.5}$$

where the subscript $\mathcal{D}$ (without α) refers to the expectation values on the unit disk in the absence of the flux. When $\mathcal{V}_\alpha$ is a primary operator, the right hand side of Eq. (3.2.5) is Δ_α/z^2 [162] and hence

$$\langle T_j(z)\rangle_{\mathcal{D},\alpha} = \frac{\Delta_\alpha}{z^2}. \tag{3.2.6}$$

Plugging the above expression and the Schwartzian derivative (3.2.4) into Eq. (3.2.3) ones get

$$\frac{\langle T(w)\mathcal{T}_{n,\alpha}(\ell)\rangle_{\mathrm{HP}}}{\langle \mathcal{T}_{n,\alpha}(\ell)\rangle_{\mathrm{HP}}} = \left[\frac{c}{24}\left(n - \frac{1}{n}\right) + \frac{\Delta_\alpha}{n}\right]\frac{(2\ell)^2}{(w-\ell)^2(w+\ell)^2}. \tag{3.2.7}$$

The comparison of Eq. (3.2.7) with the conformal Ward identity for BCFT [162] confirms that also in the presence of boundaries, the scaling dimension of the composite twist fields is

$$d_n = 2\Delta_n = \frac{c}{12}\left(n - \frac{1}{n}\right), \tag{3.2.8}$$

leading immediately to the expected result (3.2.1). Taking the Fourier transform by saddle point approximation, one obtains the asymptotic symmetry resolved moments

$$\mathcal{Z}_n(q) \simeq (2\ell)^{-\frac{c}{12}\left(n-\frac{1}{n}\right)} \sqrt{\frac{n\pi}{K\log\ell}} \mathrm{e}^{\frac{n\pi^2(q-\bar{q})^2}{K\log\ell}}. \tag{3.2.9}$$

The other situation of interest is that of an interval of length ℓ placed at distance ℓ_0 from the boundary. In this case, global conformal invariance fixes the overall scaling. Indeed, the charged moment is a two-point function $Z_n(\alpha) = \langle \mathcal{T}_{n,\alpha}(u_1)\tilde{\mathcal{T}}_{n,\alpha}(v_1)\rangle_{\mathrm{HP}}$ with $u_1 = \ell_0$ and $v_1 = \ell + \ell_0$. By image charges technique, this is related to a four-point function on the plane with images at $u_2 = -v_1$ and $v_2 = -u_1$. The scaling of a general four four-point function of composite twist fields is

$$\langle \mathcal{T}_{n,\alpha}(u_2)\tilde{\mathcal{T}}_{n,\alpha}(v_2)\mathcal{T}_{n,\alpha}(u_1)\tilde{\mathcal{T}}_{n,\alpha}(v_1)\rangle = c_{n,\alpha}^2 \left(\frac{|u_1-u_2||v_1-v_2|}{|u_1-v_1||u_2-v_2||u_1-v_2||u_2-v_1|}\right)^{2\Delta_{n,\alpha}} \mathcal{F}_{n,\alpha}(x), \tag{3.2.10}$$

where $\mathcal{F}_{n,\alpha}(x)$ is a universal function that depends on the operator content of the CFT and x is the anharmonic ratio of the four points. The desired boundary correlation is related to the square root of the bulk four-point function, and hence, specifying to the actual values of u_i and v_i, we have

$$\mathrm{Tr}\left[\rho_A^n e^{\mathrm{i}Q_A\alpha}\right] = \langle \mathcal{T}_{n,\alpha}(u_1)\tilde{\mathcal{T}}_{n,\alpha}(v_1)\rangle_{\mathrm{HP}} = c_{n,\alpha}\left(\frac{(2\ell_0+\ell)^2}{4\ell^2\ell_0(\ell+\ell_0)}\right)^{\Delta_{n,\alpha}} \mathcal{F}_{n,\alpha}(x), \tag{3.2.11}$$

where $\mathcal{F}_{n,\alpha}(x)$ is a universal function of the anharmonic ratio x in (3.1.2) that depends on the operator content of the *boundary* CFT. As $\ell_0 \gg \ell$, using $\mathcal{F}_{n,\alpha}(0) = 1$, Eq. (3.2.11) tends to the results for one interval in an infinite system (2.2.13), as it should. Conversely, for $\ell_0 \ll \ell$, one recovers the result for the interval close to the boundary, cf. Eq. (3.2.1), in which the relation between $c_{n,\alpha}$ and $\tilde{c}_{n,\alpha}$ (generalisation to $\alpha \neq 0$ of Eq. (1.4.52))

$$\frac{\tilde{c}_{n,\alpha}}{c_{n,\alpha}^{1/2}} = g^{1-n}, \tag{3.2.12}$$

is provided by the singular behaviour of $F_{n,\alpha}(x)$ close to $x = 1$.

Finally, let us briefly mention what happens for a finite system of length L with OBC on both sides (which is the most relevant situation for physical applications, as e.g., those in Refs. [248, 192]). The worldsheet of each replica is an infinite (in the time direction) strip of length L. This can be mapped to the half plane by a conformal transformation (the logarithm). Hence the net effect of having a finite system is just to replace all separations in Eqs. (3.2.1) and (3.2.11) with the appropriate chord distance, e.g. in Eq. (3.2.1) we have the replacement

$$\ell \to \frac{L}{\pi}\sin\frac{\pi\ell}{L}, \tag{3.2.13}$$

and similarly in Eq. (3.2.11). In the same way, one can consider a semi-infinite system at finite temperature, with the worldsheet being a semi-infinite cylinder that can be mapped to the half

plane by a conformal transformation. Simple algebra leads to the replacement $2\ell \to \frac{\beta}{\pi} \sinh \frac{2\pi\ell}{\beta}$ [25, 26], with β being the inverse temperature.

We conclude this section briefly mentioning what happens for the resolution of discrete symmetries (a problem that attracted some attention in recent times, see e.g. [53, 58]) in the presence of boundaries. Let us focus for concreteness on a Z_N charge. The charged moments in boundary CFTs are always given by Eq. (3.2.11), with proper scaling dimensions $\Delta_{n,\alpha}$ [53, 58]. From these, the charge moments are obtained as

$$\mathcal{Z}_n(q) = \frac{1}{N} \sum_{\alpha=0}^{N-1} Z_n(\alpha) \mathrm{e}^{-\mathrm{i}\frac{2\pi\alpha q}{N}}, \tag{3.2.14}$$

rather than Eq. (2.2.8) for the $U(1)$ charge. For other discrete symmetries, one should only adapt the sum above to the structure of the symmetry group.

3.3 Semi-infinite chain of free fermions: the block $A = [1, \ell]$

The results in the previous section are valid for an arbitrary boundary CFT. In this section, we specialise to a particular microscopic model whose low energy physics is captured by a CFT. We wish to calculate also the non-universal factors (not predicted by CFT) that enter in a parameter-free comparison with numerics.

We focus on the tight-binding model given by the Hamiltonian (2.3.1), which describes free fermions hopping on a 1D lattice and can be mapped to the XX spin chain via Jordan-Wigner transformations. The fermionic RDM (2.3.2) is equal to the spin RDM for the same subsystem A only when A is one interval (starting from the boundary if PBC are not imposed), because the Jordan-Wigner transformation is local within a compact subset. Conversely, for a non-compact bipartition $A \cup \bar{A}$ (such as for disjoint intervals with PBC or one interval away from the boundary in an open chain) the non-local nature of the Jordan-Wigner string makes the spin and fermion RDMs different [252, 253, 254]. We denote with $|A|$ the total number of sites within A (i.e. the length ℓ for a single interval).

We work with a semi-infinite chain, i.e. $l \in \mathbb{N}$, and the first site on the left is free, i.e. we choose open boundary conditions.

The fermion correlation function between two arbitrary sites i, j [221] is

$$(C_A)_{ij} = \frac{\sin\left(k_F(i-j)\right)}{\pi(i-j)} - \frac{\sin\left(k_F(i+j)\right)}{\pi(i+j)}. \tag{3.3.1}$$

For an arbitrary spatial bipartition $A \cup \bar{A}$, the elements of the correlation matrix C_A are just given by the above correlation with indices i, j restricted in A. The first term in Eq. (3.3.1) is the same as in the infinite system (cf. Eq. (2.3.3)) and it depends only on the spatial distance between the two points as a consequence of translational invariance. The second term breaks the latter symmetry and depends on the average distance from the boundary (and it vanishes for large i, j at fixed separation $|i-j|$, when only the first term survives).

Having constructed the subsystem correlation matrix, the entanglement spectrum and so the REs (total and symmetry resolved) follow from the general results in Sec. 2.3.1. In particular, the charged moments are given by Eq. (2.3.6) in terms of the eigenvalues ν_j of the matrix C_A. In the following we specialise to two bipartitions that can be handled analytically, which are the ones depicted in Fig. 3.1 with one block of ℓ sites at distance ℓ_0 from the boundary (that can be

$\ell_0 = 0$, recovering an interval starting from the boundary). The $\ell \times \ell$ correlation matrix may be written as

$$(C_A)_{ij} = f_{i-j} - f_{i+j+2\ell_0}, \qquad i,j = 1,\dots,\ell, \qquad \ell_0 = 0,1,2,\dots \tag{3.3.2}$$

with f_k the elements of the correlation matrix for the infinite system in Eq. (2.3.3). The first term in the rhs of Eq. (3.3.2) is a Toeplitz part, since it depends only on the difference of the indices, and is equal to the matrix for an infinite system; the second term is a Hankel matrix since it depends only on the *sum* of the indices and it comes from the presence of the boundary. The correlation matrix C_A in Eq. (3.3.2) is then equal to the sum of one Toeplitz matrix and a Hankel one.

3.3.1 A generalised Fisher-Hartwig formula and charged entropies

In the case of a block starting from the boundary, i.e. with $\ell_0 = 1$, the Toeplitz+Hankel matrix in Eq. (3.3.2) has been studied a lot in both the mathematical and physics literature [255, 229, 256]. The final result of interest for our paper is the conjectured form for a generalised Fisher-Hartwig expansion [229]

$$D_A(\lambda) \simeq (\lambda+1)^\ell \left(\frac{\lambda+1}{\lambda-1}\right)^{-\frac{k_F \ell}{\pi}} \sum_{m\in\mathbb{Z}} \mathrm{e}^{\mathrm{i}\frac{\pi}{2}(\beta+m)} \left[4\left(\ell+\frac{1}{2}\right)|\sin k_F|\right]^{-(m+\beta_\lambda)^2} \times \mathrm{e}^{-2\mathrm{i}k_F(\beta+m)(\ell+1/2)} G(m+1+\beta_\lambda) G(1-m-\beta_\lambda), \tag{3.3.3}$$

where β_λ is defined in Eq. (2.3.18) and $G(z)$ is the Barnes function. This formula was conjectured in Ref. [229] in such a way to reproduce the results for $m = 0$ derived rigorously in Ref. [255] and generalising heuristically to the existence of inequivalent representations of the symbol. The term $1/2$ added to ℓ has been introduced to absorb some of the subleading corrections to better match numerical evaluation of the determinant and has not a rigorous basis (we will see in the following section another reason for its presence). This asymptotic expansion has been used to compute the moments of the RDM $\mathrm{Tr}\rho_A^n$, for which the leading term corresponds to $m = 0$, while the first corrections are given by $m = \pm 1$. For the charged moments $Z_n(\alpha)$, restricting by periodicity to $\alpha \in [-\pi, \pi]$, the leading term is still given by $m = 0$, see also the discussion in Ref. [53].

The leading term

The leading behaviour of the determinant $D_A(\lambda)$ is given by

$$D_A^{(0)}(\lambda) \sim \mathrm{e}^{\mathrm{i}\left(\frac{\pi}{2}-k_F\right)\beta_\lambda} \left[(\lambda+1)\left(\frac{\lambda+1}{\lambda-1}\right)^{-\frac{k_F}{\pi}}\right]^\ell (4\ell|\sin k_F|)^{-\beta_\lambda^2} G(1-\beta_\lambda) G(1+\beta_\lambda), \tag{3.3.4}$$

(at the leading order we can drop the $1/2$ in the generalised form) so that the leading contribution to the charged moments (2.3.12) is

$$\log Z_n^{(0)}(\alpha) = \frac{1}{2\pi\mathrm{i}} \oint \mathrm{d}\lambda f_{n,\alpha}(1,\lambda) \frac{\mathrm{d}\log D_\ell^{(0)}(\lambda)}{\mathrm{d}\lambda} = a_0 + a_1\ell + a_2 \log L_k + a_3, \tag{3.3.5}$$

where

$$
\begin{aligned}
a_0 &= \frac{1}{2\pi}\left(\frac{\pi}{2}-k_F\right)\oint \mathrm{d}\lambda f_{n,\alpha}(1,x)\frac{\mathrm{d}}{\mathrm{d}\lambda}\beta_\lambda,\\
a_1 &= \frac{1}{2\pi \mathrm{i}}\oint \mathrm{d}\lambda f_{n,\alpha}(1,\lambda)\left(\frac{1-k_F/\pi}{1+\lambda}-\frac{k_F/\pi}{1-\lambda}\right),\\
a_2 &= \frac{1}{2\pi i}\oint \mathrm{d}\lambda f_{n,\alpha}(1,\lambda)\frac{\mathrm{d}(-\beta_\lambda^2)}{\mathrm{d}\lambda} = \frac{1}{\pi^2}\oint \mathrm{d}\lambda f_n(\lambda,\alpha)\frac{\beta_\lambda}{1-\lambda^2},\\
a_3 &= \frac{1}{2\pi \mathrm{i}}\oint \mathrm{d}\lambda f_{n,\alpha}(1,\lambda)\frac{\mathrm{d}\log[G(1-\beta_\lambda)G(1+\beta_\lambda)]}{\mathrm{d}\lambda}.
\end{aligned}
\tag{3.3.6}
$$

Putting everything together, the final result is

$$
\log Z_n^{(0)}(\alpha) = \frac{\mathrm{i}\alpha k_F \ell}{\pi} + \left[\frac{\mathrm{i}\alpha}{2}\left(\frac{k_F}{\pi}-\frac{1}{2}\right)\right] - \left[\frac{1}{12}\left(n-\frac{1}{n}\right)+\frac{1}{n}\left(\frac{\alpha}{2\pi}\right)^2\right]\log\left[4\ell|\sin k_F|\right] + \frac{\Upsilon(n,\alpha)}{2},
\tag{3.3.7}
$$

where the real constant $\Upsilon(n,\alpha)$ is the same as the one in Eq. (2.3.27). Let us now discuss the various terms, emphasising the differences with the case of the infinite system in Eq. (2.3.26). The purely imaginary term gives the average number of particles in the interval ℓ which is

$$
\bar{q} \equiv \langle Q_A\rangle = \frac{k_F}{\pi}\ell + \frac{1}{2}\left(\frac{k_F}{\pi}-\frac{1}{2}\right) + o(1)\,.
\tag{3.3.8}
$$

The leading piece, proportional to ℓ, is the average density also present in the infinite system. The $O(1)$ correction is the more interesting and represents the variation of the number due the inhomogeneity close to the boundary. Indeed the density at the site j is $n_j = k_F/\pi - \sin(2k_F j)/(2\pi j)$ (i.e. the correlation (3.3.1) at coinciding points). Thus, the mean number of particles in $[1,\ell]$ is

$$
\langle Q_A\rangle - \frac{k_F}{\pi}\ell = -\sum_{j=1}^{\ell}\frac{\sin(2k_F j)}{2\pi j} = -\sum_{j=1}^{\infty}\frac{\sin(2k_F j)}{2\pi j} + O(\ell^{-1}) = \frac{1}{2}\left(\frac{k_F}{\pi}-\frac{1}{2}\right)+o(1)\,.
\tag{3.3.9}
$$

At half-filling this term is obviously zero since there is no inhomogeneity.

Let us now move to the other pieces in Eq. (3.3.7). The logarithmic term agrees with the boundary CFT prediction (3.2.1) for this specific model and confirms the dimension of the modified twist fields. Interesting enough, also the non-universal constant is related to the one in the absence of boundaries and satisfies the universal relation (3.2.12) with $g=1$, as well known.

In Fig. 3.2 we present the comparison between the analytical formula (3.3.7) and the exact numerical data obtained for the charged REs for different values of n and α, at filling $k_F=\pi/2$ and $k_F=\pi/3$. It is evident that the data are slowly approaching the exact predictions, but there are large oscillating corrections to the scaling whose amplitude increases with n and α. These corrections do not come as a surprise: they have been intensively studied for the total EE both for periodic [234, 217, 235, 237, 236] and open boundary conditions [249, 229]. For the charged moments with $\alpha\neq 0$ and PBC, they have been described and characterised in Refs. [1, 53]. In the following subsection we will derive and quantify them for OBC.

The leading corrections to the scaling for the charged entropies

The corrections to the scaling are encoded in the generalised Fisher-Hartwig formula (3.3.3). The precise order in which they appear depends on the quantity to be calculated. It is straightforward to convince ourselves that for $0<\alpha<\pi$ ($-\pi<\alpha<0$) the leading correction is the

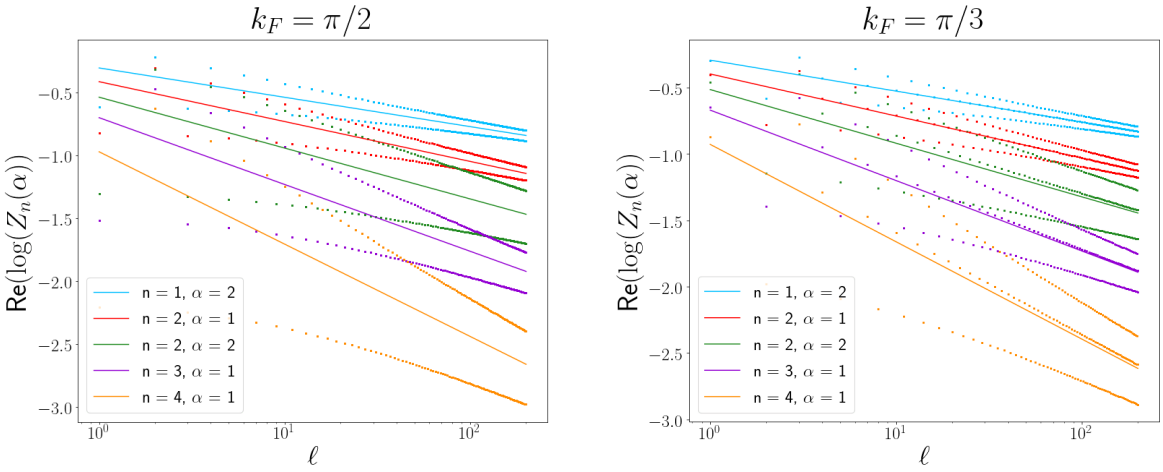


Figure 3.2: Real part of the charged REs $\log Z_n(\alpha)$ with the insertion of a flux α as functions of ℓ. The exact numerical results (symbols) are shown for different values of α and n at fillings $k_F = \pi/2$ (left) and $k_F = \pi/3$ (right). The numerical data present a slow approach to the asymptotic behaviour (3.3.7), with large oscillating corrections to the scaling.

one with $m = 1$ ($m = -1$). For $\alpha = 0$ the terms $m = \pm 1$ are of the same order. If not yet clear, all this will be evident and self-consistent at the end of the calculation in this subsection.

We perform the calculation keeping only the two terms with $m = \pm 1$ and approximate the characteristic polynomial $D_A(\lambda)$ as

$$\begin{aligned} D_A(\lambda) &\simeq D_A^{(0)}(\lambda)\left\{1 + \mathrm{i}\mathrm{e}^{-\mathrm{i}k_F\ell}\mathrm{e}^{-2\mathrm{i}k_F\ell}L_k^{-1-2\beta_\lambda}\frac{\Gamma(1+\beta)}{\Gamma(-\beta_\lambda)} - \mathrm{i}\mathrm{e}^{\mathrm{i}k_F\ell}\mathrm{e}^{2\mathrm{i}k_F\ell}L_k^{-1+2\beta_\lambda}\frac{\Gamma(1-\beta_\lambda)}{\Gamma(\beta_\lambda)}\right\} \\ &\equiv D_A^{(0)}(\lambda)(1+\Psi_\ell(\lambda)), \end{aligned} \tag{3.3.10}$$

where the leading term $D_A^{(0)}(\lambda)$ is the one in Eq. (3.3.4) and we introduced the shorthand

$$L_k = 4\left(\ell + \frac{1}{2}\right)|\sin k_F|. \tag{3.3.11}$$

The corrections to the scaling are characterised by the difference

$$d_n(\alpha) \equiv \log Z_n(\alpha) - \log Z_n^{(0)}(\alpha), \tag{3.3.12}$$

that for large L_k can be written as

$$d_n(\alpha) \simeq \frac{1}{2\pi\mathrm{i}}\oint \mathrm{d}\lambda f_{n,\alpha}(1,x)\frac{\mathrm{d}\log[1+\Psi_\ell(\lambda)]}{\mathrm{d}\lambda} = \frac{1}{2\pi\mathrm{i}}\oint \mathrm{d}\lambda f_{n,\alpha}(1,\lambda)\frac{\mathrm{d}\Psi_\ell(\lambda)}{\mathrm{d}\lambda} + \cdots. \tag{3.3.13}$$

The contour integral can be split as the sum of two contributions above and below the segment $[-1,1]$

$$d_n(\ell) \simeq \frac{1}{2\pi\mathrm{i}}\left[\int_{-1+\mathrm{i}\epsilon}^{1+\mathrm{i}\epsilon} - \int_{-1-\mathrm{i}\epsilon}^{1-\mathrm{i}\epsilon}\right]\mathrm{d}\lambda f_{n,\alpha}(1,\lambda)\frac{\mathrm{d}\Psi_\ell(\lambda)}{\mathrm{d}\lambda}. \tag{3.3.14}$$

The integral is then given by the discontinuity at the branch cut; the only discontinuous function along this cut is β_λ, that we rewrite as (for $-1 < x < 1$)

$$\beta_{x\pm\mathrm{i}\epsilon} = -\mathrm{i}w(x) \mp \frac{1}{2}, \qquad \text{with} \qquad w(x) = \frac{1}{2\pi}\log\frac{1+x}{1-x}. \tag{3.3.15}$$

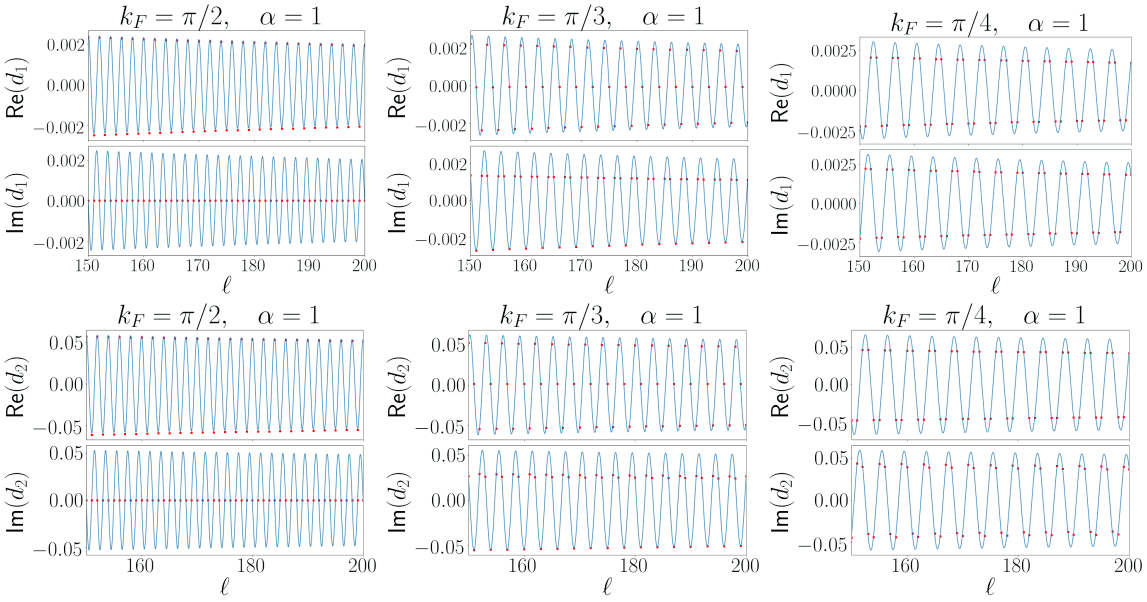


Figure 3.3: Leading corrections to the scaling for the charged entropies. The plots show the difference $d_n(\alpha)$ defined in Eq. (3.3.12). We focus on $\alpha = 1$, $n = 1, 2$ and different fillings $k_F = \pi/2$ (left), $k_F = \pi/3$ (center) and $k_F = \pi/4$ (right) as function of ℓ. The numerical data (symbols) match well the calculated leading correction to the scaling (3.3.22) from generalised Fisher-Hartwig formula both for real and imaginary parts.

Hence the discontinuities across the branch cut given by the two terms in Ψ_ℓ are respectively

$$\left[L_k^{-\mathrm{i}-2\beta}\frac{\Gamma(1+\beta)}{-\beta}\right]_{\beta=-\mathrm{i}w-\frac{1}{2}} - \left[L_k^{-\mathrm{i}-2\beta}\frac{\Gamma(1+\beta)}{-\beta}\right]_{\beta=-\mathrm{i}w+\frac{1}{2}} \simeq L_k^{2\mathrm{i}w}\gamma(w), \tag{3.3.16}$$

$$\left[L_k^{-\mathrm{i}+2\beta}\frac{\Gamma(1+\beta)}{-\beta}\right]_{\beta=-\mathrm{i}w-\frac{1}{2}} - \left[L_k^{-\mathrm{i}+2\beta}\frac{\Gamma(1+\beta)}{-\beta}\right]_{\beta=-\mathrm{i}w+\frac{1}{2}} \simeq L_k^{-2\mathrm{i}w}\gamma(-w), \tag{3.3.17}$$

where we dropped terms of order $O(L_k^{-2})$ compared to the leading ones and defined

$$\gamma(w) = \frac{\Gamma\left(\frac{1}{2} - \mathrm{i}w\right)}{\Gamma\left(\frac{1}{2} + \mathrm{i}w\right)}. \tag{3.3.18}$$

We can now perform the change of variable

$$\lambda = \tanh(\pi w), \qquad -\infty < w < \infty, \tag{3.3.19}$$

and integrate by parts using

$$\frac{\mathrm{d}}{\mathrm{d}w} f_n(\tanh(\pi w), \alpha) = \pi n \left[\tanh(\pi n w + \mathrm{i}\alpha/2) - \tanh(\pi w)\right], \tag{3.3.20}$$

to finally get

$$d_n(\alpha) \simeq \frac{\mathrm{i}n}{2}\int_{-\infty}^{\infty} \mathrm{d}w \left(\tanh(\pi w) - \tanh(\pi n w + \mathrm{i}\alpha/2)\right) \times \\ \left[\mathrm{i}\mathrm{e}^{-\mathrm{i}k_F}\mathrm{e}^{-2\mathrm{i}k_F\ell} L_k^{2\mathrm{i}w}\gamma(w) + \mathrm{i}\mathrm{e}^{\mathrm{i}k_F}\mathrm{e}^{2\mathrm{i}k_F\ell} L_k^{-2\mathrm{i}w}\gamma(-w)\right]. \tag{3.3.21}$$

This last integral can be performed on the complex plane by residue theorem. For the first piece of the integral in square brackets, we must close the contour in the upper half plane, while for the second piece in the lower half plane. In principle, we should sum over all residues inside the integration contour, but, since we are interested in the limit of large L_k, we can limit ourselves to consider the singularities closest to the real axis. For the first integral this is at $w = \mathrm{i}/(2n)(1-\alpha/\pi)$ while for the second one it is at $w = -\mathrm{i}/(2n)(1+\alpha/\pi)$. Their sum gives

$$d_n(\alpha) \simeq \mathrm{i}\mathrm{e}^{-\mathrm{i}k_F(2\ell+1)} L_k^{-\frac{1}{n}\left(1-\frac{\alpha}{\pi}\right)} \frac{\Gamma\left(\frac{1}{2}+\frac{1}{2n}-\frac{\alpha}{2\pi n}\right)}{\Gamma\left(\frac{1}{2}-\frac{1}{2n}+\frac{\alpha}{2\pi n}\right)} - \mathrm{i}\mathrm{e}^{\mathrm{i}k_F(2\ell+1)} L_k^{-\frac{1}{n}\left(1+\frac{\alpha}{\pi}\right)} \frac{\Gamma\left(\frac{1}{2}+\frac{1}{2n}+\frac{\alpha}{2\pi n}\right)}{\Gamma\left(\frac{1}{2}-\frac{1}{2n}-\frac{\alpha}{2\pi n}\right)}. \tag{3.3.22}$$

This expression represents our final result for the oscillating corrections to the scaling. Let us comment it. For $\alpha = 0$ the corrections are real and give back the result already found in Ref. [229]. Otherwise, Eq. (3.3.22) is valid only in the range $-\pi \leq \alpha \leq \pi$ and must be extended periodically outside of it. Mathematically, one can found the periodic structure using the entire sum in the generalised Fisher-Hartwig formula (3.3.3). This periodicity in α is identical to what found for PBC in Ref. [53] to which we remand for an extensive discussion. Within the principal domain $-\pi \leq \alpha \leq \pi$, the two contributions decay with different power laws (as anticipated above), so that only one of the two is dominating, according to the sign of α. However, they become comparable in magnitude as α approaches zero where one should carefully take into account both of them. Conversely, for α close to $\pm\pi$, the calculated corrections with $m = \pm 1$ become comparable with the leading term ($m = 0$) and hence a good agreement between Eq. (3.3.22) and the data is achieved only at extremely large ℓ, since in the derivation we assumed that the leading term is much larger than the corrections.

In Fig. 3.3 we report the exact numerical data for $d_n(\alpha)$ at fixed $\alpha = 1$ and $n = 1, 2$. We observe that, for different fillings, the data always match well the analytic prediction (3.3.22) both for real and imaginary part. Remarkably, the sampling at commensurate points due to the integer values of ℓ, match well the oscillating structure due to the partial fillings.

3.3.2 Symmetry resolved moments and entropies

We are finally ready to evaluate the symmetry resolved moments $\mathcal{Z}_n(q)$ as Fourier transform of $Z_n(\alpha)$. As we already did in Sec. 2.4.1 for the infinite interval case, we use a saddle-point approximation in which $Z_n(\alpha)$ is Gaussian and hence we truncate hereafter $Z_n^{(0)}(\alpha)$ in Eq. (3.3.7) at quadratic order in α. Consequently, the charged partition function can be well approximated as

$$Z_n(\alpha) = Z_n(0)\mathrm{e}^{\mathrm{i}\alpha\bar{q} - b_n\alpha^2/2}, \tag{3.3.23}$$

where

$$b_n = \frac{b}{\pi^2 n}\ln\ell - h_n, \tag{3.3.24}$$

with

$$b = \frac{1}{2}, \qquad h_n = -\frac{1}{n}\frac{1}{2\pi^2}\log(4|\sin k_F|) + \gamma_2(n). \tag{3.3.25}$$

In this way, the Fourier transform is a simple Gaussian integral, with result

$$\mathcal{Z}_n(q) = \frac{Z_n(0)}{\sqrt{2\pi b_n}}\mathrm{e}^{-\frac{(q-\bar{q})^2}{2b_n}}. \tag{3.3.26}$$

We observe that the present case we adopt a slightly different notation with respect to the case of the infinite chain, rewriting Eq. (3.3.23) in a rather generic fashion as a function of b_n. The

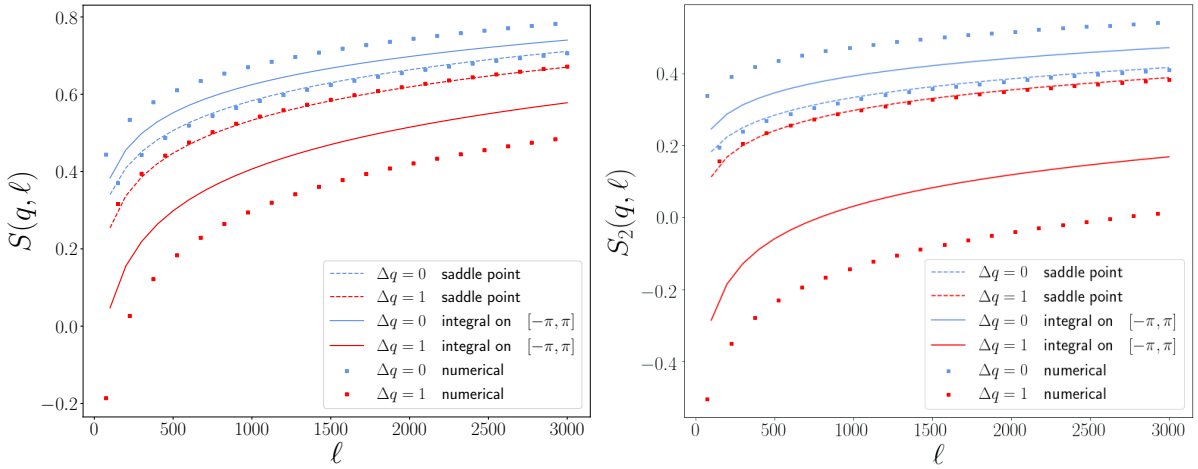


Figure 3.4: Von Neumann (left) and second Rényi (right) symmetry resolved EEs at half filling $k_F = \pi/2$ for one interval of length ℓ starting from the boundary. The analytical predictions (dashed lines) in Eq. (3.3.28) with the amplitudes in Eq. (3.3.25) are compared with the numerical data (symbols) for $\Delta q = q - \bar{q} = 0, 1$. The agreement of the saddle point results with the numerical data is rather unsatisfactory. The observed deviations are caused by the finite domain of the integral in α, and are well captured by Eq. (3.3.30) reported as full lines which falls in the middle between the data for even and odd ℓ.

reason is that in both the cases studied here (and elsewhere [62, 49, 54]) only the specific form of b_n (or h_n) matters, and the final result for the symmetry resolved REs can be conveniently rewritten as function of such amplitudes as

$$S_n(q) = S_n - \frac{1}{2}\ln(2\pi) + \frac{1}{1-n}\ln\frac{b_1(\ell,t)^{n/2}}{b_n(\ell,t)^{1/2}} - \frac{q^2}{2(1-n)}\left(\frac{1}{b_n(\ell,t)} - \frac{n}{b_1(\ell,t)}\right), \tag{3.3.27}$$

where S_n is the total entropy. Expanding for large ℓ, we have

$$S_n(q) = S_n - \frac{1}{2}\ln\left(\frac{2b}{\pi}\ln\delta_n\ell\right) + \frac{\ln n}{2(1-n)} - \frac{\pi^4 n(h_1 - nh_n)^2}{4(1-n)^2(b\ln\ell)^2} + \\ + (q-\bar{q})^2 n\pi^4 \frac{h_1 - nh_n}{2(1-n)(b\ln\ell\kappa_n)^2} + o(\ln\ell^{-2}), \tag{3.3.28}$$

where, following Ref. [1] we absorbed some subleading corrections in the amplitudes as

$$\ln\delta_n = -\frac{\pi^2 n(h_n - h_1)}{b(1-n)}, \qquad \ln\kappa_n = -\pi^2\frac{(h_1 + nh_n)}{2b}. \tag{3.3.29}$$

The above formula is valid also for the symmetry resolved Von Neumann entropy taking properly the limits of the various pieces as $n \to 1$.

In Fig. 3.4, we compare the analytical predictions for the symmetry resolved EEs with the numerical data, focusing on half filling $k_F = \pi/2$. The agreement is overall rather unsatisfactory, the asymptotic curves look rather close to data for even ℓ, but too far from those at odd ℓ. Although the oscillations are very large, we would have expected the analytic curves to be in the middle of the data, as it happens for the charged moments. Actually, the reason of this

disagreement is easily identified. Indeed, the asymptotic curve in the saddle point approximation is given by the Fourier transform of $Z_n(\alpha)$ where the integral has domain on the entire real axis, rather than the interval $[-\pi,\pi]$. The difference between the two is exponentially small in the variance b_n, and hence is usually neglected. However, the variance only grows as $\log \ell$; consequently the corrections are algebraic in ℓ and so rather visible. The data at finite, even large, ℓ should be better described by the integral on the domain $[-\pi,\pi]$, i.e.

$$\mathcal{Z}_n(q) \simeq Z_n(0)\int_{-\pi}^{\pi}\frac{\mathrm{d}\alpha}{2\pi}\mathrm{e}^{-\mathrm{i}\alpha(q-\tilde{q})-b_n\alpha^2/2} = Z_n(0)\mathrm{e}^{-\frac{\Delta q^2}{2b_n}}\frac{\mathrm{Erf}\left(\frac{\mathrm{i}\Delta q+\pi b_n}{\sqrt{2b_n}}\right)+\mathrm{Erf}\left(\frac{-\mathrm{i}\Delta q+\pi b_n}{\sqrt{2b_n}}\right)}{2\sqrt{2\pi b_n}}, \tag{3.3.30}$$

where $\mathrm{Erf}(z)$ is the error function. The symmetry resolved EEs obtained, via Eq. (**??**) are reported for $\Delta q = 0,1$ in Fig. 3.4 as continuous lines and, as expected, they fall right in the middle of the numerical data for even and odd ℓ. For extremely large ℓ, Eq. (3.3.30) clearly converges to the asymptotic result in Eq. (4.4.28). It is instructive to check analytically this slow approach, also to motivate the strong visible difference compared to the periodic case [1]. To this aim, let us focus on the case $\Delta q = 0$ which has the smallest corrections. The relative difference between the truly asymptotic behaviour and Eq. (3.3.30) is

$$\frac{\mathcal{Z}_n(0)-\mathcal{Z}_n^{\mathrm{asy}}(0)}{\mathcal{Z}_n^{\mathrm{asy}}(0)} \simeq \mathrm{Erfc}\left(\pi\sqrt{\frac{b_n}{2}}\right) \simeq \frac{\mathrm{e}^{-b_n\frac{\pi^2}{2}}}{\sqrt{\pi^3 b_n}} \sim \frac{\ell^{-\frac{b}{2n}}}{\sqrt{\log\ell}}, \tag{3.3.31}$$

where $\mathrm{Erfc}(z)$ is the complementary error function and in the last equality we only used the leading behaviour $b_n \sim b\log\ell$. It is clear that for OBC these corrections are much more severe than for the infinite system because $b = 1/2$ (instead of $b = 1$ with PBC). For example, for $n = 1$, which is the better behaving case among those in Fig. 3.4, we have corrections going like $\ell^{-1/4}$ which are extremely slow.

3.4 A general relation between Toeplitz+Hankel matrices and block Toeplitz ones

We have seen that in CFT the (charged and neutral) EEs of one interval in the middle of a semi-infinite chain are related to the ones of two intervals in an infinite chain. It is rather natural to wonder whether this correspondence has some akin for free fermions on the lattice. This is indeed the case and it is a consequence of a general relation between Toeplitz+Hankel matrices and block Toeplitz ones that we are going to show (and that in a similar form was present in Ref. [257], but for a slightly different class of matrices).

Let us start from the correlation matrix of two disjoint intervals of equal length ℓ at distance d in an infinite system. We denote this $2\ell\times 2\ell$ matrix by $C_2^{\ell,d}$ that is easily obtained from the correlation matrix of a single interval of length $2\ell+d$ given by Eq. (2.3.3) by erasing all rows and column between $\ell+1$ and $\ell+d$. It has the block structure

$$C_2^{\ell,d} = \begin{pmatrix} F & E^{d+\ell} \\ (E^{d+\ell})^T & F \end{pmatrix}, \qquad \text{with} \quad F_{i,j} = f_{i-j}, \quad E^k_{i,j} = f_{i-j+k}, \tag{3.4.1}$$

and $f_m = \frac{\sin(k_F m)}{\pi m}$ are the elements of the correlation matrix of the single interval (2.3.3), although what follows is true for arbitrary f_m such that $f_m = f_{-m}$. The four blocks in the matrix $C_2^{\ell,d}$ are Toeplitz matrices, but the total matrix is not. (Notice that by rearranging rows and

columns it is possible to write $C_2^{\ell,d}$ in such a way that it is a Toeplitz matrix in which the elementary block is a 2×2 matrix, a standard form in the literature, see e.g. [257]. However this not relevant for us.)

Let us denote by C_- the $\ell \times \ell$ correlation matrix of a block of length ℓ at distance ℓ_0 from the boundary of a semi-infinite system in Eq. (3.3.2), which can be written as

$$C_- = F - H^{2\ell_0}, \qquad \text{with} \quad H^{2\ell_0}_{i,j} = f_{i+j+2\ell_0}. \tag{3.4.2}$$

Let us also introduce the matrix

$$C_+ = F + H^{2\ell_0}, \tag{3.4.3}$$

which, incidentally, is the correlation matrix of a semi-infinite system with a Neumann boundary condition on the first site $i = 1$ (see e.g. [239]). Let us now assume that $\vec{v}_-$ is a ℓ-component vector, which is eigenvector of C_-, i.e. $C_-\vec{v}_- = \lambda_{v_-}\vec{v}_-$. Let us introduce the reverse of a vector $\vec{v}$ as $\vec{v}^R = (v_\ell, v_{\ell-1}, \dots v_1)$. Then, the 2ℓ-component vector $\vec{V}_- \equiv (\vec{v}^R_-, -\vec{v}_-)$ is an eigenvector of $C_2^{\ell,2\ell_0+1}$ with eigenvalue λ_{v_-}, as one straightforwardly shows, indeed

$$\begin{pmatrix} F & E^{2\ell_0+1+\ell} \\ (E^{2\ell_0+1+\ell})^T & F \end{pmatrix} \begin{pmatrix} \vec{v}_R \\ -\vec{v} \end{pmatrix} = \begin{pmatrix} F\vec{v}^R - E^{2\ell_0+1+\ell}\vec{v} \\ (E^{2\ell_0+1+\ell})^T\vec{v}^R - F\vec{v} \end{pmatrix}, \tag{3.4.4}$$

and the components of the top vector are

$$\sum_{j=1}^{\ell}(f_{i-j}v_{\ell+1-j} - f_{i-j+2\ell_0+1+\ell}v_j) = \sum_{j=1}^{\ell}(f_{i-j} - f_{i+j'+2\ell_0})v_{\ell+1-j}, \tag{3.4.5}$$

which is what we wanted to prove. The same goes on for the bottom vector in Eq. (3.4.4). Similarly, given an eigenvector $\vec{v}_+$ of C^+ of eigenvalue λ_{v_+}, we have that the vector $\vec{V}_+ \equiv (\vec{v}^R_+, \vec{v}_+)$ is eigenvector of $C_2^{\ell,2\ell_0+1}$ with eigenvalue λ_{v_+}. By construction, all vectors $\vec{V}_\pm$ are orthogonal and hence, since they are 2ℓ, they form a basis. The main conclusion here is that the spectrum of C_2 is the union of the spectra of C_+ and C_-, a rather remarkable result that likely is known in the literature, but we failed to find it (see however [257]). Thus we can generically relate the spectra of block Toeplitz matrices with Toeplitz+Hankel ones. We stress that these results are only valid in the fermionic basis and not in the spin one, where the structure is much more complicated because of the Jordan-Wigner string [254, 258].

Let us now move to the main objects of interest here that are the moments $Z_n(\alpha)$, both charged and neutral. Since they are just products of functionals of the eigenvalues of the respective correlation matrices, cf. Eq. (2.3.6), we have that the moment of two intervals of length ℓ at distance $2\ell_0 + 1$ in an infinite chain is the product of the moments built from C_+ and C_-. This is valid for arbitrary ℓ and ℓ_0. In the scaling limit $\ell, \ell_0 \to \infty$, with arbitrary ratio ℓ/ℓ_0, the moments built with C_+ and C_- are expected to become equal, because both boundary conditions correspond to the same boundary CFT with $g = 1$, see e.g. [259, 239]. Consequently, the scaling form of the moments of one interval at distance ℓ_0 from the boundary (with both free and Neumann conditions) is the square root of the one of two intervals of the same length at distance $2\ell_0 + 1$ in an infinite system.

3.5 Disjoint intervals in the infinite chain

En route to the calculation of the symmetry resolved entropies for a block away from the boundary, we first discuss the case of two disjoint intervals in an infinite system, since we have just

seen the two are related. In this case, the correlation matrix is given by Eq. (3.4.1). For the matrices with this structure, a generalisation of the Fisher-Hartwig formula has been conjectured in Ref. [231] for the evaluation of the total REs. Here, we just state the final result of Ref. [231] and refer the reader interested into more details to the original reference. We write the final result for a generic piecewise constant symbol $g(\theta)$ with R discontinuities at $\theta = \theta_r$ with $r = 1, \dots N$, although we are also interested in the case $R = 2$ in Eq. (2.3.16). We introduce $t_r \equiv g(\theta)$ with $\theta \in [\theta_{r-1}, \theta_r)$. We consider the subsystem $A = [u_1, v_1] \cup [u_2, v_2]$ of total length $|A| = v_1 - u_1 + v_2 - u_2$. The final result of Ref. [231] is

$$S_n(X) = A_n|A| + B_n \log \frac{(v_1-u_1)(v_2-u_2)(v_2-u_1)(u_2-v_1)}{(u_2-u_1)(v_2-v_1)} + 2C_n + \dots, \tag{3.5.1}$$

where the coefficients depend only on the symbol $g(\theta)$ and are given by

$$A_n = \frac{1}{2\pi} \int_{-\pi}^{\pi} \mathrm{d}\theta f_n(g(\theta)), \tag{3.5.2}$$

with $f_n(x) \equiv f_n(x, 0)$ in Eq. (2.3.11),

$$B_n = 2 \sum_{r=1}^{R} J_n(r, r), \tag{3.5.3}$$

$$C_n = \sum_{r=1}^{R} I_n(r) - \sum_{1 \le r \ne r' \le R} \log\left[2 - 2\cos(\theta_r - \theta_{r'})\right] J_n(r, r'), \tag{3.5.4}$$

where we defined

$$J_n(r, r') = \frac{1}{2\pi} \int_{t_{r-1}}^{t_r} \mathrm{d}\lambda \frac{\mathrm{d}f_n(\lambda)}{\mathrm{d}\lambda} \omega_{r'}(\lambda), \tag{3.5.5}$$

$$I_n(r) = \frac{1}{2\pi \mathrm{i}} \int_{t_{r-1}}^{t_r} \frac{\mathrm{d}f_n(\lambda)}{\mathrm{d}\lambda} \log\left[\frac{\Gamma\left(\frac{1}{2} - \mathrm{i}\omega_r(\lambda)\right)}{\Gamma\left(\frac{1}{2} + \mathrm{i}\omega_r(\lambda)\right)}\right] \mathrm{d}\lambda, \tag{3.5.6}$$

with

$$\omega_r(\lambda) = \frac{1}{2\pi} \log\left|\frac{\lambda - t_r}{\lambda - t_{r-1}}\right|. \tag{3.5.7}$$

For the specific case of two intervals in the ground state with only two singularities at $\pm k_F$, one finally has $A_n = 0$, $B_n = 1/6(n - 1/n)$, and $C_n = \mathrm{Y}_n$. This results agrees with the conformal field theory prediction $\mathcal{F}_n(x) = 1$ [40].

It is completely clear that for the charged entropy of two disjoint intervals, the final result is always given by Eq. (3.5.1) with the minor replacement $f_n(\lambda) \to f_n(\lambda, \alpha)$. Putting the various pieces together we arrive at

$$\log Z_n(\alpha) = A_{n,\alpha}|A| + B_{n,\alpha} \log \frac{(v_1-u_1)(v_2-u_2)(v_2-u_1)(u_2-v_1)}{(u_2-u_1)(v_2-v_1)} + 2C_{n,\alpha}, \tag{3.5.8}$$

with

$$A_{n,\alpha} = \frac{\mathrm{i}\alpha k_F}{\pi}, \tag{3.5.9}$$

$$B_{n,\alpha} = \frac{1}{6}\left(n - \frac{1}{n}\right) + \frac{2}{n}\left(\frac{\alpha}{2\pi}\right)^2, \tag{3.5.10}$$

$$C_{n,\alpha} = \mathrm{Y}_n(\alpha). \tag{3.5.11}$$

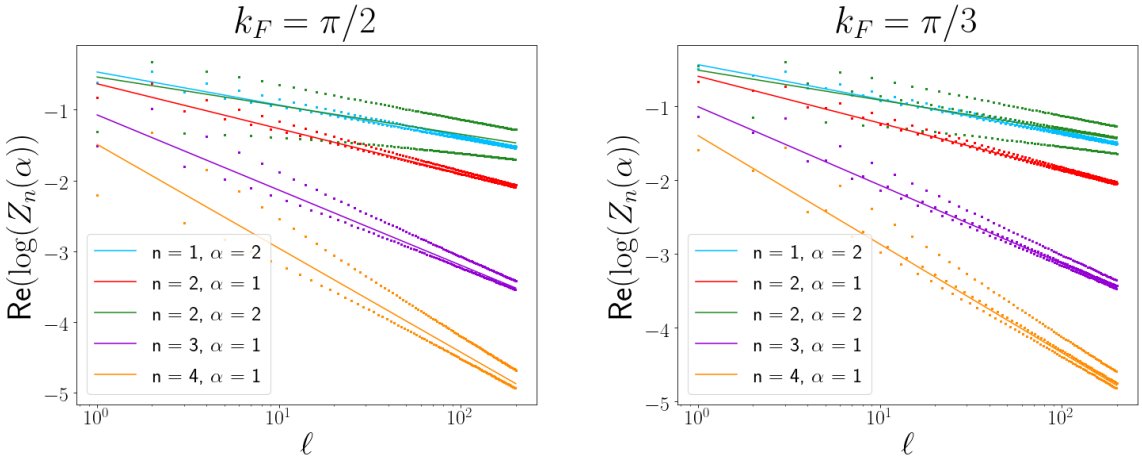


Figure 3.5: Scaling behaviour of the charged REs $\log Z_n(\alpha)$ for several values of α and n. We fix $\ell_0/\ell = 2$ and plot as function of ℓ. The numerical data (symbols) are compared with the prediction (3.6.1). The agreement is satisfactory, despite the presence of strong oscillating corrections.

3.6 Block away from the boundary

In this section, we finally move to the symmetry resolved entropies of a block A of length ℓ placed at distance ℓ_0 from the boundary (set at $x = 0$ for simplicity). As proved in Sec. 3.4, the asymptotic scaling behaviour of $Z_n(\alpha)$ is just the square root of Eq. (3.5.8) (with u_2 and v_2 being the mirror images of $u_1 = \ell_0$ and $v_1 = \ell + 2\ell_0$). Hence we have

$$\log Z_n(\alpha) = \frac{\mathrm{i}\alpha k_F}{\pi}\ell - \left(\frac{1}{12}\left(n - \frac{1}{n}\right) + \frac{1}{n}\left(\frac{\alpha}{2\pi}\right)^2\right)\log\left(\frac{4\ell^2\ell_0(\ell+\ell_0)}{(2\ell_0+\ell)^2}(2\sin k_F)^2\right) + \\ + \mathrm{Y}(n,\alpha) + o(1), \tag{3.6.1}$$

where $\mathrm{Y}(n,\alpha)$ is the same of Eq. (2.3.27). The interpretation of the three terms is the same as in Eq. (3.3.7) for the block starting from the boundary. This result is valid in the limit $\ell, \ell_0 \gg 1$ with their ratio arbitrary and confirms the CFT scaling (3.2.11). The only new relevant information is that also for $\alpha \neq 0$, the function $\mathcal{F}_{n,\alpha}(x)$ in Eq. (3.2.11) is equal to 1, as could be likely derived by field theoretical means as those in Ref. [40].

In Fig. 3.5, we show the comparison between the numerical data and the analytic prediction (3.6.1) for the REs in the presence of flux for different values of n and α, with fillings $k_F = \pi/2$ and $k_F = \pi/3$. The data are plot as function of ℓ at fixed ratio $\ell_0/\ell = 2$. As expected, the presence of oscillating corrections (with amplitude that increases as n and α get larger) strongly affect the data, but the agreement is satisfactory.

In order to investigate in a better way the correctness of Eq. (3.6.1) and to isolate the universal part, it is standard practice to construct combinations of entropies of different regions that cancel all non-universal amplitudes (for disjoint intervals the mutual information is one of them [170, 175]) and are explicitly scale invariant, i.e. they depend only on the ratio ℓ/ℓ_0 or, equivalently, on the anharmonic ratio (3.1.2). To this aim, let us first define the shorthand $\zeta_A^{(n,\alpha)}$ for $Z_n(\alpha)$ of the subsystem A, because now we need to refer explicitly to the subsystem. The

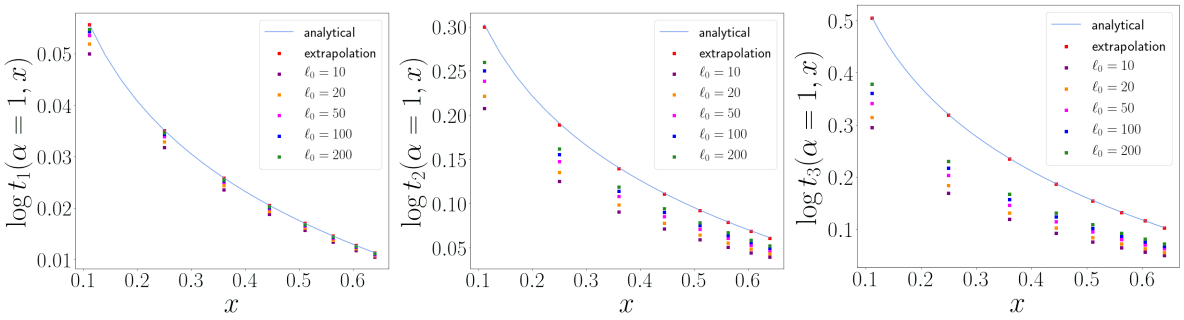


Figure 3.6: The scale invariant function $\log t_n(\alpha)$ (3.6.2) at fixed $\alpha = 1$ plotted as function of the anharmonic ratio x for $n = 1$ (left), $n = 2$ (center) and $n = 3$ (right). The numerical data are obtained at fixed anharmonic ratio x (3.1.2) for increasing values of ℓ_0 (and ℓ). The data are extrapolated to the scaling limit $\ell, \ell_0 \to \infty$ fitting with the first two corrections to the scaling. The obtained results match remarkably well our analytic prediction (3.6.4) (continuous line).

combination of interest is

$$t_n(\alpha) \equiv \mathrm{e}^{2\mathrm{i}\alpha\langle Q_{[0,\ell_0]}\rangle} \frac{\zeta^{(n,\alpha)}_{[\ell_0,\ell_0+\ell]}}{\zeta^{(n,\alpha)}_{[0,\ell_0]}\zeta^{(n,\alpha)}_{[0,\ell_0+\ell]}}\,, \tag{3.6.2}$$

where the prefactor is introduced to cancel the mean number of particles in the interval $[0, \ell_0]$. The scaling limit of $t_n(\alpha)$ can be written in terms of twist field as

$$t_n(\alpha) \equiv \mathrm{e}^{2\mathrm{i}\alpha\langle Q_{[0,\ell_0]}\rangle} \frac{\langle \mathcal{T}_{n,\alpha}(\ell_0)\tilde{\mathcal{T}}_{n,\alpha}(\ell_0+\ell)\rangle}{\langle \mathcal{T}_{n,\alpha}(\ell_0)\rangle\langle \mathcal{T}_{n,\alpha}(\ell+\ell_0)\rangle}, \tag{3.6.3}$$

in which it is clear that we are taking the ratio of the twist field correlation with its connected part, making it dimensionless and so scale invariant. Notice in particular that for $\alpha = 0$, using also the fact that the entanglement of A is the same as the one of the complement, the above ratio corresponds to the (exponential) of the RMI.

Combining Eqs. (3.6.3) and (3.6.1), it is straightforward to obtain the leading behaviour of $t_n(\alpha)$

$$\log t_n(\alpha) = -\left[\frac{1}{12}\left(n - \frac{1}{n}\right) + \frac{1}{n}\left(\frac{\alpha}{2\pi}\right)^2\right] \log \frac{\ell^2}{(2\ell_0^2 + \ell)^2} = -\left[\frac{1}{12}\left(n - \frac{1}{n}\right) + \frac{1}{n}\left(\frac{\alpha}{2\pi}\right)^2\right] \log x\,, \tag{3.6.4}$$

where in the rightmost hand side we recognised the appearance of the anharmonic ratio x as defined in Eq. (3.1.2). This result is tested against numerics in Fig. 3.6. It is clear that the date are plagued by scaling corrections. In order to achieve the scaling limit we work as follows. For some values of n and α reported in the figure, we computed the ratio $t_n(x)$ at fixed x and for increasing values of ℓ_0 from 10 to 200. The data present finite ℓ_0 corrections, which become larger as n and α increase. The leading corrections to the scaling behave $\ell_0^{-(1-\alpha/\pi)/n}$, cf. Eq. (3.3.22). There are also corrections going as $\ell_0^{-(1+\alpha/\pi)/n}$, $\ell_0^{-(2-\alpha/\pi)/n}$, and ℓ_0^{-1} and which one is the first subleading depends on n and α. We then perform a fit of the finite ℓ data, keeping the first two power-law corrections and extrapolating at $\ell \to \infty$. The data obtained following this procedure are reported in Fig. 3.6 and they match extremely well the analytic prediction (3.6.4). This is particularly remarkable for $n = 2$ and 3 when the finite ℓ data are still very far from their asymptotic values.

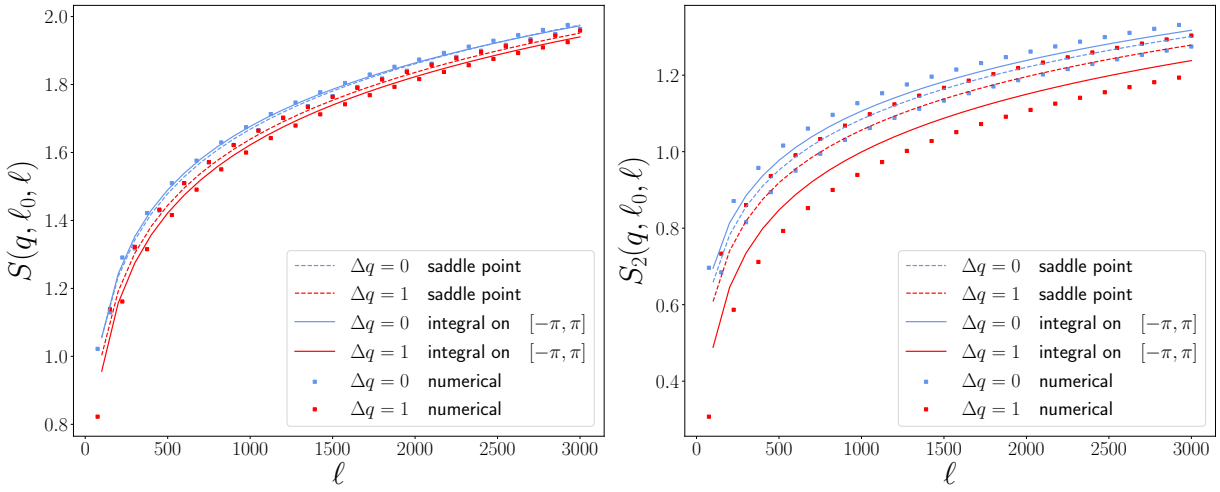


Figure 3.7: Symmetry resolved von Neumann (left) and second Rényi (right) entropies at half filling $k_F = \pi/2$ for one interval of length ℓ placed at distance ℓ_0 from the boundary of a semi-infinite chain. We focus on $\ell_0/\ell = 2$. The analytical predictions (dashed lines) in Eq. (3.3.28) with the amplitudes in Eq. (3.6.5) are compared with the numerical data (symbols) for $\Delta q = q - \bar{q} = 0, 1$. The agreement of the saddle point results with the numerical data is better than the one in Fig. 3.4. However, the observed deviations are again caused by the finite domain of the integral in α, and are well captured by Eq. (3.3.30), full line, which falls in the middle between the data for even and odd ℓ.

3.6.1 Symmetry resolution

For the symmetry resolution of moments and entropies, once again, we exploit the stationary phase approximation which implies the Gaussian approximation (3.3.23) for $Z_n(\alpha)$. The parameters defining the variance b_n for large ℓ, see Eq. (3.3.24), in this case read

$$b = 1, \qquad h_n = -\frac{1}{\pi^2 n}\left[\ln(2|\sin k_F|) + \frac{1}{2}\log\frac{4\ell_0(\ell+\ell_0)}{(2\ell_0+\ell)^2}\right] + 2\gamma_2(n). \tag{3.6.5}$$

The symmetry resolved moments and entropies (for large ℓ) are then given by Eqs. (4.4.28) and (3.3.28), respectively, with the amplitudes given in Eq. (3.6.5).

In Fig. 3.7, we compare the analytical predictions for the symmetry resolved EEs with the numerical data, focusing on half filling $k_F = \pi/2$ and on $\ell_0/\ell = 2$. Let us critically compare these results with those with $\ell_0 = 0$ in Fig. 3.4. Especially for $n = 2$, we observe that the analytic curves are not in the middle of the data for even and odd ℓ, but it is slightly shifted. The shift is much smaller than the one for $\ell_0 = 0$ and it can be described by performing the integral on $[-\pi, \pi]$ as in Eq. (3.3.30). Indeed as $\ell \to \infty$, the data crossover to those for an infinite system, where such an effect was negligible [1]. Indeed for the most relevant case $n = 1$, the two curves are extremely close.

We conclude this section by studying another universal quantity appearing in the symmetry resolution. This is related to the variance of the generalised probability distribution function $p_n(q) \equiv \frac{\mathcal{Z}_n(q)}{\mathcal{Z}_n}$. Indeed, as pointed out in Ref. [49], the difference of the variance of a given state with a reference one cancels all non universal factors. In our case, we can take the difference of the variance $\langle \Delta q^2 \rangle_n^{\rm OBC}$ for one interval at distance ℓ_0 from the boundary with the one of the infinite system $\langle \Delta q^2 \rangle_n^{\rm PBC}$. Since, the variance is just the quadratic term in $Z_n(\alpha)$, it is clear that

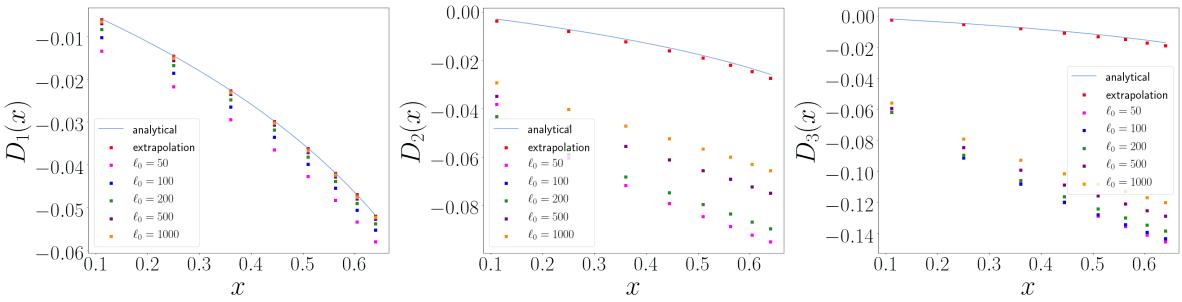


Figure 3.8: Excess of variance $D_n(x)$ in Eq. (3.6.6) as function of x at half filling $k_F = \pi/2$ for $n = 1, 2, 3$ respectively obtained from Eq. (3.6.6) (blue lines) and from numerical evaluation via correlation matrix (symbols). The numerical data are at fixed ratio x for increasing values of ℓ_0 (and ℓ). The data are extrapolated to the scaling limit $\ell, \ell_0 \to \infty$ fitting with the first two corrections to the scaling. The obtained results match very well the analytic prediction (3.6.6) (continuous line).

the difference between Eqs. (3.6.5) and the analogous quantity for the case of PBC cancels all non-universal and divergent factors, resulting finally in

$$D_n(x) \equiv \langle \Delta q^2 \rangle_n^{\mathrm{OBC}} - \langle \Delta q^2 \rangle_n^{\mathrm{PBC}} = \frac{1}{2n\pi^2} \log \frac{4\ell_0(\ell+\ell_0)}{(\ell+\ell_0)^2} = \frac{1}{2n\pi^2} \log(1-x)\,, \tag{3.6.6}$$

where in the rightmost hand side we again recognise the anharmonic ratio (3.1.2). We can compare the analytic expression of $D_n(x)$ with the numerical results, obtained from [49]

$$\langle \Delta q^2 \rangle_n = \sum_k \frac{1}{((\nu_k^{-1}-1)^n+1)} - \frac{1}{((\nu_k^{-1}-1)^n+1)^2}, \tag{3.6.7}$$

where the ν_k are again the eigenvalues of the correlation matrix corresponding to the state and bipartition of interest. The excess of variance $D_n(x)$ is then numerically evaluated as the difference between Eq. (3.6.7) evaluated for open and periodic boundary conditions. The results are shown in Fig. 3.8 for $n = 1, 2, 3$ (respectively from left to right) as function of x at half filling. The raw numerical data at finite ℓ, ℓ_0 are far from the analytic prediction (full line) but tend toward them. To be more quantitative, we extrapolate to the scaling limit with a fit that takes into account the first two corrections to the scaling that are expected to go like $\ell^{-1/n}$ and $\ell^{-2/n}$ respectively. These extrapolations are shown in Fig. 3.8 and the agreement is very good, especially when thinking that the raw data are very far away from the asymptotic ones for $n = 2, 3$.

3.7 Concluding remarks

In this Chapter, we characterised the symmetry resolved EEs in the presence of boundaries. We first reported some general results in CFT and then we specialised to spinless free fermions hopping on a 1D lattice. We focused on the case of a single block which can be either placed at the boundary or away from it. The former case can be treated with rigorous methods based on Fisher-Hartwig formulas [255, 229] that allow us to estimate also the corrections to the leading behaviour. Conversely, for the interval away from the boundary, we first derived an exact relation with the case of two intervals on the infinite line and then exploited it to use a recently

proposed conjecture for the latter case [231]. All our analytic results are tested against exact lattice computations. We found that the saddle-point approximation from charged to symmetry resolved entropies introduces algebraically decaying corrections in ℓ that are much more severe than in the periodic case. In all considered instances, we have entanglement equipartition, as expected; however we also identify the first term breaking such an equipartition.

We now briefly mention some possible generalisations and extensions of our results. First, thanks to the correspondence between the correlation matrix of the 1D lattice and the overlap matrix of a free Fermi gas [238, 242, 239], our results immediately generalise to the latter case, although we did not discuss it here. Then, we can exploit our results, to infer predictions for higher dimensional free fermionic lattices and gases with boundaries, using dimensional reduction techniques [54]. Less straightforward generalisations concern instead the effect of the boundaries in the symmetry resolved massive field theory. For integrable field theories, one should join the boundary approach of Ref. [260] with the form factors of the composite twist fields [58]. Instead for free massive theories, we should generalise the techniques of Refs. [40, 62] to the presence of boundaries.

Chapter 4

Symmetry decomposition of negativity of massless free fermions

***Summary**: In this Chapter, based on Ref. [4], we consider the problem of symmetry decomposition of the EN in free fermionic systems. Rather than performing the standard partial transpose, we use the partial time-reversal transformation which naturally encodes the fermionic statistics. The EN admits a resolution in terms of the charge imbalance between the two subsystems. We introduce a normalised version of the imbalance resolved negativity which has the advantage to be an entanglement proxy for each symmetry sector, but may diverge in the limit of pure states for some sectors. Our main focus is then the resolution of the EN for a free Dirac field at finite temperature and size. We consider both bipartite and tripartite geometries and exploit CFT to derive universal results for the charge imbalance resolved negativity. To this end, we use a geometrical construction in terms of an Aharonov-Bohm-like flux inserted in the Riemann surface defining the entanglement. We interestingly find that the EN is always equally distributed among the different imbalance sectors at leading order. Our analytical findings are tested against exact numerical calculations for free fermions on a lattice.*

4.1 Introduction

The REs are the most successful way to characterise the bipartite entanglement of a subsystem A in a pure state of a many-body quantum system [15, 20, 21, 22], also from the experimental perspective [17, 18, 24, 195, 19]. For a mixed state, the EEs are no longer good measures of entanglement since they mix quantum and classical correlations (e.g. in a high temperature state, S_1 gives the extensive result for the thermal entropy that has nothing to do with entanglement). In this case, a suitable measure of the bipartite entanglement for a general mixed state is the EN, that is defined in terms of the partial transpose of the RDM, according to the Peres criterion.

An interesting issue concerns the quantification of mixed state entanglement in fermionic systems. In particular, it has been pointed out that when ρ_A is a Gaussian fermion operator, its partial transpose is the sum of two Gaussians; from this observation a procedure to extract the integer RN was proposed [261] and was also used in many subsequent studies [262, 263, 258, 264, 265, 266, 267]. However, in this way the replica limit $n_e \to 1$ is not possible and hence,

the EN, i.e. the only genuine measure of entanglement, is not accessible. To overcome this problem, an alternative estimator of mixed state entanglement for fermionic systems has been introduced based on the time-reversal (TR) partial transpose (a.k.a *partial time reversal*) [47, 268, 269, 161, 48, 270, 271, 272]. The new estimator has been dubbed *fermionic negativity*, although it is not related to negative eigenvalues of any matrix. It turned out that not only the fermionic negativity is an entanglement monotone [271], but also that it is able to detect entanglement in mixed states where the standard negativity vanishes. For both these reasons, throughout this work, we will mainly focus on the fermionic negativity.

In this Chapter, we consider a many-body system with an internal global symmetry and address the question of how mixed state entanglement splits into contributions arising from distinct symmetry sectors.

For pure states, it has been established that the symmetry resolution of entanglement follows from the block diagonal form of the RDM [35, 33]; one of the main findings is that the EE is equally distributed among the different sectors [34]. For mixed states, the literature is limited to the pioneering work [38], where it was proven that whenever there is a conserved extensive charge, the negativity admits a resolution in terms of the charge imbalance between the two subsystems. Here, we first point out that by properly normalising the imbalance sectors (as also done in Ref. [67]) one obtains a clearer resolution of the entanglement in the imbalance; then we show that the imbalance-decomposition of negativity also holds using the partial TR definition for free fermions. We then use such decomposition to study the symmetry resolution of the entanglement of free fermions at finite temperature, exploiting the same field theory methods used for the total negativity [109, 161].

The Chapter is organised as follows. In Sect. 4.2, we provide some basic definitions and briefly review the fermionic partial TR, motivating our work by simple examples for a tripartite and a bipartite geometry. After a brief summary of the results found in [38], we proceed with the general definition of the imbalance operator and the consequent decomposition of the negativity, taking into account the normalisation of each sector. In Sect. 4.3, we review a method based on the replica trick to derive the leading order term for the RE of massless Dirac fermions in (1+1)d when both the temperature T and the system size L are finite. As a warm-up, we use this method to compute the charged REs. In Sect. 4.4 and Sect. 4.5 we then provide results for charged and imbalance resolved negativity for tripartite and bipartite settings, respectively. Numerical checks for free fermions on the lattice are also presented as a benchmark of the analytical results. We draw our conclusions in Sect. 4.6. Four appendices are also included: they provide details about the analytical and numerical computations but they also make connections with some related ideas not developed here.

4.2 Charge imbalance resolved negativity

In this section, we briefly review the definition of partial TR for fermionic density matrices following Ref. [47]. Then we present the symmetry resolution of the partial TR of the density matrix. Simple examples will lead to a general definition of the imbalance resolution of EN, both fermionic and bosonic. We closely follow Ref. [38], but we normalise differently the partial transpose in each symmetry sector, so that the symmetry resolved negativity is a genuine indicator of entanglement in the sector.

4.2.1 The fermionic partial time reversal density matrix

Let us consider a system A that is partitioned into two subsystems A_1 and A_2 such that $A = A_1 \cup A_2$. The associated RDM ρ_A has the form given in Eq. (1.2.11) (ρ_A can either be the RDM of a larger pure system $\rho_A = \mathrm{Tr}_B(\rho)$ or a mixed density matrix, e.g. thermal, for an entire system). The partial transpose of a density matrix for the subsystem A_1, defined by exchanging the matrix elements in the subsystem A_1, is

$$(|e_i^1, e_j^2\rangle \langle e_k^1, e_l^2|)^{T_1} \equiv |e_k^1, e_j^2\rangle \langle e_i^1, e_l^2| \,. \tag{4.2.1}$$

For a bosonic system, it is known [273] that the partial transpose is the same as partial time reversal in phase space. This correspondence was exploited in harmonic chains to calculate the negativity in terms of the covariance matrix [86]. However, this is no longer true for fermions. To understand why, let us consider a single-site system described by fermionic operators c and $c^\dagger$ which obey the anticommutation relation $\{c, c^\dagger\} = 1$. We introduce the Grassmann variables $\xi, \bar{\xi}$, and the fermionic coherent states $|\xi\rangle = \mathrm{e}^{-\xi c^\dagger} |0\rangle$ and $\langle\bar{\xi}| = \langle 0| e^{-c\bar{\xi}}$. In this basis, the time reversal transformation reads

$$|\xi\rangle \langle\bar{\xi}| \to |\mathrm{i}\bar{\xi}\rangle \langle \mathrm{i}\xi| \equiv (|\xi\rangle \langle\bar{\xi}|)^R. \tag{4.2.2}$$

This equation clearly shows that time reversal does not coincide with transposition because of the presence of the factor i. In the last equality we defined the time-reversal transpose, specified by the apex R so as to distinguish it from the standard transposition for which we use the apex T. This transformation rule can be generalised to a many-particle (lattice) system with a partial TR only on the degrees of freedom within A_1 and reads

$$\begin{aligned}(|\{\xi_j\}_{j\in A_1}, \{\xi_j\}_{j\in A_2}\rangle \langle \{\bar{\chi}_j\}_{j\in A_1}, \{\bar{\chi}_j\}_{j\in A_2}|)^{R_1} \\ = |\{\mathrm{i}\bar{\chi}_j\}_{j\in A_1}, \{\xi_j\}_{j\in A_2}\rangle \langle \{\mathrm{i}\xi_j\}_{j\in A_1}, \{\bar{\chi}_j\}_{j\in A_2}| \,,\end{aligned} \tag{4.2.3}$$

where $|\{\xi_j\}\rangle = \mathrm{e}^{-\sum_j \xi_j c_j^\dagger} |0\rangle$, $\langle\{\bar{\chi}_j\}| = \langle 0| \mathrm{e}^{-\sum_j c_j \bar{\chi}_j}$ are the many-particle fermionic coherent states.

Let us consider the normal-ordered occupation number basis

$$|\{n_j\}_{j\in A_1}, \{n_j\}_{j\in A_2}\rangle = (c_{m_1}^\dagger)^{n_{m_1}} \dots (c_{m_{\ell_1}}^\dagger)^{n_{m_{\ell_1}}} (c_{m'_1}^\dagger)^{n_{m'_1}} \dots (c_{m'_{\ell_2}}^\dagger)^{n_{m'_{\ell_2}}} |0\rangle \,, \tag{4.2.4}$$

where n_j's are occupation numbers in the subsystems A_1 and A_2, which have ℓ_1 and ℓ_2 sites respectively (in 1D they represent the lengths of intervals), and we use the indices $\{m_1, \dots, m_{\ell_1}\} \cup \{m'_1, \dots, m'_{\ell_2}\}$ to denote the sites within the subsystem. The definition (4.2.3) in the occupation number basis is

$$(|\{n_j\}_{A_1}, \{n_j\}_{A_2}\rangle \langle \{\bar{n}_j\}_{A_1}, \{\bar{n}_j\}_{A_2}|)^{R_1} = (-1)^{\phi(\{n_j\},\{\bar{n}_j\})} (|\{\bar{n}_j\}_{A_1}, \{n_j\}_{A_2}\rangle \langle \{n_j\}_{A_1}, \{\bar{n}_j\}_{A_2}|), \tag{4.2.5}$$

and can be viewed as the analogue of partial transposition in Eq. (4.2.1), up to the phase factor

$$\phi(\{n_j\}, \{\bar{n}_j\}) = \frac{[(\tau_1 + \bar{\tau}_1) \mathrm{mod} 2]}{2} + (\tau_1 + \bar{\tau}_1)(\tau_2 + \bar{\tau}_2), \tag{4.2.6}$$

in which $\tau_s = \sum_{j\in A_s} n_j$, $\bar{\tau}_s = \sum_{j\in A_s} \bar{n}_j$ are the number of the occupied states in the A_s intervals, $s = 1, 2$.

It is useful to rewrite the partial TR using the Majorana representation of the operator algebra. We introduce the Majorana operators as

$$f_{2j-1} = c_j + c_j^\dagger, \qquad f_{2j} = \mathrm{i}(c_j - c_j^\dagger). \tag{4.2.7}$$

The density matrix in the Majorana representation takes the form

$$\rho_A = \sum_{\substack{\kappa,\tau \\ |\kappa|+|\tau|=\text{even}}} w_{\kappa,\tau} f_{m_1}^{\kappa_{m_1}} \dots f_{2m_{\ell_1}}^{\kappa_{2m_{\ell_1}}} f_{m'_1}^{\tau_{m'_1}} \dots f_{2m'_{\ell_2}}^{\tau_{2m'_{\ell_2}}}. \tag{4.2.8}$$

Here, $f_x^0 = \mathbb{I}$ and $f_x^1 = f_x$, $\kappa_i, \tau_j \in \{0,1\}$ and κ (τ) is a $2m_{\ell_1}$-component vector ($2m'_{\ell_2}$) with norm $|\kappa| = \sum_j \kappa_j$ ($|\tau| = \sum_j \tau_j$). The constraint on the parity of $|\kappa| + |\tau|$ is due to the fact that the density matrix commutes with the total fermion-number parity operator, i.e. we focus our attention on physical states. Using Eq. (4.2.8), the partial TR with respect to the subsystem A_1 is defined by

$$\rho_A^{R_1} = \sum_{\substack{\kappa,\tau \\ |\kappa|+|\tau|=\text{even}}} \mathrm{i}^{|\kappa|} w_{\kappa,\tau} f_{m_1}^{\kappa_{m_1}} \dots f_{2m_{\ell_1}}^{\kappa_{2m_{\ell_1}}} f_{m'_1}^{\tau_{m'_1}} \dots f_{2m'_{\ell_2}}^{\tau_{2m'_{\ell_2}}}. \tag{4.2.9}$$

We should note that the matrix resulting from the partial TR is not necessarily Hermitian and may have complex eigenvalues, although $\mathrm{Tr}\rho_A^{R_1} = 1$. Nevertheless, we can still use Eq. (1.2.14) to define *a negativity* because the eigenvalues of the combined operator $[\rho_A^{R_1}(\rho_A^{R_1})^\dagger]$ are always real. Following Refs. [47, 161, 48], in the rest of the manuscript, we shall use the term negativity (or fermionic negativity) to refer to the quantity

$$\mathcal{N} \equiv \frac{\mathrm{Tr}|\rho_A^{R_1}| - 1}{2} = \frac{\mathrm{Tr}\sqrt{\rho_A^{R_1}(\rho_A^{R_1})^\dagger} - 1}{2}, \tag{4.2.10}$$

where the trace norm of the operator $\rho_A^{R_1}$ is the sum of the square roots of the eigenvalues of the product operator $\rho_A^{R_1}(\rho_A^{R_1})^\dagger$. Usually one also defines the (fermionic) RNs, as

$$R_n = \begin{cases} \mathrm{Tr}(\rho_A^{R_1}(\rho_A^{R_1})^\dagger \dots \rho_A^{R_1}(\rho_A^{R_1})^\dagger), & n \quad \text{even}, \\ \mathrm{Tr}(\rho_A^{R_1}(\rho_A^{R_1})^\dagger \dots \rho_A^{R_1}), & n \quad \text{odd}, \end{cases} \tag{4.2.11}$$

from which $\mathcal{N} = \frac{1}{2}\Big(\lim_{n_e \to 1} R_{n_e} - 1\Big)$, where n_e denotes an even $n = 2m$ [47]. We stress that the fermionic negativity (4.2.10) is not related to the presence of negative eigenvalues in the spectrum of $\rho_A^{R_1}$. Sometimes, we will refer to the standard negativity (1.2.14) as the bosonic negativity.

4.2.2 Imbalance entanglement via bosonic partial transpose

In the presence of symmetries, the RDM has a block diagonal structure which allows to identify contributions to the EE from individual charge sectors. In order to understand how symmetry is reflected in a block structure of the density matrix after partial transpose, we start with a simple example, taken from Ref. [38]. Consider a particle in one out of three boxes, A_1, A_2, B,

described by a pure state $|\Psi\rangle = \alpha|100\rangle + \beta|010\rangle + \gamma|001\rangle$. The RDM of $A = A_1 \cup A_2$ is $\rho_A = \mathrm{Tr}_B|\psi\rangle\langle\psi| = |\gamma|^2|00\rangle\langle 00| + (\alpha|10\rangle + \beta|01\rangle)(\alpha^*\langle 10| + \beta^*\langle 01|)$, i.e.

$$\rho_A = \begin{pmatrix} |\gamma|^2 & 0 & 0 & 0 \\ 0 & |\beta|^2 & \alpha^*\beta & 0 \\ 0 & \beta^*\alpha & |\alpha|^2 & 0 \\ 0 & 0 & 0 & 0 \end{pmatrix}, \tag{4.2.12}$$

in the basis $\{|00\rangle, |01\rangle, |10\rangle, |11\rangle\}$. This matrix is clearly block diagonal with respect to the total occupation number $N_A = N_1 + N_2$, where N_1 and N_2 respectively denote the particle number of the subsystem A_1 and A_2. According to Eq. (4.2.1), the partial transpose of ρ_A is

$$\rho_A^{T_1} = \begin{pmatrix} |\gamma|^2 & 0 & 0 & \alpha\beta^* \\ 0 & |\beta|^2 & 0 & 0 \\ 0 & 0 & |\alpha|^2 & 0 \\ \beta\alpha^* & 0 & 0 & 0 \end{pmatrix}. \tag{4.2.13}$$

The total negativity is $\mathcal{N} = \left|\frac{1}{2}|\gamma|^2 - \sqrt{\frac{1}{4}|\gamma|^4 + |\alpha\beta|^2}\right|$. Once we reshuffle the elements of rows and columns in the basis of $\{|10\rangle, |00\rangle, |11\rangle, |01\rangle\}$, we get

$$\rho_A^{T_1} = \begin{pmatrix} |\alpha|^2 & 0 & 0 & 0 \\ 0 & |\gamma|^2 & \alpha\beta^* & 0 \\ 0 & \beta\alpha^* & 0 & 0 \\ 0 & 0 & 0 & |\beta|^2 \end{pmatrix}, \tag{4.2.14}$$

which has a block structure where each block is labelled by the occupation imbalance $\tilde{q} = N_2 - N_1$:

$$\rho_A^{T_1} \cong (|\alpha|^2)_{\tilde{q}=-1} \oplus \begin{pmatrix} |\gamma|^2 & \alpha\beta^* \\ \beta\alpha^* & 0 \end{pmatrix}_{\tilde{q}=0} \oplus (|\beta|^2)_{\tilde{q}=1}. \tag{4.2.15}$$

The structure of the above example is easily generalised to a many-body ρ_A with subsystems A_1 and A_2 characterised by particle number operator $\hat{N}_1$ and $\hat{N}_2$; performing a partial transposition of the relation $[\rho_A, \hat{N}_A] = 0$ yields [38]

$$[\rho_A^{T_1}, \hat{N}_2 - \hat{N}_1^{T_1}] = 0, \tag{4.2.16}$$

from which we can do a block matrix decomposition according to the eigenvalues $\tilde{q}$ of the imbalance operator $\hat{\tilde{Q}} = \hat{N}_2 - \hat{N}_1^{T_1}$. Here we use $\tilde{q}$ for the eigenvalues of $\hat{\tilde{Q}}$ to make a clear distinction with the eigenvalues q of $\hat{Q}_A$. We recall that this operator $\hat{\tilde{Q}}$ is basis dependent, as stressed in [38]; it has the form of an imbalance in the Fock basis (i.e. $\hat{\tilde{Q}} = \hat{N}_2 - \hat{N}_1$), while in others it can be different (as, e.g., in the computational basis we employ, $\hat{\tilde{Q}}$ is determined by the sum of the number operators up to some additive constants, see Appendix 4.A and [38]).

Let $\Pi_{\tilde{q}}$ denote the projector onto the subspace of eigenvalue $\tilde{q}$ of the operator $\hat{\tilde{Q}}$. We define the *normalised charge imbalance partially transposed density matrix* as

$$\rho_A^{T_1}(\tilde{q}) = \frac{\Pi_{\tilde{q}}\rho_A^{T_1}\Pi_{\tilde{q}}}{\mathrm{Tr}(\Pi_{\tilde{q}}\rho_A^{T_1})}, \qquad \mathrm{Tr}(\rho_A^{T_1}(\tilde{q})) = 1, \tag{4.2.17}$$

such that

$$\rho_A^{T_1} = \oplus_{\tilde{q}} \tilde{p}(\tilde{q}) \rho_A^{T_1}(\tilde{q}). \tag{4.2.18}$$

Here, $\tilde{p}(\tilde{q}) = \mathrm{Tr}(\Pi_{\tilde{q}} \rho_A^{T_1})$ is the probability of finding $\tilde{q}$ as the outcome of a measurement of $\hat{\tilde{Q}}$ and corresponds to the sum of the diagonal elements of $\rho_A^{T_1}(\tilde{q})$. Although the eigenvalues of $\rho_A^{T_1}$ can be negative, all the diagonal elements in the Fock basis are ≥ 0 because the partial transpose leaves invariant all the elements on the diagonal and so they remain the same as those of ρ_A which are ≥ 0. This is evident in the example (4.2.14) and it is the same for any particle number. Hence $\tilde{p}(\tilde{q})$ satisfies $\tilde{p}(\tilde{q}) \geq 0$ and $\sum_{\tilde{q}} \tilde{p}(\tilde{q}) = 1$, as it should be for a probability measure. We can thus define the (normalised) *charge imbalance resolved negativity* as

$$\mathcal{N}(\tilde{q}) = \frac{\mathrm{Tr}|(\rho_A^{T_1}(\tilde{q}))| - 1}{2}. \tag{4.2.19}$$

Differently from [38], we prefer to deal with normalised quantities to preserve the natural meaning of negativity as a measure of entaglement: if in the $\tilde{q}$ sector there are no negative eigenvalues, according to Eq. (4.2.19), $\mathcal{N}(\tilde{q}) = 0$. Hence, this definition not only provides a resolution of the negativity, but also tells us in which sectors the negative eigenvalues are, i.e. where the entanglement is. The total negativity, $\mathcal{N}$, is resolved into (normalised) contributions from distinct imbalance sectors as

$$\mathcal{N} = \sum_{\tilde{q}} \tilde{p}(\tilde{q}) \mathcal{N}(\tilde{q}). \tag{4.2.20}$$

For the example of Eq. (4.2.15), the imbalance negativities are $\mathcal{N}(\pm 1) = 0$ and $\mathcal{N}(0) = \frac{1}{2}\left|1 - \sqrt{\frac{1}{2} + \left|\frac{2\alpha\beta}{|\gamma|^2}\right|^2}\right|$ with $\tilde{p}(0) = |\gamma|^2$; the only negative eigenvalue is in the sector $\tilde{q} = 0$. Eq. (4.2.20) gives back the total negativity. We stress that the imbalance decomposition of the negativity as in Eq. (4.2.20) cannot be performed for the logarithmic negativity in Eq. (1.2.15), because of the nonlinearity of the logarithm.

We conclude this section by discussing the important "pathological" case when $\tilde{p}(\tilde{q}) = 0$ for some values of the imbalance $\tilde{q}$, but $\rho_A^{T_1}(\tilde{q})$ is non-zero and so the negativity of the sectors diverges, although the total one is finite. For example, this happens setting $\gamma = 0$ in Eq. (4.2.12); in this case ρ_A corresponds to a pure state. Actually, it is obvious that every time that ρ_A is a pure state there will be some $\tilde{p}(\tilde{q}) = 0$ because $N_1 + N_2$ is fixed and hence also the parity of $N_1 - N_2$ is (so all the $\tilde{p}(\tilde{q})$'s where $\tilde{q}$ has a different parity vanish). In such case, the origin of the problem can be traced back to the fact that the (pure-state) entanglement (entropy) is better resolved in terms of N_1 or N_2 rather than in the imbalance, i.e. the symmetries of ρ_A and $\rho_A^{T_1}$ are larger than in the standard mixed case. However, mixed states with some zero $\tilde{p}(\tilde{q})$ can be also easily built, although they are difficult to encounter as mixed states in physical settings (and they all correspond to states in which there is more symmetry than the imbalance). To understand the situation better, let us recall that $\tilde{p}(\tilde{q})$ is always the sum of some diagonal elements of both $\rho_A^{T_1}(\tilde{q})$ and ρ_A. For the latter, the diagonal elements are the populations of states in the Fock basis. Hence, we need at least a few zero populations to have a vanishing $\tilde{p}(\tilde{q})$ (and, e.g., this will never happen in a Gibbs state at finite temperature). In the matrix ρ_A, if the populations in a given sector of the total charge are zero, the entire block is zero (and hence the EE of the sector is zero). However, when taking the partial transpose, the off-diagonal elements are reshuffled in the matrix and, after being re-organised in terms of the

imbalance, we can end up with some blocks with all zeros on the diagonal (and so $\tilde{p}(\tilde{q}) = 0$) but with non-zero off-diagonal elements. In these instances, we cannot normalise with $\tilde{p}(\tilde{q})$. (Have always in mind the example of Eq. (4.2.12) with $\gamma = 0$: there are two sectors in ρ_A with zero populations, $N_1 + N_2 = 0, 2$; after the partial transposition, they both end up in imbalance $\tilde{q} = 0$, see Eq. (4.2.15) which has non-zero off-diagonal terms). Anyhow, it makes sense that the imbalance negativity diverges in these cases. We are indeed facing sectors that have exactly zero populations, but still have some quantum correlations. In practice, as we shall see in the next section, these vanishing $\tilde{p}(\tilde{q})$ are encountered only in the limit of a pure state (e.g. for $T \to 0$) and so diverging imbalance negativity signals that the state is getting pure and that a better resolution of the entanglement is in N_1 or N_2 rather than in the imbalance.

The example of tripartite CFT.

As a first simple example to show the importance of the normalisation $\tilde{p}(\tilde{q})$ in the definition of imbalance resolved negativity, we reanalyse a simple known result [38] for the ground state of a Luttinger liquid (with parameter K) in a tripartite geometry. Thus, the results in this subsection describe gapless interacting 1d fermions. We focus on two adjacent intervals of length ℓ_1 and ℓ_2 respectively embedded in an infinite line.

Following [38], we start with the computation of the charged moments of the partial transpose

$$N_n^{T_1}(\alpha) \equiv \mathrm{Tr}((\rho_A^{T_1})^n e^{i\hat{\tilde{Q}}\alpha}) = \langle \mathcal{T}_n \mathcal{V}_\alpha(u_1) \mathcal{T}_{-n}^2 \mathcal{V}_{-2\alpha}(v_1) \mathcal{T}_n \mathcal{V}_\alpha(v_2) \rangle \,, \tag{4.2.21}$$

where, in the rhs, we use the correspondence with the 3-point correlation function of fluxed twist field $\mathcal{T}_n \mathcal{V}_\oslash$ with scaling dimension

$$\Delta_n(\alpha) = \frac{1}{24}\left(n - \frac{1}{n}\right) + \frac{K}{2n}\left(\frac{\alpha}{2\pi}\right)^2, \qquad \Delta_{\mathcal{T}_{n_o}^2} = \Delta_{n_o} \qquad \Delta_{\mathcal{T}_{n_e}^2} = 2\Delta_{n_e/2}. \tag{4.2.22}$$

Using these scaling dimensions, one finds

$$\log N_n^{T_1}(\alpha) = \log R_n - \frac{K}{2n}\left(\frac{\alpha}{\pi}\right)^2 \log\left[\frac{\ell_1^2 \ell_2^2}{(\ell_1 + \ell_2)\epsilon^3}\right], \tag{4.2.23}$$

where R_n are neutral RNs and ϵ is an ultraviolet cutoff. Notice in Eq. (4.2.23) only R_n does depend on the parity of n[109], while the α dependence is the same for even and odd n.

Upon performing a Fourier transform of Eq. (4.2.23), we obtain, through the saddle-point approximation, the (normalised) charge imbalance RN

$$R_n(\tilde{q}) = R_n \frac{\int_{-\pi}^{\pi} \frac{d\alpha}{2\pi} e^{-i(\tilde{q}-\bar{\tilde{q}})\alpha} e^{-\alpha^2 b_n/2}}{\left[\int_{-\pi}^{\pi} \frac{d\alpha}{2\pi} e^{-i(\tilde{q}-\bar{\tilde{q}})\alpha} e^{-\alpha^2 b_1/2}\right]^n} \simeq R_n \sqrt{\frac{(2\pi b_1)^n}{2\pi b_n}} e^{-\frac{(\tilde{q}-\bar{\tilde{q}})^2}{2}\left(\frac{1}{b_n} - \frac{n}{b_1}\right)}, \tag{4.2.24}$$

where $\bar{\tilde{q}}$ is the expectation value of the charge operator $\hat{\tilde{Q}}$ and

$$b_n = \frac{1}{\pi^2 n} \log\left[\frac{\ell_1^2 \ell_2^2}{(\ell_1 + \ell_2)\epsilon^3}\right]. \tag{4.2.25}$$

The saddle-point approximation holds for two intervals of length $\ell_1, \ell_2 \to \infty$ embedded in an infinite line at zero temperature. The replica limit $n_e \to 1$ is easily taken since there is no parity dependence in the imbalance part. For large $\ell_1, \ell_2 \to \infty$ (hence $b_n \to \infty$), we get

$$\mathcal{N}(\tilde{q}) = \mathcal{N} + o(1), \tag{4.2.26}$$

i.e. we found the equipartition of negativity in the different imbalance sectors at leading order for large subsystems. This behaviour is reminiscent of the equipartition of EE in a pure quantum system that possesses an internal symmetry [34]. It is clear that *negativity equipartition* can be shown only by properly normalising the partial transpose in each sector as done here. As an important difference compared to the EEs, we do not have additional $\log\log\ell$ [1] corrections to the symmetry resolved quantities.

4.2.3 Imbalance entanglement of fermions via partial TR

Now we are ready to understand the block structure of the partial TR density matrix and how the fermionic negativity splits according to the symmetry. We first revisit the simple example of the previous section in Eq. (4.2.12) for fermions. According to Eq. (4.2.2), the partial TR of ρ_A in Eq. (4.2.12) is

$$\rho_A^{R_1} = \begin{pmatrix} |\gamma|^2 & 0 & 0 & \mathrm{i}\alpha\beta^* \\ 0 & |\beta|^2 & 0 & 0 \\ 0 & 0 & |\alpha|^2 & 0 \\ \mathrm{i}\beta\alpha^* & 0 & 0 & 0 \end{pmatrix}, \tag{4.2.27}$$

i.e. the partial TR transformation does not spoil the block matrix structure according to the occupation imbalance $\tilde{q} = N_2 - N_1$:

$$\rho_A^{R_1} \cong \left(|\alpha|^2\right)_{\tilde{q}=-1} \oplus \begin{pmatrix} |\gamma|^2 & \mathrm{i}\alpha\beta^* \\ \mathrm{i}\beta\alpha^* & 0 \end{pmatrix}_{\tilde{q}=0} \oplus \left(|\beta|^2\right)_{\tilde{q}=1}. \tag{4.2.28}$$

The (total) fermionic negativity is

$$\mathcal{N} = \frac{|\gamma|^2}{2}\left(-1 + \sqrt{\frac{1}{2} + \frac{|\alpha\beta|^2}{|\gamma|^4} + \sqrt{\frac{1}{4} + \frac{|\alpha\beta|^2}{|\gamma|^4}}} + \sqrt{\frac{1}{2} + \frac{|\alpha\beta|^2}{|\gamma|^4} - \sqrt{\frac{1}{4} + \frac{|\alpha\beta|^2}{|\gamma|^4}}}\right). \tag{4.2.29}$$

For a many-body state, the analogue of the commutation relation in Eq. (4.2.16) now reads

$$[\rho_A^{R_1}, \hat{N}_2 - \hat{N}_1^{R_1}] = 0, \tag{4.2.30}$$

while the (normalised) charge imbalance resolved negativity is given by

$$\mathcal{N}(\tilde{q}) = \frac{\mathrm{Tr}|(\rho_A^{R_1}(\tilde{q}))| - 1}{2}, \qquad \rho_A^{R_1}(\tilde{q}) = \frac{\Pi_{\tilde{q}}\rho_A^{R_1}\Pi_{\tilde{q}}}{\mathrm{Tr}(\Pi_{\tilde{q}}\rho_A^{R_1})}. \tag{4.2.31}$$

We also define the *charge imbalance resolved RN*

$$R_n(\tilde{q}) = \begin{cases} \mathrm{Tr}(\rho_A^{R_1}(\tilde{q})\rho_A^{R_1}(\tilde{q})^\dagger \dots \rho_A^{R_1}(\tilde{q})\rho_A^{R_1}(\tilde{q})^\dagger), & n \quad \text{even}, \\ \mathrm{Tr}(\rho_A^{R_1}(\tilde{q})\rho_A^{R_1}(\tilde{q})^\dagger \dots \rho_A^{R_1}(\tilde{q})), & n \quad \text{odd}, \end{cases} \tag{4.2.32}$$

from which $\mathcal{N}(\tilde{q}) = \frac{1}{2}\Big(\lim_{n_e\to 1} R_{n_e}(\tilde{q}) - 1\Big)$. It is important to stress that the diagonal elements of $\rho_A^{R_1}$ are the same as $\rho_A^{T_1}$ (the TR operation does not touch the diagonal elements) and so the probabilities $\tilde{p}(\tilde{q})$ are identical for both the standard and the TR partial transpose. Thus, all the considerations for the vanishing of $\tilde{p}(\tilde{q})$ in the previous subsection apply also here.

For the example of Eq. (4.2.28), the imbalance negativities are $\mathcal{N}(\pm 1) = 0$ and $\mathcal{N}(0) = \frac{1}{2}\left(-1+\sqrt{\frac{1}{2}+\frac{|\alpha\beta|^2}{|\gamma|^4}+\sqrt{\frac{1}{4}+\frac{|\alpha\beta|^2}{|\gamma|^4}}}+\sqrt{\frac{1}{2}+\frac{|\alpha\beta|^2}{|\gamma|^4}-\sqrt{\frac{1}{4}+\frac{|\alpha\beta|^2}{|\gamma|^4}}}\right)$ with $\tilde{p}(0) = |\gamma|^2$. As a further check, $\sum_{\tilde{q}} \tilde{p}(\tilde{q})\mathcal{N}(\tilde{q})$ gives back the total negativity in Eq. (4.2.29).

We think it is beneficial to give another basic example (taken from Ref. [161]) of imbalance resolution with free fermions on a two-site lattice model described by the Hamiltonian

$$\hat{H} = -\Delta(c_1^\dagger c_2 + c_2^\dagger c_1), \tag{4.2.33}$$

where Δ is a tunnelling amplitude. In the basis $\{|00\rangle, |01\rangle, |10\rangle, |11\rangle\}$, the thermal density matrix is

$$\rho = \frac{\mathrm{e}^{-\beta\hat{H}}}{\mathrm{Tr}(\mathrm{e}^{-\beta\hat{H}})} = \frac{1}{2+2\cosh(\beta\Delta)}\begin{pmatrix} 1 & 0 & 0 & 0 \\ 0 & \cosh(\beta\Delta) & \sinh(\beta\Delta) & 0 \\ 0 & \sinh(\beta\Delta) & \cosh(\beta\Delta) & 0 \\ 0 & 0 & 0 & 1 \end{pmatrix}. \tag{4.2.34}$$

Let us take the partial TR

$$\rho^{R_1} = \frac{1}{2+2\cosh(\beta\Delta)}\begin{pmatrix} 1 & 0 & 0 & \mathrm{i}\sinh(\beta\Delta) \\ 0 & \cosh(\beta\Delta) & 0 & 0 \\ 0 & 0 & \cosh(\beta\Delta) & 0 \\ \mathrm{i}\sinh(\beta\Delta) & 0 & 0 & 1 \end{pmatrix}. \tag{4.2.35}$$

By reshuffling the elements of rows and columns in the basis of $\{|00\rangle, |11\rangle, |10\rangle, |01\rangle\}$, ρ^{R_1} has a block matrix structure in the occupation imbalance between the subsystem and the rest of the system that we can write explicitly as

$$\rho^{R_1} \cong \left(\tfrac{\cosh(\beta\Delta)}{2+2\cosh(\beta\Delta)}\right)_{\tilde{q}=-1} \oplus \begin{pmatrix} \frac{1}{2+2\cosh(\beta\Delta)} & \frac{\mathrm{i}\sinh(\beta\Delta)}{2+2\cosh(\beta\Delta)} \\ \frac{\mathrm{i}\sinh(\beta\Delta)}{2+2\cosh(\beta\Delta)} & \frac{1}{2+2\cosh(\beta\Delta)} \end{pmatrix}_{\tilde{q}=0} \oplus \left(\tfrac{\cosh(\beta\Delta)}{2+2\cosh(\beta\Delta)}\right)_{\tilde{q}=1}. \tag{4.2.36}$$

When the state becomes pure, i.e. $\beta\Delta \gg 1$, $\tilde{p}(\tilde{q}=0) \to 0$. The interpretation is the same as the one for the bosonic negativity: when the state is pure, the operator to resolve the symmetry is $\hat{N}_1$ (or $\hat{N}_2$), rather than the imbalance. For completeness, we report the fermionic negativity

$$\mathcal{N} = \frac{1}{2}\tanh^2\left(\frac{\beta\Delta}{2}\right), \tag{4.2.37}$$

and its splitting in the imbalance sectors: $\mathcal{N}(\pm 1) = 0$ and $\mathcal{N}(0) = \frac{1}{2}(\cosh(\beta\Delta)-1)$ with $\tilde{p}(0) = \frac{1}{\cosh(\beta\Delta)+1}$, so that $\sum_{\tilde{q}} \tilde{p}(\tilde{q})\mathcal{N}(\tilde{q}) = \tilde{p}(0)\mathcal{N}(0) = \mathcal{N}$. Notice that as $\beta \to \infty$, $\tilde{p}(0) \to 0$, $\mathcal{N}(0) \to \infty$, but their product stays finite and tends to $1/2$.

4.3 Replica approach

In this section, we first review the replica approach to the charged entropies [56] and apply it to their calculation for a massless Dirac fermion at finite temperature, a result that was not yet obtained so far. Then we adapt the method to the charged RNs. Its applications will be presented in the successive sections.

4.3.1 Charged moments of the reduced density matrix

Let us consider a system characterized by a $U(1)$ symmetry $\hat{Q}$, so that the RDM ρ_A admits a charge decomposition according to the local charge $\hat{Q}_A$. Each block corresponds to different eigenspaces of $\hat{Q}_A$, that we can label as $q \in \mathbb{Z}$. As already discussed, in a generic quantum field theory the replica trick for computing $Z_n(\alpha)$ can be implemented by inserting an Aharonov-Bohm flux through a multi-sheeted Riemann surface $\mathcal{R}_n$, such that the total phase accumulated by the field upon going through the entire surface is α [35]. The result is that $Z_n(\alpha)$ is the partition function $\mathcal{R}_{n,\alpha}$. Here we focus on a massless Dirac fermion described by the Lagrangian density

$$\mathcal{L} = \bar{\Psi}\gamma^\mu \partial_\mu \Psi, \tag{4.3.1}$$

where $\bar{\Psi} = \Psi^\dagger \gamma^0$, $\gamma^0 = \sigma^1$, $\gamma^1 = \sigma^2$. Rather than dealing with fields defined on a non trivial manifold $\mathcal{R}_{n,\alpha}$, it is more convenient to work on a single plane with a n-component field

$$\Psi = \begin{pmatrix} \psi_1 \\ \psi_2 \\ \vdots \\ \psi_n \end{pmatrix}, \tag{4.3.2}$$

where ψ_j is the field on the j-th copy. Upon crossing the cut A, the vector field Ψ transforms according to the twist matrix T_α

$$T_\alpha = \begin{pmatrix} 0 & e^{i\alpha/n} & & \\ & 0 & e^{i\alpha/n} & \\ & & \ddots & \ddots \\ (-1)^{n-1}e^{i\alpha/n} & & & 0 \end{pmatrix}. \tag{4.3.3}$$

The idea of using the twist matrix for the Dirac fermions at $\alpha = 0$ was originally suggested in [40] (see also [139]). The matrix T_α has eigenvalues

$$\lambda_k = e^{i\frac{\alpha}{n}} e^{2\pi i \frac{k}{n}}, \quad k = -\frac{n-1}{2}, \dots, \frac{n-1}{2}. \tag{4.3.4}$$

By diagonalising T_α with a unitary transformation, the problem is reduced to n decoupled and multi-valued fields ψ_k in a two dimensional spacetime. This technique is applicable only to free theories, otherwise the $k-$modes do not decouple. In particular, the charged moments become

$$Z_n(\alpha) = \prod_{k=-(n-1)/2}^{(n-1)/2} Z_{k,n}(\alpha), \tag{4.3.5}$$

where $Z_{k,n}(\alpha)$ is the partition function for a Dirac field that along A picks up a phase equal to $e^{i\frac{\alpha}{n}} e^{2\pi i \frac{k}{n}}$, or equivalently the phase picked up going around one of the entangling points u_i, v_i is $e^{i\frac{\alpha}{n}} e^{2\pi i \frac{k}{n}}$ and $e^{-i\frac{\alpha}{n}} e^{-2\pi i \frac{k}{n}}$, respectively. The main difference with respect to the standard computation for the REs is that, for a charged quantity, the boundary conditions of the multivalued fields along A depend also on the flux α and not only on the replica index. This multivaluedness can be circumvented with the same trick used for $\alpha = 0$ [40], i.e. by absorbing it in an *external* gauge field coupled to a single-valued fields $\tilde{\psi}_k$. Indeed, the singular gauge transformation

$$\psi_k(x) = e^{i \oint_C dy_\mu A_k^\mu(y)} \tilde{\psi}_k(x), \tag{4.3.6}$$

allows us to absorb the phase along A into the gauge field at the price of changing the Lagrangian density into

$$\mathcal{L}_k = \bar{\tilde{\psi}}_k \gamma^\mu (\partial_\mu + \mathrm{i} A^k_\mu) \tilde{\psi}_k. \tag{4.3.7}$$

The actual value of A^k_μ in Eq. (4.3.6) is fixed by requiring that, for any loop $\mathcal{C}$, the original boundary conditions for the multivalued field ψ_k are reproduced. This is achieved with

$$\begin{aligned} \oint_{\mathcal{C}_{u_i}} \mathrm{d}x^\mu A^k_\mu &= -\frac{2\pi k}{n} - \frac{\alpha}{n}, \\ \oint_{\mathcal{C}_{v_i}} \mathrm{d}x^\mu A^k_\mu &= +\frac{2\pi k}{n} + \frac{\alpha}{n}, \end{aligned} \tag{4.3.8}$$

where $\mathcal{C}_{u_i}$ and $\mathcal{C}_{v_i}$ are circuits around left and right endpoints of the i-th interval. If the circuit $\mathcal{C}$ does not encircle any endpoint, $\oint_{\mathcal{C}} dx^\mu A^k_\mu = 0$. If more endpoints are encircled the phases sum up. It is useful to rewrite Eq. (4.3.8) in the corresponding differential form, i.e. using Stokes' theorem

$$\epsilon^{\mu\nu} \partial_\nu A^k_\mu(x) = 2\pi \left(\frac{k}{n} + \frac{\alpha}{2\pi n} \right) \sum_{i=1}^{p} [\delta(x - u_i) - \delta(x - v_i)], \tag{4.3.9}$$

where p is the number of intervals.

After the transformation (4.3.6), the desired charged partition sum $Z_{k,n}(\alpha)$ is written as

$$Z_{k,n}(\alpha) = \langle \mathrm{e}^{\mathrm{i} \int d^2x A^k_\mu j^\mu_k} \rangle \,, \tag{4.3.10}$$

where $j^\mu_k = \bar{\tilde{\psi}}_k \gamma^\mu \tilde{\psi}_k$ is the Dirac current and A^k_μ satisfies Eq. (4.3.8) or, equivalently, (4.3.9). Eq. (4.3.10) is more easily calculated by bosonisation, which maps the Dirac current to the derivative of a scalar field and the Lagrangian of the k-th fermion to that of a real massless scalar field ϕ_k, $\mathcal{L}_k = \frac{1}{8\pi} \partial_\mu \phi_k \partial^\mu \phi_k$ (here we work with the normalisation of the boson field such that the Dirac fermion corresponds to a compactified boson with radius $R = 2$, as in [144]). Therefore we can evaluate $Z_{k,n}(\alpha)$ as the correlation function of the vertex operators $V_a(x) = \mathrm{e}^{-\mathrm{i} a \phi_k(x)}$, i.e.

$$Z_{k,n}(\alpha) = \langle \prod_{i=1}^{p} V_{\frac{k}{n} + \frac{\alpha}{2\pi n}}(u_i) V_{-\frac{k}{n} - \frac{\alpha}{2\pi n}}(v_i) \rangle \,. \tag{4.3.11}$$

An important observation about Eq. (4.3.8) is that we can arbitrarily add $2\pi m$ phase shifts, with m an integer, to the right hand side without affecting the total phase factor along the circuits $\mathcal{C}_{u_i}$ and $\mathcal{C}_{v_i}$ defined above. This ambiguity leads to inequivalent different representations of the partition function $Z_{k,n}(\alpha)$ in Eq. (4.3.5), which in turn must be written as a summation over all allowed representations. The asymptotic behaviour of each term for large subsystem size, ℓ, is a power law $\ell^{-\alpha_m}$ and the leading term corresponds to the one with the smallest exponent α_m. For the charged moments, the leading order is given by $m = 0$, but this is not the case for the EN. See Appendix 4.B for a more detailed discussion of this issue.

Let us now apply this machinery to study the charged moments of a free Dirac fermion on a torus with multiple intervals (u_a, v_a), $(a = 1, \ldots, p)$. To have more compact formulas, we rescale the spatial coordinates by the system size L. The torus is defined by two periods which, in our units, are 1 and $\tau = i\beta/L$, where $\beta = 1/T$ is the inverse temperature. The partition function depends on the boundary conditions along the two cycles, which specify the spin structure of the fermion on the torus. Let z be a holomorphic coordinate on the torus: it has the

periodicities $z = z + 1$ and $z = z + \tau$. The holomorphic component of the fermion on the torus satisfies four possible boundary conditions

$$\tilde{\psi}_k(z+1) = \mathrm{e}^{2\pi \mathrm{i} \nu_1} \tilde{\psi}_k(z), \qquad \tilde{\psi}_k(z+\tau) = \mathrm{e}^{2\pi \mathrm{i} \nu_2} \tilde{\psi}_k(z), \tag{4.3.12}$$

where ν_1 and ν_2 take the values 0 or $\frac{1}{2}$. The anti-holomorphic component is a function of $\bar{z}$ and satisfies the same boundary conditions as the holomorphic part. We denote the $\nu = (\nu_1, \nu_2)$ sector where $\nu = 1, 2, 3, 4$ corresponds to $(0,0), (0,1/2), (1/2,1/2), (1/2,0)$, respectively (for standard fermions, the physical boundary conditions are anti-periodic along both cycles and so $\nu = 3$, but the other spin structures have important applications too). Hence, we just need the correlation function of the vertex operators $V_e(z,\bar{z}) = \mathrm{e}^{\mathrm{i}e\phi(z,\bar{z})}$ on the torus with boundary conditions corresponding to the sector ν. These can be found in Ref. [144] and read

$$\langle V_{e_1}(z_1,\bar{z}_1) V_{e_2}(z_2,\bar{z}_2) \dots V_{e_N}(z_N,\bar{z}_N) \rangle_\nu = \Big| \prod_{i<j} \frac{\partial_z \theta_1(0|\tau)}{\theta_1(z_i - z_j|\tau)} \Big|^{-2e_i e_j} \Big| \frac{\theta_\nu(\sum_i (e_i z_i)|\tau)}{\theta_\nu(0|\tau)} \Big|^2. \tag{4.3.13}$$

In Eq. (4.3.13) and afterwards, we use the notation $\partial_z \theta_1(0|\tau) = \partial_z \theta_1(z|\tau)|_{z=0}$. Plugging Eq. (4.3.13) into Eq. (4.3.11), we have in sector ν

$$Z^{(\nu)}_{k,n}(\alpha) = \Big| \frac{\prod_{i<j} \theta_1(u_i - u_j|\tau)\theta_1(v_i - v_j|\tau)}{\prod_{i,j} \theta_1(u_i - v_j|\tau)} \Big(\frac{\epsilon}{L} \partial_z \theta_1(0|\tau) \Big)^p \Big|^{2(\frac{k}{n} + \frac{\alpha}{2\pi n})^2} \times \Big| \frac{\theta_\nu((\frac{k}{n} + \frac{\alpha}{2\pi n}) \sum_i (u_i - v_i)|\tau)}{\theta_\nu(0|\tau)} \Big|^2, \tag{4.3.14}$$

where ϵ is an ultraviolet cutoff which depends on both α and n, although we almost always omit such a dependence for conciseness. The total charged moments are finally obtained by taking the product (4.3.5) to get

$$\log Z^{(\nu)}_n(\alpha) = \log Z_{n,0}(\alpha) + \log Z^{(\nu)}_{n,1}(\alpha), \tag{4.3.15}$$

where the first term is spin-independent

$$\log Z_{n,0}(\alpha) = \Big[\frac{1}{6} \Big(n - \frac{1}{n} \Big) + \frac{\alpha^2}{2\pi^2 n} \Big] \log \Big| \frac{\prod_{i<j} \theta_1(u_i - u_j|\tau)\theta_1(v_i - v_j|\tau)}{\prod_{i,j} \theta_1(u_i - v_j|\tau)} \Big(\frac{\epsilon}{L} \partial_z \theta_1(0|\tau) \Big)^p \Big| \equiv \log Z_{n,0}(0) - \frac{\alpha^2}{2} \mathcal{B}^0_n, \tag{4.3.16}$$

(in the second line we implicitly defined $\mathcal{B}^0_n$) while the second one depends on the sector ν

$$\log Z^{(\nu)}_{n,1}(\alpha) = 2 \sum_{k=-(n-1)/2}^{(n-1)/2} \log \Big| \frac{\theta_\nu((\frac{k}{n} + \frac{\alpha}{2\pi n}) \sum_i (u_i - v_i)|\tau)}{\theta_\nu(0|\tau)} \Big|. \tag{4.3.17}$$

The Fourier transform of the charged moments (4.3.15) gives the symmetry resolved moments and entropies. We report only the results for $\nu = 3$, but similarly also the others may be obtained. Using the product representation of the theta functions

$$\theta_3(z|\tau) = \prod_{m=1}^{\infty} (1 - \mathrm{e}^{2\pi \mathrm{i} \tau m})(1 + \mathrm{e}^{2\pi \mathrm{i} z} \mathrm{e}^{2\pi \mathrm{i} \tau (m-1/2)})(1 + \mathrm{e}^{-2\pi \mathrm{i} z} \mathrm{e}^{2\pi \mathrm{i} \tau (m-1/2)}), \tag{4.3.18}$$

the sum over k of the spin-dependent term in Eq. (4.3.17) can be explicitly worked out as

$$\log Z^{(3)}_{n,1}(\alpha) = 2\sum_{j\geq 1}\frac{(-1)^j}{j\sinh(\pi j\beta/L)}\Big(n-\cos\Big(\frac{\alpha r j}{n}\Big)\frac{\sin(\pi jr)}{\sin(\frac{\pi jr}{n})}\Big), \tag{4.3.19}$$

where $r=\sum_i(u_i-v_i)$. Since the symmetry resolved entropies will be obtained from a saddle point, we expand at the second order in α, obtaining

$$\begin{aligned}&\log Z^{(3)}_{n,1}(\alpha)\simeq\\ &2\sum_{j\geq 1}\frac{(-1)^j}{j\sinh(\pi j\beta/L)}\Big(n-\frac{\sin(\pi jr)}{\sin(\frac{\pi jr}{n})}\Big)+\frac{\alpha^2r^2}{n^2}\sum_{j\geq 1}\frac{(-1)^j j}{\sinh(\pi j\beta/L)}\frac{\sin(\pi jr)}{\sin(\frac{\pi jr}{n})}=\mathcal{A}_n-\frac{\alpha^2}{2}\mathcal{B}^1_n.\end{aligned} \tag{4.3.20}$$

The sum converges very fast in j and very few terms are sufficient to get it. Introducing $\mathcal{B}_n\equiv\mathcal{B}^0_n+\mathcal{B}^1_n$, the charged moments of the RDM are

$$Z^{(3)}_n(\alpha)=Z^{(3)}_n(0)\mathrm{e}^{-\frac{\alpha^2}{2}\mathcal{B}_n}, \tag{4.3.21}$$

with Fourier transform

$$\mathcal{Z}^{(3)}_n(q)=Z^{(3)}_n(0)\int_{-\pi}^{\pi}\frac{\mathrm{d}\alpha}{2\pi}\mathrm{e}^{-\mathrm{i}\alpha q}\mathrm{e}^{-\frac{\alpha^2}{2}\mathcal{B}_n}\simeq\frac{Z^{(3)}_n(0)}{\sqrt{2\pi\mathcal{B}_n}}\mathrm{e}^{-\frac{q^2}{2\mathcal{B}_n}}, \tag{4.3.22}$$

where we exploited the saddle point approximation and we used that $\bar{q}$, the expectation value of the charge operator $\hat{Q}_A$, vanishes for a free Dirac field at any temperature. From the definition (2.2.6), we get the symmetry resolved REs

$$S_n(q)=S_n-\frac{1}{2}\log(2\pi\mathcal{B}_1)+O(1). \tag{4.3.23}$$

In order to make contact with some known results in literature [1, 34, 53], we report the explicit expression for $\mathcal{B}_1$ in the low and high temperature limit for $p=1$

$$\mathcal{B}_1=\begin{cases}\frac{1}{\pi^2}\log\Big(\frac{L}{\pi\epsilon}\sin\frac{\ell\pi}{L}\Big), & LT\ll 1,\\ \frac{1}{\pi^2}\log\Big(\frac{\beta}{\pi\epsilon}\sinh\frac{\ell\pi}{\beta}\Big), & LT\gg 1.\end{cases} \tag{4.3.24}$$

The result in Eq. (4.3.23) shows the presence of entanglement equipartition [34]: at leading order the entanglement is the same in the different charge sectors. In [34] this was proven for gapless interacting 1d fermions at zero temperature. As a side result, here we showed that entanglement equipartition holds also at finite size and temperature, at least for a free Dirac field.

4.3.2 Charged moments of the partial transpose

The above procedure is easily adapted to the computation of the charged moments of the partial TR defined as

$$N_n(\alpha)=\begin{cases}\mathrm{Tr}(\rho_A^{R_1}(\rho_A^{R_1})^\dagger\dots\rho_A^{R_1}(\rho_A^{R_1})^\dagger\mathrm{e}^{\mathrm{i}\hat{Q}_A\alpha}), & n \text{ even},\\ \mathrm{Tr}(\rho_A^{R_1}(\rho_A^{R_1})^\dagger\dots\rho_A^{R_1}\mathrm{e}^{\mathrm{i}\hat{Q}_A\alpha}), & n \text{ odd}.\end{cases} \tag{4.3.25}$$

Hence, in order to compute the imbalance resolved negativity, we need to study the composite operator $\rho_A^{R_1}(\rho_A^{R_1})^\dagger$. The charged moments in Eq. (4.3.25) are defined for two subsystems A_1 and A_2 with different twist matrices respectively denoted by $T_\alpha^{R_1}$ and T_α. The new twist matrix $T_\alpha^{R_1}$ for the transposed time reversed subsystem is given by

$$T_\alpha^{R_1} = \begin{pmatrix} 0 & 0 & \dots & (-1)^{n-1}\mathrm{e}^{-\mathrm{i}\alpha/n} \\ \mathrm{e}^{-\mathrm{i}\alpha/n} & 0 & & \\ 0 & \mathrm{e}^{-\mathrm{i}\alpha/n} & & \ddots \\ & & \ddots & \ddots \end{pmatrix}. \tag{4.3.26}$$

The two matrices, T_α and $T_\alpha^{R_1}$, are simultaneously diagonalisable. Consequently, we can decompose our problem into n decoupled copies in which the fields have different twist phases along the two subsystems. As a result, $N_n(\alpha)$ is decomposed as

$$N_n(\alpha) = \prod_{k=-(n-1)/2}^{(n-1)/2} Z_{R_1,k}(\alpha), \tag{4.3.27}$$

where $Z_{R_1,k}(\alpha)$ is the partition function for fields with twist phases equal to $\mathrm{e}^{-2\pi\mathrm{i}\left(\frac{k}{n}+\frac{\alpha}{2\pi n}\right)}$ and $\mathrm{e}^{2\pi\mathrm{i}\left(\frac{k}{n}+\frac{\alpha}{2\pi n}-\frac{\varphi_n}{2\pi}\right)}$, respectively along A_2 and A_1. Here $\varphi_n = \pi$ for $n = n_e$ even and $\varphi_n = \frac{n-1}{n}\pi$ for $n = n_o$ odd (as follows from the diagonalisation of Eq. (4.3.26)). In particular, the probability $p(q)$ is the Fourier transform of $N_1(\alpha) = \mathrm{Tr}[\rho^{R_1}\mathrm{e}^{\mathrm{i}\hat{\mathrm{Q}}\alpha}]$, that, with a minor abuse of terminology, we dub *charged probability*. In this case, the twist matrices along the two intervals are just phases given by $T_\alpha = \mathrm{e}^{\mathrm{i}\alpha}$ and $T_\alpha^{R_1} = T_\alpha^{-1} = \mathrm{e}^{-\mathrm{i}\alpha}$. For a system of interacting fermions (i.e. for a free compact boson with different compactification radius), the procedure outlined here does not apply. The calculation is much more cumbersome and requires to adapt the technique for the standard negativity (see [110]) to the PT case, but this has not yet been done even for the total negativity.

A Fourier transform leads us to the imbalance resolved negativities (4.2.32)

$$\mathcal{Z}_{R_1,n}(\tilde{q}) = \int_{-\pi}^{\pi}\frac{\mathrm{d}\alpha}{2\pi}\mathrm{e}^{-\mathrm{i}\alpha\tilde{q}}N_n(\alpha), \quad \tilde{p}(\tilde{q}) = \int_{-\pi}^{\pi}\frac{\mathrm{d}\alpha}{2\pi}\mathrm{e}^{-\mathrm{i}\alpha\tilde{q}}N_1(\alpha), \tag{4.3.28}$$

from which

$$R_n(\tilde{q}) = \frac{\mathcal{Z}_{R_1,n}(\tilde{q})}{\tilde{p}^n(\tilde{q})}, \qquad \mathcal{N}(\tilde{q}) = \frac{1}{2}\Big(\lim_{n_e\to 1} R_{n_e}(\tilde{q}) - 1\Big). \tag{4.3.29}$$

Let us stress the replica limit for $R_{n_e}(\tilde{q})$ is $\lim_{n_e\to 1}\frac{\mathcal{Z}_{R_1,n_e}(\tilde{q})}{\tilde{p}(\tilde{q})}$, i.e. while it is sufficient to set $n = 1$ in the denominator, the numerator requires an analytic continuation from the even sequence at $n_e \to 1$, in agreement with the definition in Eq. (4.2.10). In the following section, we compute the imbalance resolved EN for two geometries.

4.4 Charged and symmetry resolved negativities in a tripartite geometry

Let us study the negativity of two subsystems consisting of two adjacent intervals A_1, A_2, of lengths ℓ_1, ℓ_2 out of a system of length L, as depicted in Fig 4.1. We place the branch points at

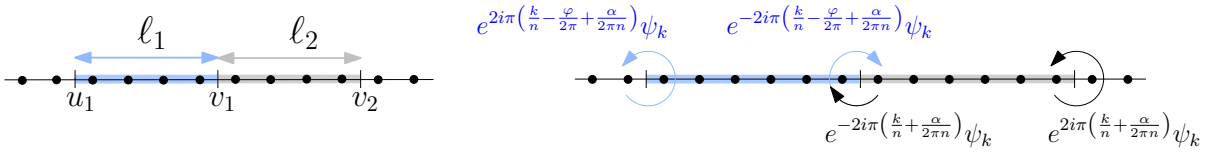


Figure 4.1: Tripartite geometry for two adjacent intervals. In the plot the interval A_1 is the blue one on the left and A_2 the grey one on the right, of length ℓ_1 and ℓ_2 respectively. B is the reminder. The partial transpose is taken on A_1. For each branch point, we report the phase taken by the field ψ_k going around it.

$u_1 = -\ell_1/L = -r_1, v_1 = u_2 = 0$, and $v_2 = \ell_2/L = r_2$ and the multivalued fields ψ_k take up a phase $\mathrm{e}^{2\pi\mathrm{i}(\frac{k}{n}+\frac{\alpha}{2\pi n}-\frac{\varphi_n}{2\pi})}$ at u_1, $\mathrm{e}^{-2\pi\mathrm{i}(\frac{k}{n}+\frac{\alpha}{2\pi n}-\frac{\varphi_n}{2\pi})}\mathrm{e}^{-2\pi\mathrm{i}(\frac{k}{n}+\frac{\alpha}{2\pi n})}$ at v_1 and $\mathrm{e}^{2\pi\mathrm{i}(\frac{k}{n}+\frac{\alpha}{2\pi n})}$ at v_2. By introducing a gauge field A^k_μ, as explained in Sect. 4.3.1, we have to impose proper monodromy conditions such that the field is almost pure gauge except at the branch points, where delta function singularities are necessary to recover the correct phases of the multivalued fields. Hence, the flux of the gauge fields is given by

$$\begin{aligned}&\frac{1}{2\pi}\epsilon^{\mu\nu}\partial_\nu A^k_\mu(x)\\&\quad=\left(\frac{k}{n}+\frac{\alpha}{2\pi n}-\frac{\varphi_n}{2\pi}\right)\delta(x-u_1)-\left(\frac{2k}{n}+\frac{\alpha}{\pi n}-\frac{\varphi_n}{2\pi}\right)\delta(x-v_1)+\left(\frac{k}{n}+\frac{\alpha}{2\pi n}\right)\delta(x-v_2).\end{aligned}\tag{4.4.1}$$

Through bosonisation, $Z^{(v)}_{R_1,k}(\alpha)$ can be written as a correlation function of vertex operators $V_a(x) = \mathrm{e}^{-\mathrm{i}a\phi_k(x)}$ as

$$\begin{aligned}Z^{(v)}_{R_1,k}(\alpha) &= \left\langle V_{\frac{k}{n}+\frac{\alpha}{2\pi n}-\frac{\varphi_n}{2\pi}}(u_1)V_{-\frac{k}{n}-\frac{\alpha}{2\pi n}+\frac{\varphi_n}{2\pi}}(v_1)V_{-\frac{k}{n}-\frac{\alpha}{2\pi n}}(v_1)V_{\frac{k}{n}+\frac{\alpha}{2\pi n}}(v_2)\right\rangle\\&= \left\langle V_{\frac{k}{n}+\frac{\alpha}{2\pi n}-\frac{\varphi_n}{2\pi}}(u_1)V_{-\frac{2k}{n}-\frac{\alpha}{\pi n}+\frac{\varphi_n}{2\pi}}(v_1)V_{\frac{k}{n}+\frac{\alpha}{2\pi n}}(v_2)\right\rangle.\end{aligned}\tag{4.4.2}$$

Using the correlation function in Eq. (4.3.13), the final result is [1]

$$\begin{aligned}&Z^{(v)}_{R_1,k}(\alpha) = |\theta_1(r_1|\tau)|^{-2(\frac{k}{n}+\frac{\alpha}{2\pi n}-\frac{\varphi_n}{2\pi})(\frac{2k}{n}+\frac{\alpha}{\pi n}-\frac{\varphi_n}{2\pi})}|\theta_1(r_2|\tau)|^{-2(\frac{k}{n}+\frac{\alpha}{2\pi n})(\frac{2k}{n}+\frac{\alpha}{\pi n}-\frac{\varphi_n}{2\pi})}\\&\quad|\theta_1(r_1+r_2|\tau)|^{2(\frac{k}{n}+\frac{\alpha}{2\pi n})(\frac{k}{n}+\frac{\alpha}{2\pi n}-\frac{\varphi_n}{2\pi})}\times\left|\frac{\epsilon}{L}\partial_z\theta_1(0|\tau)\right|^{-\Delta_k(\alpha)}\left|\frac{\theta_\nu((\frac{k}{n}+\frac{\alpha}{2\pi n})(r_2-r_1)+\frac{\varphi_n}{2\pi}r_1|\tau)}{\theta_\nu(0|\tau)}\right|^2,\end{aligned}\tag{4.4.3}$$

where

$$\Delta_k(\alpha) = -6\frac{k^2}{n^2}-6\frac{k\alpha}{n^2\pi}-3\frac{\alpha^2}{2n^2\pi^2}+3k\frac{\varphi_n}{n\pi}+3\frac{\alpha\varphi_n}{2n\pi^2}-\frac{\varphi_n^2}{2\pi^2}-2\theta(-k)(1+\frac{3k}{n}+\frac{3\alpha}{2n\pi}-\frac{\varphi_n}{\pi}),\tag{4.4.4}$$

and $\theta(x)$ is the step function. It is important to note that for $k<0$, we have to modify the flux at u_1 and v_1, φ_n, by inserting an additional 2π and -2π fluxes. Essentially, we need to find the dominant term with the lowest scaling dimension in the mode expansion, as discussed in

[1] Differently from Eq. (41) in [161] or Eq. (80) in [47], rather then using the absolute values we explicitly change $\varphi_n \to \varphi_n - 2\pi$ for $k<0$.

Appendix 4.B. Moreover, the case of odd $n = n_o$ requires particular attention: as $|\alpha| > 2/3\pi$, also the mode $k = 0$ requires an additional 2π and -2π fluxes at u_1 and v_1, respectively. Putting together the various pieces and using Eq. (4.3.27), the logarithm of the charged moments of $\rho_A^{R_1}$ are given by

$$\log N_n^{(\nu)}(\alpha) = \log N_{n,0}(\alpha) + \log N_{n,1}^{(\nu)}(\alpha), \tag{4.4.5}$$

where the spin-independent part is

$$\begin{aligned}
\log N_{n,0}(\alpha) &= \log R_n - \frac{\alpha^2}{2\pi^2 n} \log \left| \theta_1(r_1|\tau)^2 \theta_1(r_2|\tau)^2 \theta(r_1+r_2|\tau)^{-1} \Big(\frac{\epsilon}{L} \partial_z \theta_1(0|\tau) \Big)^{-3} \right|, \\
\log R_{n_o} &= -\Big(\frac{n_o^2 - 1}{12 n_o} \Big) \log \left| \theta_1(r_1|\tau) \theta_1(r_2|\tau) \theta(r_1+r_2|\tau) \Big(\frac{\epsilon}{L} \partial_z \theta_1(0|\tau) \Big)^{-3} \right|, \\
\log R_{n_e} &= -\Big(\frac{n_e^2 - 4}{12 n_e} \Big) \log \left| \theta_1(r_1|\tau) \theta_1(r_2|\tau) \Big(\frac{\epsilon}{L} \partial_z \theta_1(0|\tau) \Big)^{-2} \right| \\
&\quad - \Big(\frac{n_e^2 + 2}{12 n_e} \Big) \log \left| \theta(r_1+r_2|\tau) \Big(\frac{\epsilon}{L} \partial_z \theta_1(0|\tau) \Big)^{-1} \right|.
\end{aligned} \tag{4.4.6}$$

The first equation for $N_{n,0}(\alpha)$ is always valid for any alpha for $n = n_e$ even, but only in the region $|\alpha| < 2/3\pi$ for $n = n_o$ odd; otherwise it must be modified as

$$\begin{aligned}
\log N_{n_o,0}(\alpha) = \log R_{n_o} &- \frac{\alpha^2}{2\pi^2 n_o} \log \left| \theta_1(r_1|\tau)^2 \theta_1(r_2|\tau)^2 \theta(r_1+r_2|\tau)^{-1} \Big(\frac{\epsilon}{L} \partial_z \theta_1(0|\tau) \Big)^{-3} \right| \\
&+ \frac{|\alpha|}{n_o \pi} \log \left| \theta_1(r_1|\tau)^3 \theta_1(r_2|\tau) \theta(r_1+r_2|\tau)^{-1} \Big(\frac{\epsilon}{L} \partial_z \theta_1(0|\tau) \Big)^{-3} \right| \\
&- \frac{2}{n} \log \left| \theta_1(r_1|\tau) \Big(\frac{\epsilon}{L} \partial_z \theta_1(0|\tau) \Big)^{-1} \right|, \qquad \text{for } |\alpha| > 2/3\pi.
\end{aligned} \tag{4.4.7}$$

Hence for odd $n = n_o$, the exponent of the charged moments $N_{n_o}^{(\nu)}(\alpha)$ has a discontinuity as a function of α for $|\alpha| = \frac{2\pi}{3}$. This singular behaviour in α is reminiscent of what was found for the negativity spectrum of free fermions in [48]. Let us also note that the above result does not hold for $n_o = 1$, for which we will provide an analytical expression in the following. The spin structure dependent term is

$$\log N_{n,1}^{(\nu)}(\alpha) = 2 \sum_{k=-(n-1)/2}^{(n-1)/2} \log \left| \frac{\theta_\nu\big((\frac{k}{n} + \frac{\alpha}{2\pi n})(r_2 - r_1) + \frac{\varphi_n}{2\pi} r_1 | \tau \big)}{\theta_\nu(0|\tau)} \right|. \tag{4.4.8}$$

Although our main focus is the state with $\nu = 3$, we notice that $N_{n,1}^{(1)}(\alpha)$ above is strictly infinite because $\theta_1(0|\tau) = 0$. This is related to the fermion zero mode in this sector and is not a prerogative of the charged quantities.

In the case of intervals of equal lengths $\ell_1 = \ell_2 = \ell$ the charged logarithmic negativity (i.e., $\mathcal{E}^\nu(\alpha) \equiv \lim_{n_e \to 1} \log N_{n_e}^{(\nu)}(\alpha)$) simplifies as

$$\begin{aligned}
\mathcal{E}^\nu(\alpha) &= \mathcal{E}^{(\nu)} - \frac{\alpha^2}{2\pi^2} \log \left| \theta_1(r|\tau)^4 \theta(2r_1|\tau)^{-1} \Big(\frac{\epsilon}{L} \partial_z \theta_1(0|\tau) \Big)^{-3} \right|, \\
&\text{with} \qquad \mathcal{E}^{(\nu)} = \frac{1}{4} \log \left| \theta_1(r|\tau)^2 \theta(2r|\tau)^{-1} \Big(\frac{\epsilon}{L} \partial_z \theta_1(0|\tau) \Big)^{-1} \right| + 2 \log \left| \frac{\theta_\nu(\frac{r}{2}|\tau)}{\theta_\nu(0|\tau)} \right|,
\end{aligned} \tag{4.4.9}$$

where $r = \ell/L$.

Eq. (4.4.9) represents our final field theoretical result for the charged logarithmic negativities in a tripartite geometry with two equal intervals. We now test this prediction against exact lattice computations obtained with the techniques reported in Appendix 4.A. However, for a direct comparison without fitting parameters, we have to take into account the non-universal contribution coming from the discretisation of the spatial coordinate, i.e. the explicit expression for the cutoff ϵ in (4.4.9) that does depend also on α, but not on the size and temperature. We can exploit the latter property to deduce its exact value from the knowledge of the lattice negativities at $T = 0$ in the thermodynamic limit that can be determined via Fisher-Hartwig techniques, as reported in Appendix 4.C, cf. Eq. (4.C.21). The numerical results for the charged negativities are shown in Fig. 4.2, where four panels highlight the dependence on ℓ, T, α, and ℓ/L, respectively. The agreement with the parameter-free asymptotic results (4.4.9) is always excellent. Let us critically discuss these results. First, it is known for $\alpha = 0$, the logarithmic negativity saturates at finite temperature once $\ell T \gg 1$ [161], i.e., obeys an area law; conversely the top-left panel of Fig. 4.2 shows that $\mathcal{E}(\alpha)$ follows a volume law. This scaling can be also inferred analytically from the high-temperature limit reported in the following subsection. In the top-right panel of the same figure, we observe that $\mathcal{E}(\alpha)$ has a plateau at low temperatures, i.e when $T \ll 1/L$ so that the temperature is smaller than the energy finite-size gap (of order $1/L$); consequently the system behaves as if it is at zero temperature with exponentially small corrections in TL. For larger T a linear decrease sets up for low enough T, before an exponential high temperature behaviour takes place (this is not shown in the picture, but see next subsection). In the bottom-left panel of Fig. 4.2, we analyse the α dependence fixing ℓ and L for a few values of β. We observe a fairly good agreement between lattice and field theory, although when α gets closer to $\pm\pi$ the agreement gets worse. This is not surprising because charged quantities exactly at $\pm\pi$ are known to be singular [53] and consequently finite ℓ effects are more severe. Moreover, the plot clearly shows that $\mathcal{E}(\alpha)$ has a differentiable maximum in $\alpha = 0$ (that we need for the saddle point approximation). In the bottom-right panel, we show that the difference $\mathcal{E}(\alpha, T) - \mathcal{E}(\alpha, 0)$ is a universal function of β/L and ℓ/L: we verify this behaviour by looking at various system sizes, L, and showing that they all collapse on the same curve. The agreement also slightly improves as L increases, as it should.

Let us conclude this subsection reporting the result for the charged probability $N_1(\alpha) = \mathrm{Tr}[\rho^{R_1} e^{i\hat{\mathbb{Q}}\alpha}]$ that requires to specialise the above discussion to the case $n = 1$. Hence, $N_1^{(\nu)}(\alpha)$ reduces to one mode, $k = 0$, and Eq. (4.4.1) becomes

$$\frac{1}{2\pi}\epsilon^{\mu\nu}\partial_\nu A^0_\mu(x) = \left(\frac{\alpha}{2\pi}\right)\delta(x-u_1) - \left(\frac{\alpha}{\pi}\right)\delta(x-v_1) + \left(\frac{\alpha}{2\pi}\right)\delta(x-v_2). \tag{4.4.10}$$

As detailed in the last part of Appendix 4.B, we need to find the dominant term, i.e. with the lowest scaling dimension, in the mode expansion. In particular, it turns out that for $|\alpha/\pi| > 2/3$ an additional -2π flux has to be inserted at v_1 while an additional 2π has to be added at u_1 or, equivalently, at v_2. This is the only difference with respect to $n_o \neq 1$, when the 2π flux has to be inserted only in u_1. Hence, the final expression is given by

$$N_1^{(\nu)}(\alpha) = \begin{cases} \dfrac{|\theta_1(r_1|\tau)|^{-\frac{\alpha^2}{\pi^2}}|\theta_1(r_2|\tau)|^{-\frac{\alpha^2}{\pi^2}}|\theta_1(r_1+r_2|\tau)|^{\frac{\alpha^2}{2\pi^2}}}{|\epsilon_N/L\partial_z\theta_1(0|\tau)|^{-\frac{3\alpha^2}{2\pi^2}}}\left|\dfrac{\theta_\nu(|\frac{\alpha}{2\pi}|(r_2-r_1)|\tau)}{\theta_\nu(0|\tau)}\right|^2 & |\alpha| \leq \frac{2\pi}{3} \\ f(r_1,r_2;|\alpha|)\dfrac{\theta_1(r_1+r_2|\tau)|^{|\frac{\alpha}{\pi}|(|\frac{\alpha}{2\pi}|-1)}}{|\epsilon_N/L\partial_z\theta_1(0|\tau)|^{-\frac{3|\alpha|(-|\alpha|+2\pi)}{2\pi^2}-2}}\left|\dfrac{\theta_\nu(|\frac{\alpha}{2\pi}|(r_2-r_1)+r_1|\tau)}{\theta_\nu(0|\tau)}\right|^2 & |\alpha| > \frac{2\pi}{3} \end{cases} \tag{4.4.11}$$

where $f(x,y;q) = \frac{1}{2}[x^{2(q-1)(-2q+1)}y^{2q(-2q+1)} + x \leftrightarrow y]$. The cutoff related to the charged probability is denoted as ϵ_N. Its explicit expression, for a lattice regularisation of the Dirac field, is given in Eq. (4.C.23a) and (4.C.23b) for $|\alpha| \leq 2/3\pi$ and $|\alpha| > 2/3\pi$, respectively. This introduction of a new symbol ϵ_N is necessary in order to avoid confusion with the cutoff ϵ obtained in the replica limit as $n_e \to 1$, given explicitly for the lattice model in Eq. (4.C.22) (and it is different from $n_o = 1$).

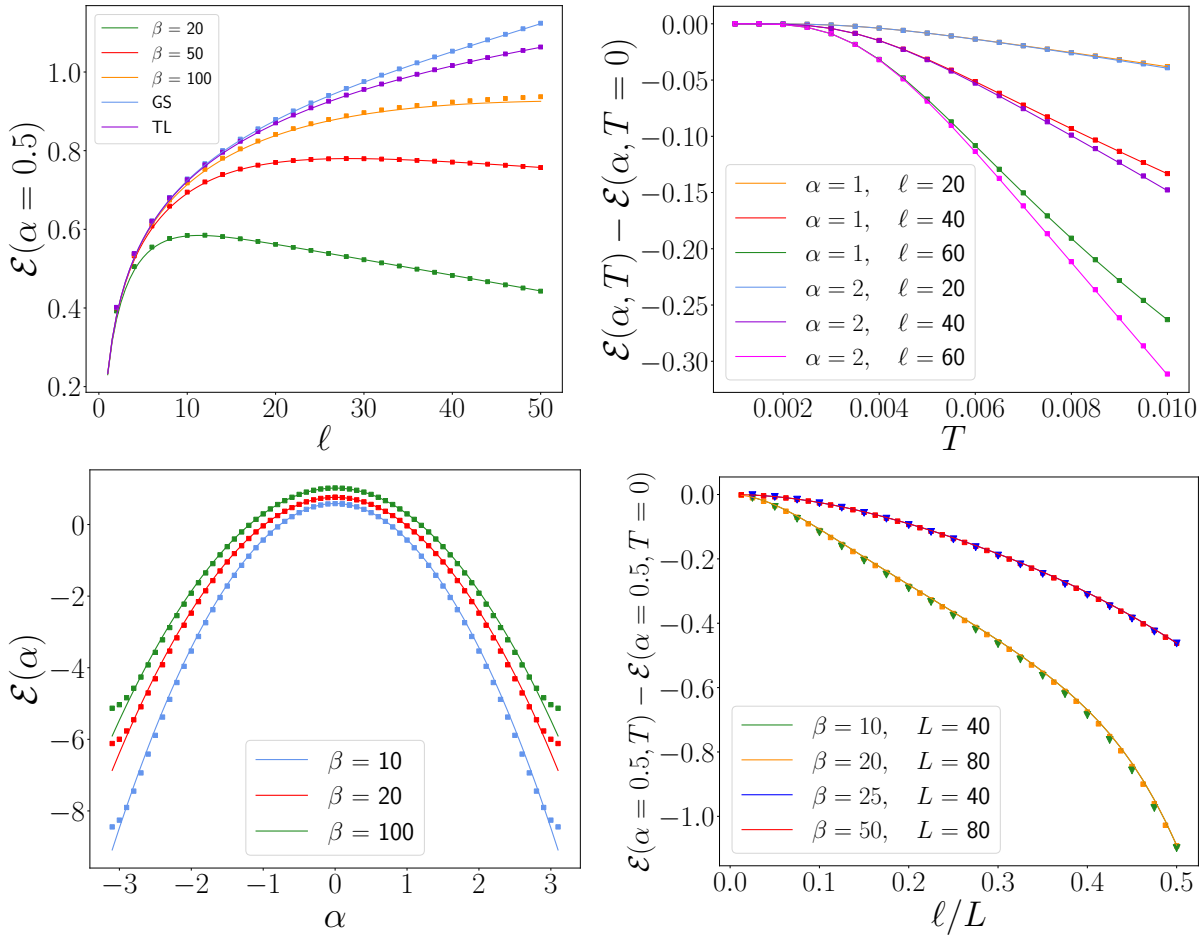


Figure 4.2: Charged negativity $\mathcal{E}(\alpha)$ in a tripartite torus with subsystem length $\ell_1 = \ell_2 = \ell$. CFT results (4.4.9), lines, against numerics on the lattice, symbols. *Top-left*: $\mathcal{E}(\alpha)$ as a function of ℓ for $\alpha = 0.5$. We consider different values of $\beta = 1/T$: in particular, GS stands for ground state, i.e. $T = 0$ while TL refers to the thermodynamic limit $T = 0, L \to \infty$. System size is fixed to $L = 200$ sites, except for the TL curve. *Top-right*: $\mathcal{E}(\alpha)$ as a function of the temperature T for different values of α and ℓ, with $L = 200$. The subtraction of the value $\mathcal{E}(\alpha, T = 0)$ cancels the dependence on the cutoff and the resulting curves are universal. *Bottom-left*: $\mathcal{E}(\alpha)$ as a function α for $L = 200$ and $\ell = 20$ for a few β. The agreement is perfect away from the boundaries $\alpha = \pm\pi$. *Bottom-right*: Scaling collapse of the charged negativity as a function of β/L and ℓ/L. We fix $\alpha = 0.5$.

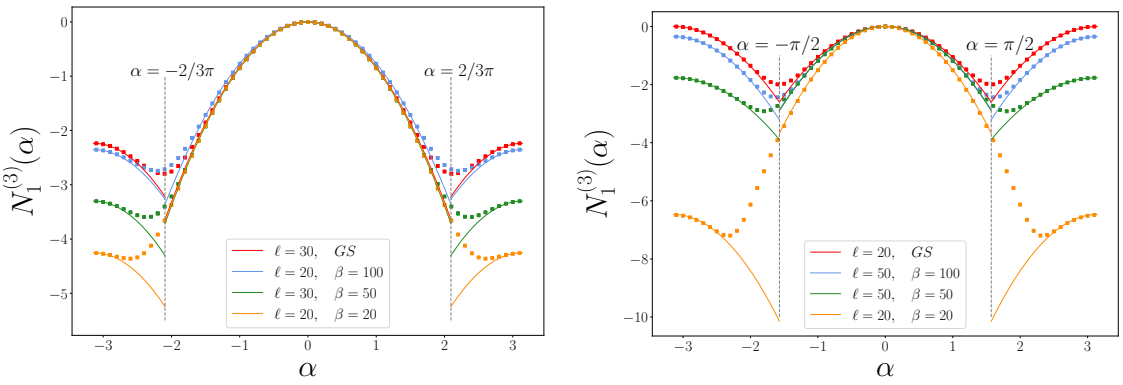


Figure 4.3: The charged probability $N_1^{(3)}(\alpha)$ for tripartite (left) and bipartite (right) geometry as a function of α. We set $L = 100$. Analytical predictions in Eqs. (4.4.11) and (4.5.8) are compared with the exact lattice computations at different β. Notice the discontinuities at $\alpha = \pm 2/3\pi$ (left) and $\alpha = \pm\pi/2$ (right).

4.4.1 Low and high temperature limits.

In this section we report the low and high temperature limits of the charged RN. Actually, the results that we are going to derive in the following for the tripartite geometry can be much more easily deduced by mapping the results in the complex plane (4.2.23) (i.e. both $L, \beta \to \infty$) to a cylinder periodic in either space or time (obtaining the forthcoming Eqs. (4.4.16) and (4.4.23), respectively). It is however a highly non trivial check for the correctness of our formulas that these results are re-obtained in the proper limits. For sake of conciseness, we focus on even $n = n_e$ and on the $\nu = 3$ sector, but similar formulas hold for all other cases.

In the low temperature limit where $\tau = \mathrm{i}\beta/L \to i\infty$, we can take advantage of the relation

$$\lim_{\beta\to\infty} \theta_1(z|\mathrm{i}\beta/L) = 2\mathrm{e}^{-\pi\beta/(4L)} \sin \pi z + O(\mathrm{e}^{-2\pi\beta/L}). \tag{4.4.12}$$

In this way we obtain for the spin-independent part

$$\log N_{n_e,0}(\alpha) = \log R_{n_e} - \frac{\alpha^2}{2\pi^2 n_e} \ln \left| \left(\frac{L}{\pi\epsilon}\right)^3 \frac{\sin^2\left(\frac{\pi\ell_1}{L}\right)\sin^2\left(\frac{\pi\ell_2}{L}\right)}{\sin\left(\frac{\pi(\ell_1+\ell_2)}{L}\right)} \right| + O(\mathrm{e}^{-2\pi/(LT)}), \tag{4.4.13}$$

while using the product representation of the theta function (4.3.18), the spin structure dependent term (4.4.8) can be rewritten as

$$\log N^{(3)}_{n_e,1}(\alpha) = \\ = 2\sum_{j=1}^{\infty} \frac{(-1)^{j+1}}{j} \frac{1}{\sinh(\pi j\beta/L)} \left(\cos(j(r_1-r_2)\alpha/n_e) \frac{\sin(\pi j r_2) - \sin(\pi j r_1)}{\sin(\pi j(r_2-r_1)/n_e)} - n_e \right). \tag{4.4.14}$$

Thus, at the leading order, Eq. (4.4.13) is the whole story at zero temperature, since in the replica limit the above expression contributes to the charged negativity as

$$\mathcal{E}_1^{(3)}(\alpha) = \lim_{n_e\to 1} \log N^{(3)}_{n_e,1}(\alpha) = 4\mathrm{e}^{-\pi/(LT)} \left(\cos((r_1-r_2)\alpha) \frac{\cos(\pi(r_2+r_1)/2))}{\cos(\pi(r_2-r_1)/2)} - 1 \right). \tag{4.4.15}$$

Putting everything together, in the low temperature limit the logarithmic charged negativity of two adjacent intervals for spatially antiperiodic fermions is given by

$$\mathcal{E}(\alpha, LT \ll 1) = \mathcal{E} - \frac{\alpha^2}{2\pi^2 n_e} \log \left| \left(\frac{L}{\pi\epsilon}\right)^3 \frac{\sin^2\left(\frac{\pi\ell_1}{L}\right)\sin^2\left(\frac{\pi\ell_2}{L}\right)}{\sin\left(\frac{\pi(\ell_1+\ell_2)}{L}\right)} \right| + O(\mathrm{e}^{-2\pi/(LT)}), \tag{4.4.16}$$

where $\mathcal{E}(LT \ll 1) = \frac{1}{4}\log\left|(\frac{L}{\pi\epsilon})\frac{\sin(\frac{\pi\ell_1}{L})\sin(\frac{\pi\ell_2}{L})}{\sin(\frac{\pi(\ell_1+\ell_2)}{L})}\right|$. We can also study the low-temperature behaviour of Eq. (4.4.11), which reads

$$N_1(\alpha, LT \ll 1) \simeq \begin{cases} -\frac{\alpha^2}{2\pi^2}\log\left|\frac{L^3}{\pi^3\epsilon_N^3}\frac{\sin^2(\frac{\pi\ell_1}{L})\sin^2(\frac{\pi\ell_2}{L})}{\sin(\frac{\pi(\ell_1+\ell_2)}{L})}\right|, & |\alpha| \le \frac{2\pi}{3} \\ \frac{(2\pi-|\alpha|)|\alpha|}{2\pi^2}\log\left|\frac{L^3}{\pi^3\epsilon_N^3}\frac{\sin^2(\frac{\pi\ell_1}{L})\sin^2(\frac{\pi\ell_2}{L})}{\sin(\frac{\pi(\ell_1+\ell_2)}{L})}\right| - \log\left|\frac{L^2}{\pi^2\epsilon_N^2}\sin(\frac{\pi\ell_1}{L})\sin(\frac{\pi\ell_2}{L})\right|. & |\alpha| > \frac{2\pi}{3}. \end{cases} \tag{4.4.17}$$

To investigate the high temperature behaviour, $\tau = \mathrm{i}\beta/L \to 0$, we can use the modular transformation rules for the theta functions:

$$\begin{aligned} \theta_1(z|\tau) &= -(-\mathrm{i}\tau)^{-1/2}\mathrm{e}^{-\mathrm{i}\pi z^2/\tau}\theta_1(z/\tau|-1/\tau), \\ \theta_3(z|\tau) &= (-\mathrm{i}\tau)^{-1/2}\mathrm{e}^{-\mathrm{i}\pi z^2/\tau}\theta_3(z/\tau|-1/\tau), \end{aligned} \tag{4.4.18}$$

and the asymptotic form of the θ_1 function in the small β limit

$$\theta_1(z/\tau|-1/\tau) = -2\mathrm{i}\mathrm{e}^{-\frac{\pi L}{4\beta}}\sinh(\frac{\pi z L}{\beta}) + O(\mathrm{e}^{\frac{3\pi L}{\beta}(z-3/4)}), \quad 0 \le z \le 1/2. \tag{4.4.19}$$

Therefore, the leading terms of the spin-independent part of the charged negativities can be written as

$$\log N_{n_e,0}(\alpha) = \log R_{n_e} + \frac{(\ell_1-\ell_2)^2\alpha^2}{2\pi n_e\beta L} - \frac{\alpha^2}{2\pi^2 n_e}\ln\left|\left(\frac{\beta}{\pi\epsilon}\right)^3\frac{\sinh^2\left(\frac{\pi\ell_1}{\beta}\right)\sinh^2\left(\frac{\pi\ell_2}{\beta}\right)}{\sinh\left(\frac{\pi(\ell_1+\ell_2)}{\beta}\right)}\right| + O(\mathrm{e}^{-\pi LT}), \tag{4.4.20}$$

while for the spin structure dependent term (4.4.8) we find

$$\begin{aligned} \log N^{(3)}_{n_e,1}(\alpha) = &-\frac{\pi}{2\beta L}\left[\left(\frac{n_e^2-1}{3n_e}\right)(\ell_2-\ell_1)^2 + n_e\ell_1(\ell_2-\ell_1) + n_e\ell_1^2\right] - \frac{(\ell_2-\ell_1)^2\alpha^2}{2\pi L\beta n_e} + \\ &- 2\sum_{j=1}^{\infty}\frac{(-1)^j}{j}\frac{1}{\sinh(\frac{\pi jL}{\beta})}\left(\cosh\left(\frac{j(\ell_1-\ell_2)\alpha}{\beta n_e}\right)\frac{\sinh(\pi\ell_2 j/\beta)-\sinh(\pi\ell_1 j/\beta)}{\sinh\left(\frac{\pi(\ell_2-\ell_1)j}{n_e\beta}\right)} - n_e\right). \end{aligned} \tag{4.4.21}$$

For fixed $\ell_{1,2}/\beta$ and $\tau = \mathrm{i}\beta/L \to 0$ we get

$$\mathcal{E}_1^{(3)}(\alpha) = -\frac{\pi\ell_1\ell_2}{2\beta L} - \frac{(\ell_2-\ell_1)^2\alpha^2}{2\pi L\beta}, \tag{4.4.22}$$

and therefore,

$$\mathcal{E}(\alpha, LT \gg 1) = \mathcal{E} - \frac{\alpha^2}{2\pi^2 n_e}\log\left|\left(\frac{\beta}{\pi\epsilon}\right)^3\frac{\sinh^2\left(\frac{\pi\ell_1}{\beta}\right)\sinh^2\left(\frac{\pi\ell_2}{\beta}\right)}{\sinh\left(\frac{\pi(\ell_1+\ell_2)}{\beta}\right)}\right| + O(\mathrm{e}^{-\pi LT}), \tag{4.4.23}$$

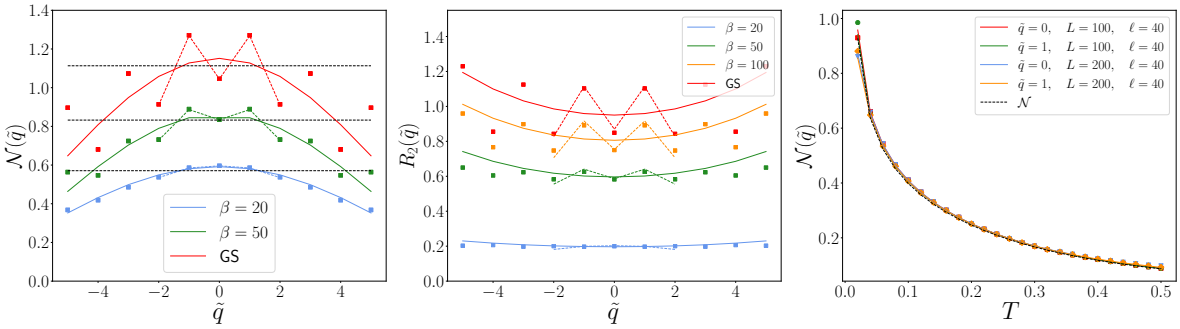


Figure 4.4: Imbalance resolved negativities for a few different values of $\tilde{q}$, $L = 200$, $\ell_1 = \ell_2 = \ell = 30$, with $n_e \to 1$ (left-panel) and $n = 2$ (middle-panel). The dashed black lines are the truly asymptotic result (4.4.32) showing equipartition, while the solid lines include the first correction due to the cutoffs as in Eq. (4.4.31). The dashed coloured lines are the ratio between the Fourier transforms without exploiting the saddle point approximation. For small q, the field theory prediction (in which the lattice cutoffs are included) well describes the numerical data. In the right-panel, $\ell = 40$ is fixed, we report two system sizes and two values of q and plot $\mathcal{N}(q)$ as a function of T. The coloured lines are Eq. (4.4.31) while the dashed one represents Eq. (4.4.32). The plot confirms the equipartition of negativity. Moreover, for large T, $\mathcal{N}(q)$ becomes a universal function of $\pi\ell T$.

where $\mathcal{E}(LT \gg 1) = \frac{1}{4}\log\left|(\frac{\beta}{\pi\epsilon})\frac{\sinh(\frac{\pi\ell_1}{\beta})\sinh(\frac{\pi\ell_2}{\beta})}{\sinh(\frac{\pi(\ell_1+\ell_2)}{\beta})}\right|$. This limit confirms analytically the volume law behaviour observed in Fig. 4.2.

The high-temperature limit of the charged probability $N_1(\alpha)$ in Eq. (4.4.11) is

$$N_1(\alpha, LT \gg 1) \simeq \begin{cases} -\frac{\alpha^2}{2\pi^2}\log\left|\frac{\beta^3}{\pi^3\epsilon_N^3}\frac{\sinh^2(\frac{\pi\ell_1}{L})\sinh^2(\frac{\pi\ell_2}{L})}{\sinh(\frac{\pi(\ell_1+\ell_2)}{L})}\right| & |\alpha| \leq \frac{2\pi}{3}, \\ \frac{(2\pi-|\alpha|)|\alpha|}{2\pi^2}\log\left|\frac{\beta^3}{\pi^3\epsilon_N^3}\frac{\sinh^2(\frac{\pi\ell_1}{L})\sinh^2(\frac{\pi\ell_2}{L})}{\sinh(\frac{\pi(\ell_1+\ell_2)}{L})}\right| - \log\left|\frac{\beta^2}{\pi^2\epsilon_N^2}\sinh(\frac{\pi\ell_1}{L})\sinh(\frac{\pi\ell_2}{L})\right|. & |\alpha| > \frac{2\pi}{3} \end{cases} \tag{4.4.24}$$

Let us conclude the subsection comparing these new results with those for the standard (bosonic) charged negativity reported in Eq. (4.2.23). At zero temperature and in the thermodynamic limit $\ell_i \ll L$, Eq. (4.4.13) matches exactly the bosonic negativity (4.2.23) (at $K = 1$ to describe free fermions) obtained in the same limit. As discussed deeply in Ref. [161] for the RN (at $\alpha = 0$), this shows that the choice of charged moments of the partial TR we made in Eq. (4.3.25) provides a partition function evaluated on the same worldsheet $\mathcal{R}_{n,\alpha}$ as the one for the moments of the standard charged partial transpose in [38].

4.4.2 Symmetry resolution

Again for conciseness of the various formulas, in this subsection we focus on the case $\ell_1 = \ell_2 = \ell$ (when also a closed-form expression for the spin-dependent part is easier to write), but more general formulas are similarly derived. Since we are ultimately using a saddle point approximation to make the Fourier transform (4.3.28), the charged moments (4.3.25) can be truncated at Gaussian level in α as

$$N_n^{(\nu)}(\alpha) = R_n^{(\nu)} \mathrm{e}^{-b_n\alpha^2/2}, \tag{4.4.25}$$

where

$$b_n = \frac{1}{\pi^2 n} \log \left| \theta_1(r_1|\tau)^4 \theta(2r_1|\tau)^{-1} \left(\frac{\epsilon}{L} \partial_z \theta_1(0|\tau) \right)^{-3} \right|. \tag{4.4.26}$$

The Fourier transform reads

$$\mathcal{Z}^{(\nu)}_{R_1,n}(\tilde{q}) = R^{(\nu)}_n \int_{-\pi}^{\pi} \frac{\mathrm{d}\alpha}{2\pi} \mathrm{e}^{-\mathrm{i}\tilde{q}\alpha} \mathrm{e}^{-\alpha^2 b_n/2}, \tag{4.4.27}$$

where we used that the expectation value of the charge imbalance operator $\hat{Q}_A$ for a free Dirac field is $\tilde{\bar{q}} = 0$ at any temperature. In the saddle point approximation the integration domain is extended to the whole real line and we end up in a simple Gaussian integral, obtaining

$$\mathcal{Z}^{(\nu)}_{R_1,n}(\tilde{q}) \simeq \frac{R^{(\nu)}_n}{\sqrt{2\pi b_n}} \mathrm{e}^{-\frac{\tilde{q}^2}{2b_n}}. \tag{4.4.28}$$

Through a similar analysis, we compute

$$\tilde{p}^{(\nu)}(\tilde{q}) = \int_{-\pi}^{\pi} \frac{\mathrm{d}\alpha}{2\pi} \mathrm{e}^{-\mathrm{i}\tilde{q}\alpha} N^{(\nu)}_1(\alpha), \tag{4.4.29}$$

which through the saddle-point approximation reads

$$\tilde{p}(\tilde{q}) \simeq \frac{\mathrm{e}^{-\frac{\tilde{q}^2}{2b_N}}}{\sqrt{2\pi b_N}} \quad b_N = \frac{1}{\pi^2} \log \left| \theta_1(r_1|\tau)^4 \theta(2r_1|\tau)^{-1} \left(\frac{\epsilon_N}{L} \partial_z \theta_1(0|\tau) \right)^{-3} \right|. \tag{4.4.30}$$

Let us note that for $\alpha \in [-\pi, \pi]$, the quantity $N^{\nu}_1(\alpha)$ has a global maximum for $\alpha = 0$ and two local maxima for $\alpha = \pm\pi$, see Fig. 4.3 (left). However, since $N^{\nu}_1(\pm\pi) < N^{\nu}_1(0)$, we can neglect the contributions to the integral coming from the regions close to the extrema at $\alpha = \pm\pi$. A similar reasoning applies to all odd charged moments $R_{n_o}(\alpha)$. Once again, let us stress the difference between the cutoff ϵ_N and the cutoff ϵ obtained in the replica limit $b = \lim_{n_e \to 1} b_{n_e}$, whose lattice expression is given in Eqs. (4.C.23a) and (4.C.22), respectively. Putting everything together, we obtain

$$R^{(\nu)}_n(\tilde{q}) = R^{(\nu)}_n \sqrt{\frac{(2\pi b_N)^n}{2\pi b_n}} \mathrm{e}^{-\frac{\tilde{q}^2}{2}\left(\frac{1}{b_n} - \frac{n}{b_N}\right)}, \qquad \mathcal{N}^{(\nu)}(q) = \frac{1}{2}\left(\mathrm{e}^{\mathcal{E}^{(\nu)}} \sqrt{\frac{b_N}{b}} \mathrm{e}^{-\frac{\tilde{q}^2}{2}\left(\frac{1}{b} - \frac{1}{b_N}\right)} - 1 \right). \tag{4.4.31}$$

When the $O(1)$ terms are negligible with respect to the leading order ones in the variance, $b_N \simeq b$, hence

$$\mathcal{N}^{(\nu)}(\tilde{q}) \simeq \mathcal{N}^{(\nu)}, \tag{4.4.32}$$

i.e. exact equipartition of negativity in the different imbalance sectors at leading order, as shown for the bosonic negativity in section (4.2.2). A similar result holds even if $\ell_1 \neq \ell_2$ in the low/high temperature limits, it would be sufficient to modify the expression of the variances in Eqs. (4.4.26) and (4.4.30).

It is instructive to explicitly write down the first term breaking the equipartition. For large L, we can expand the exponential in Eq. (4.4.31) as

$$\mathrm{e}^{-\frac{\tilde{q}^2}{2}\left(\frac{1}{b} - \frac{1}{b_N}\right)} \simeq 1 - \frac{\tilde{q}^2 \log(|\epsilon/\epsilon_N|)\pi^2}{6(\log L)^2} \equiv 1 - \frac{\gamma}{(\log L)^2} \tilde{q}^2, \tag{4.4.33}$$

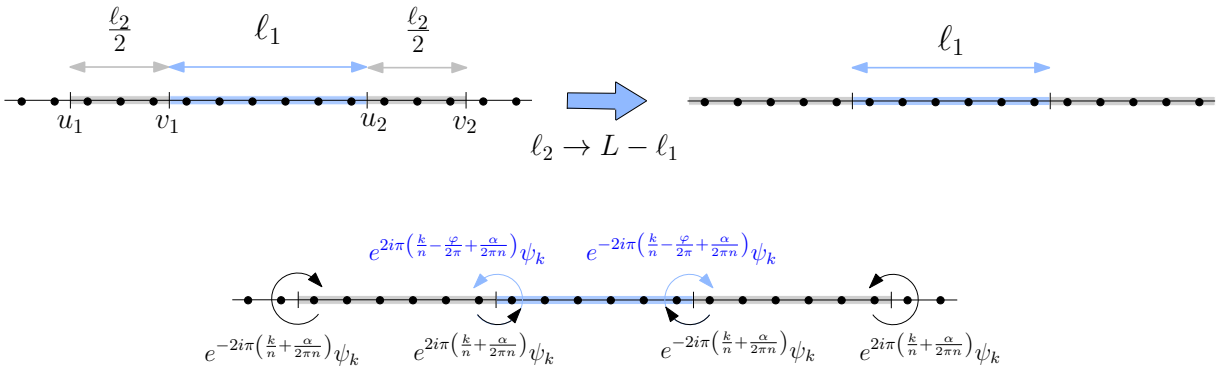


Figure 4.5: The tripartite geometry (left) of an interval of length ℓ_1 symmetrically embedded inside another subsystem of total length ℓ_2. A single interval in a chain of total length L (right) is obtained taking the limit $\ell_2 \to L - \ell_1$ of this tripartite geometry. The bottom panel shows the phase taken by the field ψ_k going around each branch point. The RDM corresponds to the union of the coloured regions, and the partial transpose is applied to the blue region.

and

$$\sqrt{\frac{b_N}{b}} \simeq 1 + \frac{\gamma'}{\log L}, \tag{4.4.34}$$

where γ and γ' are implicitly defined, also in terms of the cutoffs ϵ and ϵ_N in Appendix 4.C. To sum up, we get

$$\mathcal{N}^{(\nu)}(\tilde{q}) \simeq \mathcal{N}^{(\nu)}\Big(1 + \frac{\gamma'}{\log L} - \frac{\gamma}{(\log L)^2} q^2 + \dots\Big), \tag{4.4.35}$$

where we have derived the leading q-dependent contributions and shown that the equipartition is broken at order $1/(\log L)^2$.

In Fig. 4.4 we test the accuracy of our predictions against exact lattice numerical calculations. It is evident that equipartition is broken for all the values of ℓ, T, L we considered and the effect is more pronounced as $|\tilde{q}|$ is increased. However, the main smooth part of corrections to the scaling is captured by Eq. (4.4.31), see the full line in the plots, and does not come as a surprise. Also the presence of further subleading oscillating (in q) corrections have been observed for the resolved entropies [1] and were expected. In our case, such corrections are enhanced by the presence of the maxima at $\alpha = \pm\pi$ in $N_1(\alpha)$, see Fig. 4.4, that provide large corrections to the scaling in $\tilde{p}(\tilde{q})$. Indeed, taking the Fourier transforms without making the saddle-point approximation, the agreement between numerics and field theory is perfect. As $\ell \gg 1/T$, all these corrections become smaller and imbalance resolved negativity flattens in $\tilde{q}$, mainly as a consequence of the lowering of the maxima at $\alpha = \pm\pi$ in $N_1(\alpha)$, see Fig. 4.4.

4.5 Charged and symmetry resolved negativities in a bipartite geometry

In this section we move to the imbalance resolved negativity of a single interval at finite temperature. This geometry can be studied more effectively by considering a tripartite geometry where an interval of length ℓ_1 is symmetrically embedded inside another subsystem of total length ℓ_2, as depicted in Fig 4.5. Eventually, we take the limit $\ell_2 \to L - \ell_1$ in our calculations,

where L is the total length of the chain, in such a way that the part B becomes the empty set and consequently the system becomes bipartite.

Choosing the locations of the branch points at $u_1 = -\ell_2/(2L) = -r_2/2, v_2 = (\ell_2/2 + \ell_1)/L = r_2/2 + r_1, u_2 = \ell_1/L = r_1, v_1 = 0$, the multivalued field ψ_k takes up a phase $e^{2\pi i(\frac{k}{n}+\frac{\alpha}{2\pi n}-\frac{\varphi_n}{2\pi})}$, $e^{-2\pi i(\frac{k}{n}+\frac{\alpha}{2\pi n}-\frac{\varphi_n}{2\pi})}$ going around v_1 and u_2, respectively while going around v_2 and u_1 picks up a phase $e^{2\pi i(\frac{k}{n}+\frac{\alpha}{2\pi n})}$, $e^{-2\pi i(\frac{k}{n}+\frac{\alpha}{2\pi n})}$, respectively. As repeatedly used, this multivaluedness of the field ψ_k can be removed by introducing a single-valued field coupled to an external gauge field A^k_μ, as in Eq. (4.3.6). In order to recover the correct phases of the multivalued fields, A^k_μ has to satisfy

$$\frac{1}{2\pi}\epsilon^{\mu\nu}\partial_\nu A^k_\mu(x) = \left(\frac{2k}{n}+\frac{\alpha}{\pi n}-\frac{\varphi_n}{2\pi}\right)(\delta(x-v_1)-\delta(x-u_2)) + \left(\frac{k}{n}+\frac{\alpha}{2\pi n}\right)(\delta(x-v_2)-\delta(x-u_1)). \quad (4.5.1)$$

Therefore, $Z^{(\nu)}_{R_1,k}(\alpha)$ can be expressed as the following correlation function of vertex operators

$$Z^{(\nu)}_{R_1,k}(\alpha) = \langle V_{-\frac{k}{n}-\frac{\alpha}{2\pi n}}(u_1) V_{\frac{2k}{n}+\frac{\alpha}{\pi n}-\frac{\varphi_n}{2\pi}}(v_1) V_{-\frac{2k}{n}-\frac{\alpha}{\pi n}+\frac{\varphi_n}{2\pi}}(u_2) V_{\frac{k}{n}+\frac{\alpha}{2\pi n}}(v_2)\rangle\,. \quad (4.5.2)$$

Using Eq. (4.3.13), we have

$$Z^{(\nu)}_{R_1,k}(\alpha) = |\theta_1(r_1|\tau)|^{-2(\frac{2k}{n}+\frac{\alpha}{\pi n}-\frac{\varphi_n}{2\pi})^2}\left|\frac{\theta_1(\frac{r_2}{2}|\tau)}{\theta_1(\frac{r_2}{2}+r_1|\tau)}\right|^{-4(\frac{k}{n}+\frac{\alpha}{2\pi n})(\frac{2k}{n}+\frac{\alpha}{\pi n}-\frac{\varphi_n}{2\pi})}$$
$$|\theta_1(r_1+r_2|\tau)|^{-2(\frac{k}{n}+\frac{\alpha}{2\pi n})^2} \times \left|\frac{\epsilon}{L}\partial_z\theta_1(0|\tau)\right|^{-\Delta_k(\alpha)} \left|\frac{\theta_\nu((\frac{k}{n}+\frac{\alpha}{2\pi n})(r_2-r_1)+\frac{\varphi_n}{2\pi}r_1|\tau)}{\theta_\nu(0|\tau)}\right|, \quad (4.5.3)$$

where

$$\Delta_k(\alpha) = -10\frac{k^2}{n^2} - 10\frac{k\alpha}{n^2\pi} - 5\frac{\alpha^2}{2n^2\pi^2} + 4k\frac{\varphi_n}{n\pi} + 2\frac{\alpha\varphi_n}{n\pi^2} - \frac{\varphi_n^2}{2\pi^2} - 2\theta(-k)(1+\frac{4k}{n}+\frac{2\alpha}{n\pi}-\frac{\varphi_n}{\pi}). \quad (4.5.4)$$

Also in this case we fix the value of φ_n for $k<0$ according to the discussion in Appendix 4.B, taking care of the mode $k=0$ for $n=n_o$. This leads to the spin-independent terms

$$\log N_{n,0}(\alpha) = \log R_n - \frac{\alpha^2}{2\pi^2 n}\log\left|\frac{\theta_1(r_1|\tau)^4\theta_1\left(\frac{r_2}{2}|\tau\right)^4\theta_1(r_1+r_2|\tau)}{\theta_1\left(r_1+\frac{r_2}{2}|\tau\right)^4(\frac{\epsilon}{L}\partial_z\theta_1(0|\tau))^5}\right|,$$
$$\log N_{n_o,0}(|\alpha|>\pi/2) = \log R_{n_o} - \frac{\alpha^2}{2\pi^2 n_o}\log\left|\frac{\theta_1(r_1|\tau)^4\theta_1\left(\frac{r_2}{2}|\tau\right)^4\theta_1(r_1+r_2|\tau)}{\theta_1\left(r_1+\frac{r_2}{2}|\tau\right)^4(\frac{\epsilon}{L}\partial_z\theta_1(0|\tau))^5}\right|$$
$$+\frac{2|\alpha|}{\pi n_o}\log\left|\frac{\theta_1(r_1|\tau)^2\theta_1\left(\frac{r_2}{2}|\tau\right)}{\theta_1\left(r_1+\frac{r_2}{2}|\tau\right)(\epsilon/L\partial_z\theta_1(0|\tau))^2}\right| - \frac{2}{n}\log\left|\frac{\theta_1(r_1|\tau)}{(\frac{\epsilon}{L}\partial_z\theta_1(0|\tau))}\right|,$$
$$\log R_{n_o} = -\left(\frac{n_o^2-1}{6n_o}\right)\log\left|\frac{\theta_1(r_1|\tau)\theta_1\left(\frac{r_2}{2}|\tau\right)\theta_1(r_1+r_2|\tau)}{\theta_1\left(r_1+\frac{r_2}{2}|\tau\right)(\frac{\epsilon}{L}\partial_z\theta_1(0|\tau))^2}\right|,$$
$$\log R_{n_e} = -\left(\frac{n_e^2-4}{6n_e}\right)\log\left|\frac{\theta_1(r_1|\tau)\theta_1\left(\frac{r_2}{2}|\tau\right)}{\theta_1\left(r_1+\frac{r_2}{2}|\tau\right)(\frac{\epsilon}{L}\partial_z\theta_1(0|\tau))}\right|$$
$$-\left(\frac{n_e^2-1}{6n_e}\right)\log\left|\theta_1(r_1+r_2|\tau)(\frac{\epsilon}{L}\partial_z\theta_1(0|\tau))^{-1}\right|, \quad (4.5.5)$$

and

$$\log N_{n,1}^{(\nu)}(\alpha) = 2 \sum_{k=-(n-1)/2}^{(n-1)/2} \log \left| \frac{\theta_\nu((\frac{k}{n} + \frac{\alpha}{2\pi n})(r_2 - r_1) + \frac{\varphi_n}{2\pi} r_1 | \tau)}{\theta_\nu(0|\tau)} \right|. \tag{4.5.6}$$

for the spin structure dependent term. In this geometry, $N_{n_o}^{(\nu)}(\alpha)$ presents a discontinuity for $|\alpha| = \frac{\pi}{2}$, as shown for $n_o = 1$ in Fig. 4.3.

At this point, we derived all the needed formulas to take the limit $r_2 \to 1 - r_1$ and to reproduce the bipartite geometry in which we are interested. Using that $\theta_1(z+1) = \theta_1(z)$, the spin-independent part of the charged logarithmic negativity (for even n and for odd and $\alpha < |\pi/2|$) becomes

$$\log N_{n,0}(\alpha) = \log R_n - \frac{2\alpha^2}{\pi^2 n} \log \left| \frac{L \theta_1(r_1|\tau)}{\epsilon \partial_z \theta_1(0|\tau)} \right|, \tag{4.5.7}$$

while the spin-dependent ones are just given by (4.5.6) without major simplifications.

At this point, we analyse the charged probability $N_1(\alpha) = \mathrm{Tr}[\rho^{R_1} e^{i\hat{Q}\alpha}]$. The final expression can be read off from Eq. (4.5.5) and, after some standard manipulations, can be put in the form

$$N_1^{(\nu)}(\alpha) = \begin{cases} \left(\frac{\theta_1(r_1|\tau)}{\frac{\epsilon_N}{L} \partial_z \theta_1(0|\tau)} \right)^{-2(\frac{\alpha}{\pi})^2} \left| \frac{\theta_\nu(|\frac{\alpha}{2\pi}|(1-2r_1)|\tau)}{\theta_\nu(0|\tau)} \right|^2 & |\alpha| \leq \frac{\pi}{2}, \\ \left(\frac{\theta_1(r_1|\tau)}{\frac{\epsilon_N}{L} \partial_z \theta_1(0|\tau)} \right)^{-2(|\frac{\alpha}{\pi}|-1)^2} \left| \frac{\theta_\nu(|\frac{\alpha}{2\pi}|(1-2r_1)+r_1|\tau)}{\theta_\nu(0|\tau)} \right|^2, & |\alpha| > \frac{\pi}{2}. \end{cases} \tag{4.5.8}$$

The cutoff for the charged probability is denoted by ϵ_N and its explicit expression is given in Eq. (4.C.25a) and (4.C.25b) for $|\alpha| \leq \pi/2$ and $|\alpha| > \pi/2$, respectively. We recall that, as in the tripartite case, ϵ_N is different from the cutoff ϵ obtained in the replica limit as $n_e \to 1$ and explicitly given in Eq. (4.C.24).

4.5.1 Low and high temperature limits

In this section we report the low and high temperature limits of the charged RN, focussing, once again, on even $n = n_e$ and on the $\nu = 3$ sector. The low temperature limits of the spin-independent part, Eq. (4.5.5), can be obtained through the relation (4.4.12), finding

$$\log N_{n_e,0}(\alpha) = \log R_{n_e} - \frac{2\alpha^2}{\pi^2 n_e} \left[\log \left| \frac{L}{\pi\epsilon} \sin\left(\frac{\pi \ell_1}{L} \right) \right| \right] + O(e^{-2\pi/(LT)}), \tag{4.5.9}$$

while the low temperature limit of the spin-dependent term, Eq. (4.5.6), can be obtained through the product representation (4.3.18) of the theta functions and it reads

$$\mathcal{E}_1^{(3)}(\alpha) = \lim_{n_e \to 1} \log Z_{n_e,1}^{(3)}(\alpha) = 4 e^{-\pi/(LT)} \left(\cos((r_1 - r_2)\alpha) \frac{\cos(\pi(r_2 + r_1)/2))}{\cos(\pi(r_2 - r_1)/2)} - 1 \right). \tag{4.5.10}$$

Therefore, as $\tau = i\beta/L \to 0$ and $r_2 \to 1 - r_1$, we get in the replica limit

$$\mathcal{E}(LT \ll 1)(\alpha) = \left(\frac{1}{2} - \frac{2\alpha^2}{\pi^2} \right) \log \left| \frac{L}{\pi\epsilon} \sin\left(\frac{\pi \ell_1}{L} \right) \right| + O(e^{-2\pi/(LT)}). \tag{4.5.11}$$

We notice that Eq. (4.5.11) coincides with $2 \log \mathrm{Tr}(\rho_{A_1}^{1/2} e^{i\hat{Q}_{A_1}\alpha})$, as it should for pure states (and mentioned in the introduction for $\alpha = 0$).

The low-temperature limit of Eq. (4.5.8) is

$$\log N_1(\alpha) \simeq \begin{cases} -\frac{2\alpha^2}{\pi^2}\log\left|\frac{L}{\pi\epsilon_N}\sin(\frac{2\pi\ell_1}{L})\right|, & |\alpha|\leq\frac{\pi}{2}, \\ -\frac{2(|\alpha|-\pi)^2}{\pi^2}\log\left|\frac{L}{\pi\epsilon_N}\sin(\frac{2\pi\ell_1}{L})\right|, & |\alpha|>\frac{\pi}{2}. \end{cases} \tag{4.5.12}$$

Interestingly, the previous expansion shows that its Fourier transform vanishes for odd values of the imbalance q. This agrees with the discussion at the end of Section 4.2.3: as $\tau = i\beta/L \to 0$, the state becomes pure and the vanishing of $p(q)$ occurs because the parity of the imbalance is fixed by the conservation of $\hat{N}_1 + \hat{N}_2$. This reflects the fact that the entanglement is better resolved in subsystem charges rather than in the imbalance.

As done in Sec. 4.4.1, the high temperature limit can be obtained using the modular properties of theta functions, Eq. (4.4.18), and the relation (4.4.19). The result for the spin-independent part in Eq. (4.5.5) is

$$\log N_{n_e,0}(\alpha) = \log R_{n_e} - \frac{2\alpha^2}{\pi^2 n_e}\Big[-\frac{\pi^2\ell_1^2}{\beta L} + \log\Big|\frac{\beta}{\epsilon\pi}\sinh\Big(\frac{\pi\ell_1}{\beta}\Big)\Big|\Big] + O(\mathrm{e}^{-\pi LT}). \tag{4.5.13}$$

The spin-dependent term in Eq. (4.5.5) can be evaluated as follows

$$\begin{aligned}\log N^{(3)}_{n_e,1}(\alpha) = &-\frac{\pi}{2\beta L}\left[\left(\frac{n_e^2-1}{3n_e}\right)(L-2\ell_1)^2 + n_e\ell_1(L-2\ell_1) + n_e\ell_1^2\right] - \frac{(L-2\ell_1)^2\alpha^2}{2\pi L\beta n_e} + \\ &-2\sum_{j=1}^{\infty}\frac{(-1)^j}{j}\frac{1}{\sinh(\frac{\pi jL}{\beta})}\Big(\cosh\Big(\frac{j(L-2\ell_1)\alpha}{\beta n_e}\Big)\frac{\sinh(\pi(L-\ell_1)j/\beta) - \sinh(\varphi_{n_e}\ell_1 j/\beta)}{\sinh\left(\frac{\pi(L-2\ell_1)j}{n_e\beta}\right)} - n_e\Big),\end{aligned} \tag{4.5.14}$$

which gives in the replica limit, for $\beta/L \to 0$ and ℓ_1/β fixed,

$$\mathcal{E}_1^{(3)}(\alpha) = \frac{\pi\ell_1(\ell_1-L)}{2\beta L} - \frac{(L-2\ell_1)^2\alpha^2}{2\pi\beta L} + O(\mathrm{e}^{-\pi LT}). \tag{4.5.15}$$

To sum up, we find in the high temperature regime

$$\mathcal{E}(LT\gg 1)(\alpha) = \Big(\frac{1}{2} - \frac{2\alpha^2}{\pi^2}\Big)\Big[\log\Big|\frac{\beta}{\pi\epsilon}\sinh(\frac{\pi\ell_1}{\beta})\Big| - \frac{\pi\ell_1}{\beta}\Big] - \frac{\alpha^2 L}{2\pi\beta} + O(\mathrm{e}^{-\pi LT}). \tag{4.5.16}$$

Given the result found in Eq. (4.5.11), one could be tempted to do a conformal mapping to a cylinder periodic in time, to get

$$\mathcal{E}(LT\gg 1)(\alpha)_{\text{naive}} = \Big(\frac{1}{2} - \frac{2\alpha^2}{\pi^2}\Big)\log\Big|\frac{\beta}{\epsilon\pi}\sinh\Big(\frac{\pi\ell_1}{\beta}\Big)\Big|, \tag{4.5.17}$$

which is nothing but the finite temperature logarithmic charged entropy of order $1/2$. This naive derivation provides a wrong result whose origin has been extensively discussed in [112] and it remains the right interpretation also for $\alpha \neq 0$. Indeed, for pure states (i.e. $T \to 0$), the n_e-sheeted Riemann surface, $\mathcal{R}_{n_e,\alpha}$, decouples in two independent $(n_e/2)$-sheeted surfaces characterised by the parity of the sheets and therefore $\mathcal{E}(\alpha)(LT \ll 1) = 2\log\mathrm{Tr}(\rho_{A_1}^{1/2}\mathrm{e}^{\mathrm{i}\hat{Q}_{A_1}\alpha})$. Conversely, this decoupling of the sheets does not occur at finite temperature. The lack of decoupling is manifested in the presence of the linear terms ℓ/β and L/β in Eq. (4.5.16) which cannot be derived through a simple conformal mapping.

We also present the high-temperature limit of the charged probability in Eq. (4.5.8), that is

$$\log N_1(\alpha) \simeq \begin{cases} -\frac{2\alpha^2}{\pi^2}\left[\log\left|\frac{\beta}{\pi\epsilon_N}\sinh(\frac{2\pi\ell_1}{\beta})\right| - \frac{\pi\ell_1}{\beta}\right] - \frac{\alpha^2 L}{2\pi\beta}, & |\alpha| \leq \frac{\pi}{2}, \\ -\frac{2(\alpha-\pi)^2}{\pi^2}\log\left|\frac{\beta}{\pi\epsilon_N}\sinh(\frac{2\pi\ell_1}{\beta})\right| - \frac{2\alpha\ell_1}{\beta} + \frac{2\alpha^2\ell_1}{\pi\beta} - \frac{\alpha^2 L}{2\pi\beta}, & |\alpha| > \frac{\pi}{2}. \end{cases} \tag{4.5.18}$$

4.5.2 A semi-infinite system

A simple generalisation of the previous calculation concerns the charged logarithmic negativity for a semi-infinite system. For free fermions, the semi-infinite geometry is obtained from the infinite one by cutting the interval A_1 in half. Because of the structure of the vertex operators correlations in Eq. (4.5.2), the entanglement in the semi-infinite system is equal to half of that of the infinite one in Eq. (4.5.5). Therefore, the charged logarithmic negativity of a finite interval with length $\ell_1 = r_1 L$ is given by

$$\log N_n^{(\nu)}(\alpha) = \log R_n - \frac{\alpha^2}{\pi^2 n}\log\left|\frac{\theta_1(2r_1|\tau)}{(\frac{\epsilon}{L}\partial_z\theta_1(0|\tau))}\right| + \\ + \sum_{k=-(n-1)/2}^{(n-1)/2}\log\left|\frac{\theta_\nu((\frac{k}{n}+\frac{\alpha}{2\pi n})(1-4r_1)+\frac{\varphi_n}{\pi}r_1|\tau)}{\theta_\nu(0|\tau)}\right|. \tag{4.5.19}$$

The low and high temperature limits of this expression are obtained in analogy with the infinite line case, e.g. as $\tau \to 0$ we get

$$\mathcal{E}(\alpha) = \left(\frac{1}{4} - \frac{\alpha^2}{\pi^2}\right)\left[\log\left|\frac{\beta}{\pi\epsilon}\sinh(\frac{2\pi\ell_1}{\beta})\right| - \frac{2\pi\ell_1}{\beta}\right] - \frac{\alpha^2 L}{4\pi\beta} + O(\mathrm{e}^{-\pi LT}). \tag{4.5.20}$$

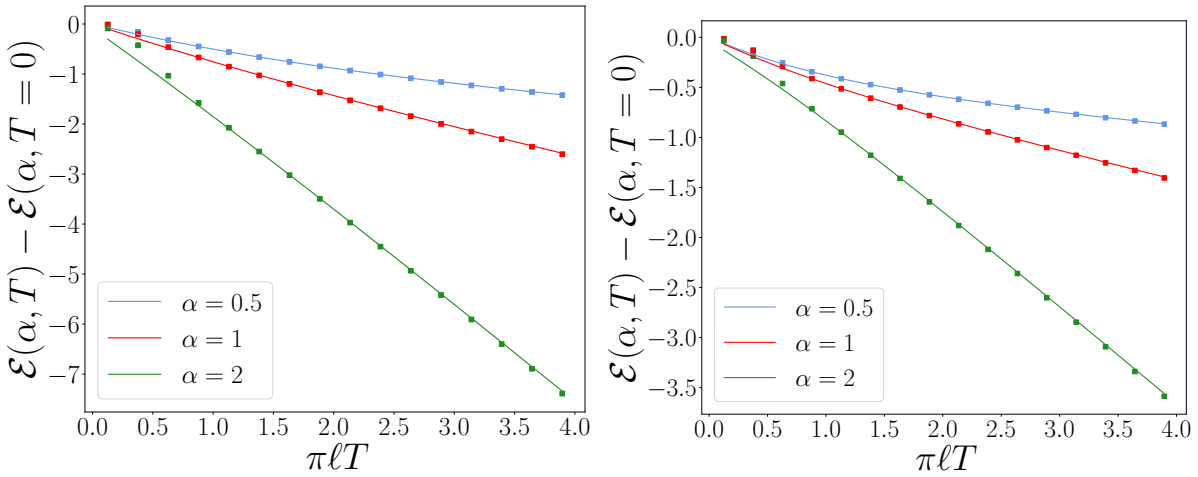


Figure 4.6: The charged logarithmic negativity for a bipartite geometry in the infinite-line (left) or semi-infinite (right). We set $L = 200$. Analytical prediction in Eqs. (4.5.16) and (4.5.20).

The correctness of these CFT charged negativities is tested against lattice calculations in Fig. 4.6. Here we plot $\mathcal{E}(\alpha, T) - \mathcal{E}(\alpha, T = 0)$ that turns out to be a universal function of $\pi\ell T$ and πLT, in agreement with Eqs. (4.5.16) and (4.5.20). As for the tripartite case, in order to test our final field theoretical results, we have taken into account the explicit expression for the cutoff

ϵ. Since it does not depend on the temperature, it can be extracted from the knowledge of the lattice charged moments $\mathrm{Tr}(\rho_{A_1}^{1/2}\mathrm{e}^{\mathrm{i}\hat{Q}_{A_1}\alpha})$ at $T=0$, derived in [1] and explicitly reported in the Appendix, see Eq. (4.C.24).

4.5.3 Symmetry resolution

As usual, the Fourier transform (4.3.28) is performed in the scaling regime with a saddle point approximation. Hence, the charged moments (4.3.25) can be truncated at Gaussian level in α as

$$N^{(\nu)}(\alpha)_n = R_n^{(\nu)}\mathrm{e}^{-\frac{\alpha^2}{2}b_n}, \tag{4.5.21}$$

where

$$b_n = \frac{4}{\pi^2 n}\log\left|\mathcal{A}_n^{(1)}\frac{L\theta_1(r_1|\tau)}{\epsilon\partial_z\theta_1(0|\tau)}\right|, \tag{4.5.22}$$

and we used a quadratic approximation for

$$\log N_{n,1}^{(\nu)}(\alpha) = \mathcal{A}_n^{(0)} - \frac{2\alpha^2}{\pi^2 n}\log\mathcal{A}_n^{(1)}. \tag{4.5.23}$$

The RN in the sector $\tilde{q}$ are

$$R_n^{(\nu)}(\tilde{q}) = \frac{\mathcal{Z}_{R_1,n}(\tilde{q})}{[\tilde{p}(\tilde{q})]^n} = R_n^{(\nu)}\frac{\int_{-\pi}^{\pi}\frac{\mathrm{d}\alpha}{2\pi}\mathrm{e}^{-\mathrm{i}\tilde{q}\alpha}\mathrm{e}^{-\alpha^2 b_n/2}}{\left[\int_{-\pi}^{\pi}\frac{\mathrm{d}\alpha}{2\pi}\mathrm{e}^{-\mathrm{i}\tilde{q}\alpha}N_1(\alpha)\right]^n}, \tag{4.5.24}$$

and, through the saddle point approximation,

$$R_n^{(\nu)} \simeq R_n^{(\nu)}\sqrt{\frac{(2\pi b_N)^n}{2\pi b_n}}\mathrm{e}^{-\frac{\tilde{q}^2}{2}\left(\frac{1}{b_n}-\frac{n}{b_N}\right)}, \qquad \mathcal{N}^{(\nu)}(\tilde{q}) \simeq \frac{1}{2}\left(\mathrm{e}^{\mathcal{E}^{(\nu)}}\sqrt{\frac{2\pi b_N}{2\pi b}}\mathrm{e}^{-\frac{\tilde{q}^2}{2}\left(\frac{1}{b}-\frac{1}{b_N}\right)}-1\right), \tag{4.5.25}$$

with

$$b = \lim_{n_e\to 1} b_{n_e}, \qquad b_N = \frac{4}{\pi^2}\log\left|\mathcal{A}_N^{(1)}\frac{L\theta_1(r_1|\tau)}{\epsilon_N\partial_z\theta_1(0|\tau)}\right|. \tag{4.5.26}$$

The explicit expressions for the cutoff ϵ and ϵ_N can be found in Eqs. (4.C.24) and (4.C.25a), respectively. When the $O(1)$ terms are negligible with respect to the leading order ones, $b \simeq b_N$ and we find the exact equipartition of negativity in the different charge sectors at leading order, i.e. $\mathcal{N}^{(\nu)}(\tilde{q}) \simeq \mathcal{N}^{(\nu)}$, on the same lines as for the tripartite case. We used that the leading contribution to the integral $\tilde{p}(\tilde{q})$ comes from the region near the saddle point $\alpha = 0$, despite the presence of two local maxima at $\alpha = \pm\pi$. This is possible as long as $T > 0$: when $T \to 0$, the secondary maxima become degenerate with the one in 0 and they cannot be neglected. Their degeneracy is indeed related to the fact that $\tilde{p}(\tilde{q})$ becomes zero for all odd $\tilde{q}$.

Finally, it is worth reporting the high temperature limits of the variances in Eq. (4.5.26), that following the steps in Sect. 4.5.1, simplify as

$$\begin{aligned} b &= \lim_{n_e\to 1}\frac{4}{\pi^2 n_e}\left[\log\left|\frac{\beta}{\pi\epsilon}\sinh(\frac{\pi\ell_1}{\beta})\right| - \frac{\pi\ell_1}{\beta} + \frac{\pi L}{4\beta}\right], \\ b_N &= \frac{4}{\pi^2}\left[\log\left|\frac{\beta}{\pi\epsilon_N}\sinh(\frac{\pi\ell_1}{\beta})\right| - \frac{\pi\ell_1}{\beta} + \frac{\pi L}{4\beta}\right]. \end{aligned} \tag{4.5.27}$$

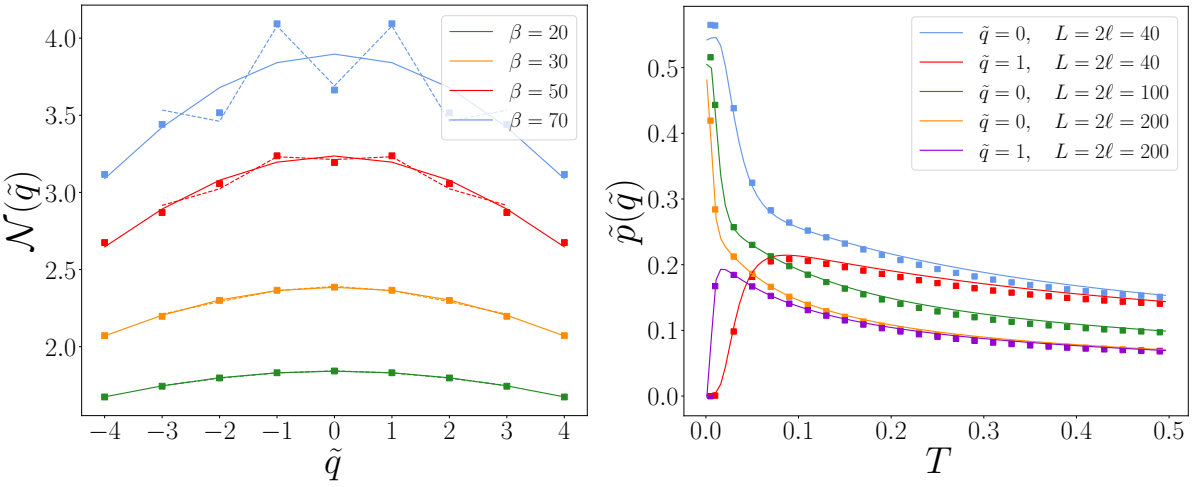


Figure 4.7: *Left*: The imbalance-resolved negativity as a function of $\tilde{q}$ in a bipartite geometry. The subsystem size is fixed, $\ell_1 = 40$, the total system sizes is also fixed, $L = 200$, while T is varied. The coloured full lines represent Eq. (4.5.25) while the dashed ones represent Eq. (4.5.24) in the replica limit. *Right*: The probability of finding $\tilde{q}$ as outcome of a measurement of $\hat{\tilde{Q}}$. As the state becomes pure (i.e. $T \to 0$), $\tilde{p}(\tilde{q}) \to 0$ for odd $\tilde{q}$, as explained in Sec. 4.2.3. The full lines correspond to the Fourier transforms of the charged probability in (4.5.8) without saddle-point approximation.

The symmetry resolved negativities for a single interval embedded inside a semi-infinite chain or in the low-temperature regime are straightforwardly derived with minor modifications of the above calculations.

Also for this bipartite geometry it is instructive to identify the first term breaking equipartition. Expanding to order $O((\log L)^{-2})$ the above expressions, we get

$$\mathcal{N}^{(v)}(\tilde{q}) \simeq \mathcal{N}^{(v)}\Big(1 - \frac{\tilde{\gamma}}{\log|\theta_1(r_1|\tau)(\partial_z\theta_1(0|\tau)/L)|)} - \frac{\tilde{q}^2\tilde{\gamma}\pi^2}{4(\log|\theta_1(r_1|\tau)(\partial_z\theta_1(0|\tau)/L)^{-1}|)^2}\Big), \tag{4.5.28}$$

where $\tilde{\gamma} = \frac{\pi^2}{8}\log(\epsilon_N\mathcal{A}/(\epsilon\mathcal{A}_N))$. Since $\mathcal{A}/\mathcal{A}_N \simeq 1$, $\tilde{\gamma}$ can be explicitly computed through the results for ϵ and ϵ_N found in Appendix 4.C.

Our analytic results for the symmetry resolved negativity are compared with the numerical data in the left panel of Figure 4.7. The equipartition of negativity is broken for all the considered values of ℓ, T, L and the effect is more evident as $|\tilde{q}|$ is increased. However, Eq. (4.5.25) can capture the smooth part of these corrections to the scaling, as shown by the full line in the plots. As $\ell \gg 1/T$, the corrections due to the presence of the maxima at $\alpha = \pm\pi$ in $N_1(\alpha)$ become smaller and the imbalance resolved negativity flattens in q, mainly as a consequence of the lowering of the maxima at $\alpha = \pm\pi$ in $N_1(\alpha)$, see Fig. 4.4. We also check the correctness of our prediction for $\tilde{p}(\tilde{q})$ in the right-panel of the same figure: we can observe that as the state becomes pure (i.e. $T \to 0$), $\tilde{p}(\tilde{q}) \to 0$ for odd $\tilde{q}$, as explained above. As already stressed many times, the divergent behaviour of negativity in the same charge sector is a consequence of the fact that the imbalance is no longer the right quantum number to resolve the entanglement.

4.6 Concluding remarks

We studied the EN in systems with a conserved local charge and we found it to be decomposable into symmetry sectors. The partial TR operation does not spoil the result found for the standard partial transposition operation [38]: the resulting operator that commutes with the partial TR density matrix is not the total charge, but rather an imbalance operator, which is essentially the difference operator between the charge in the two regions. We introduced a normalised version of the charge imbalance resolved negativity (both fermionic and bosonic) which has the great advantage to be an entanglement proxy also for the symmetry sectors, e.g. it vanishes if the standard partial transpose has only positive eigenvalues in the sector. The price to pay is that the normalised symmetry resolved negativity diverges (for some sectors) in the limit of pure states, as a consequence of the fact that the imbalance is no longer the best quantity to resolve the entanglement. Another interesting property of this normalisation for the sector partial transpose is the *negativity equipartition*, i.e. the entanglement is the same in all imbalance sectors, in full analogy to entropy equipartition for pure states [34].

We then considered the (1+1)d CFT corresponding to free massless Dirac fermions at finite temperature T and finite size L. We derived field theory predictions for the distribution of negativity in both tripartite and bipartite settings (i.e. the entanglement between two adjacent intervals and the one between one interval and the remainder, respectively). We tested our prediction against numerical computations for a lattice version of the Dirac field, in which the non-universal terms are fixed from exact analytic computations. In both geometries, we find that, at leading order, the charge imbalance resolved negativity satisfies entanglement equipartition. We identify the subleading terms responsible for the breaking of equipartition in the lattice model.

There are different aspects that this work leaves open for further study. The first one concerns the calculation of the time evolution of the charged and imbalance resolved negativity to understand if and how the quasiparticle picture remains true within the sectors of an internal local symmetry of a quantum many-body system, as recently done for the resolved entropies [3]. Secondly, one may use the corner transfer matrix to investigate the symmetry decomposition of negativity in gapped one-dimensional models by combining former studies of the total negativity [104] with those for symmetry resolution [56]. Eventually, the generalisation of one-dimensional results to higher dimensions can be done using the dimensional reduction approach, as already done for the total negativity in [161]. Decoupling the initial d-dimensional problem into one-dimensional ones in a mixed space-momentum representation [54] would allow to generalise the above results to higher dimensional Fermi surfaces.

4.A Appendix: Numerical methods

In this first appendix, we report how to numerically calculate the charged negativity associated with the partial TR (4.2.9) for free fermions on a lattice described by the hopping Hamiltonian on a chain

$$H_{FF} = -\sum_{j=0}^{L-2} c_{j+1}^\dagger c_j + c_0^\dagger c_{L-1} + \text{H.c.}, \tag{4.A.1}$$

with anti-periodic condition (corresponding to the $\nu = 3$ sector discussed in the main text). The technique is a straightforward generalisation to $\alpha \neq 0$ of the one presented in [161]. This method is used throughout the main text to obtain all lattice numerical results.

Even though we use the computational basis of the Majorana modes, for particle-number conserving systems such as the lattice model in Eq. (4.A.1), the covariance matrix is simplified into the form $\sigma_2 \otimes \Gamma$, with $\Gamma = \mathbb{I} - 2C$, $C_{ij} = \text{Tr}(\rho c_i^\dagger c_j)$ is the correlation matrix and σ_2 is the second Pauli matrix (see Ref. [48] for a more detailed discussion). For a thermal state, the single-particle correlator reads

$$C_{ij} = \sum_k \frac{u_k^*(i) u_k(j)}{e^{\beta\omega_k} + 1}, \tag{4.A.2}$$

where ω_k and $u_k(i)$ are the single-particle eigenvalues and eigenvectors of the Hamiltonian (4.A.1). For a bipartite Hilbert space $\mathcal{H}_A \otimes \mathcal{H}_B$ where $A = A_1 \cup A_2$, the covariance matrix takes a block form

$$\Gamma = \begin{pmatrix} \Gamma_{11} & \Gamma_{12} \\ \Gamma_{21} & \Gamma_{22} \end{pmatrix}, \tag{4.A.3}$$

where Γ_{11} and Γ_{22} are the reduced covariance matrices of the two subsystems A_1 and A_2, respectively, while Γ_{12} and $\Gamma_{21}^\dagger$ contain the cross correlations between them. By simple Gaussian states' manipulations, the correlation matrices associated with $\rho_A^{R_1}$, $(\rho_A^{R_1})^\dagger$ can be written as [161]

$$\Gamma_\pm = \begin{pmatrix} -\Gamma_{11} & \pm i\Gamma_{12} \\ \pm i\Gamma_{21} & \Gamma_{22} \end{pmatrix}. \tag{4.A.4}$$

The objects we are interested in are $N_{n_e} = \text{Tr}[(\rho^{R_1}(\rho^{R_1})^\dagger)^{n_e/2} e^{i\hat{\tilde{Q}}\alpha}]$ and $N_1(\alpha) = \text{Tr}[\rho^{R_1} e^{i\hat{\tilde{Q}}\alpha}]$. The imbalance of the relativistic Dirac field corresponds to the discretised operator $\hat{\tilde{Q}} = \hat{N}_{A_1\cup A_2} - 1/2(\ell_1 + \ell_2)$. Notice that in this basis, $\hat{Q}$ is not the difference, but the sum of the number operators. Furthermore, it presents a shift compared to the number operator of the non-relativistic fermions. The single particle correlation matrix associated to the normalised composite density operator $\rho_x = \rho^{R_1}(\rho^{R_1})^\dagger / Z_x$ is [161, 254]

$$\Gamma_x = (\mathbb{I} + \Gamma_+\Gamma_-)^{-1}(\Gamma_+ + \Gamma_-), \tag{4.A.5}$$

where the normalisation factor is $Z_x = \text{Tr}(\Gamma_x) = \text{Tr}(\rho_A^2)$. In terms of eigenvalues of correlation matrices, we can write [161]

$$\begin{aligned} \log N_n(\alpha) = &- i\alpha\frac{\ell_1+\ell_2}{2} + \sum_{j=1}^N \log\left[\left(\frac{1-\nu_j^x}{2}\right)^{n/2} + e^{i\alpha}\left(\frac{1+\nu_j^x}{2}\right)^{n/2}\right] + \\ &+ \frac{n}{2}\sum_{j=1}^N \log\left[\zeta_j^2 + (1-\zeta_j)^2\right], \end{aligned} \tag{4.A.6}$$

where ν_j^{x} and ζ_j are eigenvalues of the matrices Γ_{x} (4.A.5) and C (4.A.2), respectively. In terms of the eigenvalues ν's of $\Gamma_\pm$ (4.A.4) (Γ_+ and Γ_- have the same spectrum), the charged normalisation $N_1(\alpha)$ is

$$\log N_1(\alpha) = -\mathrm{i}\alpha\frac{\ell_1+\ell_2}{2} + \sum_{j=1}^{N}\log\left[\left(\frac{1-\nu_j}{2}\right) + \mathrm{e}^{\mathrm{i}\alpha}\left(\frac{1+\nu_j}{2}\right)\right]. \tag{4.A.7}$$

Taking the Fourier transform of the numerical data for $N_{n_e}(\alpha)$ and $N_1(\alpha)$, we finally obtain the imbalance resolved negativities.

4.B Appendix: Mode expansion of charged moments of ρ_A and $\rho_A^{R_1}$

Following Ref. [40], we report some details about the transformation of the trace formulas into a product of n decoupled partition functions for non-interacting systems with conserved $U(1)$ charge. As mentioned in the main text, after diagonalising the twist matrices a partition function on a multi-sheet geometry can be decomposed as

$$Z_n(\alpha) = \prod_k Z_{k,n}(\alpha), \qquad Z_{k,n}(\alpha) = \langle \mathrm{e}^{\mathrm{i}\int d^2x A^k_\mu j^\mu_k}\rangle, \tag{4.B.1}$$

in which

$$\epsilon^{\mu\nu}\partial_\nu A_{k,\mu}(x) = 2\pi\sum_{i=1}^{2p}\nu_{k,i}(\alpha)\delta(x-u_i), \tag{4.B.2}$$

where $2\pi\nu_{k,i}(\alpha)$ is the vorticity of gauge flux determined by the eigenvalues of the twist matrix, p are the intervals defined between a pair of points u_{2i-1} and u_{2i}. The vorticities satisfy the neutrality condition $\sum_i \nu_{k,i}(\alpha) = 0$ for every k. As already stressed, there are several representations of the partition function $Z_{k,n}(\alpha)$. In order to obtain the asymptotic behaviour, one needs to take the sum over all the representations

$$\tilde{Z}_{k,n}(\alpha) = \sum_{\{m_i\}} Z^{(m)}_{k,n}(\alpha), \quad Z^{(m)}_{k,n}(\alpha) = \langle \mathrm{e}^{\mathrm{i}\int d^2x A^{(m)}_{k,\mu} j^\mu_k}\rangle,$$

$$\epsilon^{\mu\nu}\partial_\nu A^{(m)}_{k,\mu}(x) = 2\pi\sum_{i=1}^{2p}\tilde{\nu}_{k,i}(\alpha)\delta(x-u_i), \tag{4.B.3}$$

where m_i is a set of integers and $\tilde{\nu}_{k,i}(\alpha) = \nu_{k,i}(\alpha) + m_i$ are shifted flux vorticities obeying $\sum_i m_i = 0$ because of neutrality condition. By the bosonisation technique, we may write

$$\tilde{Z}_{k,n}(\alpha) = E_{\{m_i\}}\prod_{i<j}\frac{1}{|u_i-u_j|^{-2\tilde{\nu}_{k,i}(\alpha)\tilde{\nu}_{k,j}(\alpha)}} \quad \xrightarrow{\ell\to\infty} \quad \tilde{Z}_{k,n}(\alpha) \sim \sum_{\{m_i\}}\frac{E_{\{m_i\}}}{\ell^{\sum_i \tilde{\nu}^2_{k,i}(\alpha)}}, \tag{4.B.4}$$

where ℓ is a length scale and we absorbed all non-universal effects (e.g. cutoff and microscopic details in the case of lattice models) in the constants $E_{\{m_i\}}$. In the large ℓ limit, the leading order term(s) is (are) the one(s) which minimises the quantity $\sum_i \tilde{\nu}^2_{k,i}(\alpha)$. As shown in the following appendix, this is identical to (and consistent with) the condition derived from the generalised Fisher-Hartwig conjecture. We now carry out this procedure for $N_{n_e}(\alpha)$ in (4.3.27) for two adjacent intervals. We need to minimise the quantity

$$f_{m_1m_2m_3}(\nu) = (\nu - 1/2 + m_1)^2 + (\nu + m_2)^2 + (-2\nu + 1/2 + m_3)^2, \tag{4.B.5}$$

for a given $\nu = \frac{k}{n} + \frac{\alpha}{2\pi n}$, with $k = -\frac{n-1}{2}, \dots, \frac{n-1}{2}$, by finding the integers (m_1, m_2, m_3) constrained by $\sum_i m_i = 0$. The triplet (m_1, m_2, m_3) that minimises Eq. (4.B.5) is

$$\begin{cases} (0,0,0), & \nu \geq 0, \\ (1,0,-1), & \nu < 0. \end{cases} \tag{4.B.6}$$

For the charged probability in Eq. (4.4.11), we need to minimise

$$f_{m_1 m_2 m_3}(\nu) = (\nu + m_1)^2 + (\nu + m_2)^2 + (-2\nu + m_3)^2, \tag{4.B.7}$$

for $\nu = \frac{\alpha}{2\pi}$. In this case, the minimising sets of triplets are

$$\begin{cases} (0,0,0), & |\nu| \leq 1/3, \\ (-1,0,1), (0,-1,1), & \nu > 1/3, \\ (1,0,-1), (0,1,-1), & \nu < -1/3, \end{cases} \tag{4.B.8}$$

where in the two last lines the two reported triplets are degenerate.

A similar derivation can be carried out for $N_{n_e}(\alpha)$ in Eq. (4.3.27) for the geometry in Fig. 4.5. The quantity to minimise is

$$f_{m_1 m_2 m_3 m_4}(\nu) = (\nu + m_1)^2 + (-\nu + m_2)^2 + (-2\nu + 1/2 + m_3)^2 + (2\nu - 1/2 + m_4)^2, \tag{4.B.9}$$

where now we have four integers (m_1, m_2, m_3, m_4) constrained by $\sum_i m_i = 0$. The quadruplet (m_1, m_2, m_3, m_4) that minimises Eq. (4.B.11) is

$$\begin{cases} (0,0,0,0), & \nu \geq 0, \\ (0,0,1,-1), & \nu < 0. \end{cases} \tag{4.B.10}$$

For the charged probability in Eq. (4.5.8), where $\nu = \frac{\alpha}{2\pi}$, we have to minimise

$$f_{m_1 m_2 m_3 m_4}(\nu) = (\nu + m_1)^2 + (-\nu + m_2)^2 + (-2\nu + m_3)^2 + (2\nu + m_4)^2, \tag{4.B.11}$$

by choosing the quadruplet

$$\begin{cases} (0,0,0,0), & |\alpha| \leq \pi/2, \\ (0,0,1,-1), & |\alpha| > \pi/2. \end{cases} \tag{4.B.12}$$

4.C Appendix: Lattice-dependent terms and Fisher-Hartwig conjecture

We focus on the evaluation of the explicit cutoffs induced by the lattice for the charged RN, for the ground state of the Hamiltonian (4.A.1). Analogous results for the charged REs and EEs have already been worked out in [1]. The evaluation of the charged negativity relies on the Fisher-Hartwig conjecture for the determinant of Toeplitz matrices. Here we closely follow the derivation for the negativity at $T = 0$ [47]. We focus on a chain of length L with sites labelled by $j = [0, L-1]$; the intervals are $A_1 = [0, \ell - 1]$ and $A_2 = [\ell_1, \ell_2 - 1]$. The non-universal additive constant does not depend on the finiteness of the chain. Denoting by $\tilde{u}_i(r_j) = \langle r_j | \tilde{u}_i \rangle$ the single particle eigenstate, the wave function describing the ground state of the Hamiltonian has the form of a Slater determinant

$$\langle \{r_j\} | \Psi \rangle = \det[\tilde{u}_i(r_j)]. \tag{4.C.1}$$

Hence, the partition function $Z_{R_1,k}(\alpha)$ in Eq. (4.3.27) is

$$Z_{R_1,k}(\alpha) = \det M^{R_1,k}_{mm'}(\alpha) = \det\left(\langle \tilde{u}_m | T^{R_1}_{\alpha,k} | \tilde{u}_{m'}\rangle\right), \tag{4.C.2}$$

where $T^{R_1}_{\alpha}$ is a diagonal matrix whose entries $[T^{R_1}_{\alpha}]_{jj} = T^{R_1}_{\alpha,k}(j)$ are

$$T^{R_1}_{\alpha,k}(j) = \begin{cases} e^{i\varphi - 2\pi i\frac{k}{n} - i\frac{\alpha}{n}} & 0 \le j < \ell_1, \\ e^{i2\pi\frac{k}{n} + i\frac{\alpha}{n}} & \ell_1 \le j < \ell_1 + \ell_2, \\ 1 & \ell_1 + \ell_2 \le j < L, \end{cases} \tag{4.C.3}$$

where the phase are fixed according to the conventions in Figure 4.1. Writing explicitly the single particle eigenstates as plane waves $\tilde{u}_i(r_j) = \frac{1}{\sqrt{L}} e^{i\frac{\pi m}{L} j}$, $m = \pm 1, \pm 3, ..., \pm(L/2-1)$, we obtain

$$M^{R_1,k}_{mm'}(\alpha) = \langle \tilde{u}_m | T^{R_1}_{\alpha,k} | \tilde{u}_{m'}\rangle = \frac{1}{L}\sum_{j=0}^{L-1} e^{-i\frac{\pi j}{L}(m-m')} T^{R_1}_{\alpha,k}(j) = \\ = \frac{1}{2\pi}\int_0^{2\pi} d\theta e^{-i\theta(m-m')/2} \tilde{T}^{R_1}_{\alpha,k}(\theta), \tag{4.C.4}$$

The last identity in (4.C.4) is obtained in the scaling regime $L \to \infty$, $\ell \to \infty$ and ℓ/L fixed and $\tilde{T}^{R_1}_{\alpha,k}(\theta)$ is the continuum limit ($j \to \frac{L\theta}{2\pi}$) of Eq. (4.C.3), i.e.

$$\tilde{T}^{R_1}_{\alpha,k}(\theta) = \begin{cases} e^{i\varphi - 2\pi i\frac{k}{n} - i\frac{\alpha}{n}} & 0 < \theta < \pi r_1 \\ e^{i2\pi\frac{k}{n} + i\frac{\alpha}{n}} & \pi r_1 < \theta < \pi(r_1 + r_2), \\ 1 & \pi(r_1 + r_2) < \theta < 2\pi \end{cases} \tag{4.C.5}$$

where we introduced $r_i = 2\ell_i/L$. Hence, in this basis, the matrix $M^{R_1,k}_{mm'}(\alpha)$ is a Toeplitz matrix where $(m-m')/2 = 0, 1, 2, \ldots, (L/2-1)$ which implies that the size of the matrix is $\frac{L}{2} \times \frac{L}{2}$.

The asymptotic evaluation of the determinant of a Toeplitz matrix is based on a special standard structure that we now describe. In general, a Toeplitz matrix has the form $T_L[\phi] = (\phi_{i-j})$, where ϕ_k is the k-th Fourier coefficient of the *symbol* $\phi(\theta)$. The Fisher-Hartwig conjecture gives the asymptotic behaviour of the determinant of Toeplitz matrices whose symbol admits a canonical factorisation as

$$\phi(\theta) = \psi(\theta)\prod_{r=1}^{R} t_{\beta_r,\theta_r}(\theta) u_{\alpha_r,\theta_r}(\theta), \tag{4.C.6}$$

where

$$t_{\beta_r,\theta_r}(\theta) = \exp[-i\beta_r(\pi - \theta + \theta_r)], \quad \theta_r < \theta < 2\pi + \theta_r, \tag{4.C.7}$$

$$u_{\alpha_r,\theta_r}(\theta) = (2 - 2\cos(\theta - \theta_r))^{\alpha_r}, \quad \mathrm{Re}[\alpha_r] > -\frac{1}{2}, \tag{4.C.8}$$

$\psi(\theta)$ is a smooth vanishing function with zero winding number and R is the number of discontinuities of $\phi(\theta)$. For $L \to \infty$, the Fisher-Hartwig formula gives

$$\det T_L[\phi] = (\mathcal{F}[\psi])^L \left(\prod_{r=1}^{R} L^{\alpha_i^2 - \beta_i^2}\right) E_{\mathrm{FH}}, \tag{4.C.9}$$

where

$$\mathcal{F}[\psi] = \exp\left(\frac{1}{2\pi}\int_0^{2\pi} \ln\psi(\theta)\mathrm{d}\theta\right), \tag{4.C.10}$$

and

$$\begin{aligned} E_{\mathrm{FH}} = E[\psi]\prod_{i=1}^{R}\frac{G(1+\alpha_i+\beta_i)G(1+\alpha_i-\beta_i)}{G(1+2\alpha_i)}\prod_{1\le \mathrm{i}\ne j\le R}\left(1-\mathrm{e}^{\mathrm{i}(\theta_i-\theta_j)}\right)^{-(\alpha_i+\beta_i)(\alpha_j-\beta_j)} \\ \times\prod_{i=1}^{R}\left(\psi_-\left(\mathrm{e}^{\mathrm{i}\theta_i}\right)\right)^{-\alpha_i-\beta_i}\left(\psi_+\left(\mathrm{e}^{-\mathrm{i}\theta_i}\right)\right)^{-\alpha_i+\beta_i} \end{aligned} \tag{4.C.11}$$

assuming that $\psi(\theta)$ admits the Wiener-Hopf factorisation

$$\psi(\theta) = \mathcal{F}[\psi]\psi_+\left(\exp(i\theta)\right)\psi_-\left(\exp(-i\theta)\right). \tag{4.C.12}$$

Here $E[\psi] = \exp\left(\sum_{k=1}^{\infty} k s_k s_{-k}\right)$, with s_k corresponding to the k-th Fourier coefficient of $\ln\psi(\theta)$, and G are the Barnes G-function

$$G(1+z) = (2\pi)^{z/2}e^{-(z+1)z/2-\gamma_E z^2/2}\prod_{n=1}^{\infty}[(1+z/n)^n e^{-z+z^2/(2n)}], \tag{4.C.13}$$

and γ_E the Euler constant.

In the case of the negativity for two adjacent intervals and even $n = n_e$, the *symbol* $\phi(\theta)$ is given by

$$\phi(\theta) = \begin{cases} e^{i\pi-2\pi\mathrm{i}(k/n+\alpha/(2\pi n))}, & -\pi r_1 < \theta < 0, \\ e^{2\pi\mathrm{i}(k/n+\alpha/(2\pi n))}, & 0 < \theta < \pi r_2, \\ 1, & \pi r_2 < \theta < 2\pi - \pi r_1, \end{cases} \tag{4.C.14}$$

Therefore, it has three discontinuities and admits the following canonical factorization:

$$\phi(\theta) = \psi(\theta)t_{\beta_1(k),-\pi r_1}(\theta)t_{\beta_2(k),\pi r_2}(\theta)t_{\beta_3(k),0}(\theta), \tag{4.C.15}$$

where

$$\psi(\theta) = e^{i\pi r_1/2 - i\pi(\frac{k}{n}+\frac{\alpha}{2\pi n})(r_1-r_2)}, \tag{4.C.16}$$

$$\beta(k) = \frac{k}{n}+\frac{\alpha}{2\pi n} = \beta_1(k)+\frac{1}{2} = \beta_2(k), \tag{4.C.17}$$

$$\beta_3(k) = -2\beta(k)+\frac{1}{2}, \tag{4.C.18}$$

so we can apply the conjecture with $R = 3$ and $\alpha_i = 0$. When $\beta < 0$, we have $|\beta_3| > 1/2$ and the FH conjecture in its original form breaks down (we can also use the most general hypothesis in which the Fisher-Hartwig conjecture works, i.e. if we introduce the seminorm $|||\beta||| = \max_{j,k}|\beta_k - \beta_k|$, where $1 \le j,k \le 3$, the conjecture has been verified for $|||\beta||| < 1$ [**FH**]). In this case we should use the generalised Fisher-Hartwig conjecture, see e.g. [**FH**, 217] in which one sums over all the inequivalent representations of the symbol, i.e. summing over all possible $\{\hat{\beta}_i\}$ such that

$$\hat{\beta}_i = \beta_i + n_i, \qquad \sum_{i=1}^{R} n_i = 0. \tag{4.C.19}$$

The leading terms is given by the set(s) of integers $\{n_i\}$ that minimises the function $\sum_{i=1}^{R} \hat{\beta}_i^2$. This is identical to the condition derived in Sec. 4.B. We denote the corresponding set of solutions by $\mathcal{M}_\beta$. The Toeplitz determinant is sum of the standard form (4.C.9) corresponding to these solutions. Then, the asymptotic behaviour of the Toeplitz determinant in (4.C.2) is

$$\begin{aligned} Z_{R_1,k}(\alpha) = &(2-2\cos(2\pi\ell_1/L))^{-(|k/n+\alpha/(2\pi n)|-1/2)(2|k/n+\alpha/(2\pi n)|-1/2)} \\ &\times (2-2\cos(2\pi\ell_2/L))^{-|k/n+\alpha/(2\pi n)|(2|k/n+\alpha/(2\pi n)|-1/2)} \\ &\times (2-2\cos(2\pi(\ell_1+\ell_2)/L))^{|k/n+\alpha/(2\pi n)|(|k/n+\alpha/(2\pi n)|-1/2)} \\ &\times J_\alpha(k)(L)^{\Delta_k(\alpha)}, \end{aligned} \tag{4.C.20}$$

where $\Delta_k(\alpha)$ is given by Eq. (4.4.4) and $J_\alpha(k) = \prod_{i=1}^{3} G(1+\beta_i(k))G(1-\beta_i(k))$. Using standard manipulation of the Barnes G-function, we can rewrite the $O(1)$ terms as

$$\begin{aligned} \Big(\frac{n^2-2}{4n}+\frac{3\alpha^2}{2\pi^2 n}\Big)\log\epsilon = &\sum_{k=-\frac{(n-1)}{2}}^{k=\frac{(n-1)}{2}} \log 2^{2\Delta_k} J_\alpha(k) = -\log 2\Big(\frac{n^2-2}{4n}+\frac{3\alpha^2}{2\pi^2 n}\Big) \\ &-(1+\gamma_E)\Big(\frac{n}{4}-\frac{1}{2n}+\frac{3\alpha^2}{2n\pi^2}\Big)+\sum_{m=1}^{\infty}\frac{-2\pi^2+n^2\pi^2+6\alpha^2}{4mn\pi^2} \\ &+\sum_{m=1}^{\infty} 2m\log\frac{(\frac{2}{m^3n^3})^n\Gamma[\frac{2+n-2nm}{4}-\frac{\alpha}{2\pi}]\Gamma[\frac{2+n-2nm}{4}+\frac{\alpha}{2\pi}]\Gamma[\frac{1+n+2nm}{2}-\frac{\alpha}{2\pi}]\Gamma[\frac{1-n+2nm}{2}-\frac{\alpha}{2\pi}]}{\Gamma[\frac{2-n-2nm}{4}-\frac{\alpha}{2\pi}]\Gamma[\frac{2-n-2nm}{4}+\frac{\alpha}{2\pi}]\Gamma[\frac{1-n+2nm}{2}+\frac{\alpha}{2\pi}]\Gamma[\frac{1-n+2nm}{2}-\frac{\alpha}{2\pi}]}. \end{aligned} \tag{4.C.21}$$

Eq. (4.C.21) is well approximated by the expansion at the second order in α since higher corrections $O(\alpha^4)$ are negligible for most practical purposes (this is in full analogy with the charged entropies [1]). In particular, in the replica limit $n_e \to 1$ we have

$$-\left(\frac{1}{4}-\frac{3\alpha^2}{2\pi^2}\right)\log\epsilon \simeq 0.47295 - 0.29990\alpha^2. \tag{4.C.22}$$

In conclusion, the Fisher-Hartwig technique allows us to re-derive the leading CFT terms (at $T=0$) and also provides the cutoff due to lattice regularisation.

Similar derivation can be carried out to compute the cutoff ϵ_N of the charged probability in Eq. (4.4.11) and we report the final result

$$\frac{3\alpha^2}{2\pi^2}\log\epsilon_N \simeq -0.34514\alpha^2 \quad |\alpha| \le 2\pi/3 \tag{4.C.23a}$$

$$-\left(1-\frac{|\alpha|}{\pi}\right)\frac{|\alpha|}{\pi}\log\epsilon_N \simeq -3.21853 + 1.93194|\alpha| - 0.30748\alpha^2 \quad |\alpha| > 2\pi/3 \tag{4.C.23b}$$

For a bipartite geometry, the lattice cutoff ϵ can be computed using the equivalence between the (charged) negativity and the (charged) $\frac{1}{2}$ RE for pure states, exploiting the results of Ref. [1], i.e.

$$-(\frac{1}{2}-\frac{2\alpha^2}{\pi^2})\log\epsilon \simeq 0.94590 - 0.36978\alpha^2. \tag{4.C.24}$$

We also write down the final result for the cutoff ϵ_N of the charged probability in Eq. (4.5.8)

$$\frac{2\alpha^2}{\pi^2}\log\epsilon_N \simeq -0.46020\alpha^2, \quad |\alpha| \le \pi/2, \tag{4.C.25a}$$

$$\frac{(\pi-|\alpha|)^2}{\pi^2}\log\epsilon_N \simeq -0.46020(|\alpha|-\pi)^2, \quad |\alpha| > \pi/2. \tag{4.C.25b}$$

As already discussed in the main text, the knowledge of the exact expression for this non-universal quantities is relevant in order to test our analytical predictions against numerical data without any fitting parameter.

4.D Appendix: Twisted partial transpose

For $T = 0$, the fermionic RN in CFT (4.2.11) is equal [161] to the bosonic RN for both even and odd values of n, also in the charged case [38]. The definition (4.2.11) has been employed since $\rho_A^{R_1}$ is not necessarily Hermitian. Then, the trace norm in terms of square root of the eigenvalues of the composite operator $\rho_{\rm x} = \rho_A^{R_1}(\rho_A^{R_1})^\dagger$ provides a well-defined EN for fermions. However, one can also introduce a hermitian partial transpose, which is suitable to define another fermionic negativity because of its real spectrum [48]. This is done by considering the composite operator $\tilde{\rho}_{\rm x} = (\rho_A^{\tilde{R}_1})^2$, in terms of the twisted partial transpose $\rho_A^{\tilde{R}_1} = \rho_A^{R_1}(-1)^{F_1}$, with $(-1)^{F_1}$ the fermion number parity in A_1. The associated charged moments are $\tilde{N}_n = {\rm Tr}[(\rho_A^{\tilde{R}_1})^n {\rm e}^{{\rm i}\hat{\tilde{Q}}\alpha}]$. The use of the composite operator $\tilde{\rho}_{\rm x}$ is distinct from the previous one. In fact, the $T_\alpha^{\tilde{R}_1}$ matrix which glues together $\rho_A^{\tilde{R}_1}$ is

$$T_\alpha^{\tilde{R}_1} = \begin{pmatrix} 0 & 0 & \dots & -{\rm e}^{-{\rm i}\alpha/n} \\ {\rm e}^{-{\rm i}\alpha/n} & 0 & & \\ 0 & {\rm e}^{-{\rm i}\alpha/n} & & \ddots \\ & & \ddots & \ddots \end{pmatrix}. \tag{4.D.1}$$

The technical difference is that the twist phases of the two intervals are now $e^{2\pi{\rm i}(\frac{k}{n}+\frac{\alpha}{2\pi n}-\frac{\varphi_n}{2\pi})}$ and $e^{-2\pi{\rm i}\left(\frac{k}{n}+\frac{\alpha}{2\pi n}\right)}$, with $\varphi_n = \pi$ for both n even and odd. This means that for n even the two RN are equal (and indeed the negativity may be obtained from the replica limit $n_e \to 1$ of both). Hence, we report the final results for the two geometries studied in the main text for $n = n_o$.

1. Adjacent intervals: The spin-independent part of the moments of negativity are given by

$$\begin{aligned} \log \tilde{N}_{n_o,0}(\alpha) = \log \tilde{R}_{n_o} - \frac{\alpha^2}{2\pi^2 n_o} \log |\theta_1(r_1|\tau)^2 \theta_1(r_2|\tau)^2 \theta(r_1+r_2|\tau)^{-1} (\frac{\epsilon}{L}\partial_z \theta_1(0|\tau))^{-3}| \\ + \frac{|\alpha|}{2n_o\pi} \log |\theta_1(r_1|\tau)^3 \theta_1(r_2|\tau) \theta(r_1+r_2|\tau)^{-1} (\frac{\epsilon}{L}\partial_z \theta_1(0|\tau))^{-3}|, \end{aligned} \tag{4.D.2}$$

while the spin structure dependent term is the same as Eq. (4.4.8) with $\varphi_{n_o} = \pi$.

2. Bipartite geometry: In this case, one has

$$\begin{aligned} \log \tilde{N}_{n_o,0}(\alpha) = \log \tilde{R}_{n_o} - \frac{\alpha^2}{2\pi^2 n_o} \log \left| \frac{\theta_1(r_1|\tau)^4 \theta_1\left(\frac{r_2}{2}|\tau\right)^4 \theta_1(r_1+r_2|\tau)}{\theta_1\left(r_1+\frac{r_2}{2}|\tau\right)^4 (\frac{\epsilon}{L}\partial_z\theta_1(0|\tau))^5} \right| \\ + \frac{|\alpha|}{\pi n_o} \log \left| \frac{\theta_1(r_1|\tau)^2 \theta_1\left(\frac{r_2}{2}|\tau\right)}{\theta_1\left(r_1+\frac{r_2}{2}|\tau\right) (\frac{\epsilon}{L}\partial_z\theta_1(0|\tau))^2} \right|, \end{aligned} \tag{4.D.3}$$

for the spin-independent part while the spin structure dependent term is the same as Eq. (4.5.6) with $\varphi_{n_o} = \pi$.

Chapter 5

Exact quench dynamics of symmetry resolved entanglement in a free fermion chain

Summary: *The study of the entanglement dynamics plays a fundamental role in understanding the behaviour of many-body quantum systems out of equilibrium. In the presence of a globally conserved charge, further insights are provided by the knowledge of the resolution of entanglement in the various symmetry sectors. This Chapter is based on Refs. [3, 5], in which we initiated the study of the evolution of the symmetry resolved entanglement after a global quantum quench in quantum many-body systems. We also extend our analysis defining and quantifying a symmetry resolved mutual information (MI). We find that EEs display a time delay that depends on the charge sector that we characterise exactly. Both EEs and MI show effective equipartition in the scaling limit of large time and subsystem size. Furthermore, we argue that the behaviour of the charged entropies can be quantitatively understood in the framework of the quasiparticle picture for the spreading of entanglement, and hence we expect that a proper adaptation of our results should apply to a large class of integrable systems. We also find that the number entropy grows logarithmically with time before saturating to a value proportional to the logarithm of the subsystem size.*

5.1 Introduction

The time evolution of the entanglement in extended quantum systems starting from a non-equilibrium configuration became in the last decade a fundamental question with ramifications into many problems of contemporary physics, such as the equilibration and thermalisation of isolated many-body systems [176, 177, 178, 179, 180], the emergence of thermodynamic entropy [181, 182, 183, 184], and the effectiveness of classical computers to simulate the quantum dynamics [185, 186, 187, 188, 189].

In particular, in the experimental paper [19], the authors pointed out that a refined understanding of how the entanglement arises from the various symmetry sectors is necessary to better grasp the full many-body dynamics. Even though the study of *the symmetry resolution of*

entanglement became a very active research area of the last years [35, 34, 1, 2, 49, 3, 33, 38, 39, 62, 53, 56, 57, 55, 54, 63, 64, 66, 58, 65, 50, 4, 67, 68, 59, 69, 51, 52, 60], only few results are available for out-of-equilibrium situations [39, 3, 67, 53].

In this work, we present the analysis of the time evolution of the symmetry resolved entanglement after a global quench. In the context of free fermions and conformal field theories, we are able to provide analytical results for the relevant time-dependent quantities, and shed light on two new physical phenomena. First, the symmetry resolved REs start evolving with a calculable time delay that depends on the charge sector. Second, there is an effective equipartition of the entanglement in the limit of large subsystem size. We argue that these phenomena occur in more general quantum systems, as they can be understood from the quasiparticle picture for the spreading of entanglement. We also syudy the dynamics of two relevant quantities, namely a suitably defined symmetry resolved MI and the number entropy. We focus on exact lattice calculations for two distinct quenches and compare our results with the quasiparticle picture predictions.

This paper is organised as follows. In Sect. 5.2 we provide the definition of the symmetry resolved MI. We then introduce the model of free fermions that we consider in Sect. 5.3. Sections 5.4 and 5.5 are devoted to the analytical study of the dynamics of the symmetry resolved quantities in a free fermionic system after a quench from two distinct initial states: the Néel state and the Majumdar-Ghosh dimer state, respectively. In Sect. 5.6 we use the CFT approach to global quanches to derive the time evolution of the symmetry resolved entropies for a free compactified bosonic theory, describing the scaling limit of the system. In Sect. 5.7 we give an interpretation of our results in the framework of the quasiparticle picture for the dynamics of entanglement in integrable models. Finally, we give a summary of the results and future outlook of this work in Sect. 5.8.

5.2 Symmetry resolution and flux insertion

We consider an extended quantum system with an internal $U(1)$ symmetry generated by a local operator Q. Considering a bipartition in two complementary subsystems A and B,such that Q splits as sum of operators that act on the degrees of freedom of the two parts, $Q = Q_A + Q_B$, the symmetry resolution of the entanglement and REs can be performed following Sect. 2.2.

The MI defined in Eq. (1.2.9) is constructed from three different EEs and so from three different RDMs ρ_{A_1}, ρ_{A_2}, and $\rho_{A_1\cup A_2}$. Each of them admits its independent symmetry decomposition, and it is not obvious how to combine them to construct a symmetry resolved quantity, and whether it is possible at all. We propose to define the *symmetry resolved mutual information* as follows:

$$I_1^{A_1:A_2}(q) = \sum_{q_1=0}^{q} p(q_1, q-q_1)\Big(S_1^{A_1}(q_1) + S_1^{A_2}(q-q_1)\Big) - S_1^{A_1\cup A_2}(q), \tag{5.2.1}$$

where the superscripts A_1, A_2 or $A_1 \cup A_2$ indicate to which system the various quantities pertain to. The idea of Eq. (5.2.1) is that for a given charge sector q of the whole subsystem A, we take a weighted sum over the contributions from charge sectors q_1 and q_2 of A_1 and A_2 such that $q_1 + q_2 = q$. The weight $p(q_1, q-q_1)$ is the probability that a simultaneous measurement of the charges Q_{A_1} and Q_{A_2} yields q_1 and $q-q_1$, respectively, while the charge sector of the whole

system A is fixed to q. It is given by

$$p(q_1, q-q_1) = \frac{\mathcal{Z}_1^{A_1:A_2}(q_1, q-q_1)}{\mathcal{Z}_1^{A_1\cup A_2}(q)} \tag{5.2.2a}$$

where $\mathcal{Z}_1^{A_1:A_2}(q_1, q-q_1)$ is the probability of obtaining q_1 and $q-q_1$ by simultaneous measure of the charge in A_1 and A_2, respectively, and satisfies

$$\sum_{q_1=0}^{q} p(q_1, q-q_1) = 1. \tag{5.2.2b}$$

The above definition of symmetry resolved MI is sort of natural, but does not represent a measure of the total correlations within the symmetry sector (e.g., we shall see that it can be negative) and does not account for many processes (e.g., the total charge q of A should not be split as a direct sum of eigenvalues q_1, q_2). It is very likely that a more appropriate symmetry resolved MI can be defined and we strongly hope that this manuscript will boost the research in this direction. In spite of all these caveats, we will see that the symmetry resolved MI defined in Eq. (5.2.1) satisfies an equipartition for small $q - \langle Q_A \rangle$ after a quench.

In full analogy with $\mathcal{Z}_1^A(q)$, $\mathcal{Z}_1^{A_1:A_2}(q_1, q-q_1)$ can be reconstructed from the knowledge of a more complicated charged moment given by

$$Z_1^{A_1:A_2}(\alpha, \beta) = \mathrm{Tr}[\rho_A \mathrm{e}^{\mathrm{i}\alpha Q_{A_1} + \mathrm{i}\beta Q_{A_2}}] \tag{5.2.3}$$

and performing the double Fourier transform

$$\mathcal{Z}_1^{A_1:A_2}(q_1, q_2) = \int_{-\pi}^{\pi} \frac{\mathrm{d}\alpha}{2\pi} \frac{\mathrm{d}\beta}{2\pi} \mathrm{e}^{-\mathrm{i}q_1\alpha} \mathrm{e}^{-\mathrm{i}q_2\beta} Z_1^{A_1:A_2}(\alpha, \beta). \tag{5.2.4}$$

The charged moment $Z_1^{A_1:A_2}(\alpha, \beta)$ is a new quantity that, to the best of our knowledge, has not yet been studied in the literature, even in equilibrium.

Similarly to the EE, it is possible to reconstruct the total MI from the symmetry resolved ones. We have

$$I_1^{A_1:A_2} = \sum_q p(q) I_1^{A_1:A_2}(q) + S^{A_1,n} + S^{A_2,n} - S^{A_1\cup A_2,n} = \sum_q p(q) I_1^{A_1:A_2}(q) + I^{A_1:A_2,n}, \tag{5.2.5}$$

where the notation $S^{s,n}$ stands for the number entropy associated with system s, and $p(q) = \mathcal{Z}_1^{A_1\cup A_2}(q)$. The last equality defines the number MI $I^{A_1:A_2,n} \equiv S^{A_1,n} + S^{A_2,n} - S^{A_1\cup A_2,n}$.

5.3 Free fermions

We study the time evolution of the symmetry resolved entanglement after a global quench in the tight-binding model. So we consider a one-dimensional lattice with L sites and endowed with periodic boundary conditions, with hamiltonian

$$H = \sum_{j=1}^{L} (c_j^\dagger c_{j+1} + c_{j+1}^\dagger c_j), \tag{5.3.1}$$

where c_j and $c_j^\dagger$ are the canonical spinless fermionic annihilation and creation operators on site j, that satisfy the anticommutation relations $\{c_i, c_j^\dagger\} = \delta_{i,j}$ and $\{c_i, c_j\} = \{c_i^\dagger, c_j^\dagger\} = 0$.

We consider a subsystem A of length ℓ and its complement B, of length $L - \ell$. Because of locality, the global conserved charge Q trivially splits as a sum over A and B,

$$Q = \sum_{j\in A} c_j^\dagger c_j + \sum_{j\in B} c_j^\dagger c_j = Q_A + Q_B. \tag{5.3.2}$$

We will study both the cases in which A is a block of ℓ consecutive sites or the union of two disjoint blocks $A = A_1 \cup A_2$ where the subsystems have respective lengths ℓ_1 and $\ell_2 = \ell - \ell_1$ and are separated by d lattice sites. The RDM of A is always written in terms of the correlations matrix $C_A = \langle c_x^\dagger c_{x'} \rangle$ with $x, x' \in A$ [221, 211, 212], using the property that the many-body time-dependent state is a Slater determinant and so ρ_A is a Gaussian operator at any time. Using the standard algebra of Gaussian operators, the charged moments $Z_n(\alpha)$ defined in Eq. (2.2.9) can be expressed as [35]

$$\log Z_n(\alpha) = \mathrm{Tr} \log \left[(C_A)^n e^{i\alpha} + (1 - C_A)^n \right]. \tag{5.3.3}$$

For later convenience, we introduce the $\ell \times \ell$ matrix J_A defined as $C_A = \frac{1}{2}(\mathbb{I}_\ell + J_A)$, with eigenvalues ν_i. In terms of the latter, the charged moments are recast as

$$\log Z_n(\alpha) = \sum_{i=1}^{\ell} \log \left[\left(\frac{1+\nu_i}{2} \right)^n e^{i\alpha} + \left(\frac{1-\nu_i}{2} \right)^n \right]. \tag{5.3.4}$$

To perform analytical calculations, it is useful to express the charged moments as a Taylor series in $\mathrm{Tr} J_A^m$. We thus introduce the function $h_{n,\alpha}(x)$ and the coefficients $c_{n,\alpha}(m)$ as

$$h_{n,\alpha}(x) = \log \left[\left(\frac{1+x}{2} \right)^n e^{i\alpha} + \left(\frac{1-x}{2} \right)^n \right] \equiv \sum_{m=0}^{\infty} c_{n,\alpha}(m) x^m \tag{5.3.5}$$

and conclude

$$\log Z_n(\alpha) = \sum_{m=0}^{\infty} c_{n,\alpha}(m) \mathrm{Tr} J_A^m. \tag{5.3.6}$$

As we shall see in the following sections, the precise form of the coefficients $c_{n,\alpha}(m)$ is never needed and hence will not be reported.

In the case of disjoint intervals, the matrix $J_{A_1 \cup A_2}$ has a structure

$$J_{A_1\cup A_2} = \begin{pmatrix} J_{11} & J_{12} \\ J_{21} & J_{22} \end{pmatrix}, \tag{5.3.7}$$

in which the notation J_{ab}, $a, b = 1, 2$, refers to correlations between sites in A_a and A_b. We recall that for disjoint blocks, fermionic and spin entanglement are not equal [253, 252, 254] and here we focus only on the fermionic one. The computation of $Z_n^A(\alpha)$ is not affected by the fact that A is not a connected block. Instead, to compute the symmetry resolved MI, we need to evaluate $Z_1^{A_1:A_2}(\alpha, \beta)$ defined in Eq. (5.2.3). Since the RDM ρ_A does not commute with the charges Q_{A_1} and Q_{A_2} of the two disjoint subsystems, the method used to compute $Z_n(\alpha)$ and find Eq. (5.3.4) does not apply. To circumvent this problem, we adapt a technique devised in [274] to compute the full counting statistics of the magnetisation in the transverse field Ising chain. The idea is to express $Z_1^{A_1:A_2}(\alpha, \beta)$ in terms of a trace of two non-commuting putative density matrices. We recast Eq. (5.2.3) as

$$Z_1^{A_1:A_2}(\alpha, \beta) = \tilde{Z}_A \mathrm{Tr}_A(\rho_A \tilde{\rho}_A) \tag{5.3.8}$$

were

$$\tilde{\rho}_A = \frac{1}{\tilde{Z}_A} e^{i\alpha Q_{A_1} + i\beta Q_{A_2}}, \quad \tilde{Z}_A = \mathrm{Tr}_A \left(e^{i\alpha Q_{A_1} + i\beta Q_{A_2}} \right) \tag{5.3.9}$$

and the normalisation $\tilde{Z}_A$ ensures that $\mathrm{Tr}_A \tilde{\rho}_A = 1$. It is simply given by

$$\tilde{Z}_A = (1 + e^{i\alpha})^{\ell_1} (1 + e^{i\beta})^{\ell_2}. \tag{5.3.10}$$

Obviously, $\tilde{\rho}_A$ is not a true density matrix (it is not even hermitian), but it is a very simple Gaussian operator and can be associated to a two-point correlation matrix. We can thus use the rules for composition of Gaussian operators. In particular, the trace of a product of two $\ell \times \ell$ density matrices ρ_1 and ρ_2 is [254, 275]

$$\mathrm{Tr}(\rho_1 \rho_2) = \det \left(\frac{\mathbb{I}_\ell + J_1 J_2}{2} \right) \tag{5.3.11}$$

where

$$J_j = 2C_j - \mathbb{I}_\ell, \quad [C_j]_{x,x'} = \mathrm{Tr}(\rho_j c_x^\dagger c_{x'}). \tag{5.3.12}$$

To ease the comparison with Ref. [274] we mention that for free fermionic systems without particle number conservation (i.e. the Ising and XY spin chain), one also has to consider correlations of the form $\mathrm{Tr}(\rho_j c_x^\dagger c_{x'}^\dagger)$ and $\mathrm{Tr}(\rho_j c_x c_{x'})$. For that reason, the size of the correlation matrices are 2ℓ instead of ℓ, and the right-hand side of Eq. (5.3.11) is then written with an overall square root in [274].

For the case of interest here, the two correlation matrices are

$$\begin{aligned} [C_A]_{x,x'} &= \mathrm{Tr}_A(\rho_A c_x^\dagger c_{x'}), \quad x, x' \in A, \\ [\tilde{C}_A]_{x,x'} &= \mathrm{Tr}_A(\tilde{\rho}_A c_x^\dagger c_{x'}), \quad x, x' \in A. \end{aligned} \tag{5.3.13}$$

Of course, C_A is the usual correlation matrix related to $J_{A_1 \cup A_2}$ given in Eq. (5.3.7), by definition. The second one, $\tilde{C}_A$, is very easy to compute because Q_{A_1} and Q_{A_2} are diagonal operators in terms of the fermion operators c_j. We then find

$$\begin{aligned} \mathrm{Tr}_A(\tilde{\rho}_A c_x^\dagger c_{x'}) &= \delta_{x,x'} \begin{cases} \frac{1}{\tilde{Z}_A} e^{i\alpha} (1 + e^{i\alpha})^{\ell_1 - 1} (1 + e^{i\beta})^{\ell_2} & x \in A_1, \\ \frac{1}{\tilde{Z}_A} e^{i\beta} (1 + e^{i\alpha})^{\ell_1} (1 + e^{i\beta})^{\ell_2 - 1} & x \in A_2, \end{cases} \\ &= \delta_{x,x'} \begin{cases} \frac{e^{i\alpha}}{1 + e^{i\alpha}} & x \in A_1, \\ \frac{e^{i\beta}}{1 + e^{i\beta}} & x \in A_2. \end{cases} \end{aligned} \tag{5.3.14}$$

Finally, combining Eqs. (5.3.8), (5.3.10), (5.3.11) and (5.3.14), we have

$$Z_1^{A_1:A_2}(\alpha, \beta) = (1 + e^{i\alpha})^{\ell_1} (1 + e^{i\beta})^{\ell_2} \det \left(\frac{\mathbb{I}_\ell + J_{\alpha\beta}}{2} \right) \tag{5.3.15}$$

where

$$J_{\alpha\beta} = \begin{pmatrix} J_{11} & J_{12} \\ J_{21} & J_{22} \end{pmatrix} \cdot \begin{pmatrix} \frac{e^{i\alpha} - 1}{e^{i\alpha} + 1} \mathbb{I}_{\ell_1} & 0 \\ 0 & \frac{e^{i\beta} - 1}{e^{i\beta} + 1} \mathbb{I}_{\ell_2} \end{pmatrix}. \tag{5.3.16}$$

Similarly to the charged entropies, we write $Z_1^{A_1:A_2}(\alpha, \beta)$ as an expansion in terms of the traces of the powers of $J_{\alpha\beta}$, namely

$$\log Z_1^{A_1:A_2}(\alpha, \beta) = \ell_1 \log(1 + e^{i\alpha}) + \ell_2 \log(1 + e^{i\beta}) + \sum_{m=0}^{\infty} \tilde{c}(m) \mathrm{Tr} J_{\alpha\beta}^m \tag{5.3.17}$$

where $\tilde{c}(m)$ are the Taylor coefficient of the function $\tilde{h}(x) = \log[(1+x)/2]$.

In this work, we focus on the quench dynamics starting from two low-entangled initial states $|\psi_0\rangle$ that are invariant under $U(1)$ symmetry and with a resulting time-dependent correlation matrix $C_A(t) = \langle\psi_0|e^{itH}c_x^\dagger c_{x'}e^{-itH}|\psi_0\rangle$ which is exactly known when H is the tight-binding Hamiltonian (5.3.1). Those are the Néel and the dimer state, denoted by $|N\rangle$ and $|D\rangle$, respectively, defined as

$$\begin{aligned} |N\rangle &= \prod_{j=1}^{L/2} c_{2j}^\dagger|0\rangle, \\ |D\rangle &= \prod_{j=1}^{L/2} \frac{c_{2j}^\dagger - c_{2j-1}^\dagger}{\sqrt{2}}|0\rangle. \end{aligned} \tag{5.3.18}$$

5.4 Quench from the Néel state

The correlation function after a quench from the Néel state $|N\rangle$ in the tight-binding model (5.3.1) is known in the thermodynamic limit and reads (see, e.g., [209])

$$[C(t)]_{x,x'} = \frac{\delta_{x,x'}}{2} + \frac{(-1)^{x'}}{2}\int_{-\pi}^{\pi}\frac{dk}{2\pi}e^{ik(x-x')+4it\cos k}. \tag{5.4.1}$$

As explained in Sect. 5.3, the expression of the time-dependent correlation matrix is the starting point to compute the charged moments, and hence symmetry resolved entanglement measures. In the following subsection, we separately consider the situations where the subsystem A is a single interval of adjacent sites and where $A = A_1 \cup A_2$ is made of two disjoint intervals.

5.4.1 Single interval

In this subsection we study the case where A is a connected interval of ℓ neighbouring sites in an infinite chain. The correlation matrix is then simply $C_A = \frac{1}{2}(\mathbb{I}_\ell + J_A)$ with

$$[J_A(t)]_{x,x'} = (-1)^{x'}\int_{-\pi}^{\pi}\frac{dk}{2\pi}e^{ik(x-x')+4it\cos k}, \quad x,x' \in \{1,2,\dots,\ell\}. \tag{5.4.2}$$

Because of the structure of the initial state, we only work with ℓ even.

Charged moments

The first step to compute the charged moments $Z_n(\alpha)$ is the evaluation of the trace of powers of J_A. With the exact expression (5.4.2), it is possible to perform this calculation analytically using the multidimentional stationary phase approximation in the scaling limit where $t, \ell \to \infty$ with a fixed finite ratio t/ℓ. Actually, the computation of $\mathrm{Tr}J_A(t)^j$ is a simple adaptation of the calculations reported in Ref. [257], and the final result (see Appendix 5.A for the details of the evaluation) can be written as

$$\mathrm{Tr}J_A(t)^{2j} = \ell - \int_{-\pi}^{\pi}\frac{dk}{2\pi}\min(\ell, 2v_k t), \quad \mathrm{Tr}J_A(t)^{2j+1} = 0, \tag{5.4.3}$$

with $v_k = 2|\sin k|$. We note that, with our normalisation, the maximal velocity $v_M = \max_k v_k$ is $v_M = 2$. To compute the charged moments $Z_n(\alpha)$, we evaluate the sum (5.3.6) with (5.4.3).

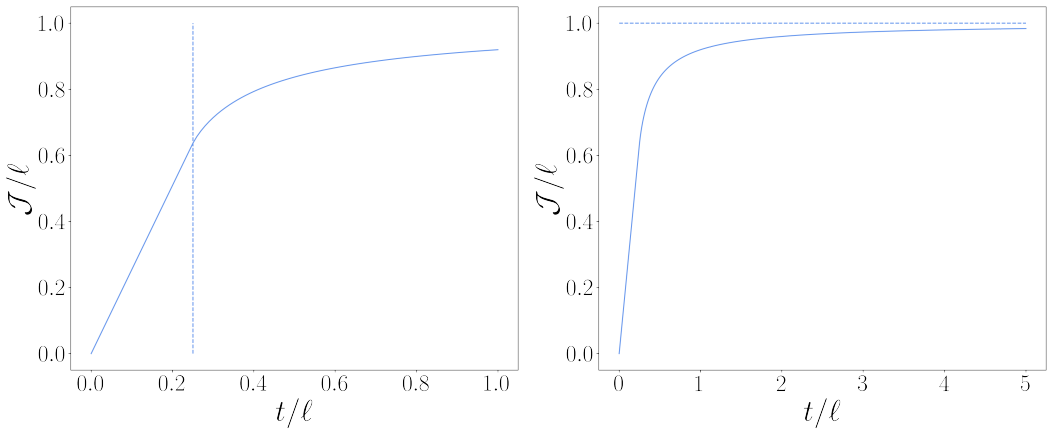


Figure 5.1: Time evolution of $\mathcal{J}/\ell$ in Eq. (5.4.8) as a function of t/ℓ. *Left:* The crossover between the linear growth and the saturation; the vertical dashed line indicates the time at which the transition occurs, i.e. $t/\ell = 1/4$ (in agreement with $t/\ell = 1/(2v_M)$ and $v_M = 2$). *Right:* For large time, $\mathcal{J}/\ell$ saturates to 1 (horizontal dashed line).

We use the fact that $\mathrm{Tr} J_A(t)^m$ only depends on the parity of the exponent for $m > 0$, and $\mathrm{Tr} J_A(t)^0 = \ell$. We then find

$$\log Z_n(\alpha) = \ell c_{n,\alpha}(0) + \mathrm{Tr} J_A(t)^2 \sum_{m=1}^{\infty} c_{n,\alpha}(2m), \tag{5.4.4}$$

where the coefficients $c_{n,\alpha}(k)$ are defined in (5.3.5). To proceed, we notice that the coefficient $c_{n,\alpha}(0)$, as well as the sum $\sum_{m=1}^{\infty} c_{n,\alpha}(2m)$ in fact correspond to the function $h_{n,\alpha}(x)$ from Eq. (5.3.5) evaluated in certain simple points. Indeed, we have

$$\begin{aligned} c_{n,\alpha}(0) &= h_{n,\alpha}(0) = (1-n)\log 2 + \log\cos\frac{\alpha}{2} + \mathrm{i}\frac{\alpha}{2}, \\ \sum_{m=1}^{\infty} c_{n,\alpha}(2m) &= \left(\frac{h_{n,\alpha}(1) + h_{n,\alpha}(-1)}{2} - c_{n,\alpha}(0)\right) = (n-1)\log 2 - \log\cos\frac{\alpha}{2}. \end{aligned} \tag{5.4.5}$$

It immediately follows that

$$\log Z_n(\alpha) = \mathrm{i}\ell\frac{\alpha}{2} + \int_{-\pi}^{\pi}\frac{\mathrm{d}k}{2\pi}\mathrm{Re}[h_{n,\alpha}(0)]\min(\ell, 2v_k t), \tag{5.4.6}$$

or

$$Z_n(\alpha) = \left(\frac{\cos\frac{\alpha}{2}}{2^{n-1}}\right)^{\mathcal{J}} \mathrm{e}^{\mathrm{i}\ell\frac{\alpha}{2}} \tag{5.4.7}$$

where we introduced the quantity

$$\mathcal{J} \equiv \ell - \mathrm{Tr} J_A(t)^2 = \int_{-\pi}^{\pi}\frac{\mathrm{d}k}{2\pi}\min(\ell, 2v_k t). \tag{5.4.8}$$

The function $\mathcal{J}(t)$ is an increasing function of time, going from $\mathcal{J}(t=0) = 0$ to $\mathcal{J}(t=\infty) = \ell$. Its time evolution is separated in two distinct regimes. For short times $t < \ell/(2v_M)$, $\mathcal{J}(t) \propto t$ increases linearly with time. On the other hand, for $t > \ell/(2v_M)$, $\mathcal{J}(t)$ slowly saturates to its asymptotic value ℓ. These behaviours are illustrated in Fig. 5.1. The ratio $\mathcal{J}(t)/\ell$ is a scaling function of t/ℓ, a fact that we will use repeatedly in what follows.

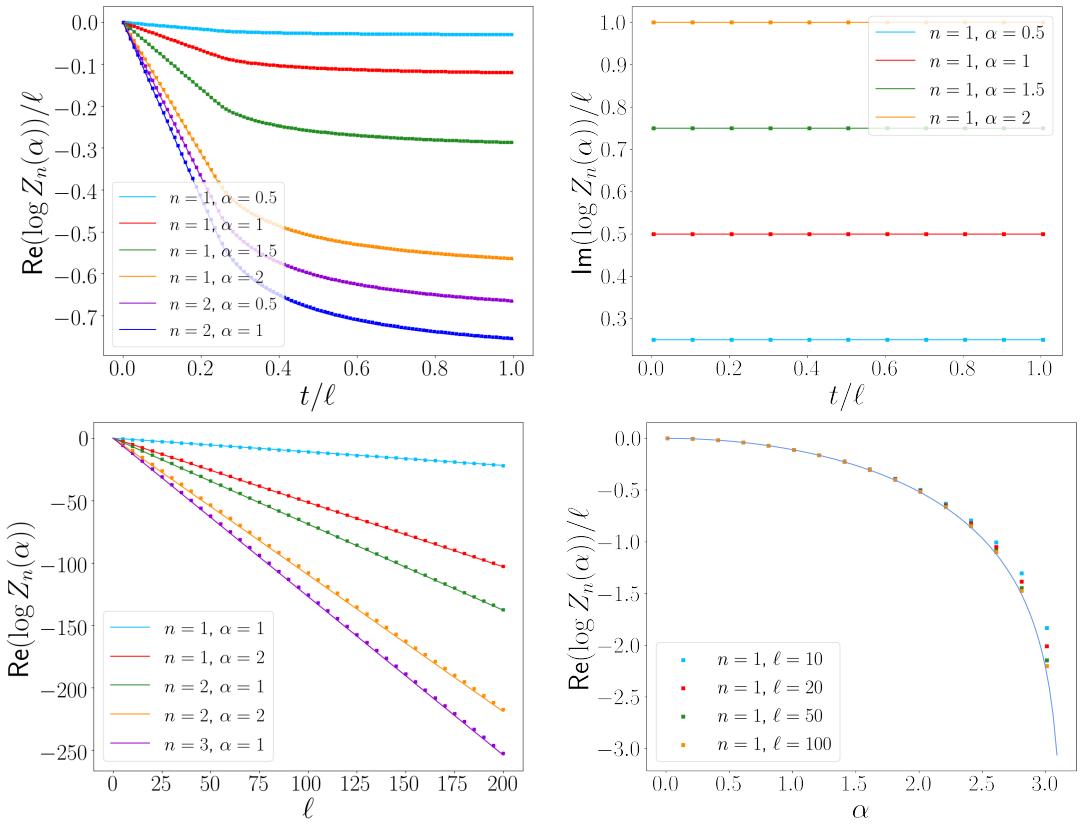


Figure 5.2: Comparison between the asymptotic result (5.4.7) (solid lines) and exact numerical data (symbols) for $\log Z_n(\alpha)$ after a quench from the Néel state in the free fermion model (5.3.1). *Top left:* Time evolution of the real part of $\log Z_n(\alpha)$ as a function of t/ℓ with $\ell = 120$. *Top right*: Time evolution of the imaginary part of $\log Z_n(\alpha)$ as a function of t/ℓ with $\ell = 20$ and $n = 1$. *Bottom left:* Real part of $\log Z_n(\alpha)$ as a function of ℓ with $t/\ell = 0.5$. *Bottom right:* Real part of $\log Z_n(\alpha)$ as a function of α with $t/\ell = 0.5$ and $n = 1$.

In Fig. 5.2 we compare the prediction (5.4.7) for the charged moments $Z_n(\alpha)$ with ab-initio computations. The dependence of $Z_n(\alpha)$ in t and ℓ is perfectly reproduced by the exact result, as can be seen from top left, right and bottom left panels. For this quench, the imaginary part is trivial since it is given by the average conserved charge. Concerning the α-dependence, we observe that away from $\alpha = \pi$, the analytic prediction and numerical data match perfectly, even for relatively small ℓ. However, as α gets closer to $\pm\pi$, the difference between the numerical results and the exact prediction gets larger. To highlight this phenomenon, we zoom on the region in the vicinity of $\alpha = \pi$ in Fig. 5.3. It is clear that for large ℓ, the data approach the asymptotic result for any $\alpha \neq \pi$. As is well known also in equilibrium, see e.g. [1, 53], as α gets closer to $\pm\pi$, the match between the numerical data and the analytical predictions only holds for very large values of ℓ. Additional subleading terms (vanishing in the scaling limit) in the development of $\mathcal{J}$ should be considered to correctly describe the large corrections in finite size. However, this point will not affect the asymptotic behaviour of the symmetry resolved quantities which are calculated by a saddle point integral close to $\alpha = 0$ and will not be further discussed.

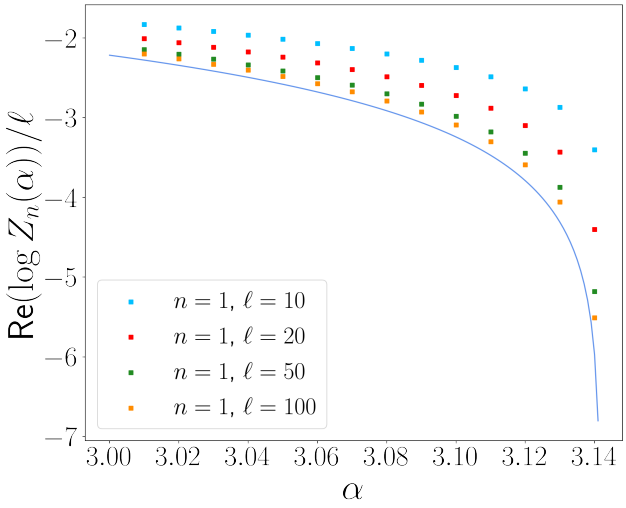


Figure 5.3: Real part of $\log Z_n(\alpha)$ after a quench from the Néel state in the free fermion model (5.3.1) as a function of α with $t/\ell = 0.5$ and $n = 1$ near the value $\alpha = \pi$.

Fourier transform

The symmetry resolved moments $\mathcal{Z}_n(q)$ with $q = \Delta q + \langle Q_A \rangle$ are defined as the Fourier transform of the charged moments $Z_n(\alpha)$. Using Eq. (2.2.8), the asymptotic formula (5.4.7), and $\langle Q_A \rangle = \ell/2$, we have

$$\mathcal{Z}_n(q) \simeq 2^{(1-n)\mathcal{J}} \int_{-\pi}^{\pi} \frac{\mathrm{d}\alpha}{2\pi} \left(\cos\frac{\alpha}{2}\right)^{\mathcal{J}} \mathrm{e}^{-\mathrm{i}\alpha\Delta q}. \tag{5.4.9}$$

First of all, we stress that this formula is valid for arbitrary Δq, but only for asymptotically large $\mathcal{J}$ because we used the asymptotic behaviour of $Z_n(\alpha)$. Indeed, as we shall see, the integral in Eq. (5.4.9) can be also negative for small $\mathcal{J}$. Furthermore, in the scaling limit Δq should be taken proportional to ℓ (or, equivalently, t), otherwise one obtains trivial results.

Since the n-dependence in Eq. (5.4.9) is trivial, we focus on $n = 1$. The integral in Eq. (5.4.9) can be evaluated in closed form in terms of the Euler Beta function $B(x,y) = \frac{\Gamma(x)\Gamma(y)}{\Gamma(x+y)}$, where $\Gamma(z)$ is the Gamma function. The result reads [1]

$$\zeta_1(q) = 2^{-\mathcal{J}} \frac{\Gamma(\mathcal{J}+1)}{\Gamma\left(\frac{\mathcal{J}+2\Delta q+2}{2}\right)\Gamma\left(\frac{\mathcal{J}-2\Delta q+2}{2}\right)}, \tag{5.4.10}$$

and we recall

$$\mathcal{Z}_1(q) \simeq \zeta_1(q), \qquad \text{for } \mathcal{J} \gg 1. \tag{5.4.11}$$

We now discuss the properties of the function $\zeta_1(q)$ and in particular its limit for $\mathcal{J} \gg 1$ when it tends to the physical probability $\mathcal{Z}_1(q)$.

The function $\Gamma(z)$ has poles when z is a negative integer. Since $\mathcal{J} \geq 0$, it follows that $\zeta_1(q)$ vanishes when $\mathcal{J} < 2|\Delta q|$ is an even integer. For other values of $\mathcal{J}$ in the regime $\mathcal{J} < 2|\Delta q|$, the function $\zeta_1(q)$ oscillates in ℓ around zero, as can be seen in Fig. 5.4 (top panels). The amplitude

[1] Eq. (5.4.9) is an integral representation of the reciprocal β function, see Wikipedia. Alternatively, see Eq. 3.631-9 in Gradshteyn and Ryzhik's, *Table of Integrals, Series, and Products*, 5th edition, Academic Press.

of these oscillations decays quickly to zero and, in the scaling limit, averages to $\zeta_1(q) \simeq \mathcal{Z}_1(q) \simeq 0$ for all the relevant physics. Actually, the last zero of $\zeta_1(q)$ is at position $\mathcal{J} = 2|\Delta q| - 2$ and afterward it monotonically increases with $\mathcal{J}$ (see Fig. 5.4, bottom panels). At $\mathcal{J} = 2|\Delta q|$, we have $\zeta_1(q) = 2^{-\mathcal{J}} = 2^{-2|\Delta q|}$. Thus, in the scaling limit, when Δq also grows with ℓ, the entire window $2|\Delta q| - 2 < \mathcal{J} < 2|\Delta q|$ shrinks to zero length, and $\mathcal{Z}_1(q)$ can be considered zero up to $\mathcal{J} = 2|\Delta q|$. Anyhow, for finite q, $\mathcal{Z}_1(q)$ is expected to grow from $\mathcal{J} = 2|\Delta q| - 2$. We illustrate these behaviours in Fig. 5.4 for relatively small values of ℓ.

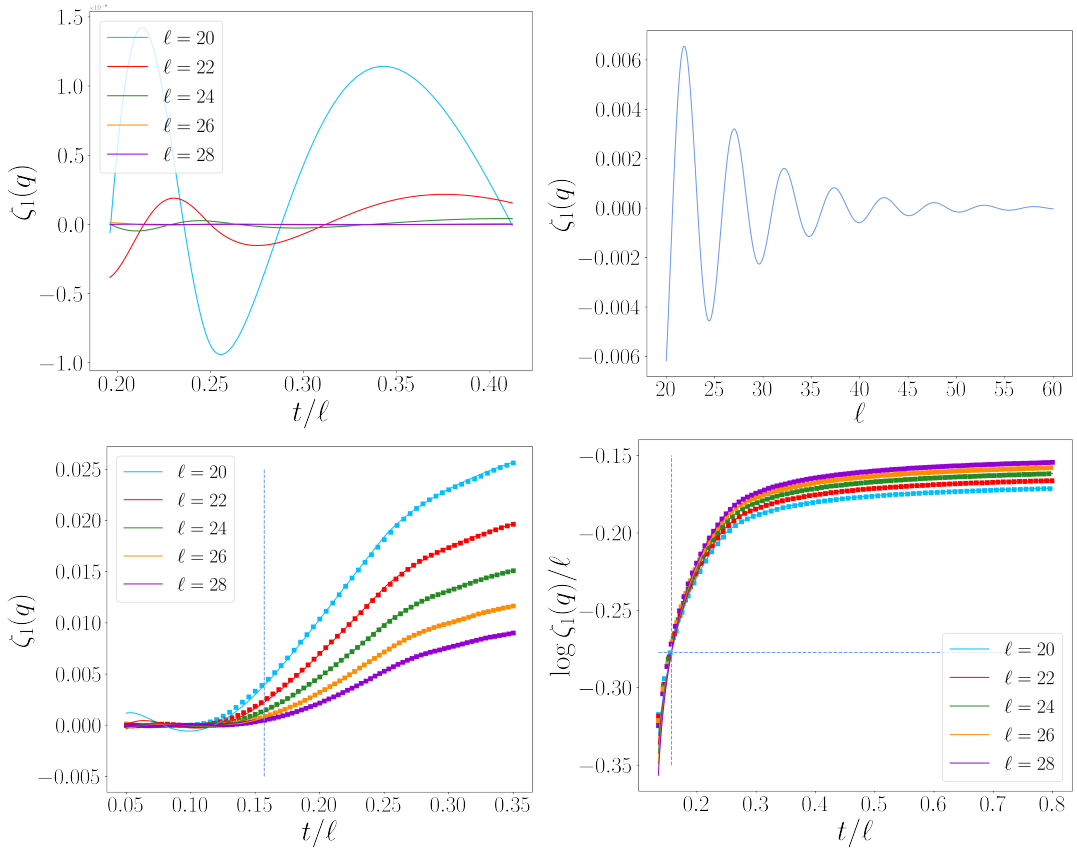


Figure 5.4: Study of the function $\zeta_1(q)$ in Eq. (5.4.10) that tends to the physical probability $\mathcal{Z}_1(q)$ for large $\mathcal{J}$ after a quench from the Néel state in the tight-biding model (5.3.1). *Top*: Short time regime $\mathcal{J} < 2|\Delta q|$. *Left:* $\zeta_1(q)$ as a function of $\mathcal{J}/\ell$ for $q = \ell$ and various values of ℓ. As ℓ increases, $\zeta_1(q)$ quickly averages to zero. *Right:* $\zeta_1(q)$ as a function of ℓ with $q = 9\ell/10$ and fixed $\mathcal{J} = \ell/100$. *Bottom*: $\zeta_1(q)$ (left) and $(\log \zeta_1(q))/\ell$ (right) as a function of $\mathcal{J}/\ell$ with $q = 7\ell/10$. We compare the exact formula of Eq. (5.4.10) for $\zeta_1(q)$ (solid lines) with numerical data for $\mathcal{Z}_1(q)$ (symbols). The vertical dashed lines are placed at $\mathcal{J}/\ell = 2|\Delta q|/\ell = 2/5$ in both panels. *Left:* $\zeta_1(q)$ starts growing monotonically at $\mathcal{J} = 2|\Delta q| - 2$. *Right:* The horizontal dashed line is at position $\log \zeta_1(q) = -2|\Delta q| \log 2$. All the curves collapse on the point $\zeta_1(q) = 2^{-\mathcal{J}}$ at $\mathcal{J} = 2|\Delta q|$.

In the regime $\mathcal{J} > 2|\Delta q| \gg 1$, we use Stirling formula to derive the asymptotic behaviour

of $\zeta_1(q)$ and hence of $\mathcal{Z}_1(q)$. We find

$$\log \mathcal{Z}_1(q) = -\Big(\frac{\mathcal{J}}{2} + |\Delta q|\Big) \log\Big(1 + \frac{2|\Delta q|}{\mathcal{J}}\Big) - \Big(\frac{\mathcal{J}}{2} - |\Delta q|\Big) \log\Big(1 - \frac{2|\Delta q|}{\mathcal{J}}\Big) + \frac{1}{2}\log\Big(\frac{4\mathcal{J}}{(\mathcal{J}+2\Delta q)(\mathcal{J}-2\Delta q)}\Big) - \frac{1}{2}\log 2\pi. \quad (5.4.12)$$

The first line of Eq. (5.4.12) contains the leading terms, the second one gives the first corrections, and sub-leading terms are omitted. We stress that the corrections due to the subleading terms in $Z_n(\alpha)$ enter at an order higher than the ones in Eq. (5.4.12).

We have seen that in the scaling regime $\mathcal{Z}_1(q)$ is zero for short $\mathcal{J}$ and starts growing at $\mathcal{J} = 2\Delta q$. These relations can be transferred from the auxiliary variable $\mathcal{J}$ to the physical time t. The crossover between the zero probability regime and the growing one takes place at a time t_D that we dub *delay time*. The latter is defined by the relation $\mathcal{J}(t_D) = 2|\Delta q|$. In general, this relation is not explicit. However, from Eq. (5.4.8), we have that for $2v_M t < \ell$

$$\mathcal{J} = 2t \int_{-\pi}^{\pi} \frac{\mathrm{d}k}{2\pi} v_k, \quad 2v_M t < \ell. \quad (5.4.13)$$

Since $v_k = 2|\sin k|$ and $v_M = 2$, we find

$$4t_D \int_{-\pi}^{\pi} \frac{\mathrm{d}k}{2\pi} |\sin k| = 2|\Delta q|, \quad 4t_D < \ell, \quad (5.4.14)$$

and conclude

$$t_D = \pi \frac{|\Delta q|}{4}, \quad \text{for} \quad |\Delta q| < \frac{\ell}{\pi}. \quad (5.4.15)$$

For larger $|\Delta q|$, there is no closed form for t_D. In Fig. 5.5 we compare the numerical solution of $\mathcal{J}(t_D) = 2|\Delta q|$ (symbols) with the linear result $t_D = \pi\frac{|\Delta q|}{4}$ (solid line). For $|\Delta q| < \frac{\ell}{\pi}$ the match is perfect, but for larger Δq the delay grows very quickly.

Even though the scaling behaviour of $\mathcal{Z}_1(q)$ is completely encoded in Eq. (5.4.10), we also analyse it with the saddle point approximation. The reason is that this method is useful in the cases where there are no analytical formulas like Eq. (5.4.10). We recast Eq. (5.4.9) as

$$\mathcal{Z}_1(q) = \int_{-\pi}^{\pi} \frac{\mathrm{d}\alpha}{2\pi} \mathrm{e}^{\ell h(\alpha)}, \quad h(\alpha) = -\mathrm{i}\alpha\frac{\Delta q}{\ell} + \frac{\mathcal{J}}{\ell}\log\cos\frac{\alpha}{2}, \quad (5.4.16)$$

so that the saddle point α^*, defined as $h'(\alpha^*) = 0$, is

$$\alpha^* = -2\mathrm{i}\,\mathrm{arctanh}\left(\frac{2\Delta q}{\mathcal{J}}\right) = \mathrm{i}\log\left(\frac{\mathcal{J}-2\Delta q}{\mathcal{J}+2\Delta q}\right). \quad (5.4.17)$$

We have two regimes, (i) $\mathcal{J} < 2|\Delta q|$, where α^* has a real part, and (ii) $\mathcal{J} > 2|\Delta q|$, where α^* is purely imaginary. In the first regime, the real part of α^* leads to a non-zero imaginary part of $h(\alpha^*)$ and $\mathcal{Z}_1(q)$ oscillates quickly in ℓ around zero. This behaviour is the same as the one we found by analyzing the exact formula (5.4.10). In the scaling limit, these oscillations average to zero for all the relevant physics.

Conversely, for $t > t_D$ (i.e. $\mathcal{J} > 2|\Delta q|$), we deform the integration contour to pass through α^* while remaining in the analyticity region of the integrand. The saddle point method gives

$$\mathcal{Z}_1(q) = \mathrm{e}^{\ell h(\alpha^*)} \sqrt{\frac{1}{2\pi\ell|h''(\alpha^*)|}}. \quad (5.4.18)$$

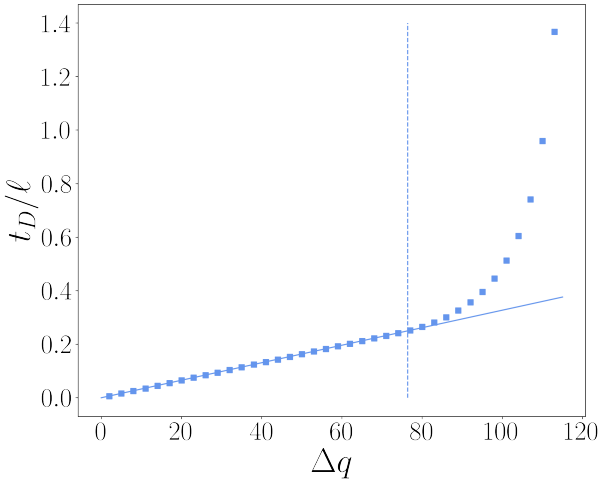


Figure 5.5: Delay t_D obtained from the numerical solution of $\mathcal{J}(t_D) = 2|\Delta q|$ for $\ell = 240$ (symbols) compared with the linear result $t_D = \pi\frac{|\Delta q|}{4}$ (solid line), valid up to $\Delta q = \frac{\ell}{\pi}$ (dashed vertical line).

The logarithm of this equation precisely gives back Eq. (5.4.12), as expected. In the limit where $\mathcal{J} \gg |\Delta q|$ we have

$$\mathcal{Z}_1(q) \simeq \sqrt{\frac{2}{\mathcal{J}\pi}}\mathrm{e}^{-\frac{2\Delta q^2}{\mathcal{J}}} \tag{5.4.19}$$

at leading order.

Symmetry resolved Rényi entropies

We now turn to the evaluation of the symmetry resolved REs. Plugging Eq. (5.4.9) into Eq. (2.2.6), $S_n(q)$ reads

$$S_n(q) = \mathcal{J}\log 2 + \log \mathcal{Z}_1(q) \tag{5.4.20}$$

and does not depend on n. In the scaling regime $\mathcal{J} > 2|\Delta q| \gg 1$, $\log \mathcal{Z}_1(q)$ is given by (5.4.12).

Following the discussion of the previous section, in the scaling limit, the entropies start to grow for $t > t_D$. In the top panels of Fig. 5.6, we compare ab-initio calculations of $S_n(q)$ and the exact prediction (5.4.20), finding perfect agreement. In particular, Fig. 5.6 convincingly shows that the numerical results for $S_n(q)$ do not depend on n. We thus focus on $S(q)$ for the rest of this subsection. We also compare the prediction (5.4.15) for the delay with the numerical results at a finite ℓ (we fix $\ell = 240$ and we calculated the delay time as the time when $S(q)/\ell = 0.007$) in the bottom right panel of Fig. 5.6 and again find a very good agreement.

If in the scaling limit with ℓ, we also take $\mathcal{J} \gg |\Delta q|$, we can use Eq. (5.4.12) and plug it into (5.4.20). Expanding the result in powers of $|\Delta q|/\mathcal{J}$, we find

$$S_n(q) = \mathcal{J}\left(\log 2 - 2\Big(\frac{\Delta q}{\mathcal{J}}\Big)^2\right). \tag{5.4.21}$$

Eq. (5.4.21) implies that for small $|\Delta q|$ there is an effective equipartition of entanglement between the various symmetry sectors, with violations of order $(\Delta q)^2/\ell$. We report this prediction

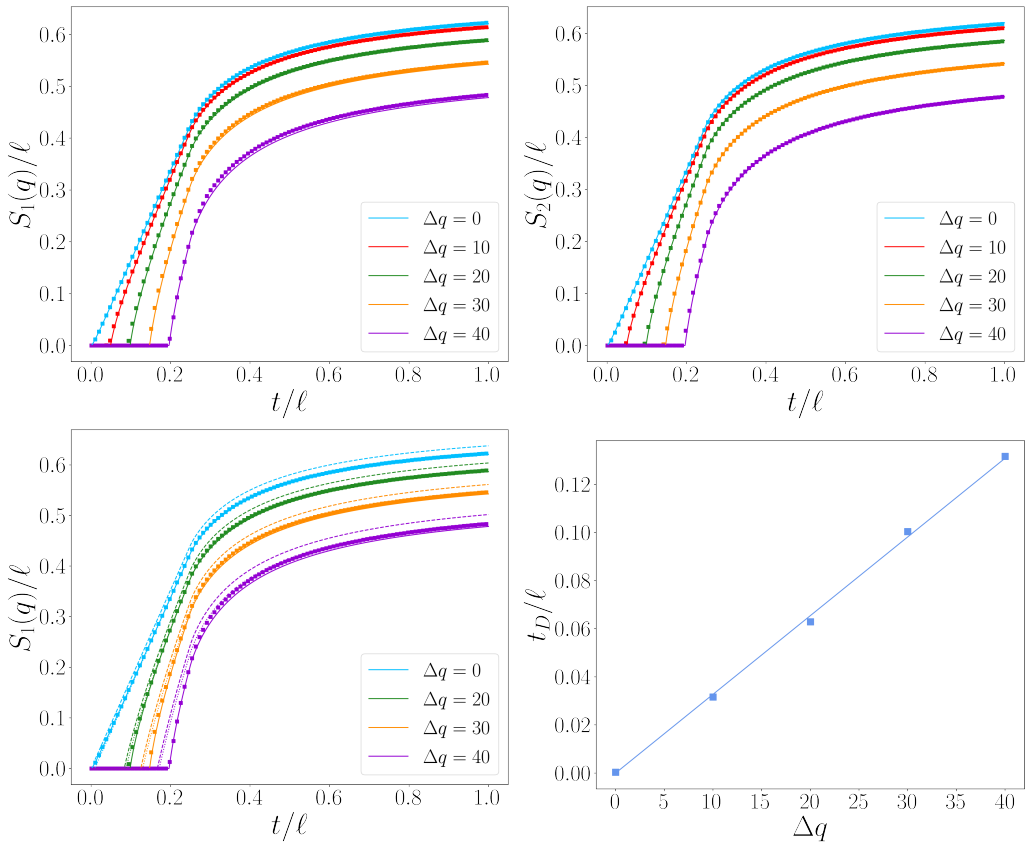


Figure 5.6: *Top and bottom left:* Time evolution of the symmetry resolved EEs $S_n(q)$ after a quench from the Néel state in the tight-binding model (5.3.1). The symbols are the exact numerical results for $\ell = 160$ and various Δq. The solid lines are our prediction (5.4.20) that perfectly match the numerical data. *Bottom left:* The dashed lines are the saddle-point approximation (5.4.21) and the dotted ones are the same approximation with the logarithmic correction. *Bottom right:* Delay time t_D for various Δq and $\ell = 240$. The solid line is the analytic prediction (5.4.15) and the symbols are the numerical results. They are obtained as the time for which $S(q)/\ell = 0.007$.

as dashed lines in the bottom left panel of Fig. 5.6. There appears to be some discrepancies, close to the delay time, between this approximation and the numerical results, even for small $|\Delta q|$, where one would expect the approximation to be very accurate. The reason for such disagreement is, obviously, that at the delay time $\mathcal{J}(t_D) = 0$ and so the subleading terms in (5.4.21) cannot be neglected. Looking at Eq. (5.4.12) (or equivalently Eq. (5.4.18)), we see that the first correction to $S_n(q)$ in the large-ℓ expansion is proportional to $\log \ell$. In the same panel of Fig. 5.6, we add this correction and report $\frac{\mathcal{J}}{\ell}\left(\log 2 - 2\left(\frac{\Delta q}{\mathcal{J}}\right)^2\right) - 1/(2\ell)\log \ell$ as the dotted lines. These curves get closer to the numerical data and fit them perfectly for $t \gg t_D$, i,e, in the region where $\mathcal{J}$ is significantly larger than $|\Delta q|$. This correction is subleading in the scaling limit and hence we conclude that Eq. (5.4.21) correctly reproduces the numerical data in the large-ℓ limit.

Total and number entropy

A final question worth investigating is whether our results for the symmetry resolved EE are coherent with the known results for the dynamics of the total EE S. To this aim, we should also investigate the contribution of the number entropy S^n to the total entanglement. The number entropy S^n is defined in Eq. (2.2.2), providing in our case

$$S^n = -\sum_{q=0}^{\ell} \mathcal{Z}_1(q) \log \mathcal{Z}_1(q) \tag{5.4.22}$$

and, using the same asymptotic calculations as in Sect. 5.4.1 and Eq. (5.4.19), we find

$$S^n = \sqrt{\frac{2}{\mathcal{J}\pi}} \sum_{\Delta q=-\ell/2}^{\ell/2} \Big(\frac{2\Delta q^2}{\mathcal{J}} + \frac{1}{2}\log\frac{\mathcal{J}\pi}{2}\Big) \mathrm{e}^{-\frac{2\Delta q^2}{\mathcal{J}}} \tag{5.4.23}$$

for $\mathcal{J} \gg |\Delta q|$. The latter condition is not met for the extreme values of $|\Delta q|$ in the sum, where instead we have $\mathcal{J} \sim |\Delta q|$. However, such values of the subsystem charge have a very low probability and so this approximation is expected to give excellent results, as we will soon confirm numerically. Since we are in the limit of large ℓ, we transform the sums into Gaussian integrals. Their evaluation is straightforward and we have

$$S^n = \frac{1}{2}\Big(1 + \log\frac{\mathcal{J}\pi}{2}\Big), \tag{5.4.24}$$

i.e. the number entropy grows logarithmically with time until saturation to a value which is proportional to $\log \ell$. Such behaviour is reminiscent of what found in many other different contexts [276, 277, 278].

In Fig. 5.7 we compare this result (solid lines) with ab-initio calculations of S^n (symbols), and find perfect agreement. The inset in the left panel shows the time-evolution of S^n in a log-linear scale and highlights the logarithmic growth in time before the saturation. It directly follows from Eq. (5.4.24) that the large-time limit of the number entropy is $\lim_{t\to\infty} S^n = \frac{1}{2}\Big(1 + \log\frac{\ell\pi}{2}\Big)$, reported as a dotted horizontal line in the left panel of Fig. 5.7. This analysis shows that in the scaling limit, the number entropy has a negligible contribution to the total entropy, $\lim_{t\to\infty} S^n/S = \mathcal{O}(\ell^{-1}\log\ell)$.

For the total entropy, we plug Eq. (5.4.20) into Eq. (2.2.2) and find

$$S = \sum_{q=0}^{\ell} \mathcal{Z}_1(q)\mathcal{J}\log 2, \tag{5.4.25}$$

where we used the relation $p(q) = \mathcal{Z}_1(q)$ from Eq. (2.2.7). The latter satisfies $\sum_{q=0}^{\ell}\mathcal{Z}_1(q) = 1$, as it should. We thus recover the known result for the total EE after a quench from the Néel state [193, 127], namely

$$S = \log 2 \int \frac{\mathrm{d}k}{2\pi} \min(\ell, 2v_k t). \tag{5.4.26}$$

For large times, we have $\lim_{t\to\infty} S = \ell \log 2$. We finally mention that it is straightforward to show that the number entropy exactly compensate for the $\log\ell$ subleading corrections present in the entanglement of each symmetry sector.

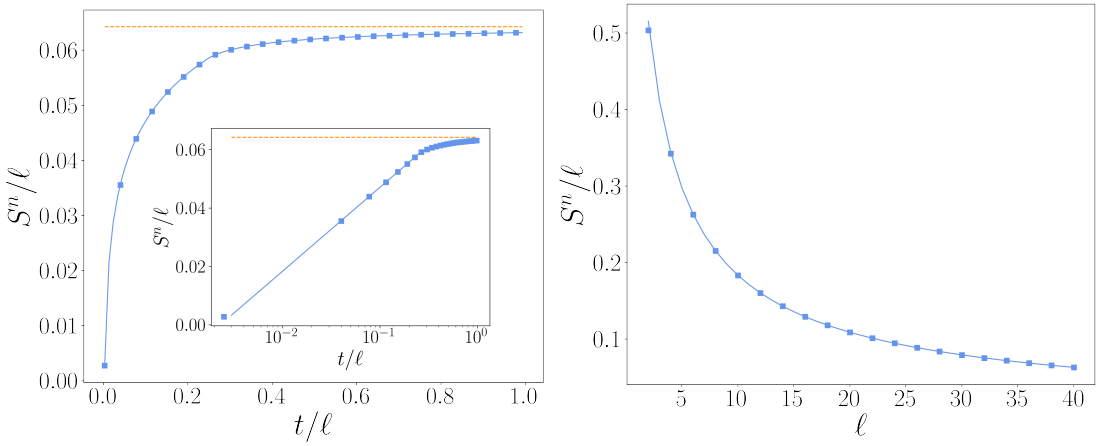


Figure 5.7: Evolution of S^n after a quench from the Néel state in the tight-binding model (5.3.1) as a function of t/ℓ for $\ell = 40$ (left panel), and as a function of ℓ with $t/\ell = 1$ (right panel). The prediction (5.4.24) (solid line) perfectly matches the numerical results (symbols). In the left panel, the horizontal dotted line is the asymptotic value $\frac{1}{2\ell}\left(1 + \log\frac{\ell\pi}{2}\right)$ for large times. In the same panel, the inset shows S^n as a function of t/ℓ in a log-linear scale.

5.4.2 Disjoint intervals

In this subsection, we move to the analysis of the charged and symmetry resolved entropies for two disjoint intervals, as well as the symmetry resolved MI.

The starting point is the correlation matrix $C_{A_1\cup A_2}(t)$ that encodes correlations within the system $A = A_1 \cup A_2$ where the two subsystems have respective lengths ℓ_1 and $\ell_2 = \ell - \ell_1$, and are separated by d lattice sites. The correlation matrix has the form

$$C_{A_1\cup A_2}(t) = \begin{pmatrix} C_{11}(t) & C_{12}(t) \\ C_{21}(t) & C_{22}(t) \end{pmatrix} \tag{5.4.27}$$

with

$$[C_{11}(t)]_{j,k} = [C(t)]_{j,k}, \qquad j,k = 1,\dots \ell_1, \tag{5.4.28}$$
$$[C_{22}(t)]_{j,k} = [C(t)]_{j+d,k+d}, \qquad j,k = 1,\dots \ell_2, \tag{5.4.29}$$
$$[C_{12}(t)]_{j,k} = [C(t)]_{j,k+d}, \qquad j = 1,\dots \ell_1, \quad k = 1,\dots \ell_2, \tag{5.4.30}$$
$$[C_{21}(t)]_{j,k} = [C(t)]_{j+d,k}, \qquad j = 1,\dots \ell_2, \quad k = 1,\dots \ell_1, \tag{5.4.31}$$

where the matrix elements are given in Eq. (5.4.1).

Charged moments

In order to compute the charged moments and the symmetry resolved entanglement measures, we compute the trace of arbitrary powers of the matrix $J_{A_1\cup A_2}(t) = 2C_{A_1\cup A_2}(t) - \mathbb{I}_\ell$. We perform the computation of $\mathrm{Tr}J_{A_1\cup A_2}(t)^m$ in the scaling limit $t, \ell, \ell_1, \ell_2, d \to \infty$ where the various ratios are kept constant. The calculation uses the multidimensional stationary phase approximation, and generalises the methods used in [257] to the case of an arbitrary separation d. We

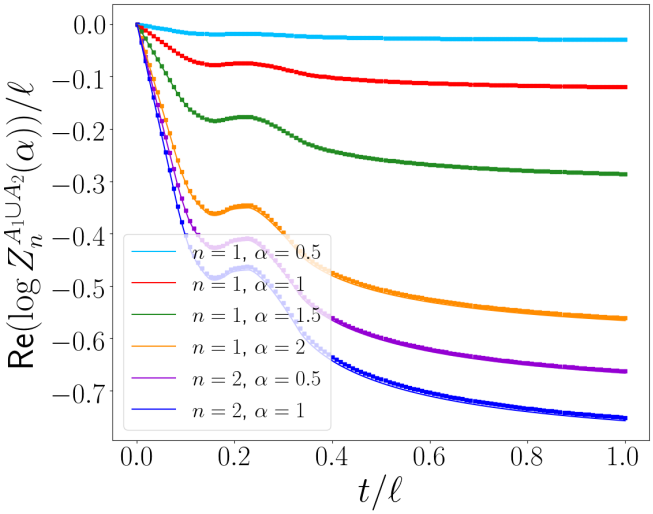


Figure 5.8: Time evolution of the charged moments $Z_n^{A_1\cup A_2}(\alpha)$ after a quench from the Néel state in the tight-binding model (5.3.1) as a function of t/ℓ with $\ell_1 = 100$, $\ell_2 = 140$ and $d = 80$. The analytical prediction of Eq. (5.4.33) (solid lines) perfectly matches the numerical data (symbols).

find

$$\begin{aligned}\mathrm{Tr}J_{A_1\cup A_2}(t)^{2j} &= \ell - \int \frac{\mathrm{d}k}{2\pi}[\min(\ell_1, 2v_k t) + \min(\ell_2, 2v_k t)] \\ &\quad + \int \frac{\mathrm{d}k}{2\pi}[\max(d, 2v_k t) + \max(d+\ell, 2v_k t) - \max(d+\ell_1, 2v_k t) - \max(d+\ell_2, 2v_k t)], \\ \mathrm{Tr}J_{A_1\cup A_2}(t)^{2j+1} &= 0,\end{aligned} \tag{5.4.32}$$

with $v_k = 2|\sin k|$. We note that the case $d = 0$ reduces to the known result of Eq. (5.4.3) for a single interval. The computation of the charged moments $Z_n^{A_1\cup A_2}(\alpha)$ proceeds exactly as for the case of a single interval discussed in Sect. 5.4.1. We thus find

$$Z_n^{A_1\cup A_2}(\alpha) = \left(\frac{\cos\frac{\alpha}{2}}{2^{n-1}}\right)^{\mathcal{J}_d} \mathrm{e}^{\mathrm{i}\ell\frac{\alpha}{2}} \tag{5.4.33}$$

where we introduced

$$\begin{aligned}\mathcal{J}_d \equiv& \ell - \mathrm{Tr}J_{A_1\cup A_2}(t)^2 \\ =& \int \frac{\mathrm{d}k}{2\pi}[\min(\ell_1, 2v_k t) + \min(\ell_2, 2v_k t)] \\ &- \int \frac{\mathrm{d}k}{2\pi}[\max(d, 2v_k t) + \max(d+\ell, 2v_k t) - \max(d+\ell_1, 2v_k t) - \max(d+\ell_2, 2v_k t)].\end{aligned} \tag{5.4.34}$$

In Fig. 5.8 we compare the prediction (5.4.33) for $Z_n^{A_1\cup A_2}(\alpha)$ with ab-initio calculations and find perfect agreement.

Fourier transform and symmetry resolved Rényi entropies

The calculations for the symmetry resolved moments and REs are exactly the same as the computations of Secs. 5.4.1 and 5.4.1 where $\mathcal{J}$ is systematically replaced by $\mathcal{J}_d$. We thus have

$$S_n^{A_1\cup A_2}(q) = \mathcal{J}_d \log 2 + \log \mathcal{Z}_1^{A_1\cup A_2}(q), \quad \mathcal{Z}_1^{A_1\cup A_2}(q) \simeq 2^{-\mathcal{J}_d} \frac{\Gamma(\mathcal{J}_d+1)}{\Gamma\left(\frac{\mathcal{J}_d+2\Delta q+2}{2}\right)\Gamma\left(\frac{\mathcal{J}_d-2\Delta q+2}{2}\right)}, \tag{5.4.35}$$

and

$$S_n^{A_1\cup A_2}(q) = \mathcal{J}_d \left(\log 2 - 2\left(\frac{\Delta q}{\mathcal{J}_d}\right)^2\right), \quad \mathcal{Z}_1^{A_1\cup A_2}(q) \simeq \sqrt{\frac{2}{\mathcal{J}_d\pi}} \mathrm{e}^{-\frac{2\Delta q^2}{\mathcal{J}_d}}, \tag{5.4.36}$$

in the limit where ℓ is large and $\mathcal{J} \gg |\Delta q|$. We do not report numerical tests for these symmetry resolved entropies because they do not to add any information compared to the single interval case.

Symmetry resolved mutual information

We now turn to the computation of the symmetry resolved MI defined as in Eq. (5.2.1). The first step is to compute $Z_1^{A_1:A_2}(\alpha,\beta)$. To do so, we compute the trace of powers of the matrix $J_{\alpha\beta}$ in Eq. (5.3.16). We adapt the calculations of Sect. 5.4.2 for the trace of $J_{A_1\cup A_2}$ and find

$$\begin{aligned}
\mathrm{Tr} J_{\alpha\beta}(t)^{2j} &= \left(\frac{\mathrm{e}^{\mathrm{i}\alpha}-1}{\mathrm{e}^{\mathrm{i}\alpha}+1}\right)^{2j}\left[\ell_1 - \int \frac{\mathrm{d}k}{2\pi}\min(\ell_1, 2v_k t)\right] \\
&+ \left(\frac{\mathrm{e}^{\mathrm{i}\beta}-1}{\mathrm{e}^{\mathrm{i}\beta}+1}\right)^{2j}\left[\ell_2 - \int \frac{\mathrm{d}k}{2\pi}\min(\ell_2, 2v_k t)\right] \\
+(-1)^j\left(\tan\frac{\alpha}{2}\tan\frac{\beta}{2}\right)^j &\int \frac{\mathrm{d}k}{2\pi}[\max(d,2v_k t)+\max(d+\ell,2v_k t)-\max(d+\ell_1,2v_k t)-\max(d+\ell_2,2v_k t)], \\
\mathrm{Tr} J_{\alpha\beta}(t)^{2j+1} &= 0.
\end{aligned} \tag{5.4.37}$$

The re-summation in Eq. (5.3.17) is direct and we find

$$\begin{aligned}
\log Z_1^{A_1:A_2}(\alpha,\beta) = \mathrm{i}\frac{\ell_1\alpha+\ell_2\beta}{2} &+ \log\left(\cos\frac{\alpha}{2}\right)\mathcal{J}_{A_1} + \log\left(\cos\frac{\beta}{2}\right)\mathcal{J}_{A_2} \\
&+ \frac{1}{2}\log\left(1+\tan\frac{\alpha}{2}\tan\frac{\beta}{2}\right)(\mathcal{J}_{A_1}+\mathcal{J}_{A_2}-\mathcal{J}_d)
\end{aligned} \tag{5.4.38}$$

where $\mathcal{J}_d$ is given in Eq. (5.4.34) and the straightforward notation $\mathcal{J}_{A_{1,2}} = \mathcal{J}|_{\ell\to\ell_{1,2}} = \int \frac{\mathrm{d}k}{2\pi}\min(\ell_{1,2}, 2v_k t)$. As a consistency check, $Z_1^{A_1:A_2}(\alpha,\alpha)$ is equal to the charged moment $Z_1^{A_1\cup A_2}(\alpha)$ given in Eq. (5.4.33). We compare the prediction of Eq. (5.4.38) with numerical results in Fig. 5.9 and find a perfect agreement.

To perform the double Fourier transform in Eq. (5.2.4) for $\mathcal{Z}_1^{A_1:A_2}(q_1, q-q_1)$, we exploit the saddle point approximation and expand $Z_1^{A_1:A_2}(\alpha,\beta)$ at quadratic order, obtaining

$$\log Z_1^{A_1:A_2}(\alpha,\beta) = \mathrm{i}\frac{\ell_1\alpha+\ell_2\beta}{2} - \frac{\alpha^2}{8}\mathcal{J}_{A_1} - \frac{\beta^2}{8}\mathcal{J}_{A_2} + \frac{\alpha\beta}{8}(\mathcal{J}_{A_1}+\mathcal{J}_{A_2}-\mathcal{J}_d). \tag{5.4.39}$$

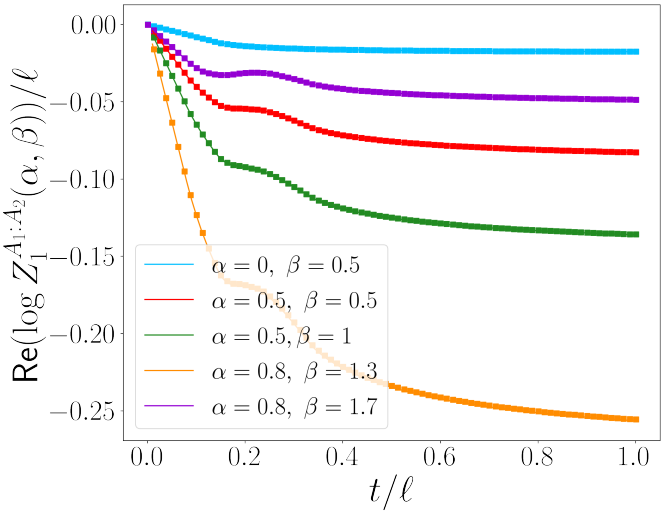


Figure 5.9: Time evolution of $Z_1^{A_1:A_2}(\alpha,\beta)$ after a quench from the Néel state in the tight-binding model (5.3.1) as a function of t/ℓ with $\ell_1 = 100$, $\ell_2 = 140$ and $d = 80$. The analytical prediction of Eq. (5.4.38) (solid lines) perfectly matches the numerical data (symbols).

In this approximation, the Fourier transform is given as

$$\mathcal{Z}_1^{A_1:A_2}(q_1, q-q_1) = \frac{2}{\pi\sqrt{\mathcal{J}_{A_1}\mathcal{J}_{A_2} - \frac{\mathcal{J}_m^2}{4}}} \mathrm{e}^{-\frac{8}{4\mathcal{J}_{A_1}\mathcal{J}_{A_2}-\mathcal{J}_m^2}\left[\Delta q_1^2\mathcal{J}_{A_2}+(\Delta q-\Delta q_1)^2\mathcal{J}_{A_1}+\Delta q_1(\Delta q-\Delta q_1)\mathcal{J}_m\right]} \tag{5.4.40}$$

where we have introduced $\mathcal{J}_m = (\mathcal{J}_{A_1} + \mathcal{J}_{A_2} - \mathcal{J}_d)$ to lighten the notations, and we have $\Delta q = q - \ell/2$ and $\Delta q_1 = q_1 - \ell_1/2$. Importantly, the weight $p(q_1, q-q_1) = \mathcal{Z}_1^{A_1:A_2}(q_1, q-q_1)/\mathcal{Z}_1^{A_1\cup A_2}(q)$ defined in Eq. (5.2.2) satisfies $\sum_{q_1=0}^{q} p(q_1, q-q_1) = 1$ also when the sum is approximated as an integral and the quantities are given by their Gaussian approximations of Eqs. (5.4.36) and (5.4.40).

Using the Gaussian expression for each term involved in the definition of Eq. (5.2.1) and the same type of asymptotic calculations as in the previous sections, we find

$$\begin{aligned} I_1^{A_1:A_2}(q) = (\mathcal{J}_{A_1} + \mathcal{J}_{A_2} - \mathcal{J}_d)\log 2 - \frac{1}{2}\Big(\log\frac{\mathcal{J}_{A_1}\mathcal{J}_{A_2}\pi}{2\mathcal{J}_d}\Big) - \frac{4\mathcal{J}_{A_1}\mathcal{J}_{A_2} - \mathcal{J}_m^2}{8\mathcal{J}_d}\Big(\frac{1}{\mathcal{J}_{A_1}} + \frac{1}{\mathcal{J}_{A_2}}\Big) \\ - 2\Delta q^2\Big\{\Big(\frac{-\mathcal{J}_{A_1} + \mathcal{J}_{A_2} - \mathcal{J}_d}{2\mathcal{J}_d}\Big)^2\frac{1}{\mathcal{J}_{A_1}} + \Big(\frac{\mathcal{J}_{A_1} - \mathcal{J}_{A_2} - \mathcal{J}_d}{2\mathcal{J}_d}\Big)^2\frac{1}{\mathcal{J}_{A_2}} - \frac{1}{\mathcal{J}_d}\Big\}. \end{aligned} \tag{5.4.41}$$

Eq. (5.4.41) implies that at the leading order there is equipartition of the symmetry resolved MI. Furthermore, for $t < d/4$ and in the limit $t \to \infty$, the subleading term vanishes, because $\mathcal{J}_d = \mathcal{J}_{A_1} + \mathcal{J}_{A_2}$ in these two regimes, and the equipartition is broken at higher order. In Fig. 5.10 we compare the prediction (5.4.41) (solid lines) with the ab-initio calculation of Eq. (5.2.1) where the entropies have been replaced by their expressions in terms of Gamma functions, and the weights are replaced by their Gaussian expressions (symbols). We find a perfect agreement between asymptotic prediction and exact numerics. The slight negative values for early times arise from the term $-\frac{1}{2}\log\frac{\mathcal{J}_{A_1}\mathcal{J}_{A_2}\pi}{2\mathcal{J}_d}$ in Eq. (5.4.41). This term is at most of order $\log\ell$ and is

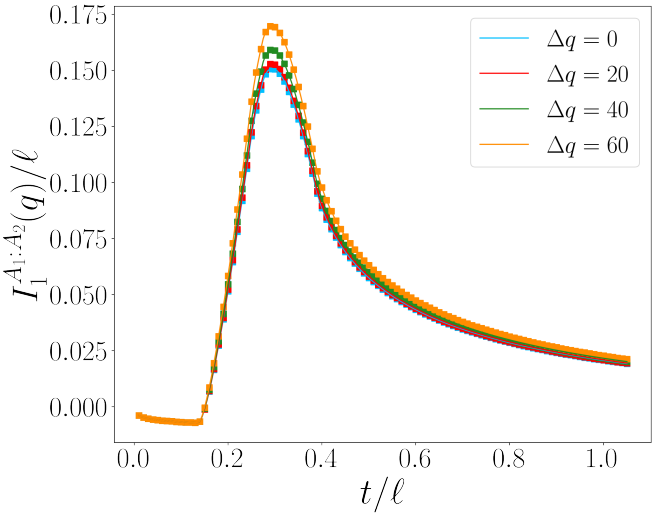


Figure 5.10: Time evolution of $I_1^{A_1:A_2}(q)$ after a quench from the Néel state in the tight-binding model (5.3.1) as a function of t/ℓ with $\ell_1 = 180$, $\ell_2 = 220$ and $d = 220$ for various values of Δq. We compare the approximation of Eq. (5.4.41) (solid lines) with the exact result given by Eq. (5.2.1) where the entropies are replaced by their exact formulas of the form of Eq. (5.4.20) and the weights are given by their Gaussian approximations (symbols).

negligible in the scaling limit. We do not observe any other time delays that depend on the charge sector. The reason is that from its definition of Eq. (5.2.1), $I_1^{A_1:A_2}(q)$ mixes quantities from different charge sectors for the subsystems. For intermediate times, the equipartition is broken at order $\Delta q^2/\ell$.

The leading term in Eq. (5.4.41) is the total MI,

$$\begin{aligned} I_1^{A_1:A_2} &= (\mathcal{J}_{A_1} + \mathcal{J}_{A_2} - \mathcal{J}_d)\log 2 \\ &= \log 2 \int \frac{\mathrm{d}k}{2\pi} [\max(d, 2v_k t) + \max(d+\ell, 2v_k t) - \max(d+\ell_1, 2v_k t) - \max(d+\ell_2, 2v_k t)]. \end{aligned} \tag{5.4.42}$$

This immediately follow from the definition of Eq. (1.2.9) and the exact results of Eqs. (5.4.20) and (5.4.36) for the EE. This integral is precisely the form predicted by the quasiparticle picture for the spreading of entanglement between two non-complementary subsystems [279]. It is vanishing for times $t < d/4$ as well as in the large-time limit. To verify the consistency of our calculations, we must recover the total MI from the symmetry resolved ones with the combination given in Eq. (5.2.5). Using the same Gaussian results as before, Eq. (5.4.41) and the asymptotic result for the number entropy of Eq. (5.4.24), we indeed find

$$\sum_{q=0}^{\ell} \mathcal{Z}_1^{A_1\cup A_2}(q) I_1^{A_1:A_2}(q) + S^{A_1,n} + S^{A_2,n} - S^{A_1\cup A_2,n} = (\mathcal{J}_{A_1} + \mathcal{J}_{A_2} - \mathcal{J}_d)\log 2. \tag{5.4.43}$$

5.5 Quench from the dimer state

For the quench from the dimer state $|D\rangle$ (cf. Eq. (5.3.18)) in the tight binding model, the starting point is also the correlation matrix. For this quench, it is convenient to write it in a block form as follows (see e.g. [280]):

$$[C(t)]_{j,k} = \left\langle \begin{pmatrix} c^\dagger_{2j-1} \\ c^\dagger_{2j} \end{pmatrix} \begin{pmatrix} c_{2k-1} & c_{2k} \end{pmatrix} \right\rangle = \frac{1}{2}(\delta_{j,k}\mathbb{I}_2 + \Pi_{k-j}) \tag{5.5.1}$$

where Π_m is

$$\Pi_m = \mathrm{i}\int_{-\pi}^{\pi} \frac{\mathrm{d}k}{2\pi} \mathrm{e}^{-\mathrm{i}mk} \begin{pmatrix} -f(k,t) & g(k,t) \\ -g(k,t)^* & f(k,t) \end{pmatrix} \tag{5.5.2}$$

with

$$\begin{aligned} f(k,t) &= \mathrm{i}\sin k \sin(2\cos(k)t), \\ g(k,t) &= \mathrm{e}^{-\mathrm{i}k}(\cos k + \mathrm{i}\sin k \cos(2\cos(k)t)). \end{aligned} \tag{5.5.3}$$

5.5.1 Single interval

Similarly to the Néel quench, we start by considering the case where A is a block of ℓ consecutive sites. The correlation matrix $C_A(t) = \frac{1}{2}(\mathbb{I}_\ell + J_A(t))$ is the $\ell \times \ell$ matrix whose entries are $[C(t)]_{j,k}$ given in Eq. (5.5.1) with $j,k \in \{1,\dots,\ell/2\}$.

Charged moments

We compute of the trace of $J_A(t)^m$ in the scaling limit where $t, \ell \to \infty$ with a fixed finite ratio. The computation is exaclty the same as in [257] and we find

$$\mathrm{Tr}J_A(t)^{2j} = \ell - \int \frac{\mathrm{d}k}{2\pi}(1 - [\cos k]^{2j}) \min(\ell, 2v_k t), \quad \mathrm{Tr}J_A(t)^{2j+1} = 0 \tag{5.5.4}$$

with $v_k = 2|\sin k|$. As for the quench from the Néel state, the maximal velocity is $v_M = 2$. We evaluate the sum (5.3.6) with (5.5.4) and find

$$\log Z_n(\alpha) = \mathrm{i}\ell\frac{\alpha}{2} + \int \frac{\mathrm{d}k}{2\pi} \mathrm{Re}[h_{n,\alpha}(\cos k)] \min(\ell, 2v_k t) \tag{5.5.5}$$

where $h_{n,\alpha}(x)$ is given in Eq. (5.3.5). This result is very similar to Eq. (5.4.6) for the Néel quench, with the difference that the function $h_{n,\alpha}(x)$ is now evaluated in $x = \cos k$ and hence cannot be factorised out of the integral. In Fig. 5.11 we compare this prediction with the exact numerical data for the charged moments and find a very good agreement. As observed for the Néel quench and in many other cases, the corrections to the scaling are larger as α gets closer to $\pm\pi$ and as n increases.

Fourier transform and symmetry resolved Rényi entropies

The symmetry resolved moments $\mathcal{Z}_n(q)$ with $q = \Delta q + \langle Q_A \rangle$ are defined in Eq. (2.2.8). With Eq. (5.5.5) and $\langle Q_A \rangle = \ell/2$, we have

$$\mathcal{Z}_n(q) = \int \frac{\mathrm{d}\alpha}{2\pi} \mathrm{e}^{-\mathrm{i}\alpha\Delta q + \int \frac{\mathrm{d}k}{2\pi} \mathrm{Re}[h_{n,\alpha}(\cos k)] \min(\ell, 2v_k t)}. \tag{5.5.6}$$

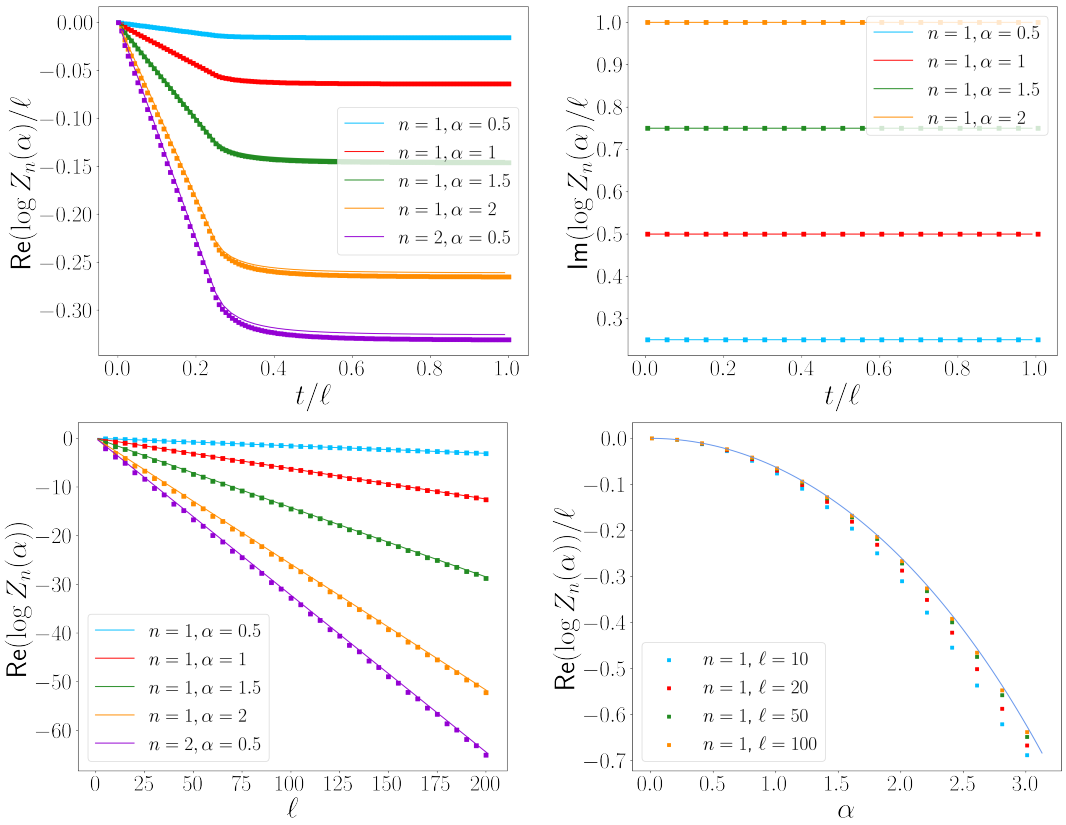


Figure 5.11: Comparison between the exact result (5.5.5) (solid lines) and numerical results (symbols) for $\log Z_n(\alpha)$ after a quench from the dimer state in the free fermion model (5.3.1). *Top left:* Time evolution of the real part of $\log Z_n(\alpha)$ as a function of t/ℓ with $\ell = 120$. *Top right*: Time evolution of the imaginary part of $\log Z_n(\alpha)$ as a function of t/ℓ with $\ell = 20$ and $n = 1$. *Bottom left:* Real part of $\log Z_n(\alpha)$ as a function of ℓ with $t/\ell = 0.5$. *Bottom right:* Real part of $\log Z_n(\alpha)$ as a function of α with $t/\ell = 0.5$ and $n = 1$.

Contrarily to the Néel quench, there is no closed-form expression similar to Eq. (5.4.10) for this integral. We can nonetheless infer the validity of our two main results, namely the existence of a time delay that grows linearly in $|\Delta q|$ for small values of $|\Delta q|$, and an effective equipartition of entanglement broken at order $(\Delta q)^2/\ell$.

For the delay, we analyse Eq. (5.5.6) with the saddle point approximation in the regime where $2v_M t < \ell$. The saddle point equation is

$$-\mathrm{i}\Delta q + \mathrm{i}t \int \frac{\mathrm{d}k}{2\pi} \partial_{\mathrm{i}\alpha} \left(\mathrm{Re}[h_{n,\alpha}(\cos k)]\right) 2v_k = 0 \tag{5.5.7}$$

and admits a solution for imaginary α only. In that case, the integral $\int \frac{\mathrm{d}k}{2\pi} \partial_{\mathrm{i}\alpha} \left(\mathrm{Re}[h_{n,\alpha}(\cos k)]\right) 2v_k$ is a monotonic function of $\mathrm{i}\alpha$, going from $4/\pi$ at $\alpha = -\mathrm{i}\infty$ to $-4/\pi$ at $\alpha = \mathrm{i}\infty$. It thus follows that Eq. (5.5.7) only admits a solution for $t > \frac{\pi|\Delta q|}{4}$. Hence we find precisely the same delay as for the Néel quench, with the same self-consistency relation $|\Delta q| < \ell/\pi$, as given in Eq. (5.4.15).

For the equipartition, we expand the charged moments at quadratic order in α,

$$\log Z_n(\alpha) = \mathrm{i}\ell\frac{\alpha}{2} + \log Z_n(0) - \frac{\alpha^2}{8}\mathcal{J}^{(n)} \tag{5.5.8}$$

with

$$\mathcal{J}^{(n)} = \int \frac{\mathrm{d}k}{2\pi} j_n(k)\, \min\big(\ell, 2v_k t\big), \tag{5.5.9}$$

where

$$j_n(k) = \frac{4\sin^{2n} k}{((1+\cos k)^n + (1-\cos k)^n)^2}. \tag{5.5.10}$$

In the following, we also need the value of the derivative of $j_n(k)$ with respect to n at $n = 1$. It reads

$$(\partial_n j_n(k))|_{n=1} = [-(1-\cos k)\log(1-\cos k) - (1+\cos k)\log(1+\cos k) + 2\log\sin k]\sin^2 k. \tag{5.5.11}$$

These $\mathcal{J}^{(n)}$ integrals generalise $\mathcal{J}$ of Eq. (5.4.8). In particular, we have $\mathcal{J}^{(0)} = \mathcal{J}$. With this quadratic expansion, we compute the Fourier transform and find

$$\mathcal{Z}_n(q) = Z_n(0)\mathrm{e}^{-\frac{2\Delta q^2}{\mathcal{J}^{(n)}}}\sqrt{\frac{2}{\pi\mathcal{J}^{(n)}}}. \tag{5.5.12}$$

Plugging this result in Eq. (2.2.6), we find at leading order

$$S_n(q) = S_n - \frac{2\Delta q^2}{(1-n)}\Big\{\frac{1}{\mathcal{J}^{(n)}} - \frac{n}{\mathcal{J}^{(1)}}\Big\} \tag{5.5.13}$$

where we used that $\log Z_1(0) = 0$ and the total entropy is $S_n = \frac{1}{1-n}\log Z_n(0)$. The symmetry resolved EE is obtained as the limit $n \to 1$ of Eq. (5.5.13), and reads

$$S(q) = S - \frac{2\Delta q^2}{\mathcal{J}^{(1)}}\Big\{\frac{(\partial_n \mathcal{J}^{(n)})|_{n=1}}{\mathcal{J}^{(1)}} + 1\Big\} \tag{5.5.14}$$

where $S = -(\partial_n Z_n(0))|_{n=1}$. Equations (5.5.13) and (5.5.14) are physically equivalent to Eq. (5.4.21). Similarly to the case of a quench from the Néel state, the match with the numerical data is better when we include the sub-leading terms that arise from the square root in Eq. (5.5.12). The result reads

$$S_n(q) = S_n - \frac{2\Delta q^2}{(1-n)}\Big\{\frac{1}{\mathcal{J}^{(n)}} - \frac{n}{\mathcal{J}^{(1)}}\Big\} + \frac{1}{2}\log\frac{2}{\pi} - \frac{1}{2(1-n)}\log\frac{\mathcal{J}^{(n)}}{(\mathcal{J}^{(1)})^n} \tag{5.5.15}$$

and the limit $n \to 1$ is

$$S(q) = S - \frac{2\Delta q^2}{\mathcal{J}^{(1)}}\Big\{\frac{(\partial_n \mathcal{J}^{(n)})|_{n=1}}{\mathcal{J}^{(1)}} + 1\Big\} + \frac{1}{2}\log\frac{2}{\pi} + \frac{1}{2}\Big(\frac{(\partial_n \mathcal{J}^{(n)})|_{n=1}}{\mathcal{J}^{(1)}} - \log\mathcal{J}^{(1)}\Big). \tag{5.5.16}$$

We compare these predictions with ab-initio results in Fig. 5.12. As expected, the delay is not well reproduced by the approximation for large $|\Delta q|$, but the asymptotic values match convincingly. The reason of this disagreement at intermediate times is the same as for the Néel quench and is not discussed again here. In the same figure we report the delays for $S(q)$ and $S_2(q)$ and compare them with the prediction $t_D = \frac{\pi|\Delta q|}{4}$. For $S(q)$, the match is perfect. We expect that finite-size effects play an increasing role for larger values of n and $|\Delta q|$, and indeed the match is less precise for $S_2(q)$ at large $|\Delta q|$.

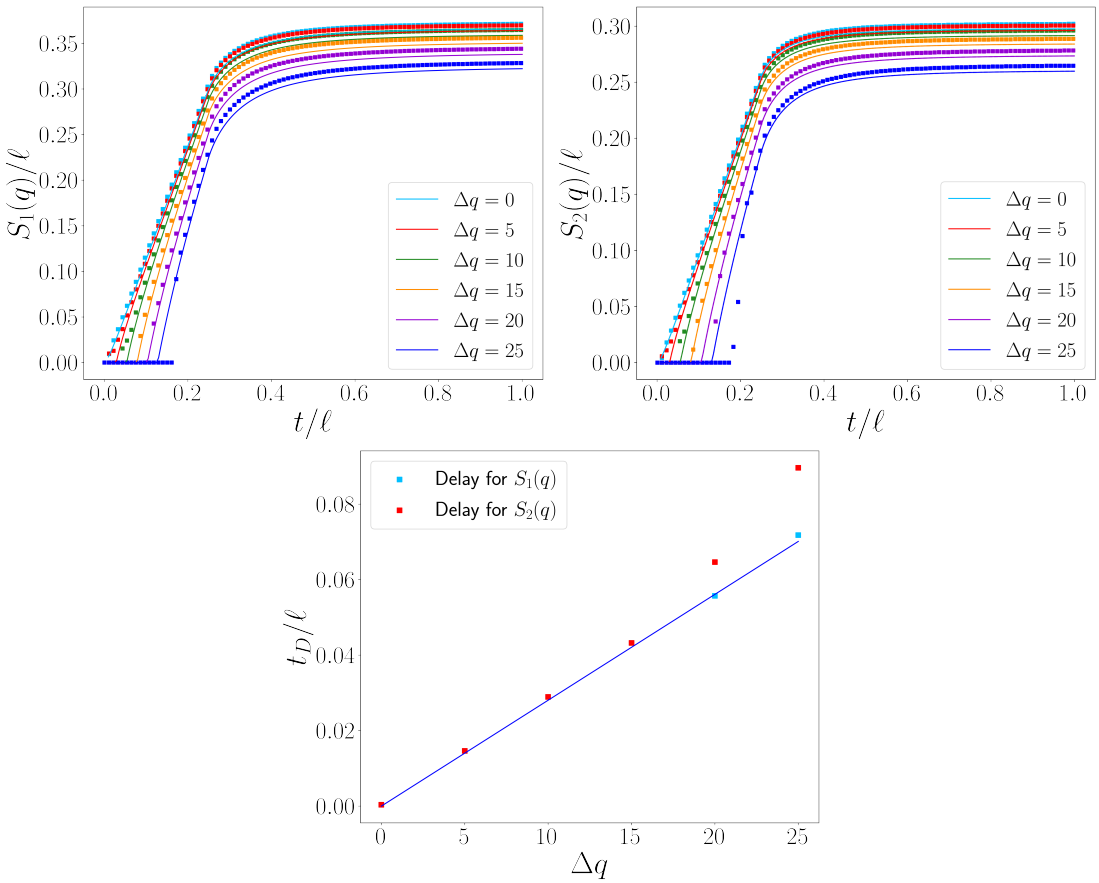


Figure 5.12: *Top:* Time evolution of the symmetry resolved entropies $S(q)$ and $S_2(q)$ after a quench from the dimer state in the tight-binding model (5.3.1) for $\ell = 140$ and various Δq. We compare the predictions of Eqs. (5.5.15) and (5.5.16) (solid lines) with numerical data (symbols). *Bottom:* Delay time t_D for various Δq and $\ell = 280$. The solid line is the analytic prediction $t_D = \frac{\pi|\Delta q|}{4}$ and the symbols are the numerical results. They are obtained as the time for which $S_{1,2}(q)/\ell = 0.011$.

Total and number entropy

The total entropies are given by $S_n = \frac{1}{1-n} \log Z_n(0)$. With Eq. (5.5.5) we have

$$S_n = \frac{1}{1-n} \int \frac{\mathrm{d}k}{2\pi} h_{n,0}(\cos k) \min(\ell, 2v_k t) \tag{5.5.17}$$

where

$$h_{n,0}(\cos k) = \log \left[\left(\frac{1+\cos k}{2} \right)^n + \left(\frac{1-\cos k}{2} \right)^n \right] \tag{5.5.18}$$

is a specialisation of Eq. (5.3.5). The term $n_k = \frac{1+\cos k}{2}$ is the mode occupation in the steady state. The limit $n \to 1$ yields

$$S = \int \frac{\mathrm{d}k}{2\pi} (-n_k \log n_k - (1-n_k) \log(1-n_k)) \min(\ell, 2v_k t) \tag{5.5.19}$$

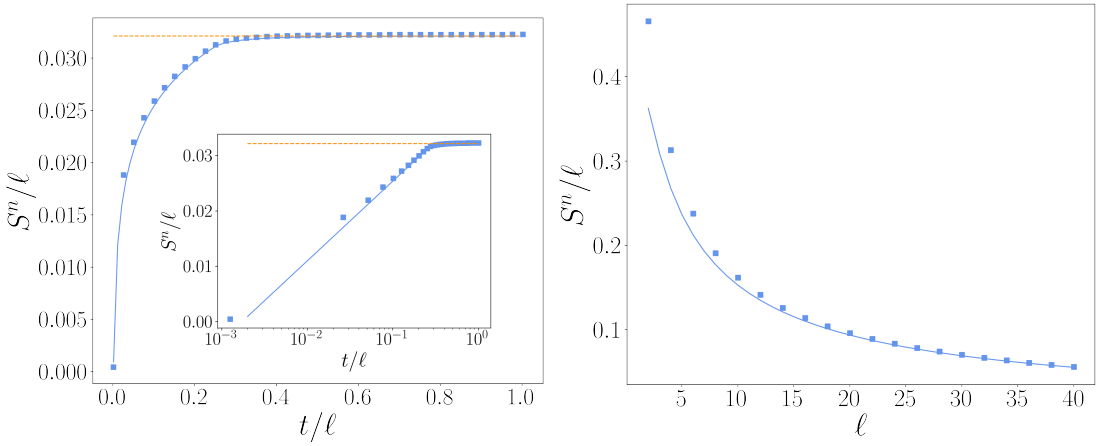


Figure 5.13: Evolution of S^n after a quench from the dimer state in the tight-binding model (5.3.1) as a function of t/ℓ for $\ell = 80$ (left panel), and as a function of ℓ with $t/\ell = 1$ (right panel). The prediction (5.5.21) (solid line) perfectly matches the numerical results (symbols). In the left panel, the horizontal dotted line is the asymptotic value $\frac{1}{2\ell}\left(1+\log\frac{\ell\pi}{4}\right)$ for large times. In the same panel, the inset shows S^n as a function of t/ℓ in a log-linear scale.

that matches the quasiparticle prediction [193, 127]. As in the case of a quench from the Néel state, we recover the total EE S from the symmetry resolved quantities using Eq. (2.2.2). To see this, we plug the Gaussian approximations (5.5.12) and (5.5.16) into Eq. (2.2.2) and find

$$S = -(\partial_n Z_n(0))|_{n=1} + \frac{(\partial_n \mathcal{J}^{(n)})|_{n=1}}{\mathcal{J}^{(1)}}\left(\frac{1}{2} - \sqrt{\frac{2}{\pi\mathcal{J}^{(1)}}}\sum_{q=0}^{\ell}\frac{2\Delta q^2}{\mathcal{J}^{(1)}}\mathrm{e}^{-\frac{2\Delta q^2}{\mathcal{J}^{(1)}}}\right) \tag{5.5.20}$$

where we also used $\sum_q \mathcal{Z}_1(q) = 1$. In the large-$\ell$ limit, the sum in the right-hand side becomes a Gaussian integral. The whole parenthesis then vanishes and we recover $S = -(\partial_n Z_n(0))|_{n=1}$, as desired.

The number entropy is given in Eq. (5.4.22) and only depends on $\mathcal{Z}_1(q)$. We use the quadratic approximation (5.5.12) and find that the calculations are exactly the same as in Sect. 5.4.1 where $\mathcal{J}$ is replaced by $\mathcal{J}^{(1)} = \int \frac{\mathrm{d}k}{2\pi}(1-\cos^2 k)\min(\ell, 2v_k t)$. We thus find

$$S^n = \frac{1}{2}\left(1+\log\frac{\mathcal{J}^{(1)}\pi}{2}\right). \tag{5.5.21}$$

In Fig. 5.13 we compare this result (solid lines) with ab-initio calculations of S^n (symbols), and find perfect agreement. The inset in the left panel shows the time-evolution of S^n in a log-linear scale. We note that $\mathcal{J}^{(1)}$ saturates to the value $\ell/2$ for large times, so that $\lim_{t\to\infty} S^n = \frac{1}{2}\left(1+\log\frac{\ell\pi}{4}\right)$. This asymptotic value is reported as a dotted horizontal line in the left panel of Fig. 5.13. Similarly to the quench from the Néel state, the number entropy grows logarithmically with time before saturation, and has negligible contribution to the total entropy in the large-time limit, $\lim_{t\to\infty} S^n/S = \mathcal{O}(\ell^{-1}\log\ell)$.

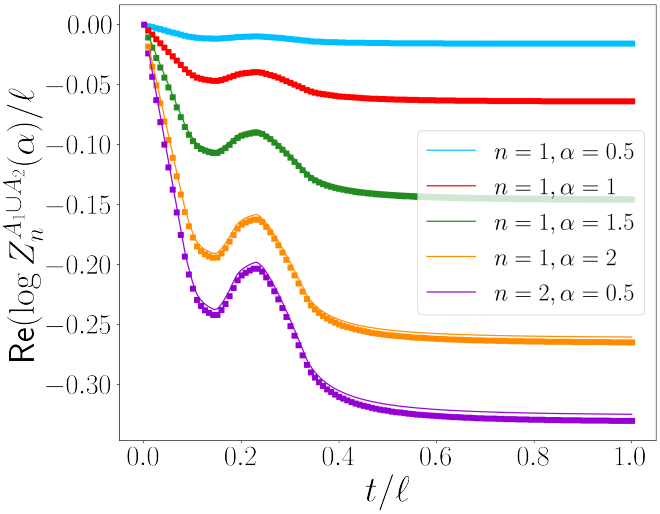


Figure 5.14: Time evolution of the charged moments $Z_n^{A_1\cup A_2}(\alpha)$ after a quench from the dimer state in the tight-binding model (5.3.1) as a function of t/ℓ with $\ell_1 = 100$, $\ell_2 = 140$ and $d = 80$. The analytical prediction of Eq. (5.5.23) (solid lines) perfectly matches the numerical data (symbols).

5.5.2 Disjoint intervals

We now turn to the case where the system A is composed of two disjoint subsystems A_1 and A_2 of lengths ℓ_1 and $\ell_2 = \ell - \ell_1$ and separated by a distance d. The correlation matrix has the form of Eqs. (5.4.27) and (5.4.28) with the entries given in Eq. (5.5.1).

Charged moments

Similarly to the calculations of Sect. 5.4.2, we compute the trace of arbitrary powers of the matrix $J_{A_1\cup A_2}(t) = 2C_{A_1\cup A_2}(t) - \mathbb{I}_\ell$. We perform the computation of $\mathrm{Tr}J_{A_1\cup A_2}(t)^m$ in the scaling limit $t, \ell, \ell_1, \ell_2, d \to \infty$ where the various ratios are kept constant. We find

$$\begin{aligned}\mathrm{Tr}J_{A_1\cup A_2}(t)^{2j} &= \ell - \int \frac{\mathrm{d}k}{2\pi}(1-[\cos k]^{2j})[\min(\ell_1, 2v_k t) + \min(\ell_2, 2v_k t)] \\ &+ \int \frac{\mathrm{d}k}{2\pi}(1-[\cos k]^{2j})[\max(d, 2v_k t) + \max(d+\ell, 2v_k t) - \max(d+\ell_1, 2v_k t) - \max(d+\ell_2, 2v_k t)], \\ \mathrm{Tr}J_{A_1\cup A_2}(t)^{2j+1} &= 0,\end{aligned} \tag{5.5.22}$$

with $v_k = 2|\sin k|$. We note that the case $d = 0$ reduces to the known result (5.5.4) for a single interval. The calculation is similar to case of a single interval as presented in Sect. 5.5.1, and we find

$$\begin{aligned}\log Z_n^{A_1\cup A_2}(\alpha) &= \mathrm{i}\ell\frac{\alpha}{2} + \int \frac{\mathrm{d}k}{2\pi}\mathrm{Re}[h_{n,\alpha}(\cos k)](\min(\ell_1, 2v_k t) + \min(\ell_2, 2v_k t)) \\ &- \int \frac{\mathrm{d}k}{2\pi}\mathrm{Re}[h_{n,\alpha}(\cos k)](\max(d, 2v_k t) + \max(d+\ell, 2v_k t) - \max(d+\ell_1, 2v_k t) - \max(d+\ell_2, 2v_k t)).\end{aligned} \tag{5.5.23}$$

We compare the prediction of Eq. (5.5.23) for $Z_n^{A_1\cup A_2}(\alpha)$ with ab-initio calculations in Fig. 5.14 and find perfect agreement.

Fourier transform and symmetry resolved Rényi entropies

In order to perform analytical calculations, we approximate $\log Z_n^{A_1\cup A_2}(\alpha)$ at quadratic order in α,

$$\log Z_n^{A_1\cup A_2}(\alpha) = \mathrm{i}\ell\frac{\alpha}{2} + \log Z_n^{A_1\cup A_2}(0) - \frac{\alpha^2}{8}\mathcal{J}_d^{(n)} \tag{5.5.24}$$

with

$$\begin{aligned}\mathcal{J}_d^{(n)} &= \int \frac{\mathrm{d}k}{2\pi} j_n(k)(\min(\ell_1, 2v_k t) + \min(\ell_2, 2v_k t)) \\ &- \int \frac{\mathrm{d}k}{2\pi} j_n(k)(\max(d, 2v_k t) + \max(d+\ell, 2v_k t) - \max(d+\ell_1, 2v_k t) - \max(d+\ell_2, 2v_k t)).\end{aligned} \tag{5.5.25}$$

where $j_n(k)$ is given in Eq. (5.5.10). As in the case of a single interval, these $\mathcal{J}_d^{(n)}$ integrals generalise $\mathcal{J}_d$ of Eq. (5.4.34). In particular, we have $\mathcal{J}_d^{(0)} = \mathcal{J}_d$. We follow Sect. 5.5.1 and find

$$\mathcal{Z}_n^{A_1\cup A_2}(q) = Z_n^{A_1\cup A_2}(0)\mathrm{e}^{-\frac{2\Delta q^2}{\mathcal{J}_d^{(n)}}}\sqrt{\frac{2}{\pi\mathcal{J}_d^{(n)}}}, \tag{5.5.26}$$

$$S_n^{A_1\cup A_2}(q) = S_n^{A_1\cup A_2} - \frac{2\Delta q^2}{(1-n)}\Big\{\frac{1}{\mathcal{J}_d^{(n)}} - \frac{n}{\mathcal{J}_d^{(1)}}\Big\} + \frac{1}{2}\log\frac{2}{\pi} - \frac{1}{2(1-n)}\log\frac{\mathcal{J}_d^{(n)}}{(\mathcal{J}_d^{(1)})^n}, \tag{5.5.27}$$

for $|\Delta q| \ll \ell$. We used that $\log Z_1^{A_1\cup A_2}(0) = 0$ and the total entropy is $S_n^{A_1\cup A_2} = \frac{1}{1-n}\log Z_n^{A_1\cup A_2}(0)$. The symmetry resolved EE is

$$S^{A_1\cup A_2}(q) = S_1^{A_1\cup A_2} - \frac{2\Delta q^2}{\mathcal{J}_d^{(1)}}\Big\{\frac{(\partial_n\mathcal{J}_d^{(n)})|_{n=1}}{\mathcal{J}_d^{(1)}} + 1\Big\} + \frac{1}{2}\log\frac{2}{\pi} + \frac{1}{2}\Big(\frac{(\partial_n\mathcal{J}_d^{(n)})|_{n=1}}{\mathcal{J}_d^{(1)}} - \log\mathcal{J}_d^{(1)}\Big). \tag{5.5.28}$$

Symmetry resolved mutual information

We now turn to the computation of the symmetry resolved MI after a quench from the dimer state. Most of the results and computations are similar to those presented in Sect. 5.4.2 in the case of a quench from the Néel state. The first step is to compute $Z_1^{A_1:A_2}(\alpha,\beta)$ and hence the trace of powers of the matrix $J_{\alpha\beta}$ defined in Eq. (5.3.16). We adapt the calculations of Sect. 5.5.2

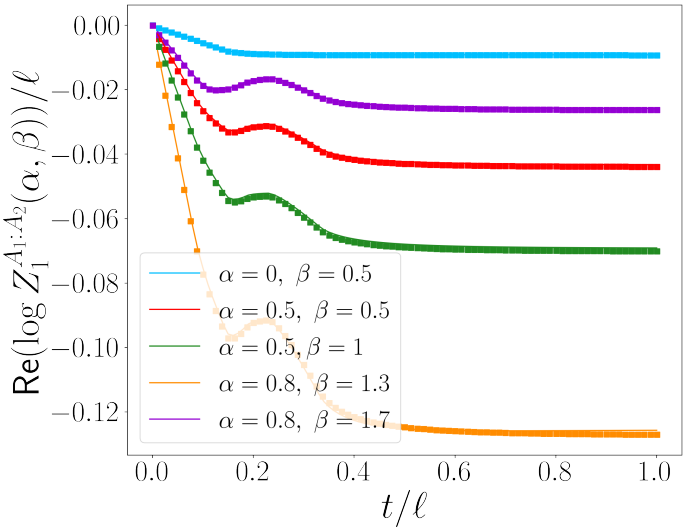


Figure 5.15: Time evolution of $Z_1^{A_1:A_2}(\alpha,\beta)$ after a quench from the dimer state in the tight-binding model (5.3.1) as a function of t/ℓ with $\ell_1 = 100$, $\ell_2 = 140$ and $d = 80$. The analytical prediction of Eq. (5.5.32) with the cut-off $\Lambda = 6$ (solid lines) perfectly matches the numerical data (symbols).

for the trace of $J_{A_1\cup A_2}$ and find

$$\begin{aligned}\mathrm{Tr}J_{\alpha\beta}(t)^{2j} &= \left(\frac{e^{i\alpha}-1}{e^{i\alpha}+1}\right)^{2j}\left[\ell_1 - \int\frac{dk}{2\pi}(1-[\cos k]^{2j})\min(\ell_1,2v_kt)\right]\\ &+\left(\frac{e^{i\beta}-1}{e^{i\beta}+1}\right)^{2j}\left[\ell_2 - \int\frac{dk}{2\pi}(1-[\cos k]^{2j})\min(\ell_2,2v_kt)\right]\\ +\int\frac{dk}{2\pi}\xi(k,j)&[\max(d,2v_kt)+\max(d+\ell,2v_kt)-\max(d+\ell_1,2v_kt)-\max(d+\ell_2,2v_kt)],\\ \mathrm{Tr}J_{\alpha\beta}(t)^{2j+1} &= 0,\end{aligned} \tag{5.5.29}$$

where

$$\xi(k,j) = \sum_{s=1}^{j}\sum_{t=0}^{2j-2s}(-1)^t\left(\frac{e^{i\alpha}-1}{e^{i\alpha}+1}\right)^{s+t}\left(\frac{e^{i\beta}-1}{e^{i\beta}+1}\right)^{2j-s-t}\gamma_{s,t,j}\cos k^{2j-2s}\sin k^{2s} \tag{5.5.30}$$

and

$$\gamma_{s,t,j} = \frac{sj}{(2j-s-t)(s+t)}\binom{2j-s-t}{s}\binom{s+t}{s}. \tag{5.5.31}$$

The re-summation in Eq. (5.3.17) yields the formal expression

$$\begin{aligned}\log Z_1^{A_1:A_2}(\alpha,\beta) &= i\frac{\ell_1\alpha+\ell_2\beta}{2} + \int\frac{dk}{2\pi}\mathrm{Re}[h_{1,\alpha}(\cos k)]\min(\ell_1,2v_kt) + \int\frac{dk}{2\pi}\mathrm{Re}[h_{1,\beta}(\cos k)]\min(\ell_2,2v_kt)\\ &+\int\frac{dk}{2\pi}\Xi(k)(\max(d,2v_kt)+\max(d+\ell,2v_kt)-\max(d+\ell_1,2v_kt)-\max(d+\ell_2,2v_kt))\end{aligned} \tag{5.5.32}$$

with the infinite sum

$$\Xi(k) = \sum_{j=1}^{\infty} \tilde{c}(2j)\xi(k,j), \quad \tilde{c}(2j) = -\frac{1}{2j}, \tag{5.5.33}$$

where we recall that the coefficients $\tilde{c}(j)$ are the Taylor coefficients of the function $\tilde{h}(x) = \log[(1+x)/2]$. To plot these charged moments, we use a cut-off Λ for the maximal value of the index j in the infinite sum and check the stability with varying the cutoff. Let us stress that the function $\gamma_{s,t,j}$ in Eq. (5.5.31) satisfies the crucial relation

$$\sum_{t=0}^{2j-2s} (-1)^t \gamma_{s,t,j} = \binom{j}{s}. \tag{5.5.34}$$

With this, it is a simple calculation to show that $Z_1^{A_1:A_2}(\alpha,\alpha)$ indeed reduces to $Z_1^{A_1\cup A_2}(\alpha)$ given in Eq. (5.5.23), as expected. We compare the prediction of Eq. (5.5.32) with ab-initio calculations in Fig. 5.15 and find perfect agreement.

Despite the cumbersome form of $Z_1^{A_1:A_2}(\alpha,\beta)$ in terms of an infinite sum, we are nonetheless able to extract the quadratic orders in α and β. We find

$$\log Z_1^{A_1:A_2}(\alpha,\beta) = \mathrm{i}\frac{\ell_1\alpha+\ell_2\beta}{2} - \frac{\alpha^2}{8}\mathcal{J}_{A_1}^{(1)} - \frac{\beta^2}{8}\mathcal{J}_{A_2}^{(1)} + \frac{\alpha\beta}{8}(\mathcal{J}_{A_1}^{(1)} + \mathcal{J}_{A_2}^{(1)} - \mathcal{J}_d^{(1)}), \tag{5.5.35}$$

and the double Fourier transform is

$$\mathcal{Z}_1^{A_1:A_2}(q_1,q-q_1) = \frac{2}{\pi\sqrt{\mathcal{J}_{A_1}^{(1)}\mathcal{J}_{A_2}^{(1)} - \frac{(\mathcal{J}_m^{(1)})^2}{4}}} \mathrm{e}^{-\frac{8}{4\mathcal{J}_{A_1}^{(1)}\mathcal{J}_{A_2}^{(1)} - (\mathcal{J}_m^{(1)})^2}\left[\Delta q_1^2\mathcal{J}_{A_2}^{(1)} + (\Delta q - \Delta q_1)^2\mathcal{J}_{A_1}^{(1)} + \Delta q_1(\Delta q - \Delta q_1)\mathcal{J}_m^{(1)}\right]} \tag{5.5.36}$$

with $\mathcal{J}_m^{(1)} = (\mathcal{J}_{A_1}^{(1)} + \mathcal{J}_{A_2}^{(1)} - \mathcal{J}_d^{(1)})$ to lighten the notations, where $\mathcal{J}_{A_{1,2}}^{(n)}$ is simply $\mathcal{J}^{(n)}$ from Eq. (5.5.9) where ℓ is replaced by $\ell_{1,2}$, and $\mathcal{J}_d^{(n)}$ is given in Eq. (5.5.25). We also have $\Delta q = q - \ell/2$ and $\Delta q_1 = q_1 - \ell_1/2$. These two results are the same as Eqs. (5.4.39) and (5.4.40) where the $\mathcal{J}_s$ integrals are systematically replaced by $\mathcal{J}_s^{(1)}$. In a similar fashion as for the quench from the Néel state, the weight $p(q_1,q-q_1) = \mathcal{Z}_1^{A_1:A_2}(q_1,q-q_1)/\mathcal{Z}_1^{A_1\cup A_2}(q)$ defined in Eq. (5.2.2) satisfies $\sum_{q_1=0}^{q} p(q_1,q-q_1) = 1$.

To compute the symmetry resolved MI, we use Eq. (5.2.1) and replace each quantity by its Gaussian approximation, namely Eqs. (5.5.12), (5.5.36), (5.5.16) and (5.5.28). The calculations are similar to those of Sect. 5.4.2. We find

$$\begin{aligned}
I_1^{A_1:A_2}(q) &= S^{A_1} + S^{A_2} - S^{A_1\cup A_2} - \frac{1}{2}\Big(\log\frac{\mathcal{J}_{A_1}^{(1)}\mathcal{J}_{A_2}^{(1)}\pi}{2\mathcal{J}_d^{(1)}}\Big) + \frac{1}{2}\Big(\frac{\partial_n(\mathcal{J}_{A_1}^{(n)})|_{n=1}}{\mathcal{J}_{A_1}^{(1)}} + \frac{\partial_n(\mathcal{J}_{A_2}^{(n)})|_{n=1}}{\mathcal{J}_{A_2}^{(1)}} - \frac{\partial_n(\mathcal{J}_d^{(n)})|_{n=1}}{\mathcal{J}_d^{(1)}}\Big) \\
&- \frac{4\mathcal{J}_{A_1}^{(1)}\mathcal{J}_{A_2}^{(1)} - (\mathcal{J}_m^{(1)})^2}{8\mathcal{J}_d^{(1)}}\Big\{\frac{1}{\mathcal{J}_{A_1}^{(1)}}\Big(\frac{\partial_n(\mathcal{J}_{A_1}^{(n)})|_{n=1}}{\mathcal{J}_{A_1}^{(1)}} + 1\Big) + \frac{1}{\mathcal{J}_{A_2}^{(1)}}\Big(\frac{\partial_n(\mathcal{J}_{A_2}^{(n)})|_{n=1}}{\mathcal{J}_{A_2}^{(1)}} + 1\Big)\Big\} \\
&- 2\Delta q^2\Big\{\Big(\frac{-\mathcal{J}_{A_1}^{(1)} + \mathcal{J}_{A_2}^{(1)} - \mathcal{J}_d^{(1)}}{2\mathcal{J}_d^{(1)}}\Big)^2\Big(\frac{\partial_n(\mathcal{J}_{A_1}^{(n)})|_{n=1}}{(\mathcal{J}_{A_1}^{(1)})^2} + \frac{1}{\mathcal{J}_{A_1}^{(1)}}\Big) + \Big(\frac{\mathcal{J}_{A_1}^{(1)} - \mathcal{J}_{A_2}^{(1)} - \mathcal{J}_d^{(1)}}{2\mathcal{J}_d^{(1)}}\Big)^2\Big(\frac{\partial_n(\mathcal{J}_{A_2}^{(n)})|_{n=1}}{(\mathcal{J}_{A_2}^{(1)})^2} + \frac{1}{\mathcal{J}_{A_2}^{(1)}}\Big)\Big\} \\
&+ 2\Delta q^2\Big(\frac{\partial_n(\mathcal{J}_d^{(n)})|_{n=1}}{(\mathcal{J}_d^{(1)})^2} + \frac{1}{\mathcal{J}_d^{(1)}}\Big).
\end{aligned} \tag{5.5.37}$$

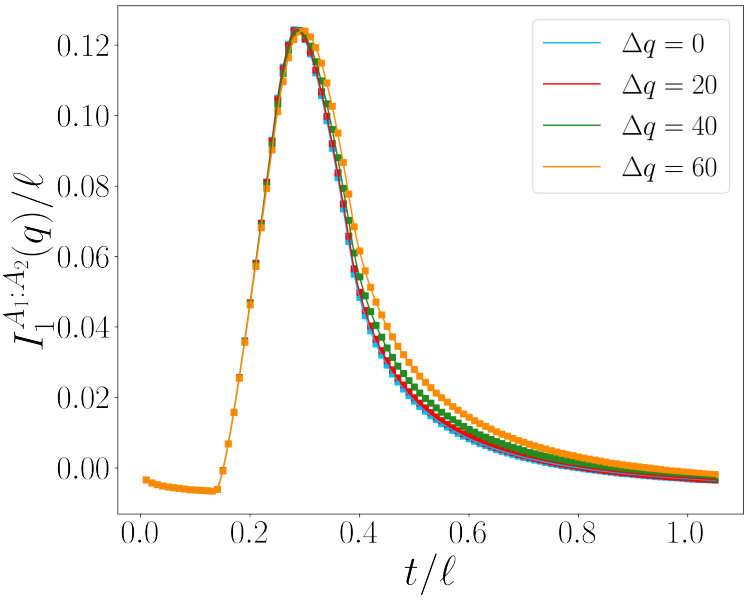


Figure 5.16: Time evolution of $I_1^{A_1:A_2}(q)$ after a quench from the dimer state in the tight-binding model (5.3.1) as a function of t/ℓ with $\ell_1 = 180$, $\ell_2 = 220$ and $d = 220$ for various values of Δq. We compare the approximation of Eq. (5.5.37) (solid lines) with the definition of Eq. (5.2.1) where the various quantities are replaced by their Gaussian approximations with the first corrections (symbols).

We compare this prediction with the definition of Eq. (5.2.1) where the various quantities are replaced by their Gaussian approximations in Fig. 5.16, and find a perfect match. The result of Eq. (5.5.37) has the same physical interpretation as Eq. (5.4.41), namely the first three terms of the right-hand side precisely yield the quasiparticle prediction for the total MI, equipartition is broken at order $\Delta q^2/\ell$ for intermediate times and at higher order for $t < d/4$ and $t \to \infty$, since $\mathcal{J}_d^{(n)} = \mathcal{J}_{A_1}^{(n)} + \mathcal{J}_{A_2}^{(n)}$ in those regimes. As for the quench from the Néel state, the combination of Eq. (5.2.5) yields the total MI, namely

$$\sum_{q=0}^{\ell} \mathcal{Z}_1^{A_1\cup A_2}(q) I_1^{A_1:A_2}(q) + S^{A_1,n} + S^{A_2,n} - S^{A_1\cup A_2,n} = I_1^{A_1:A_2} \tag{5.5.38}$$

where

$$\begin{aligned} I_1^{A_1:A_2} = -\int \frac{\mathrm{d}k}{2\pi} \partial_n h_{n,0}(\cos k)|_{n=1} (\max(d, 2v_k t) + \max(d+\ell, 2v_k t) \\ - \max(d+\ell_1, 2v_k t) - \max(d+\ell_2, 2v_k t)). \end{aligned} \tag{5.5.39}$$

5.6 Conformal field theory results

The CFT approach to global quantum quenches has been developed in Refs. [192, 190, 198]. The main idea, as discussed in Sect. 1.5.2, is that the correlation functions at time t, following a quantum quench from a low entangled state $|\psi_0\rangle$, can be mapped to the path integral in a strip in Euclidean time of width $2\tau_0$ in which the operators are inserted at τ which must be

analytically continued to $\tau \to \tau_0 + it$. The variable τ_0 is an appropriate extrapolation length which, in some sense [190], measures the distance of the initial state from an ideal conformally invariant boundary state, and hence the results are valid only for times t and separations ℓ much larger than τ_0. The total REs within this approach have been obtained [192] exploiting the fact that they are related to two-point correlators of properly defined twist fields. The very same ideas apply to the charged moments of a compact boson φ (which includes free fermions), with conserved charge $Q_A = \int_A dx \partial_x \varphi$. Indeed, the moments $Z_n(\alpha)$ are correlations of composite twist fields $\mathcal{T}_{n,\alpha}$ [35] of dimension $\Delta_{n,\alpha} = \frac{1}{12}(n - \frac{1}{n}) + \frac{K}{n}\frac{\alpha^2}{4\pi^2}$, with K related to the compactification radius. Hence, the expectation value in the strip is the same as the one for the total moments $Z_n(\alpha = 0)$ [192] with the change of the conformal dimension. Thus, after the analytic continuation, we have

$$Z_n(\alpha) = c_{n,\alpha} \left[\frac{\pi^2}{4\tau_0^2} \frac{\cosh\left(\frac{\pi\ell}{2\tau_0}\right) + \cosh\left(\frac{\pi v t}{\tau_0}\right)}{2\sinh^2\left(\frac{\pi\ell}{4\tau_0}\right)\cosh^2\left(\frac{\pi v t}{2\tau_0}\right)} \right]^{2\Delta_{n,\alpha}}, \tag{5.6.1}$$

with $c_{n,\alpha}$ a normalisation constant. For large ℓ/τ_0 and t/τ_0, this simplifies to

$$\log Z_n(\alpha) = \log Z_n(0) - \frac{K\alpha^2}{4\pi n} \frac{\min[2vt, \ell]}{\tau_0}. \tag{5.6.2}$$

This result resembles free fermions ones (5.4.7) and (5.5.5) with $\langle Q_A \rangle = 0$ and with the difference that there is a single velocity v. As a consequence of this single velocity and of the too simple dependence on α and n in Eq. (5.6.2), the symmetry resolved moments and entropies do not show the time delay t_D in Eq. (5.4.14) and the functional form in t, ℓ is different. The conclusion is that while CFT captures *universal aspects of the charged entropy*, it expectedly fails to reproduce non-universal ones for the symmetry resolved quantities such as the time delay t_D. Instead, the entanglement equipartition trivially follows from the Gaussian form of Eq. (5.6.2).

5.7 Quasiparticle picture for the charged moments

In this section we use the quasiparticle picture to get general results for the dynamics of the charged moments for the EE. On the one hand, this picture provides a physical explanation of the findings of the previous sections. On the other hand, it gives a generalisation valid for any free-fermion (or free-boson) model for arbitrary REs. It also suggests a conjecture for the charged entropies for arbitrary interacting models, but many quantitative details are still missing and its validity should eventually be tested against numerical simulations. Concerning the MI, it seems more complicated to find a quasiparticle description for the required charged moment $Z_n(\alpha, \beta)$.

5.7.1 Dynamics of the entanglement entropies

The quasiparticle description can be used to derive analytical predictions for free fermions [193]. The main idea of Ref. [193] is that the kernel $s(k)$ in Eq. (1.5.22) can be read off from the limit $t \to \infty$, where the density of EE equals the density of the thermodynamic entropy in the stationary state, leading to

$$s(k) = \frac{1}{2\pi}(-n_k \log n_k - (1 - n_k)\log(1 - n_k)) \tag{5.7.1}$$

and so

$$S = \int \frac{\mathrm{d}k}{2\pi}(-n_k \log n_k - (1-n_k)\log(1-n_k))\min(\ell, 2v_k t). \tag{5.7.2}$$

Here n_k is the probability of occupation of the mode k in the steady state. For simplicity, we recast the sum of the two integrals as the integral where the function $\min(\ell, 2v_k t)$ is included in the integrand. As anticipated, for free models, Eq. (1.5.22) also holds for the RE with the replacement [204]

$$s(k) \to s_n(k) = \frac{1}{2\pi}\frac{1}{1-n}\log[n_k^n + (1-n_k)^n]\,. \tag{5.7.3}$$

At this point, it is very natural to generalise the quasiparticle result to charged moments with the natural conjecture

$$\log Z_n(\alpha) = \mathrm{i}\alpha\langle Q_A\rangle + \int \frac{\mathrm{d}k}{2\pi}\log[n_k^n \mathrm{e}^{\mathrm{i}\alpha} + (1-n_k)^n]\min(\ell, 2v_k t). \tag{5.7.4}$$

This conjecture matches the exact results for the two quenches considered here where $n_k = 1/2$ (Néel case) and $n_k = (1+\cos k)/2$ (dimer case).

Actually, within free fermion models, the validity of the quasiparticle result (5.7.4) can be inferred from the following argument. For the RE, the quasiparticles conjecture is

$$S_n(t) = \frac{1}{1-n}\int \frac{\mathrm{d}k}{2\pi} h_{n,0}(x_k)\min(\ell, 2v_k t) = \frac{1}{1-n}\sum_{j=0}^{\infty} c_{n,0}(2j)\int \frac{\mathrm{d}k}{2\pi} x_k^{2j}\min(\ell, 2v_k t), \tag{5.7.5}$$

where x_k is related to the probability of occupation of the mode k by $n_k = (1+x_k)/2$ and $h_{n,0}(x)$ is given in Eq. (5.3.5) and has been expanded in x (as in the rightmost side of Eq. (5.3.5)). In terms of the function $s_n(k)$, it is just $h_{n,0}(2n_k - 1) = 2\pi(1-n)s_n(k)$. Similarly, the starting formula for the RE in terms of the correlation matrix can be expanded as

$$S_n(t) = \frac{1}{1-n}\sum_{i=1}^{\ell}\log\left[\left(\frac{1+\nu_i}{2}\right)^n + \left(\frac{1-\nu_i}{2}\right)^n\right] = \frac{1}{1-n}\sum_{j=0}^{\infty} c_{n,0}(2j)\mathrm{Tr}J(t)^{2j}. \tag{5.7.6}$$

Matching Eqs. (5.7.6) and (5.7.5) and properly keeping track of the normalisations (i.e. $\sum_{j=0}^{\infty} c_{n,0}(2j) = h_{n,0}(1) = 0$ and $\mathrm{Tr}J(t)^0 = \ell$), we get

$$\mathrm{Tr}J(t)^{2j} = \ell + \int \frac{\mathrm{d}k}{2\pi}(x_k^{2j} - 1)\min(\ell, 2v_k t). \tag{5.7.7}$$

Plugging Eq. (5.7.7) in Eq. (5.3.6), we obtain the desired result (5.7.4). As for the total entropies, we conjecture that in the presence of different species of quasiparticles, the result of Eq. (5.7.4) generalises to a sum over the different species.

5.7.2 Discussion about the dynamics of the mutual information

For the charged moment $\log Z_n^{A_1\cup A_2}(\alpha)$ it is straightforward to adapt the argument of the previous subsection to get

$$\log Z_n^{A_1\cup A_2}(\alpha) = \mathrm{i}\alpha\langle Q_A\rangle + \int \frac{\mathrm{d}k}{2\pi}\mathrm{Re}[h_{n,\alpha}(x_k)][\min(\ell_1, 2v_k t) + \min(\ell_2, 2v_k t)]$$
$$- \int \frac{\mathrm{d}k}{2\pi}\mathrm{Re}[h_{n,\alpha}(x_k)][\max(d, 2v_k t) + \max(d+\ell, 2v_k t) - \max(d+\ell_1, 2v_k t) - \max(d+\ell_2, 2v_k t)]. \tag{5.7.8}$$

This equation precisely matches our analytical results from Eqs. (5.4.33) with $x_k = 0$ for the quench from the Néel state, and (5.5.23) with $x_k = \cos k$ in the case of the quench from the dimer state. As in the case of a single interval, we conjecture that in the presence of different species of quasiparticles, the result of Eq. (5.7.8) generalises to a sum over the different species.

However, to determine the symmetry resolved MI we also need the moment $Z_n(\alpha, \beta)$ defined in Eq. (5.2.3). Unfortunately, this quantity has a more complicated structure (it requires the manipulation of non-commuting operators as in Eq. (5.3.15)). As already shown for the full counting statistics of the Ising model [274], the quasiparticle picture fails to capture the complex structure of this kind of objects. The complicated function Ξ (cf. Eq. (5.5.32) for the charged moment after the dimer quench) is a clear manifestation of this problem.

5.8 Concluding remarks

In this Chapter, we studied the symmetry resolved entanglement after a quantum quench in the one-dimensional tight binding model. We start from the calculation of the charged moments $Z_n(\alpha)$ (cf. Eq. (2.2.9)) that have been exactly determined by adapting the multidimensional stationary phase calculation of Ref. [257]. Our results for $Z_n(\alpha)$ are also valid when the subsystem A consists of two (or more) disjoint intervals. From the charged moments, the symmetry resolved entropy is obtained by Fourier transform and saddle point approximation in the charge flux. The structure of charged moments leads to two main physical results. First, the symmetry resolved entanglement with charge $\Delta q = q - \langle Q_A \rangle$ starts evolving only after a (calculable) delay time proportional to $|\Delta q|$. Second, for small $|\Delta q|$ there is an effective equipartition of entanglement broken at order $\Delta q^2/\ell$. We also introduced a symmetry resolved MI (5.2.1) that requires the computation of a charged moment with two independent flux insertions, see Eq. (5.2.3). We worked out exact predictions for this more complicated charged moment for two quenches in our models. We also found that the number entropy grows logarithmically with time before saturating to a value proportional to the logarithm of the subsystem size.

Our results for free fermions naturally lead to a conjecture based on the quasiparticle picture for $Z_n(\alpha)$ that can generically be written as

$$\log Z_n(\alpha) = \mathrm{i}\alpha\langle Q_A \rangle + \sum_m \int \frac{\mathrm{d}k}{2\pi} s^m_{n,\alpha}(k) \min(\ell, 2v_m(k)t) \tag{5.8.1}$$

where the sum is over the independent quasiparticles' species (where the velocities $v_m(k)$ also depend on the state [106]). To give predictive power to this conjecture we should still devise a way to fix the kernel $s^m_{n,\alpha}(k)$, but how to do this is still not know for an interacting model, as already discussed for the RE in Refs. [204, 205, 206, 207, 208]. The solution is known only in the neighbourhood of $n = 1$ where the kernel is the Yang-Yang entropy [193]. It would already be interesting to generalise this result at $n = 1$ and small $\alpha \neq 0$, that would be enough for the saddle-point approximation necessary to get the symmetry resolution. Independently of the details of the function $s^m_{n,\alpha}(k)$, the form of the conjecture (5.8.1) is sufficient to deduce the two main physical results, i.e. existence of the delay time and equipartition for small $|\Delta q|$ for a generic integrable model. Moreover, the logarithmic growth of the number entropy follows from the behaviour of $Z_1(\alpha)$ close to $\alpha = 0$ and so follows generically from Eq. (5.8.1).

Conversely, the charged moment $Z_n(\alpha, \beta)$ in Eq. (5.2.3) turned out to contain information which is not accessible by the quasiparticles picture, see Eq. (5.5.32) for a concrete example. This is not surprising, since a similar conclusion was drawn for the generating function of

the subsystem magnetisation of the Ising model after a quench in Ref. [274], an object whose microscopic structure is very similar to $Z_n(\alpha, \beta)$ (see also [281]).

We conclude this Chapter by speculating on some generalisations of our results. A first question is whether symmetry resolved entropies can be obtained in inhomogeneous settings, as done for the total entropy in Refs. [282, 283, 284, 285, 248, 286]. Then, it is natural to wonder if some of the techniques developed for non-integrable models [287, 288, 289, 290, 291, 292, 293, 294, 295, 296, 297] apply to the symmetry resolved quantities and whether our main physical findings, time delay and equipartition, are robust.

5.A Evaluation of $\mathrm{Tr} J_A(t)^{2n}$

In this Appendix, we illustrate the procedure to evaluate the even powers $\mathrm{Tr} J_A(t)^{2m}$ for the Néel quench, to obtain the result in Eq. (5.4.3). We show the procedure for the case $m = 1$ and the generalisation to higher powers. We start with the evaluation of

$$\begin{aligned}\mathrm{Tr} J_A^2(t) &= \sum_{j_1=1}^{\ell}\sum_{j_2=1}^{\ell} J_{j_1 j_2} J_{j_2 j_1} \\ &= \sum_{j_1=1}^{\ell}\sum_{j_2=1}^{\ell} (-1)^{j_1}(-1)^{j_2}\int_{-\pi}^{\pi}\frac{\mathrm{d}k_1}{2\pi}\int_{-\pi}^{\pi}\frac{\mathrm{d}k_2}{2\pi} \mathrm{e}^{4\mathrm{i}t(\cos k_1+\cos k_2)}\mathrm{e}^{\mathrm{i}k_1(j_1-j_2)}\mathrm{e}^{\mathrm{i}k_2(j_2-j_1)} \\ &= \sum_{j_1=1}^{\ell}\sum_{j_2=1}^{\ell} \int_{-\pi}^{\pi}\frac{\mathrm{d}k_1}{2\pi}\int_{-\pi}^{\pi}\frac{\mathrm{d}k_2}{2\pi} \mathrm{e}^{4\mathrm{i}t(\cos k_1+\cos k_2)}\mathrm{e}^{\mathrm{i}j_1(k_1-k_2+\pi)}\mathrm{e}^{\mathrm{i}j_2(k_2-k_1-\pi)}.\end{aligned} \tag{5.A.1}$$

The general structure for higher m is

$$\mathrm{Tr} J_A^{2m}(t) = \sum_{j_1,j_2,\cdots,j_{2m}} \int \prod_{i=1}^{2m}\frac{\mathrm{d}k_i}{2\pi} \mathrm{e}^{4\mathrm{i}t\sum_{i=1}^{2m}\cos k_i}\mathrm{e}^{\mathrm{i}j_1(k_1-k_{2m}+\pi)}\mathrm{e}^{\mathrm{i}j_2(k_2-k_1-\pi)}\ldots\mathrm{e}^{\mathrm{i}j_{2m}(k_{2m}-k_{2m-1}-\pi)}. \tag{5.A.2}$$

In order to absorb the oscillating sign, we have used exponentials of the form $\mathrm{e}^{\mathrm{i}j_a(k_a-k_{a-1}+(-1)^{a+1}\pi)}$, where we identify $k_0 \equiv k_{2m}$, to ensure that $\sum_{a=1}^{2m}(k_a - k_{a-1} + (-1)^{a+1}\pi) = 0$.

Let us go back to the case $m = 1$. We can recast the Eq. (5.A.1) as

$$\mathrm{Tr} J_A^2(t) = \int_{-\pi}^{\pi}\int_{-\pi}^{\pi}\frac{\mathrm{d}k_1}{2\pi}\frac{\mathrm{d}k_2}{2\pi}\mathrm{e}^{4\mathrm{i}t(\cos k_1+\cos k_2)}\sum_{j_1=1}^{\ell}\mathrm{e}^{\mathrm{i}j_1(k_1-k_2+\pi)}\sum_{j_2=1}^{\ell}\mathrm{e}^{\mathrm{i}j_2(k_2-k_1-\pi)}. \tag{5.A.3}$$

We can use the identity

$$\sum_{j_1}^{\ell}\mathrm{e}^{\mathrm{i}jK} = \mathrm{e}^{\mathrm{i}K\left(\frac{\ell+1}{2}\right)}\frac{\sin\left(\frac{\ell}{2}K\right)}{\sin\left(\frac{K}{2}\right)}, \tag{5.A.4}$$

so that the expression of $\mathrm{Tr} J_A^2(t)$ becomes

$$\mathrm{Tr} J_A^2(t) = \int_{-\pi}^{\pi}\int_{-\pi}^{\pi}\frac{\mathrm{d}k_1}{2\pi}\frac{\mathrm{d}k_2}{2\pi}\mathrm{e}^{4\mathrm{i}t(\cos k_1+\cos k_2)}\frac{\sin\left(\frac{\ell}{2}(k_1-k_2+\pi)\right)}{\sin\left(\frac{(k_1-k_2+\pi)}{2}\right)}\frac{\sin\left(\frac{\ell}{2}(k_2-k_1-\pi)\right)}{\sin\left(\frac{(k_2-k_1-\pi)}{2}\right)}. \tag{5.A.5}$$

The sine in the numerator can be replaced using the identity $\sin(a) = \frac{a}{2}\int_{-1}^{1} d\xi \cos(\xi a)$, so that

$$\begin{aligned}\mathrm{Tr} J_A^2(t) = \left(\frac{\ell}{2}\right)^2 \int_{-\pi}^{\pi}\int_{-\pi}^{\pi}\frac{\mathrm{d}k_1}{2\pi}\frac{\mathrm{d}k_2}{2\pi}\int_{-1}^{1}\int_{-1}^{1}\mathrm{d}\xi_1\mathrm{d}\xi_2\mathrm{e}^{4\mathrm{i}t(\cos k_1+\cos k_2)}\times \\ \times\frac{\cos\left(\frac{\ell\xi}{2}(k_1-k_2+\pi)\right)}{\mathrm{sinc}\left(\frac{(k_1-k_2+\pi)}{2}\right)}\frac{\cos\left(\frac{\ell\xi}{2}(k_2-k_1-\pi)\right)}{\mathrm{sinc}\left(\frac{(k_1-k_2+\pi)}{2}\right)}.\end{aligned} \tag{5.A.6}$$

We anticipate that, performing the saddle point approximation for this integral, we will evaluate it in the stationary points $k_{2a} = k$ and $k_{2a-1} = (k - \pi)$, in corrispondence of which we have

$\mathrm{sinc}(0) = 1$. So from now on we will omit these factors to lighten the calculations. We consider the integrals in $\mathrm{d}\xi_i$, and rewriting the cosines as exponentials and rearranging the terms we obtain the identity

$$\begin{aligned}&\int_{-1}^{1}\int_{-1}^{1}\mathrm{d}\xi_1\mathrm{d}\xi_2\cos\left(\frac{\ell\xi}{2}(k_1-k_2+\pi)\right)\cos\left(\frac{\ell\xi}{2}(k_2-k_1-\pi)\right)=\\&=\int_{-1}^{1}\int_{-1}^{1}\mathrm{d}\xi_1\mathrm{d}\xi_2\frac{1}{2}\left[\cos\left(\frac{\ell}{2}(\xi_1-\xi_2)(k_1-k_2+\pi)\right)+\cos\left(\frac{\ell}{2}(\xi_1+\xi_2)(k_2-k_1-\pi)\right)\right].\end{aligned} \tag{5.A.7}$$

Due to the symmetry of the integration domain, the two terms in the rhs contribute to the integral with the same amount, so we obtain the identity

$$\begin{aligned}\int_{-1}^{1}\mathrm{d}\xi_1\mathrm{d}\xi_2\cos\left(\frac{\ell\xi}{2}(k_1-k_2+\pi)\right)\cos\left(\frac{\ell\xi}{2}(k_2-k_1-\pi)\right)=\\\int_{-1}^{1}\mathrm{d}\xi_1\mathrm{d}\xi_2\cos\left(\frac{\ell}{2}(\xi_1-\xi_2)(k_1-k_2+\pi)\right).\end{aligned} \tag{5.A.8}$$

With the change of integration $\zeta_0 = \xi_1$ and $\zeta_1 = \xi_2 - \xi_1$ the integral becomes

$$\int_{-1}^{1}\mathrm{d}\zeta_0\int_{-1-\zeta_0}^{1-\zeta_0}\mathrm{d}\zeta_1\cos\left[\frac{\ell}{2}\zeta_1(k_1-k_2)+\frac{\ell\pi}{2}\zeta_1\right] \tag{5.A.9}$$

We observe that the function in the integral depends only on ζ_1, so we invert the order of integration as follow

$$\begin{aligned}\int_{-1}^{1}\mathrm{d}\zeta_0\int_{-1-\zeta_0}^{1-\zeta_0}\mathrm{d}\zeta_1 f(\zeta_1)&=\int_{-2}^{0}\mathrm{d}\zeta_1\int_{-1-\zeta_1}^{1}\mathrm{d}\zeta_0 f(\zeta_1)+\int_{0}^{2}\mathrm{d}\zeta_1\int_{-1}^{1-\zeta_1}\mathrm{d}\zeta_0 f(\zeta_1)\\&=\int_{-2}^{0}\mathrm{d}\zeta_1 f(\zeta_1)(2+\zeta_1)+\int_{0}^{2}\mathrm{d}\zeta_1 f(\zeta_1)(2-\zeta_1),\end{aligned} \tag{5.A.10}$$

where the domain of the first integral is represented by the triangle in the lower half (ζ_0, ζ_1) plane of Fig. 5.17, and that of the second integral by the triangle in the upper half plane. We can rewrite the two terms in a more compact form, observing that in both cases the term in the parenthesis is positive. Moreover, for $-2 < \zeta < 0$ we want to recover the first integral, and analogously for the second. So we can easily verify that all these conditions are met by rewriting the sum of the two integrals as

$$\int_{\mathbb{R}} f(\zeta_1)\Omega(\zeta_1), \tag{5.A.11}$$

where

$$\Omega(\zeta_1) = \max\left[0, \min(1, 1+\zeta_1) + \min(1, 1-\zeta_1)\right]. \tag{5.A.12}$$

So we obtain that

$$\mathrm{Tr}J_A^2(t) = \left(\frac{\ell}{2}\right)^2\int_{-\pi}^{\pi}\int_{-\pi}^{\pi}\frac{\mathrm{d}k_1}{2\pi}\frac{\mathrm{d}k_2}{2\pi}\mathrm{d}\zeta_1 e^{4it(\cos k_1+\cos k_2)}\cos\left(\frac{\ell}{2}\zeta_1(k_1-k_2)+\frac{\ell\pi}{2}\zeta_1\right)\Omega(\zeta_1). \tag{5.A.13}$$

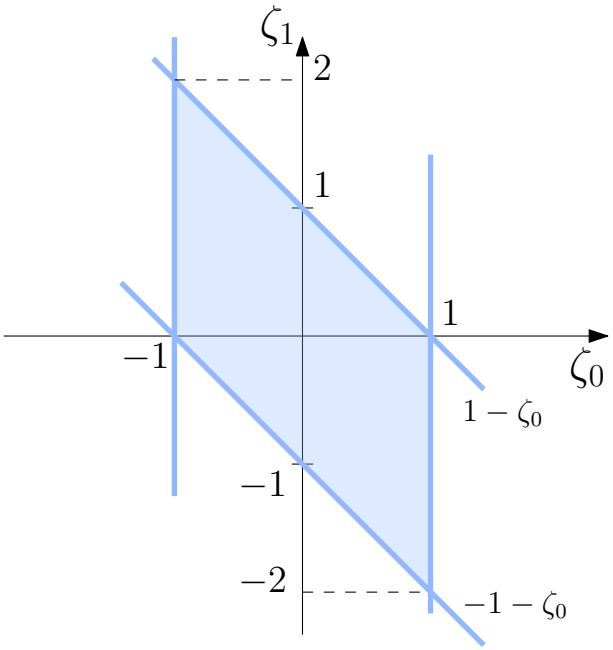


Figure 5.17: Domain of integration in the plane (ζ_0, ζ_1)

For the generic case $m > 1$, we can do an analogous treatment. The expression for the rhs of Eq.(5.A.8) becomes

$$\int_{-1}^{1} \cdots \int_{-1}^{1} \mathrm{d}\xi_1 \cdots \mathrm{d}\xi_{2m} \cos\left[\frac{\ell}{2}\sum_{j=1}^{2m}(\xi_{j+1}-\xi_j)(k_j-k_{2m}) + \frac{\ell\pi}{2}\sum_{j=1}^{2m}(-1)^j\xi_j\right], \tag{5.A.14}$$

and the change of variable

$$\zeta_0 = \xi_1, \qquad \zeta_j = \xi_{j+1}-\xi_j, \qquad j = 1, \cdots, 2m-1, \tag{5.A.15}$$

gives

$$\int_{-1}^{1} \cdots \int_{-1}^{1} \mathrm{d}\zeta_0 \cdots \mathrm{d}\xi_{2m-1} \cos\left[\frac{\ell}{2}\sum_{j=1}^{2m}\zeta_j(k_j-k) + \frac{\ell\pi}{2}\sum_{j=1}^{m}\zeta_{2j-1}\right], \tag{5.A.16}$$

where we set $k \equiv k_{2m}$. The change of order of integration can be generalised as

$$\int_{-1}^{1} \mathrm{d}\zeta_0 \cdots \int_{-1-(\zeta_0+\cdots+\zeta_{2m-2})}^{1-(\zeta_0+\cdots+\zeta_{2m-2})} \mathrm{d}\zeta_{2m-1} f(\zeta_1, \cdots, \zeta_{2m-1}) = \int_{\mathbb{R}^{2m-1}} \mathrm{d}^{2m-1}\vec{\zeta}\,\Omega(\vec{\zeta})f(\vec{\zeta}), \tag{5.A.17}$$

with $\vec{\zeta} = (\zeta_1, \cdots, \zeta_{2m-1})$ and

$$\Omega(\zeta_1, \cdots, \zeta_{2m-1}) = \max\left[0, \min_{j=1,\cdots,2m-1}\left(1, 1-\sum_{i=1}^{j}\zeta_i\right) + \min_{j=1,\cdots,2m-1}\left(1, 1+\sum_{i=1}^{j}\zeta_i\right)\right]. \tag{5.A.18}$$

We can now introduce the stationary phase approximation for the evaluation of the integrals. This method is used to compute integrals of the form

$$I(\ell) = \int_{\mathbb{R}} \mathrm{d}x g(x) \mathrm{e}^{\mathrm{i}\ell f(x)}, \tag{5.A.19}$$

when the parameter $\ell \to \infty$. Under certain conditions, that are met in our case, the result is

$$\lim_{\ell\to\infty} I(\ell) = g(x_0)\mathrm{e}^{\mathrm{i}\ell f(x_0)} \left(\frac{2\pi}{\ell}\right)^{\frac{a}{2}} |\det \mathrm{Hess}(f)|^{-\frac{1}{2}} + o(\ell^{-\frac{m}{2}}) \tag{5.A.20}$$

where x_0 is such that $\nabla f(x_0) = 0$.

We start from the case $m = 1$, so we rewrite the integral in Eq.(5.A.13) as

$$\mathrm{Tr}J_A^2(t) = \left(\frac{\ell}{2}\right)^2 \int_{-\pi}^{\pi} \frac{\mathrm{d}k}{(2\pi)^2} \left[\mathrm{d}k_1 \mathrm{d}\zeta_1 \mathrm{e}^{\mathrm{i}4t(\cos k + \cos k_1)} \cos\left(\frac{\ell}{2}\zeta_1(k_1 - k) + \frac{\ell\pi}{2}\zeta_1\right) \Omega(\zeta_1)\right]. \tag{5.A.21}$$

We can apply the stationary phase method to the term in the square parenthesis. We have in our case

$$\begin{aligned} f(k_1, \zeta_1) &= \frac{4t}{\ell}\cos k_1 + \frac{4t}{\ell}\cos k + \epsilon\left(\frac{1}{2}\zeta_1(k_1 - k) + \frac{\pi}{2}\zeta_1\right), \\ g(\zeta_1) &= \Omega(\zeta_1), \end{aligned} \tag{5.A.22}$$

and the dimension of the integral is $a = 2$. The stationary point is

$$k_1 = k - \pi, \qquad \zeta_1 = -\epsilon\frac{8t}{\ell}\sin k. \tag{5.A.23}$$

The determinant of the Hessian of f is 2^{-2}. We observe that the function f evaluated in correspondence of the stationary point gives 0, while

$$g(k_1, \zeta_1) = \Omega(\zeta_1) = \max\left[0, \min\left(1, 1 + \frac{8t}{\ell}\sin k\right) + \min\left(1, 1 - \frac{8t}{\ell}\sin k\right)\right]. \tag{5.A.24}$$

According to the argument of the min function, we can have the two cases

$$4t|\sin k| > \ell \quad \Rightarrow \quad \Omega(\zeta_1) = \max[0, 2 - \frac{8t}{\ell}|\sin k|] = 0, \tag{5.A.25}$$

$$4t|\sin k| < \ell \quad \Rightarrow \quad \Omega(\zeta_1) = \max[0, 1 + 1 - \frac{8t}{\ell}|\sin k|] = 2 - \frac{8t}{\ell}|\sin k|. \tag{5.A.26}$$

So we have

$$\begin{aligned} \lim_{\ell\to\infty} \mathrm{Tr}J^2(t) &= \left(\frac{\ell}{2}\right)^2 \frac{1}{2\pi} \int_{4t|\sin k|<\ell} \frac{\mathrm{d}k}{2\pi}\left(2 - \frac{8t}{\ell}|\sin k|\right) \frac{2\pi}{\ell}(2^{-2})^{-\frac{1}{2}} \\ &= \int_{4t|\sin k|<\ell} \frac{\mathrm{d}k}{2\pi}\left(\ell - 4t|\sin k|\right). \end{aligned} \tag{5.A.27}$$

In the case $m > 1$, the generalization is straightforward. The dimension of the integral becomes $a = 4m - 2$, and the stationary point is

$$\begin{aligned} k_{2j-1} &= k - \pi, & k_{2j} &= k, \\ \zeta_{2j-1} &= -\epsilon\frac{8t}{\ell}\sin k, & \zeta_{2j} &= \epsilon\frac{8t}{\ell}\sin k. \end{aligned} \tag{5.A.28}$$

The determinant of the Hessian is 2^{2-4m}. The function f evaluated at the stationary point vanishes, while the function g gives

$$\Omega(\zeta_1, \cdots, \zeta_{2m-1}) = \begin{cases} 2 - \frac{8t}{\ell}|\sin k| & \text{if} \quad 4t|\sin k| < \ell \\ 0 & \text{if} \quad 4t|\sin k| > \ell \end{cases} \tag{5.A.29}$$

So we get

$$\lim_{\ell\to\infty} \mathrm{Tr} J^{2m}(t) = \left(\frac{\ell}{2}\right)^{2m} \frac{1}{(2\pi)^{2m-1}} \int_{4t|\sin k|<\ell} \frac{\mathrm{d}k}{2\pi} \left(2 - \frac{8t}{\ell}|\sin k|\right) \left(\frac{2\pi}{\ell}\right)^{2m-1} (2^{-2-4m})^{-\frac{1}{2}}$$
$$= \int_{4t|\sin k|<\ell} \frac{\mathrm{d}k}{2\pi} \left(\ell - 4t|\sin k|\right). \tag{5.A.30}$$

So we obtain that the result is independent on the value of m. We can recast the expression of $\mathrm{Tr} J^{2m}(t)$ as

$$\lim_{\ell\to\infty} \mathrm{Tr} J^{2m}(t) = \ell \int_{4t|\sin k|>\ell} \frac{\mathrm{d}k}{2\pi} - \ell \int_{4t|\sin k|>\ell} \frac{\mathrm{d}k}{2\pi} + \int_{4t|\sin k|<\ell} \frac{\mathrm{d}k}{2\pi} (\ell - 4t|\sin k|) =$$
$$= \ell \left(\int_{4t|\sin k|>\ell} \frac{\mathrm{d}k}{2\pi} + \int_{4t|\sin k|<\ell} \frac{\mathrm{d}k}{2\pi} \right) - \left(\ell \int_{4t|\sin k|>\ell} + \int_{4t|\sin k|<\ell} 4t|\sin k| \right) =$$
$$= \ell - \left[\ell \int_{4t|\sin k|>\ell} \frac{\mathrm{d}k}{2\pi} + \int_{4t|\sin k|<\ell} \frac{\mathrm{d}k}{2\pi} 4t|\sin k| \right] \tag{5.A.31}$$

We can rewrite the condition in the square parenthesis observing that, according to which one is smaller between ℓ and $4t|\sin k|$, we have that the integrand contains one of the two. So we can summarize this observation as

$$\lim_{\ell\to\infty} \mathrm{Tr} J^{2m}(t) = \ell - \int \frac{\mathrm{d}k}{2\pi} \min(\ell, 4t|\sin k|), \tag{5.A.32}$$

and find the expression of the even powers of $\mathrm{Tr} J_A(t)$ given in Eq. (5.4.3).

Appendix A

Conformal Field Theory

A.1 The conformal group

Let us consider the d-dimensional space $\mathbb{R}^d$ with flat metric $g_{\mu\nu} = \eta_{\mu\nu} = \text{diag}(-1, \cdots, 1, \cdots)$ of signature (p, q), with $p + q = d$, and let $\text{d}s^2 = g_{\mu\nu}\text{d}x^\mu \text{d}x^\nu$ be the line element [144, 298]. A differentiable map φ is a *conformal transformation* if it leaves the metric invariant up to a scale change

$$\varphi \quad : \quad g_{\mu\nu}(x) \to g'_{\mu\nu}(x') = \Lambda(x) g_{\mu\nu}(x), \tag{A.1.1}$$

where the function $\Lambda(x)$ is called *scale factor*. Under coordinate transformation $x \to x'$, the corresponding transformation of the metric tensor is $g_{\mu\nu}(x) \to g'_{\mu\nu}(x') = \frac{\partial x'^\alpha}{\partial x^\mu} \frac{\partial x'^\beta}{\partial x^\nu} g_{\alpha\beta}(x)$, so for a flat space the condition for a conformal transformation is

$$\eta_{\alpha\beta} \frac{\partial x'^\alpha}{\partial x^\mu} \frac{\partial x'^\beta}{\partial x^\nu} = \Lambda(x) \eta_{\mu\nu}. \tag{A.1.2}$$

For $\Lambda(x) = 1$, the condition above identifies the Poincaré group, that consists of translations and Lorentz rotations. For $\Lambda(x) = \textit{constant}$, it corresponds to global global scale transformations. Given two vectors v and w, such transformations preserve the angle $v \cdot w / (v^2 w^2)^{1/2}$ between them, with $v \cdot w = g_{\mu\nu} v^\mu w^\nu$.

A.1.1 Conditions for conformal invariance

Let us consider an infinitesimal transformation

$$x^\mu \to x^\mu + \epsilon^\mu + \mathcal{O}(\epsilon^2). \tag{A.1.3}$$

Correspondingly, the left-hand side of Eq. (A.1.2) becomes

$$\begin{aligned} \eta_{\alpha\beta} \frac{\partial x'^\alpha}{\partial x^\mu} \frac{\partial x'^\beta}{\partial x^\nu} &= \eta_{\alpha\beta} \left(\delta^\alpha_\mu + \frac{\partial \epsilon^\alpha}{\partial x^\mu} + \mathcal{O}(\epsilon^2) \right) \left(\delta^\beta_\nu + \frac{\partial \epsilon^\beta}{\partial x^\nu} + \mathcal{O}(\epsilon^2) \right) \\ &= \eta_{\mu\nu} + \eta_{\mu\beta} \frac{\partial \epsilon^\beta}{\partial x^\nu} + \eta_{\alpha\nu} \frac{\partial \epsilon^\alpha}{\partial x^\mu} + \mathcal{O}(\epsilon^2) \\ &= \eta_{\mu\nu} \left(\frac{\partial \epsilon_\mu}{\partial x^\nu} + \frac{\partial \epsilon_\nu}{\partial x^\mu} \right) + \mathcal{O}(\epsilon^2). \end{aligned}$$

Introducing the notation $\partial/\partial x^\mu = \partial_\mu$, one obtains the following requirement

$$\partial_\mu \epsilon_\nu + \partial_\nu \epsilon_\mu = f(x)\eta_{\mu\nu}, \tag{A.1.4}$$

where the function $f(x)$ can be determined by taking the trace of both sides of the equation above

$$\begin{aligned} \eta^{\mu\nu}\left(\partial_\mu \epsilon_\nu + \partial_\nu \epsilon_\mu\right) &= f(x)\eta^{\mu\nu}\eta_{\mu\nu} \\ 2\partial^\mu \epsilon_\mu &= f(x)d \\ \Rightarrow \quad f(x) &= \frac{2}{d}\partial^\mu \epsilon_\mu. \end{aligned}$$

So the coordinate transformation is conformal if it verifies

$$\partial_\mu \epsilon_\nu + \partial_\nu \epsilon_\mu = \frac{2}{d}(\partial \cdot \epsilon)\eta_{\mu\nu}. \tag{A.1.5}$$

Comparing with Eq. (A.1.2), it follows that $\Lambda(x) = 1 + \frac{2}{d}(\partial \cdot \epsilon)$.

From the condition in Eq. (A.1.5), it is also possible to derive other important relations. Let us start taking the derivative with respect to ∂^ν and summing over ν

$$\begin{aligned} \partial^\nu\left(\partial_\mu \epsilon_\nu + \partial_\nu \epsilon_\mu\right) &= \frac{2}{d}\partial^\nu(\partial \cdot \epsilon)\eta_{\mu\nu} \\ \partial_\mu(\partial \cdot \epsilon) + \Box \epsilon_\mu &= \partial_\mu(\partial \cdot \epsilon), \end{aligned}$$

where $\Box = \partial^\mu \partial_\mu$. Taking the derivative ∂_ν of the equation above, one gets

$$\partial_\mu \partial_\nu(\partial \cdot \epsilon) + \Box \partial_\nu \epsilon_\mu = \frac{2}{d}\partial_\mu \partial_\nu(\partial \cdot \epsilon).$$

Interchanging $\mu \leftrightarrow \nu$ in the previous expression and taking the sum of the two,

$$\begin{aligned} 2\partial_\mu \partial_\nu(\partial \cdot \epsilon) + \Box\left(\partial_\mu \epsilon_\nu + \partial_\nu \epsilon_\mu\right) &= \frac{4}{d}\partial_\mu \partial_\nu(\partial \cdot \epsilon) \\ 2\partial_\mu \partial_\nu(\partial \cdot \epsilon) + \Box\left(\frac{2}{d}(\partial \cdot \epsilon)\eta_{\mu\nu}\right) &= \frac{4}{d}\partial_\mu \partial_\nu(\partial \cdot \epsilon) \\ \left(\eta_{\mu\nu}\Box + (d-2)\partial_\mu \partial_\nu\right)(\partial \cdot \epsilon) &= 0 \end{aligned}$$

where Eq. (A.1.5) has been used in the first passage. By contracting with $\eta^{\mu\nu}$ one finally gets

$$(d\Box + (d-2)\partial^\nu \partial_\nu)(\partial \cdot \epsilon) = 0$$

$$(d-1)\Box(\partial \cdot \epsilon) = 0. \tag{A.1.6}$$

Another useful expression can be obtained by taking derivatives ∂_ρ of Eq. (A.1.5) and permuting cyclically the indices

$$\begin{aligned} \partial_\rho \partial_\mu \epsilon_\nu + \partial_\rho \partial_\nu \epsilon_\mu &= \frac{2}{d}\eta_{\mu\nu}\partial_\rho(\partial \cdot \epsilon) \\ \partial_\nu \partial_\rho \epsilon_\mu + \partial_\mu \partial_\rho \epsilon_\nu &= \frac{2}{d}\eta_{\rho\mu}\partial_\nu(\partial \cdot \epsilon) \\ \partial_\mu \partial_\nu \epsilon_\rho + \partial_\nu \partial_\mu \epsilon_\rho &= \frac{2}{d}\eta_{\nu\rho}\partial_\mu(\partial \cdot \epsilon) \end{aligned}$$

Subtracting the first line from the sum of the last two one obtains the relation

$$2\partial_\mu \partial_\nu \epsilon_\rho = \frac{2}{d}(-\eta_{\mu\nu}\partial_\rho + \eta_{\rho\mu}\partial_\nu + \eta_{\nu\rho}\partial_\mu)(\partial \cdot \epsilon). \tag{A.1.7}$$

A.1.2 Conformal group in $d \geq 3$

Let us now determine the conformal group for dimensions $d \geq 3$. From Eq. (A.1.6), one can observe that the term $(\partial \cdot \epsilon)$ is at most linear in x^μ, that is, it can be written as $(\partial \cdot \epsilon) = A + B_\mu x^\mu$. This means that ϵ_μ is at most quadratic in the coordinates, and so it can be written as

$$\epsilon_\mu = a_\mu + b_{\mu\nu} x^\nu + c_{\mu\nu\rho} x^\nu x^\rho, \tag{A.1.8}$$

where $a_\mu, b_{\mu\nu}, c_{\mu\nu\rho}$ are constants and $c_{\mu\nu\rho} = c_{\mu\rho\nu}$. Since the constraints for conformal invariance are independent from the position, each term in the equation above can be treated separately.

- The constant term a_μ has no constraints, and it represents an infinitesimal translation $x'^\mu = x^\mu + a^\mu$. The generator of such infinitesimal transformation is the momemtum operator $P_\mu = -\mathrm{i}\partial_\mu$.

- The linear term can be determined by inserting Eq. (A.1.8) into Eq. (A.1.5),

$$b_{\nu\mu} + b_{\mu\nu} = \frac{2}{d}(\eta^{\rho\sigma} b_{\sigma\rho})\eta_{\mu\nu} \tag{A.1.9}$$

  This implies that $b_{\mu\nu}$ can be split into the sum of a symmetric and an antisymmetric part

$$b_{\mu\nu} = \alpha\eta_{\mu\nu} + m_{\mu\nu} \tag{A.1.10}$$

  with $m_{\mu\nu} = -m_{\nu\mu}$. The symmetric term $\alpha\eta_{\mu\nu}$ is an infinitesimal scale trasformation $x'^\mu = (1+\alpha)x^\mu$. The corresponding generator is $D = -\mathrm{i}x^\mu\partial_\mu$. The antisymmetric term is an infinitesimal rotation $x'^\mu = (\delta^\mu_\nu + m^\mu_\nu)x^\nu$, whose generator is the angular momentum operator $L_{\mu\nu} = \mathrm{i}(x_\mu\partial_\nu - x_\nu\partial_\mu)$.

- The quadratic term can be studied by inserting Eq. (A.1.8) into Eq. (A.1.7), obtaining

$$c_{\mu\nu\rho} = \eta_{\mu\rho} b_\nu + \eta_{\mu\nu} b_\rho - \eta_{\nu\rho} b_\mu, \qquad \text{with} \quad b_\mu \equiv \frac{1}{d} c^\sigma_{\sigma\mu} \tag{A.1.11}$$

  The corresponding infinitesimal transformation is the so called *special confrormal transformation* (SCT) $x'^\mu = x^\mu + 2(x \cdot b)x^\mu - b^\mu x^2$.

The corresponding finite transformations are

$$\begin{array}{ll} x'^\mu = x^\mu + a^\mu & \textit{translation} \\ x'^\mu = \alpha x^\mu & \textit{dilation} \\ x'^\mu = M^\mu_\nu x^\nu & \textit{rotation} \\ x'^\mu = \frac{x^\mu - b^\mu x^2}{1 - 2b\cdot x + b^2 x^2} & \textit{SCT} \end{array} \tag{A.1.12}$$

Let us now determine the conformal group for dimension $d \geq 3$. The generators of the group are found to be

$$\begin{array}{ll} P_\mu = -\mathrm{i}\partial_\mu & \textit{translation} \\ D = -\mathrm{i}x^\mu\partial_\mu & \textit{dilation} \\ L_{\mu\nu} = \mathrm{i}(x_\mu\partial_\nu - x_\nu\partial_\mu) & \textit{rotation} \\ K_\mu = \mathrm{i}(2x_\mu x^\nu\partial_\nu - \mathbf{x}^2\partial_\mu) & \textit{SCT} \end{array} \tag{A.1.13}$$

In order to identify the conformal group, let us consider the conformal algebra, which is the Lie algebra associated to the group. The dimension of the algebra is determined by the number of generators, which are respectively

$$d \quad \text{translations} + 1 \quad \text{dilations} + d \quad \text{special conformal} + \frac{d(d-1)}{2} \quad \text{rotations}$$

$$\Rightarrow \frac{(d+2)(d+1)}{2} \quad \text{generators.}$$

They can be recast to obtain a new set of generators

$$\begin{aligned} J_{\mu\nu} &= L_{\mu\nu} & J_{-1,\mu} &= \frac{1}{2}(P_\mu - K_\mu) \\ J_{-1,0} &= D & J_{0,\mu} &= \frac{1}{2}(P_\mu + K_\mu) \end{aligned} \tag{A.1.14}$$

with $J_{ab} = -J_{ba}$ and $a, b \in \{-1, 0, 1, \cdots, d\}$, which satisfy the $SO(d+1,1)$ commutation relations

$$[J_{ab}, J_{cd}] = \mathrm{i}(\eta_{ad}J_{bc} + \eta_{bc}J_{ad} - \eta_{ac}J_{bd} - \eta_{bd}J_{ac}). \tag{A.1.15}$$

For the Euclidean space $\mathbb{R}^{d,0}$, the diagonal metric is $\eta_{ab} = \mathrm{diag}(-1, 1, \cdots, 1)$, and the commutation relations above identify the algebra $so(d+1,1)$. For the Minkowski space $\mathbb{R}^{d-1,1}$, the metric is $\eta_{ab} = \mathrm{diag}(-1, -1, 1, \cdots, 1)$ and the corresponding algebra is $so(d,2)$. In general, for the case of dimension $d = p + q \geq 3$, the condformal group of $\mathbb{R}^{p,q}$ is $SO(p+1, q+1)$.

A.1.3 Constraints of conformal invariance in d dimensions

Let us now study the consequences of conformal invariance on correlation functions, which are the objects of main interest in quantum field theory. To this purpose, it is convenient to express the conformal transformations in terms of the jacobian, that is related to the scale factor Λ of Eq. (A.1.2) by the relation

$$\left|\frac{\partial x}{\partial x'}\right| = \frac{1}{\sqrt{\det g'_{\mu\nu}}} = \Lambda^{-d/2}. \tag{A.1.16}$$

The next step is to define the proper requirements in order to have a conformal invariant theory. Let us consider a set of fields $\{\Phi_i\}$, which can be in general infinite, containing also the derivatives of the fields Φ_i. One of the requirements for conformal invariance is the existence of a subset $\{\phi\} \subset \{\Phi\}$, called *quasi-primary fields*, that under global conformal transformation $x \mapsto x'$ transform as

$$\phi_j(x) \to \left|\frac{\partial x'}{\partial x}\right|^{\frac{d_j}{d}} \phi_j(x'), \tag{A.1.17}$$

where d_j is the so called *scaling dimension* of ϕ_j. Then, the theory is covariant under such transformation, i.e., the correlation functions satisfy

$$\langle \phi_1(x_1), \cdots, \phi_n(x_n)\rangle = \left|\frac{\partial x'}{\partial x}\right|^{\frac{d_1}{d}}_{x=x_1} \cdots \left|\frac{\partial x'}{\partial x}\right|^{\frac{d_n}{d}}_{x=x_n} \langle \phi_1(x'_1), \cdots, \phi_n(x'_n)\rangle\,. \tag{A.1.18}$$

The remaining fields $\{\Phi_i\}$ can be expressed as linear combinations of the quasi-primary fields and their derivatives. The last requirement is the existence of a vacuum state $|0\rangle$, invariant under the global conformal group.

Let us now study the consequences of the covariance property in Eq. (A.1.18) on the 2 and 3-point correlation functions. For 2-point functions, invariance under translations and rotations implies that the left hand side of Eq. (A.1.18) depends only on the distance $r_{12} \equiv |x_1 - x_2|$ between the points,

$$\langle \phi_1(x_1)\phi_2(x_2)\rangle = f(|x_1 - x_2|). \tag{A.1.19}$$

Moreover, invariance under dilations $x \to \lambda x$ implies

$$\langle \phi_1(x_1)\phi_2(x_2)\rangle = \lambda^{d_1+d_2} \langle \phi_1(\lambda x_1)\phi_2(\lambda x_2)\rangle . \tag{A.1.20}$$

Comparing the two relations, one obtains that the function f is such that $f(x) = \lambda^{d_1+d_2} f(\lambda x)$. Then the symmetries of CFT imply the two-point function to be of the form

$$\langle \phi_1(x_1)\phi_2(x_2)\rangle = \frac{C_{12}}{|x_1 - x_2|^{d_1+d_2}}, \tag{A.1.21}$$

with C_{12} normalization constant depending on the fields. Let us now study the consequences of invariance under SCT. For these transformations, the jacobian is

$$\left|\frac{\partial x'}{\partial x}\right| = \frac{1}{(1 - 2b\cdot x + b^2x^2)^d},$$

and the distance between the points transforms as

$$|x'_i - x'_j| = \frac{|x_i - x_j|}{(1 - 2b\cdot x_i + b^2x_i^2)^{1/2}(1 - 2b\cdot x_j + b^2x_j^2)^{1/2}}.$$

The substitution of the last two relations in Eq. (A.1.18) gives the following condition

$$\frac{C_{12}}{|x_1 - x_2|^{d_1+d_2}} = \frac{C_{12}(\gamma_1\gamma_2)^{(d_1+d_2)/2}}{\gamma_1^{d_1}\gamma_2^{d_2}|x_1 - x_2|^{d_1+d_2}},$$

with $\gamma_i \equiv (1 - 2b\cdot x_i + b^2x_i^2)$. It is immediate to see that this condition is satisfied only if $d_1 = d_2$. So for 2-point functions, one has

$$\langle \phi_1(x_1)\phi_2(x_2)\rangle = \begin{cases} \frac{C_{12}}{|x_1-x_2|^{d_1+d_2}}, & \text{if } d_1 = d_2, \\ 0, & \text{if } d_1 \neq d_2. \end{cases} \tag{A.1.22}$$

An analogous reasoning leads to the following form of the three point functions

$$\langle \phi_1(x_1)\phi_2(x_2)\phi_3(x_3)\rangle = \frac{C_{123}}{x_{12}^{d_1+d_2-d_3}x_{23}^{d_2+d_3-d_1}x_{13}^{d_1+d_3-d_2}}. \tag{A.1.23}$$

A.1.4 Conformal group in $d = 2$

Let us now focus on the case of $d = 2$ dimensions. The coordinates on the plane will be denoted as (z^0, z^1). The condition for conformal invariance given by Eq. (A.1.5) implies

$$\partial_0\epsilon_0 = +\partial_1\epsilon_1, \qquad \partial_0\epsilon_1 = -\partial_1\epsilon_0, \tag{A.1.24}$$

which are the Cauchy-Riemann equations. A complex function having real and imaginary parts which satisfy Eq. (A.1.24) is an holomorphic function. This suggests the introduction of the complex variables

$$\begin{aligned} z &= x^0 + \mathrm{i}x^1, & \epsilon &= \epsilon^0 + \mathrm{i}\epsilon^1, & \partial_z &= \frac{1}{2}(\partial_0 - \mathrm{i}\partial_1), \\ \bar{z} &= x^0 - \mathrm{i}x^1, & \bar{\epsilon} &= \epsilon^0 - \mathrm{i}\epsilon^1, & \partial_{\bar{z}} &= \frac{1}{2}(\partial_0 + \mathrm{i}\partial_1), \end{aligned} \tag{A.1.25}$$

so that $\epsilon(z)$ is holomorphic, and consequently also the function $f(z) = z + \epsilon(z)$. Then, a holomorphic function $f(z) = z + \epsilon(z)$ generates an infinitesimal conformal transformation $z \mapsto f(z)$. Correspondingly, the metric tensor transforms as

$$\mathrm{d}s^2 = \mathrm{d}z\mathrm{d}\bar{z} \quad \mapsto \quad \frac{\partial f}{\partial z}\frac{\partial \bar{f}}{\partial \bar{z}}\mathrm{d}z\mathrm{d}\bar{z}, \tag{A.1.26}$$

so that one can see that for $d = 2$ the scale factor is $\Lambda = |\partial f/\partial z|^2$.

The Witt and Virasoro algebras

For two dimensional infinitesimal conformal transformations, as seen in the previous section, the function $\epsilon(z)$ is holomorphic in some open set. It can be in general assumed that such function is meromorphic, i. e., it has isolated singularities around this open set. Then, it is possible to perform a Laurent expansion around a point, let us say $z = 0$, so that an infinitesimal conformal transformation can be written as

$$\begin{aligned} z' = f(z) = z + \epsilon(z) = z + \sum_{n\in\mathbb{Z}} \epsilon_n \left(-z^{n+1}\right), \\ \bar{z}' = \bar{f}(\bar{z}) = \bar{z} + \bar{\epsilon}(\bar{z}) = \bar{z} + \sum_{n\in\mathbb{Z}} \bar{\epsilon}_n \left(-\bar{z}^{n+1}\right), \end{aligned} \tag{A.1.27}$$

with $\epsilon, \bar{\epsilon}$ infinitesimal constants. For a given n, the generators of such transformations are

$$l_n = -z^{n+1}\partial_z, \qquad \bar{l}_n = -\bar{z}^{n+1}\partial_{\bar{z}}. \tag{A.1.28}$$

Since $n \in \mathbb{Z}$, there is an infinite number of independent conformal transformations for $d = 2$. The algebra of the generators can be determined from the commutation relations between the generators in Eq. (A.1.28),

$$\begin{aligned} [l_m, l_n] &= z^{m+1}\partial_z(z^{n+1}\partial_n) - z^{n+1}\partial_z(z^{m+1}\partial_n) \\ &= -(m-n)z^{m+n+1}\partial_z \\ &= (m-n)l_{m+n}, \\ [\bar{l}_m, \bar{l}_n] &= (m-n)\bar{l}_{m+n}, \\ [l_m, \bar{l}_n] &= 0. \end{aligned} \tag{A.1.29}$$

The first two relations identify two copies of the so-called *Witt algebra*, and commute between them as it is evident from the third equation. Then, it follows that the algebra of infinitesimal conformal transformations in an Euclidean two-dimensional space is infinite dimensional. As it is evident from Eq. (A.1.28), the generators $l_m, \bar{l}_m$ are not everywhere defined on the Euclidean plane $\mathbb{R}^2 \simeq \mathbb{C}$, and this suggests to work on the Riemann sphere $S^2 \simeq \mathbb{C} \cup \{\infty\}$, which is the

conformal compactification of $\mathbb{R}^2$. For $z = 0$, the generators will now be nonsingular only for $n \geq -1$. Another ambiguous point is represented by $z = \infty$, that can be studies introducing the variable $w = -1/z$ and sending $w \to 0$. The generators can be rewritten as

$$l_n = -\left(-\frac{1}{w}\right)^{n-1} \partial_w, \tag{A.1.30}$$

and they are nonsingular in $w = 0$ only for $n \leq 1$. Then, one can conclude that the conformal transformations globally defined on the Riemann sphere are generated by $\{l_{-1}, l_0, l_1\} \cup \{\bar{l}_{-1}, \bar{l}_0, \bar{l}_1\}$.

Let us now determine the corresponding conformal group.

- $l_{-1} = -\partial_z$ is the generator of translations $z \to z + b$.
- $l_0 = -z\partial_z$ generates transformations $z \to az$ with $a \in \mathbb{C}$. Introducing polar coordinates $z = re^{i\phi}$, the generators can be rewritten as

  $$l_0 = -\frac{1}{2} r\partial_r + \frac{i}{2}\partial_\phi, \qquad \bar{l}_0 = -\frac{1}{2} r\partial_r - \frac{i}{2}\partial_\phi, \tag{A.1.31}$$

  so that one can construct their linear combintions

  $$l_0 + \bar{l}_0 = -r\partial_r, \qquad i(l_0 - \bar{l}_0) = -\partial_\phi. \tag{A.1.32}$$

  It is evident that $l_0 + \bar{l}_0$ is the generator of two dimensional dilations, and $i(l_0 + \bar{l}_0)$ is the generator of rotations.
- l_1 correspond to SCTs. Those are translations for the variable $w = -1/z$. In fact, the translation $w \to w + c$ is equivalent to $z \to \frac{z}{cz+1}$, that is the finite version of the infinitesimal transformation $cl_1 z = -cz^2$.

All these operators generate transformations of the form

$$z \mapsto \frac{az + b}{cz + d}, \qquad a, b, c, d \in \mathbb{C} \tag{A.1.33}$$

with $ad - bc = 1$. This is the group $SL(2, \mathbb{C})/\mathbb{Z}_2 \simeq SO(3, 1)$ of projective conformal transformations. The quotient by $\mathbb{Z}_2$ comes from the invariance of Eq. (A.1.33) for $(a, b, c, d) \leftrightarrow (-a, -b, -c, -d)$.

The Witt algebra admits a central extension, called *Virasoro algebra*. Denoting its elements with $L_n, n \in \mathbb{Z}$, the Virasoro algebra has the following commutation relations

$$[L_m, L_n] = (m - n)L_{m+n} + \frac{c}{12}(m^3 - m)\delta_{m+n,0} \tag{A.1.34}$$

where the constant c is called *central charge*.

Primary fields

For a two dimensional Euclidean space, it is natural to do the identification $\mathbb{R}^2 \simeq \mathbb{C}$, by introducing the complex variables $z = x^0 + ix^1$ and $\bar{z} = x^0 - ix^1$. Since the relations given in

Eq. (A.1.29) identify two independent copies of the Witt algebra, one can treat z and $\bar{z}$ as independent variables, and instead of $\mathbb{C}$ one can consider the space $\mathbb{C}^2$. Then the corresponding complexification $\mathbb{R}^2 \to \mathbb{C}^2$ is

$$\phi(x^0, x^1) \to \phi(z, \bar{z}), \tag{A.1.35}$$

with $\{x^0, x^1\} \in \mathbb{R}^2$ and $\{z, \bar{z}\} \in \mathbb{C}^2$. Let us consider a field $\phi(z, \bar{z})$, with conformal dimension $(\Delta, \bar{\Delta})$. From Eq. (A.6.5), ϕ is called quasi-primary field if, under conformal transformation $z \mapsto f(z)$, it transforms as

$$\phi(z, \bar{z}) \mapsto \phi'(z, \bar{z}) = \left(\frac{\partial f}{\partial z}\right)^{\Delta} \left(\frac{\partial \bar{f}}{\partial \bar{z}}\right)^{\bar{\Delta}} \phi(f(z), \bar{f}(\bar{z})). \tag{A.1.36}$$

If, in addition, the field ϕ transforms as Eq. (A.1.36) for any conformal transformation (not necessarily global), then ϕ is called a *primary field*. It follows that a primary field is always quasi-primary, but the converse is not true. An example of quasi-primary that is not primary is the energy-momentum tensor, that will be introduced in the next Section.

Let us now derive the transformation of a primary field under infinitesimal conformal transformations. Let us consider the map $f(z) = z + \epsilon(z)$, with $\epsilon \ll 1$, so that, up to first order in $\epsilon(z)$, one has

$$\begin{aligned} \left(\frac{\partial f}{\partial z}\right)^{\Delta} &= 1 + \Delta \partial_z \epsilon(z) + \mathcal{O}(\epsilon^2), \\ \phi(z + \epsilon(z), \bar{z}) &= \phi(z) + \epsilon(z)\partial_z \phi(z, \bar{z}) + \mathcal{O}(\epsilon^2). \end{aligned} \tag{A.1.37}$$

Putting these expressions into Eq. (A.1.36), one obtains

$$\phi(z, \bar{z}) \mapsto \phi(z, \bar{z}) + (\Delta \partial_z \epsilon + \epsilon \partial_z + \bar{\Delta} \partial_{\bar{z}} \bar{\epsilon} + \bar{\epsilon} \partial_{\bar{z}}) \phi(z, \bar{z}). \tag{A.1.38}$$

Then, under infinitesimal conformal transformations the field $\phi(z, \bar{z})$ transforms as

$$\delta_{\epsilon, \bar{\epsilon}} \phi(z, \bar{z}) = (\Delta \partial_z \epsilon + \epsilon \partial_z + \bar{\Delta} \partial_{\bar{z}} \bar{\epsilon} + \bar{\epsilon} \partial_{\bar{z}})\, \phi(z, \bar{z}). \tag{A.1.39}$$

A.2 The energy-momentum tensor

The relationship between symmetries and conservation laws is summarized in *Noether's theorem*, which states that for every continuous symmmetry there exists a current j_μ that is conserved, that is

$$\partial^\mu j_\mu = 0. \tag{A.2.1}$$

In the case of a theory with conformal symmetry, the conserved current associated the infinitesimal conformal transformation in Eq. (A.1.3) is

$$j_\mu = T_{\mu\nu} \epsilon^\nu, \tag{A.2.2}$$

where $T_{\mu\nu}$ is a symmetric tensor called *energy-momentum tensor*.

In $\epsilon^\mu = \text{cnst}$, the conservation of the current implies

$$\begin{aligned} 0 = \partial^\mu j_\mu = \partial^\mu \left(T_{\mu\nu} \epsilon^\nu\right) = \left(\partial^\mu T_{\mu\nu}\right) \epsilon^\nu \\ \Rightarrow \quad \partial^\mu T_{\mu\nu} = 0. \end{aligned} \tag{A.2.3}$$

For a general transformation $\epsilon^\mu(x) \neq \text{cnst}$, using the fact that $T_{\mu\nu}$ is symmetric one has

$$0 = \partial^\mu j_\mu = (\partial^\mu T_{\mu\nu})\epsilon^\nu + T_{\mu\nu}(\partial^\mu \epsilon^\nu) = \frac{1}{2} T_{\mu\nu}\eta^{\mu\nu}(\partial\cdot\epsilon)\frac{2}{d} = \frac{1}{d} T^\mu_\mu(\partial\cdot\epsilon). \tag{A.2.4}$$

Since the equation above has to be valid for any infinitesimal transformation, it follows that *in CFT, the energy momentum tensor $T_{\mu\nu}$ is traceless*, i.e.,

$$T^\mu_\mu = 0. \tag{A.2.5}$$

A.2.1 Energy-momentum tensor for $d = 2$

In the case of 2-dimensional CFTs, using the change of coordinates from the real to the complex plane

$$x^0 = \frac{1}{2}(z + \bar{z}), \qquad x^1 = \frac{1}{2\mathrm{i}}(z - \bar{z}), \tag{A.2.6}$$

the components of the energy-momentum tensor in the complex z-plane can be obtained using the usual transformation $T_{\mu\nu} = \frac{\partial x^\alpha}{\partial x^\mu}\frac{\partial x^\beta}{\partial x^\nu} T_{\alpha\beta}$,

$$\begin{aligned} T_{zz} &= \frac{1}{4}(T_{00} - 2\mathrm{i}T_{10} - T_{11}), \\ T_{\bar{z}\bar{z}} &= \frac{1}{4}(T_{00} + 2\mathrm{i}T_{10} - T_{11}), \\ T_{z\bar{z}} &= T_{\bar{z}z} = \frac{1}{4}(T_{00} + T_{11}) = \frac{1}{4}T^\mu_\mu = 0. \end{aligned} \tag{A.2.7}$$

Using the conservation law in Eq. (A.2.3) and the tracelessness condition in Eq. (A.2.7) it follows that

$$\partial_{\bar{z}} T_{zz} = 0, \qquad \partial_z T_{\bar{z}\bar{z}} = 0. \tag{A.2.8}$$

Then, the two non-vanishing components of the stress-energy tensor are a *chiral* and *anti-chiral* field

$$T(z) \equiv T_{zz}(z,\bar{z}), \qquad \bar{T}(\bar{z}) \equiv T_{\bar{z}\bar{z}}(z,\bar{z}). \tag{A.2.9}$$

A.3 Radial Quantization

Let us consider a 2-dimensional flat Euclidean space, with time and space coordinates x^0 and x^1 respectively. In Minkowski space, the time coordinate can be obtained by Wick's rotation $x^0 \to \mathrm{i}x^0$. In order to avoid infrared divergencies, the space coordinate x^1 is compactified on a circle of radius R, that can be usually chosen to be $R = 1$. This defines a cylinder of infinite length, in the complex coordinates $w = x^0 + \mathrm{i}x^1$, with $w \sim w + 2\pi\mathrm{i}$. Then, the cylinder can be mapped to the complex plane using the conformal mapping

$$z = \mathrm{e}^w = \mathrm{e}^{(x^0 + \mathrm{i}x^1)}. \tag{A.3.1}$$

This transformation sends the past and future $x^0 = \pm\infty$ on the cylinder to the points $z = 0, \infty$ of the plane, and the equal time surfaces $x^0 = \text{cnst}$ to circles of constant radius in the z-plane, as shown in Fig. A.1. Moreover, the time translations $x^0 \mapsto x^0 + a$ are mapped to complex dilation $z \mapsto \mathrm{e}^a z$, and the space translations $x^1 \mapsto x^1 + b$ are mapped to rotations. So the role of the Hamiltonian, which is the generator of time translations, is played in the conformal

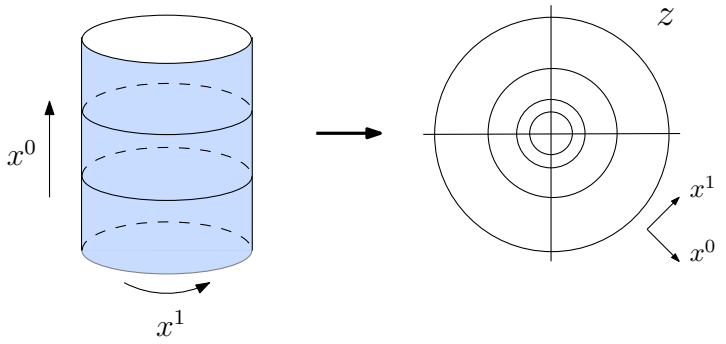


Figure A.1: Conformal mapping from the cylinder to the complex plane.

plane by the dilation operator. Analogously the momentum, that is the generator of space translations, corresponds to rotations. The Hilbert space of the system is then built up on surfaces of constant radius. This procedure for defining a quantum theory on the plane is known as *radial quantization*.

A.4 Operator product expansion

In presence of a conserved charge $j_\mu = T_{\mu\nu}\epsilon^\nu$ associated to a conformal symmetry, the corresponding conserved charged is

$$Q = \int \mathrm{d}x^1 j_0, \qquad \text{at} \quad x^0 = \text{cnst}. \tag{A.4.1}$$

In radial quantization, the integral of $\int \mathrm{d}x^1$ over a surface of equal time $x^0 = \text{cnst}$ corresponds to a contour integral over a surface of radius $|z| = \text{cnst}$. Then the conserved charge in Eq. (A.4.1) expressed in complex coordinates is given by the following contour integral

$$Q = \frac{1}{2\pi \mathrm{i}} \oint_{\mathcal{C}} \left(\mathrm{d}z T(z)\epsilon(z) + \mathrm{d}\bar{z}\bar{T}(\bar{z})\bar{\epsilon}(\bar{z})\right), \tag{A.4.2}$$

where both the integrations $\mathrm{d}z$ and $\mathrm{d}\bar{z}$ over the contour $\mathcal{C}$ are taken in the counter-clockwise direction. The infinitesimal variation of a field $\phi(z,\bar{z})$ generated by the charge Q is then given by the equal-time commutator $\delta\phi = [Q,\phi]$, that is

$$\delta_{\epsilon,\bar{\epsilon}}\phi(w,\bar{w}) = \frac{1}{2\pi \mathrm{i}} \oint_{\mathcal{C}} \mathrm{d}z[T(z)\epsilon(z), \phi(w,\bar{w})] + \frac{1}{2\pi \mathrm{i}} \oint_{\mathcal{C}} \mathrm{d}\bar{z}[\bar{T}(\bar{z})\bar{\epsilon}(\bar{z}), \phi(w,\bar{w})]. \tag{A.4.3}$$

The correlation functions in quantum field theory are expressed as time-ordered product of operators. In radial quantization, this condition translates to the *radial ordering* operators, that is

$$R\left(A(z)B(w)\right) \equiv \begin{cases} A(z)B(w), & \text{if} \quad |z| > |w|, \\ B(w)A(z), & \text{if} \quad |w| > |z|. \end{cases} \tag{A.4.4}$$

Then the contour integral having the form of Eq. (A.4.3) can be evaluated as

$$\begin{aligned} \oint \mathrm{d}z\,[A(z), B(w)] &= \oint_{|z|>|w|} \mathrm{d}z A(z)B(w) - \oint_{|z|<|w|} \mathrm{d}z B(w)A(z) \\ &= \oint_{\mathcal{C}(w)} \mathrm{d}z R\left(A(z)B(w)\right), \end{aligned} \tag{A.4.5}$$

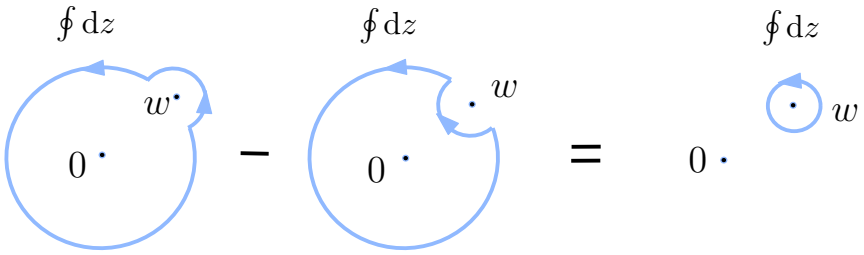


Figure A.2: Sum of contour integrals in Eq. (A.4.5).

as is shown pictorially in Fig. A.2. Then, Eq. (A.4.3) can be rewritten as

$$\delta_{\epsilon,\bar{\epsilon}}\phi(w,\bar{w}) = \frac{1}{2\pi \mathrm{i}} \oint_{\mathcal{C}(w)} \left(\mathrm{d}z\epsilon(z)R\left(T(z)\phi(w,\bar{w})\right) + \mathrm{d}\bar{z}\bar{\epsilon}(\bar{z})R\left(\bar{T}(\bar{z})\phi(w,\bar{w})\right)\right). \tag{A.4.6}$$

This expression can be compared with the one obtained using Eq. (A.1.39), that is

$$\begin{aligned}\partial_{\epsilon,\bar{\epsilon}}\phi(w,\bar{w}) = {} & \Delta\left(\partial_w\epsilon(w)\phi(w,\bar{w})\right) + \epsilon(w)\left(\partial_w\phi(w,\bar{w})\right) \\ & + \bar{\Delta}\left(\partial_{\bar{w}}\bar{\epsilon}(\bar{w})\phi(w,\bar{w})\right) + \bar{\epsilon}(\bar{w})\left(\partial_{\bar{w}}\phi(w,\bar{w})\right).\end{aligned} \tag{A.4.7}$$

Using the identities

$$\begin{aligned}\Delta\left(\partial_w\epsilon(w)\phi(w,\bar{w})\right) &= \frac{1}{2\pi \mathrm{i}} \oint_{\mathcal{C}(w)} \mathrm{d}z\Delta\frac{\epsilon(z)}{(z-w)^2}\phi(w,\bar{w}), \\ \epsilon(w)\left(\partial_w\phi(w,\bar{w})\right) &= \frac{1}{2\pi \mathrm{i}} \oint_{\mathcal{C}(w)} \mathrm{d}z\frac{\epsilon(z)}{(z-w)}\partial_w\phi(w,\bar{w}),\end{aligned} \tag{A.4.8}$$

and analogously for the anti-holomorphic part, one obtains

$$R\left(T(z)\phi(w,\bar{w})\right) = \frac{\Delta}{(z-w)^2}\phi(w,\bar{w}) + \frac{1}{(z-w)}\partial_w\phi(w,\bar{w}) + \text{non-singular terms}. \tag{A.4.9}$$

The expression above is called *operator product expansion* (OPE). From Eq. (A.4.9), an operator $\phi(z,\bar{z})$ is primary field of conformal dimension $(\Delta,\bar{\Delta})$ if the OPE between such operator and the energy-momentum tensor has the form

$$\begin{aligned}R(T(z)\phi(w,\bar{w})) &= \frac{\Delta}{(z-w)^2}\phi(w,\bar{w}) + \frac{1}{(z-w)}\partial_w\phi(w,\bar{w}) + \text{non-singular terms}, \\ R(\bar{T}(\bar{z})\phi(w,\bar{w})) &= \frac{\bar{\Delta}}{(\bar{z}-\bar{w})^2}\phi(w,\bar{w}) + \frac{1}{(\bar{z}-\bar{w})}\partial_{\bar{w}}\phi(w,\bar{w}) + \text{non-singular terms}.\end{aligned} \tag{A.4.10}$$

A.4.1 Operator product expansion of the energy-momentum tensor

The OPE of the energy-momentum tensor with itself is

$$\begin{aligned}T(z)T(w) &= \frac{c/2}{(z-w)^4} + \frac{2T(w)}{(z-w)^2} + \frac{\partial_w T(w)}{(z-w)} + \text{non-singular terms}, \\ \bar{T}(\bar{z})\bar{T}(\bar{w}) &= \frac{\bar{c}/2}{(\bar{z}-\bar{w})^4} + \frac{2\bar{T}(\bar{w})}{(\bar{z}-\bar{w})^2} + \frac{\partial_{\bar{w}}\bar{T}(\bar{w})}{(\bar{z}-\bar{w})} + \text{non-singular terms},\end{aligned} \tag{A.4.11}$$

where c is the central charge and $|z| > |w|$. To prove Eq. (A.4.11), let us write the Laurent expansion of the energy-momentum tensor

$$T(z) = \sum_{n\in\mathbb{Z}} z^{-n-2} L_n, \tag{A.4.12}$$

where

$$L_n = \frac{1}{2\pi \mathrm{i}} \oint \mathrm{d}z z^{n+1} T(z). \tag{A.4.13}$$

For a conformal transformation of the form $\epsilon(z) = -\epsilon_n z^{n+1}$, Eq. (A.4.2) can be rewritten as

$$Q_n = \oint \frac{\mathrm{d}z}{2\pi\mathrm{i}} T(z) \left(-\epsilon_n z^{n+1}\right) = -\epsilon_n \sum_{m\in\mathbb{Z}} \oint \frac{\mathrm{d}z}{2\pi\mathrm{i}} L_m z^{n-m-1} = -\epsilon_n L_n. \tag{A.4.14}$$

So the Laurent modes of the energy-momentum tensor in Eq. (A.4.13), can be identified with the generators of infinitesimal conformal transformation. In order to prove Eq. (A.4.11), it is necessary to verify that their commutator satisfies Eq. (A.1.34)

$$\begin{aligned}
[L_m, L_n] &= \oint \frac{\mathrm{d}z}{2\pi\mathrm{i}} \oint \frac{\mathrm{d}w}{2\pi\mathrm{i}} z^{m+1} w^{n+1} \left[T(z), T(w)\right] \\
&= \oint_{\mathcal{C}(0)} \frac{\mathrm{d}w}{2\pi\mathrm{i}} w^{n+1} \oint_{\mathcal{C}(w)} \frac{\mathrm{d}z}{2\pi\mathrm{i}} z^{m+1} R\left(T(z)T(w)\right) \\
&= \oint_{\mathcal{C}(0)} \frac{\mathrm{d}w}{2\pi\mathrm{i}} w^{n+1} \oint_{\mathcal{C}(w)} \frac{\mathrm{d}z}{2\pi\mathrm{i}} z^{m+1} \left(\frac{c/2}{(z-w)^4} + \frac{2T(w)}{(z-w)^2} + \frac{\partial_w T(w)}{(z-w)}\right) \\
&= \oint \frac{\mathrm{d}w}{2\pi\mathrm{i}} \left(\frac{c}{12}(m+1)m(m-1)w^{m+n+1} + 2(m+1)w^{m+n+1}T(w) + w^{m+n+2}\partial_w T(w)\right) \\
&= (m-n)L_{m+n} + \frac{c}{12}(m^3 - m)\delta_{m,-n}.
\end{aligned} \tag{A.4.15}$$

So, Eq. (A.4.11) is the correct OPE between two energy-momentum tensors.

A.4.2 Conformal transformations of the energy-momentum tensor

From the OPE in Eq. (A.4.11), it is evident that in general $T(z)$ is not a primary fields. It can be shown that, under conformal transformations $f(z)$, the energy-momentum behaves as

$$T'(z) = \left(\frac{\partial f}{\partial z}\right)^2 T\left(f(z)\right) + \frac{c}{12}\{f(z), z\}, \tag{A.4.16}$$

where $\{f(z), z\}$ is the so-called *Schwarzian derivative*

$$\{w, z\} = \frac{1}{(\partial_z w)^2}\left((\partial_z w)(\partial_z^3 w) - \frac{3}{2}(\partial_z^2 w)^2\right). \tag{A.4.17}$$

Let us verify Eq. (A.4.16) in the case of an infinitesimal transformation $f(z) = z + \epsilon(z)$. Using Eq. (A.4.6), the variation of the energy-momentum tensor under this transformation is

$$\begin{aligned}
\delta_\epsilon T(z) &= \frac{1}{2\pi\mathrm{i}} \oint_{\mathcal{C}(z)} \mathrm{d}w \epsilon(w) T(w) T(z) = \\
&= \frac{1}{2\pi\mathrm{i}} \oint_{\mathcal{C}(z)} \mathrm{d}w \epsilon(w) \left(\frac{c/2}{(w-z)^4} + \frac{2T(z)}{(w-z)^2} + \frac{\partial_z T(z)}{w-z} + \dots\right) \\
&= \frac{c}{12}\partial_z^3 \epsilon(z) + 2T(z)\partial_z \epsilon(z) + \epsilon(z)\partial_z T(z).
\end{aligned} \tag{A.4.18}$$

This expression can be compared with the one obtained using the expression of the variation of the energy-momentum tensor in Eq. (A.4.16)

$$\begin{aligned}\delta_\epsilon T(z) &= T'(z) - T(z)\\ &= (1+\partial_z\epsilon(z))^2\,(T(z)+\epsilon(z)\partial_z T(z)) + \frac{c}{12}\frac{1}{(1+\partial_z\epsilon)^2}\left((1+\partial_z\epsilon)\partial_z^3\epsilon - \frac{3}{2}(\partial_z^2\epsilon)^2\right) - T(z)\\ &\simeq (1+\partial_z\epsilon(z))^2\,(T(z)+\epsilon(z)\partial_z T(z)) + \frac{c}{12}\partial_z^3\epsilon(z) - T(z)\\ &= \frac{c}{12}\partial_z^3\epsilon(z) + 2T(z)\partial_z\epsilon(z) + \epsilon(z)\partial_z T(z),\end{aligned} \tag{A.4.19}$$

that is the result of that in Eq. (A.4.18).

The expansion in Laurent modes can be generalized to an arbitrary holomorphic primary field of conformal dimension $(\Delta, 0)$ as follows

$$\phi(z) = \sum_{n\in\mathbb{Z}-\Delta} \phi_n z^{-n-\Delta}, \tag{A.4.20}$$

where the modes ϕ_n satisfy

$$\phi_n = \oint \frac{\mathrm{d}z}{2\pi\mathrm{i}} z^{\Delta+n-1}\phi(z). \tag{A.4.21}$$

In analogy with Eq. (A.4.15), let us evaluate

$$\begin{aligned}[L_m, \phi_n] &= \oint \frac{\mathrm{d}w}{2\pi\mathrm{i}} w^{\Delta+n-1}(\Delta(m+1)w^m\phi(w) + w^{m+1}\partial\phi(w))\\ &= \oint \frac{\mathrm{d}w}{2\pi\mathrm{i}} w^{\Delta+m+n-1}(\Delta(m+1) - (\Delta+m+n))\phi(w)\\ &= (m(\Delta-1)-n)\phi_{m+n},\end{aligned} \tag{A.4.22}$$

for all $n, m \in \mathbb{Z}$. If Eq. (A.4.11) and Eq. (A.4.22) hold for $m = -1, 0, 1$, the field $\phi(z)$ is a quasi-primary field. Using this relation, it can be shown that the energy-momentum tensor is a quasi-primary field with conformal dimension $(\Delta, \bar{\Delta}) = (2, 0)$.

A.5 Conformal Ward identity

The Ward identities are generally identities verified by correlation functions as a consequence of symmetries possessed by a theory. Let us illustrate the procedure to derive the conformal Ward identities verified by correlations functions of primary fields ϕ_i. The starting point is the evaluation of

$$\left\langle \oint \frac{\mathrm{d}z}{2\pi\mathrm{i}} \epsilon(z)T(z)\phi_1(w_1,\bar{w}_1)\cdots\phi_N(w_N,\bar{w}_N)\right\rangle. \tag{A.5.1}$$

The contour integral encircling the points w_i can be evaluated as sum over small contours around each of the points as shown in Fig. A.3, so the expression above can be written as

$$\begin{aligned}&= \sum_{i=1}^N \left\langle \phi_1(w_1,\bar{w}_1)\cdots\left(\oint_{\mathcal{C}(w_i)} \frac{\mathrm{d}z}{2\pi\mathrm{i}}\epsilon(z)T(z)\phi_i(w_i,\bar{w}_i)\right)\cdots\phi_N(w_N,\bar{w}_N)\right\rangle\\ &= \sum_{i=1}^N \left\langle \phi_1(w_1,\bar{w}_1)\cdots\left(\Delta_i\partial\epsilon(w_1) + \epsilon(w_i)\partial_{w_i}\right)\phi_i(w_i,\bar{w}_i)\cdots\phi_N(w_N,\bar{w}_N)\right\rangle\end{aligned} \tag{A.5.2}$$

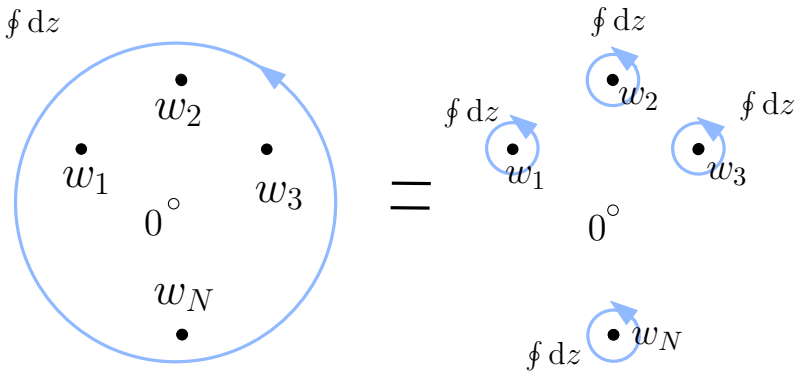


Figure A.3: The contour integral in Eq. (A.5.1) is equivalent to the sum of the contours around each point w_i

where the last identity is given by Eq. (A.1.39). Using the identities in Eq. (A.4.8), one obtains

$$0 = \oint \frac{\mathrm{d}z}{2\pi \mathrm{i}} \epsilon(z) \Big[\langle T(z)\phi_1(w_1,\bar{w}_1)\cdots\phi_N(w_N,\bar{w}_N)\rangle - \sum_{i=1}^{N} \left(\frac{\Delta_i}{(z-w_i)^2} + \frac{1}{z-w_i}\partial_{w_i} \right) \langle \phi_1(w_1,\bar{w}_1)\cdots\phi_N(w_N,\bar{w}_N)\rangle \Big]. \tag{A.5.3}$$

This relation is true for arbitrary $\epsilon(z)$ of the form $\epsilon(z) = -z^{n+1}$ with $n \in \mathbb{Z}$. So the integrand must vanish, giving the so-called *Conformal Ward identity*

$$\langle T(z)\phi_1(w_1,\bar{w}_1)\cdots\phi_N(w_N,\bar{w}_N)\rangle = \sum_{i=1}^{N} \left(\frac{\Delta_i}{(z-w_i)^2} + \frac{1}{z-w_i}\partial_{w_i} \right) \langle \phi_1(w_1,\bar{w}_1)\cdots\phi_N(w_N,\bar{w}_N)\rangle \,. \tag{A.5.4}$$

A.6 Two-point function

Let us derive the 2-point function of quasi-primary fields

$$\langle \phi_1(z)\phi_2(w)\rangle = g(z,w). \tag{A.6.1}$$

The form of the function g can be derived using the properties of invariance under conformal transformations. The invariance under L_{-1}, that generates the translations $f(z) = z + a$, requires that $g(z,w) = g(z-w)$. The invariance under L_0, that generates the scale transformation $f(z) = \lambda z$, gives

$$\langle \phi_1(z)\phi_2(w)\rangle \to \langle \lambda^{\Delta_1}\phi_1(\lambda z)\lambda^{\Delta_2}\phi_2(\lambda w)\rangle = \lambda^{\Delta_1+\Delta_2} g(\lambda(z-w)). \tag{A.6.2}$$

Combining with the previous condition, one gets

$$g(z-w) = \frac{C_{12}}{(z-w)^{\Delta_1+\Delta_2}}, \tag{A.6.3}$$

where C_{12} is the so-called structure constant. From the invariance under L_1, that is under transformation $f(z) = -1/z$, it follows that

$$\begin{aligned}\langle \phi_1(z)\phi_2(w)\rangle \to \left\langle \frac{1}{z^{2\Delta_1}}\frac{1}{w^{2\Delta_2}}\phi_1\left(-\frac{1}{z}\right)\phi_2\left(-\frac{1}{w}\right) = \right\rangle \\ = \frac{1}{z^{2\Delta_1}w^{2\Delta_2}}\frac{C_{12}}{\left(-\frac{1}{z}+\frac{1}{w}\right)^{\Delta_1+\Delta_2}}.\end{aligned} \tag{A.6.4}$$

The result above is equal to the condition in Eq. (A.6.3) only if $\Delta_1 = \Delta_2$. It follows that the form of the 2-point function of two quasi-primary fields is

$$\langle \phi_i(z)\phi_j(w)\rangle = \frac{C_{ij}\delta_{\Delta_i,\Delta_j}}{(z-w)^{2\Delta_i}}. \tag{A.6.5}$$

For example, using the OPE of the energy-momentum tensor, one obtains the following 2-point function

$$\langle T(z)T(w)\rangle = \frac{c/2}{(z-w)^4}. \tag{A.6.6}$$

References

[1] R. Bonsignori, P. Ruggiero, and P. Calabrese. "Symmetry resolved entanglement in free fermionic systems". In: *Journal of Physics A: Mathematical and Theoretical* 52.47 (2019), p. 475302. DOI: 10.1088/1751-8121/ab4b77. URL: https://doi.org/10.1088/1751-8121/ab4b77.

[2] R. Bonsignori and P. Calabrese. "Boundary effects on symmetry resolved entanglement". In: *Journal of Physics A: Mathematical and Theoretical* 54.1 (2020), p. 015005. DOI: 10.1088/1751-8121/abcc3a. URL: https://doi.org/10.1088/1751-8121/abcc3a.

[3] G. Parez, R. Bonsignori, and P. Calabrese. "Quasiparticle dynamics of symmetry-resolved entanglement after a quench: Examples of conformal field theories and free fermions". In: *Phys. Rev. B* 103.4 (2021), p. L041104. DOI: 10.1103/PhysRevB.103.L041104. URL: https://link.aps.org/doi/10.1103/PhysRevB.103.L041104.

[4] S. Murciano, R. Bonsignori, and P. Calabrese. "Symmetry decomposition of negativity of massless free fermions". In: *SciPost Phys.* 10.5 (2021), p. 111. DOI: 10.21468/SciPostPhys.10.5.111. URL: https://scipost.org/10.21468/SciPostPhys.10.5.111.

[5] G. Parez, R. Bonsignori, and P. Calabrese. "Exact quench dynamics of symmetry resolved entanglement in a free fermion chain". In: *arXiv:2106.13115* (2021). URL: https://arxiv.org/abs/2106.13115.

[6] G. Parez, R. Bonsignori, and P. Calabrese. "Quench dynamics of symmetry resolved entanglement negativity in a free fermion chain". In: *In preparation* (2021).

[7] E. Schrödinger. "Discussion of Probability Relations Between Separated Systems". In: *Proceedings of the Cambridge Philosophical Society* 32 (1936), 446–451. URL: https://doi.org/10.1017/S0305004100013554.

[8] A. Einstein et al. "Can Quantum-Mechanical Description of Physical Reality Be Considered Complete?" In: *Phys. Rev.* 47.10 (1935), pp. 777–780. DOI: 10.1103/PhysRev.47.777. URL: https://link.aps.org/doi/10.1103/PhysRev.47.777.

[9] J. S. Bell. "On the Einstein Podolsky Rosen paradox". In: *Physics Physique Fizika* 1.3 (1964), pp. 195–200. DOI: 10.1103/PhysicsPhysiqueFizika.1.195. URL: https://link.aps.org/doi/10.1103/PhysicsPhysiqueFizika.1.195.

[10] A. Aspectand J. Dalibard and G. Roger. "Experimental Test of Bell's Inequalities Using Time-Varying Analyzers". In: *Phys. Rev. Lett.* 49.25 (1982), pp. 1804–1807. DOI: 10.1103/PhysRevLett.49.1804. URL: https://link.aps.org/doi/10.1103/PhysRevLett.49.1804.

[11] A. K. Ekert. "Quantum cryptography based on Bell's theorem". In: *Phys. Rev. Lett.* 67.6 (1991), pp. 661–663. DOI: 10.1103/PhysRevLett.67.661. URL: https://link.aps.org/doi/10.1103/PhysRevLett.67.661.

[12] C. H. Bennett et al. "Mixed-state entanglement and quantum error correction". In: *Phys. Rev. A* 54.5 (1996), pp. 3824–3851. DOI: 10.1103/PhysRevA.54.3824. URL: https://link.aps.org/doi/10.1103/PhysRevA.54.3824.

[13] J. D. Bekenstein. "Black Holes and Entropy". In: *Phys. Rev. D* 7.8 (1973), pp. 2333–2346. DOI: 10.1103/PhysRevD.7.2333. URL: https://link.aps.org/doi/10.1103/PhysRevD.7.2333.

[14] S. Hawking. "Black hole explosions?" In: *Nature* 248 (1974), 30–31. DOI: 10.1038/248030a0. URL: https://doi.org/10.1038/248030a0.

[15] L.Amico et al. "Entanglement in many-body systems". In: *Rev. Mod. Phys.* 80.2 (2008), pp. 517–576. DOI: 10.1103/RevModPhys.80.517. URL: https://link.aps.org/doi/10.1103/RevModPhys.80.517.

[16] B. Zeng et al. *Quantum Information Meets Quantum Matter*. The address: Springer-Verlag New York, 2019. ISBN: 978-1-4939-9082-5. DOI: 10.1007/978-1-4939-9084-9.

[17] R. Islam et al. "Measuring entanglement entropy in a quantum many-body system". In: *Nature* 528 (2015). DOI: 10.1038/nature15750. URL: http://dx.doi.org/10.1038/nature15750.

[18] A. M. Kaufman et al. "Quantum thermalization through entanglement in an isolated many-body system". In: *Science* 353.6301 (2016), pp. 794–800. ISSN: 0036-8075. DOI: 10.1126/science.aaf6725. eprint: https://science.sciencemag.org/content/353/6301/794.full.pdf. URL: https://science.sciencemag.org/content/353/6301/794.

[19] A. Lukin et al. "Probing entanglement in a many-body–localized system". In: *Science* 364.6437 (2019), pp. 256–260. ISSN: 0036-8075. DOI: 10.1126/science.aau0818. eprint: https://science.sciencemag.org/content/364/6437/256.full.pdf. URL: https://science.sciencemag.org/content/364/6437/256.

[20] P. Calabrese, J. Cardy, and B. Doyon. "Entanglement entropy in extended quantum systems". In: *Journal of Physics A: Mathematical and Theoretical* 42.50 (2009), p. 500301. DOI: 10.1088/1751-8121/42/50/500301. URL: https://doi.org/10.1088/1751-8121/42/50/500301.

[21] J. Eisert, M. Cramer, and M. B. Plenio. "Colloquium: Area laws for the entanglement entropy". In: *Rev. Mod. Phys.* 82.1 (2010), pp. 277–306. DOI: 10.1103/RevModPhys.82.277. URL: https://link.aps.org/doi/10.1103/RevModPhys.82.277.

[22] N. Laflorencie. "Quantum entanglement in condensed matter systems". In: *Physics Reports* 646 (2016). Quantum entanglement in condensed matter systems, pp. 1–59. ISSN: 0370-1573. DOI: https://doi.org/10.1016/j.physrep.2016.06.008. URL: https://www.sciencedirect.com/science/article/pii/S0370157316301582.

[23] R. Islam et al. "Quantum entanglement in condensed matter systems". In: *Nature* 528 (2015), p. 77. URL: https://www.nature.com/articles/nature15750.

[24] A. Elben et al. "Rényi Entropies from Random Quenches in Atomic Hubbard and Spin Models". In: *Phys. Rev. Lett.* 120.5 (2018), p. 050406. DOI: 10.1103/PhysRevLett.120.050406. URL: https://link.aps.org/doi/10.1103/PhysRevLett.120.050406.

[25] P. Calabrese and J. Cardy. "Entanglement entropy and quantum field theory". In: *Journal of Statistical Mechanics: Theory and Experiment* 2004.06 (2004), P06002. DOI: 10.1088/1742-5468/2004/06/p06002. URL: https://doi.org/10.1088/1742-5468/2004/06/p06002.

[26] P. Calabrese and J. Cardy. "Entanglement entropy and conformal field theory". In: *Journal of Physics A: Mathematical and Theoretical* 42.50 (2009), p. 504005. DOI: 10.1088/1751-8113/42/50/504005. URL: https://doi.org/10.1088/1751-8113/42/50/504005.

[27] C. Holzhey, F. Larsen, and F Wilczek. "Geometric and renormalized entropy in conformal field theory". In: *Nuclear Physics B* 424.3 (1994), pp. 443–467. ISSN: 0550-3213. DOI: https://doi.org/10.1016/0550-3213(94)90402-2. URL: https://www.sciencedirect.com/science/article/pii/0550321394904022.

[28] G. Vidal et al. "Entanglement in Quantum Critical Phenomena". In: *Phys. Rev. Lett.* 90.22 (2003), p. 227902. DOI: 10.1103/PhysRevLett.90.227902. URL: https://link.aps.org/doi/10.1103/PhysRevLett.90.227902.

[29] M. M. Wolf et al. "Area Laws in Quantum Systems: Mutual Information and Correlations". In: *Phys. Rev. Lett.* 100.7 (2008), p. 070502. DOI: 10.1103/PhysRevLett.100.070502. URL: https://link.aps.org/doi/10.1103/PhysRevLett.100.070502.

[30] M. Kormos and Z. Zimborás. "Temperature driven quenches in the Ising model: appearance of negative Rényi mutual information". In: *Journal of Physics A: Mathematical and Theoretical* 50.26 (2017), p. 264005. DOI: 10.1088/1751-8121/aa70f6. URL: https://doi.org/10.1088/1751-8121/aa70f6.

[31] S. O. Scalet et al. "Computable Rényi mutual information: Area laws and correlations". In: *ArXiv:2103.01709* (2021). URL: https://arxiv.org/abs/2103.01709.

[32] G. Vidal and R. F. Werner. "Computable measure of entanglement". In: *Phys. Rev. A* 65.3 (2002), p. 032314. DOI: 10.1103/PhysRevA.65.032314. URL: https://link.aps.org/doi/10.1103/PhysRevA.65.032314.

[33] N. Laflorencie and S. Rachel. "Spin-resolved entanglement spectroscopy of critical spin chains and Luttinger liquids". In: *Journal of Statistical Mechanics: Theory and Experiment* 2014.11 (2014), P11013. DOI: 10.1088/1742-5468/2014/11/p11013. URL: https://doi.org/10.1088/1742-5468/2014/11/p11013.

[34] J. C. Xavier, F. C. Alcaraz, and G. Sierra. "Equipartition of the entanglement entropy". In: *Phys. Rev. B* 98.4 (2018), p. 041106. DOI: 10.1103/PhysRevB.98.041106. URL: https://link.aps.org/doi/10.1103/PhysRevB.98.041106.

[35] M. Goldstein and E. Sela. "Symmetry-Resolved Entanglement in Many-Body Systems". In: *Phys. Rev. Lett.* 120.20 (2018), p. 200602. DOI: 10.1103/PhysRevLett.120.200602. URL: https://link.aps.org/doi/10.1103/PhysRevLett.120.200602.

[36] J. H. Bardarson, F. Pollmann, and J. E. Moore. "Unbounded growth of entanglement in models of many-body localization". In: *Phys. Rev. Lett.* 109.017202 (2012). URL: http://dx.doi.org/10.1103/PhysRevLett.109.017202.

[37] R. Vosk and E. Altman. "Dynamical Quantum Phase Transitions in Random Spin Chains". In: *Phys. Rev. Lett.* 112.217204 (2014). URL: http://dx.doi.org/10.1103/PhysRevLett.112.217204.

[38] E. Cornfeld, M. Goldstein, and E. Sela. "Imbalance entanglement: Symmetry decomposition of negativity". In: *Phys. Rev. A* 98.3 (2018), p. 032302. DOI: 10.1103/PhysRevA.98.032302. URL: https://link.aps.org/doi/10.1103/PhysRevA.98.032302.

[39] N. Feldman and M. Goldstein. "Dynamics of charge-resolved entanglement after a local quench". In: *Phys. Rev. B* 100.23 (2019), p. 235146. DOI: 10.1103/PhysRevB.100.235146. URL: https://link.aps.org/doi/10.1103/PhysRevB.100.235146.

[40] H. Casini, C. D. Fosco, and M. Huerta. "Entanglement and alpha entropies for a massive Dirac field in two dimensions". In: *Journal of Statistical Mechanics: Theory and Experiment* 2005.07 (2005), P07007–P07007. DOI: 10.1088/1742-5468/2005/07/p07007. URL: https://doi.org/10.1088/1742-5468/2005/07/p07007.

[41] J. S. Dowker. "Conformal weights of charged Rényi entropy twist operators for free scalar fields in arbitrary dimensions". In: *Journal of Physics A: Mathematical and Theoretical* 49.14 (2016), p. 145401. DOI: 10.1088/1751-8113/49/14/145401. URL: https://doi.org/10.1088/1751-8113/49/14/145401.

[42] J. S. Dowker. "Charged Renyi entropies for free scalar fields". In: *Journal of Physics A: Mathematical and Theoretical* 50.16 (2017), p. 165401. DOI: 10.1088/1751-8121/aa6178. URL: https://doi.org/10.1088/1751-8121/aa6178.

[43] H. Casini and M. Huerta. "Entanglement entropy in free quantum field theory". In: *Journal of Physics A: Mathematical and Theoretical* 42.50 (2009), p. 504007. DOI: 10.1088/1751-8113/42/50/504007. URL: https://doi.org/10.1088/1751-8113/42/50/504007.

[44] A. Belin et al. "Holographic charged Rényi entropies". In: *J. High Energ. Phys* 12.059 (2013). DOI: 10.1088/1751-8121/aa6178. URL: https://doi.org/10.1007/JHEP12(2013)059.

[45] P. Caputa, G. Mandal, and R. Sinha. "Dynamical entanglement entropy with angular momentum and $U(1)$ charge". In: *J. High Energ. Phys.* 2013.52 (2013). URL: https://doi.org/10.1007/JHEP11(2013)052.

[46] P. Caputa, M. Nozaki, and T. Numasawa. "Charged entanglement entropy of local operators". In: *Phys. Rev. D* 93.10 (2016), p. 105032. DOI: 10.1103/PhysRevD.93.105032. URL: https://link.aps.org/doi/10.1103/PhysRevD.93.105032.

[47] H. Shapourian, K. Shiozaki, and S. Ryu. "Partial time-reversal transformation and entanglement negativity in fermionic systems". In: *Phys. Rev. B* 95.16 (2017), p. 165101. DOI: 10.1103/PhysRevB.95.165101. URL: https://link.aps.org/doi/10.1103/PhysRevB.95.165101.

[48] H. Shapourian et al. "Twisted and untwisted negativity spectrum of free fermions". In: *SciPost Phys.* 7.037 (2019). URL: https://arxiv.org/pdf/1906.04211.pdf.

[49] L. Capizzi, P. Ruggiero, and P. Calabrese. "Symmetry resolved entanglement entropy of excited states in a CFT". In: *Journal of Statistical Mechanics: Theory and Experiment* 2020.7 (2020), p. 073101. DOI: 10.1088/1742-5468/ab96b6. URL: https://doi.org/10.1088/1742-5468/ab96b6.

[50] B. Estienne, Y. Ikhlef, and A. Morin-Duchesne. "Finite-size corrections in critical symmetry-resolved entanglement". In: *arXiv:2010.10515 (2020)* (). URL: https://arxiv.org/abs/2010.10515.

[51] H. H. Chen. "Symmetry decomposition of relative entropies in conformal field theory". In: *J. High Energ. Phys.* 2021.84 (2021). DOI: 10.1007/JHEP07(2021)084. URL: https://doi.org/10.1007/JHEP07(2021)084.

[52] L. Capizzi and P. Calabrese. "Symmetry resolved relative entropies and distances in conformal field theory". In: *arXiv:2105.08596* (2021). URL: https://arxiv.org/abs/2105.08596.

[53] S. Fraenkel and M. Goldstein. "Symmetry resolved entanglement: exact results in 1D and beyond". In: *Journal of Statistical Mechanics: Theory and Experiment* 2020.3 (2020), p. 033106. DOI: 10.1088/1742-5468/ab7753. URL: https://doi.org/10.1088/1742-5468/ab7753.

[54] Sara Murciano, Paola Ruggiero, and Pasquale Calabrese. "Symmetry resolved entanglement in two-dimensional systems via dimensional reduction". In: *Journal of Statistical Mechanics: Theory and Experiment* 2020.8 (2020), p. 083102. DOI: 10.1088/1742-5468/aba1e5. URL: https://doi.org/10.1088/1742-5468/aba1e5.

[55] M. T. Tan and S. Ryu. "Particle number fluctuations, Rényi entropy, and symmetry-resolved entanglement entropy in a two-dimensional Fermi gas from multidimensional bosonization". In: *Phys. Rev. B* 101.23 (2020), p. 235169. DOI: 10.1103/PhysRevB.101.235169. URL: https://link.aps.org/doi/10.1103/PhysRevB.101.235169.

[56] S. Murciano, G. Di Giulio, and P. Calabrese. "Symmetry resolved entanglement in gapped integrable systems: a corner transfer matrix approach". In: *SciPost Phys.* 8.3 (2020), p. 46. DOI: 10.21468/SciPostPhys.8.3.046. URL: https://scipost.org/10.21468/SciPostPhys.8.3.046.

[57] Pasquale Calabrese et al. "Full counting statistics in the gapped XXZ spin chain". In: *EPL (Europhysics Letters)* 129.6 (2020), p. 60007. DOI: 10.1209/0295-5075/129/60007. URL: https://doi.org/10.1209/0295-5075/129/60007.

[58] D.X. Horváth and P. Calabrese. "Symmetry resolved entanglement in integrable field theories via form factor bootstrap". In: *J. High Energ. Phys.* 2020.131 (2020). DOI: 10.1007/JHEP11(2020)131. URL: https://doi.org/10.1007/JHEP11(2020)131.

[59] D.X. Horváth, L. Capizzi, and P. Calabrese. "$U(1)$ symmetry resolved entanglement in free $1+1$ dimensional field theories via form factor bootstrap". In: *arXiv:2103.03197* (2021). URL: https://arxiv.org/abs/2103.03197.

[60] D. X. Horvath, P. Calabrese, and O. A. Castro-Alvaredo. "Branch Point Twist Field Form Factors in the sine-Gordon Model II: Composite Twist Fields and Symmetry Resolved Entanglement". In: *arXiv:2105.13982* (2021). URL: https://arxiv.org/abs/2105.13982.

[61] L. Capizzi et al. "Entanglement of the 3-State Potts Model via Form Factor Bootstrap: Total and Symmetry Resolved Entropies". In: *arXiv:2108.10935* (2021). URL: https://arxiv.org/abs/2108.10935.

[62] S. Murciano, G. Di Giulio, and P. Calabrese. "Entanglement and symmetry resolution in two dimensional free quantum field theories". In: *J. High Energ. Phys* 2008.073 (2020). DOI: 10.1007/JHEP08(2020)073. URL: https://doi.org/10.1007/JHEP08(2020)073.

[63] X. Turkeshi et al. "Entanglement equipartition in critical random spin chains". In: *Phys. Rev. B* 102.1 (2020), p. 014455. DOI: 10.1103/PhysRevB.102.014455. URL: https://link.aps.org/doi/10.1103/PhysRevB.102.014455.

[64] K. Monkman and J. Sirker. "Operational entanglement of symmetry-protected topological edge states". In: *Phys. Rev. Research* 2.4 (2020), p. 043191. DOI: 10.1103/PhysRevResearch.2.043191. URL: https://link.aps.org/doi/10.1103/PhysRevResearch.2.043191.

[65] D. Azses and E. Sela. "Symmetry-resolved entanglement in symmetry-protected topological phases". In: *Phys. Rev. B* 102.23 (2020), p. 235157. DOI: 10.1103/PhysRevB.102.235157. URL: https://link.aps.org/doi/10.1103/PhysRevB.102.235157.

[66] E. Cornfeld et al. "Entanglement spectroscopy of non-Abelian anyons: Reading off quantum dimensions of individual anyons". In: *Phys. Rev. B* 99.11 (2019), p. 115429. DOI: 10.1103/PhysRevB.99.115429. URL: https://link.aps.org/doi/10.1103/PhysRevB.99.115429.

[67] V. Vitale et al. "Symmetry-resolved dynamical purification in synthetic quantum matter". In: *ArXiv:2101.07814* (2020). URL: https://arxiv.org/abs/2101.07814.

[68] A. Neven et al. "Symmetry-resolved entanglement detection using partial transpose moments". In: *arXiv:2103.07443* (2021). URL: https://arxiv.org/abs/2103.07443.

[69] S. Zhao, C. Northe, and R. Meyer. "Symmetry-Resolved Entanglement in AdS_3/CFT_2 coupled to $U(1)$ Chern-Simons Theory". In: *J. High Energ. Phys.* 2021.30 (2021). DOI: 10.1007/JHEP07(2021)030. URL: https://doi.org/10.1007/JHEP07(2021)030.

[70] A. Neumaier. *Coherent Quantum Physics*. De Gruyter, 2019. DOI: doi:10.1515/9783110667387-015.

[71] J. Preskill. "Quantum iInformation and Computation". Lecture notes. 1998.

[72] V. Moretti. "Mathematical Foundations of Quantum Mechanics: An Advanced Short Course". Lecture notes.

[73] A. Peres. "Separability Criterion for Density Matrices". In: *Phys. Rev. Lett.* 77.8 (1996), pp. 1413–1415. DOI: 10.1103/PhysRevLett.77.1413. URL: https://link.aps.org/doi/10.1103/PhysRevLett.77.1413.

[74] M. Horodecki, P. Horodecki, and R. Horodecki. "Separability of mixed states: necessary and sufficient conditions". In: *Phys. Lett. A* 223 (1996), pp. 1–8. DOI: https://doi.org/10.1016/S0375-9601(96)00706-2.

[75] M. B. Plenio and S. Virmani. "An introduction to entanglement measures". In: *Quantum Inf. Comput.* 7.1 (2007), pp. 1–51. DOI: 10.26421/QIC7.1-2-1. URL: https://doi.org/10.26421/QIC7.1-2-1.

[76] V. Vedral et al. "Quantifying Entanglement". In: *Phys. Rev. Lett.* 78.12 (1997), pp. 2275–2279. DOI: 10.1103/PhysRevLett.78.2275. URL: https://link.aps.org/doi/10.1103/PhysRevLett.78.2275.

[77] E. Chitambar et al. "Everything You Always Wanted to Know About LOCC (But Were Afraid to Ask)". In: *Commun. Math. Phys.* 328 (2014), 303–326. DOI: https://doi.org/10.1007/s00220-014-1953-9.

[78] C. H. Bennett et al. "Quantum nonlocality without entanglement". In: *Phys. Rev. A* 59.2 (1999), pp. 1070–1091. DOI: 10.1103/PhysRevA.59.1070. URL: https://link.aps.org/doi/10.1103/PhysRevA.59.1070.

[79] R. Horodecki et al. "Quantum entanglement". In: *Rev. Mod. Phys.* 81.2 (2009), pp. 865–942. DOI: 10.1103/RevModPhys.81.865. URL: https://link.aps.org/doi/10.1103/RevModPhys.81.865.

[80] M. A. Nielsen. "Conditions for a Class of Entanglement Transformations". In: *Phys. Rev. Lett.* 83.2 (1999), pp. 436–439. DOI: 10.1103/PhysRevLett.83.436. URL: https://link.aps.org/doi/10.1103/PhysRevLett.83.436.

[81] M. A. Nielsen and I. L. Chuang. *Quantum Computation and Quantum Information: 10th Anniversary Edition*. Cambridge University Press, 2010. DOI: 10.1017/CBO9780511976667.

[82] P. Calabrese and A. Lefevre. "Entanglement spectrum in one-dimensional systems". In: *Phys. Rev. A* 78.3 (2008), p. 032329. DOI: 10.1103/PhysRevA.78.032329. URL: https://link.aps.org/doi/10.1103/PhysRevA.78.032329.

[83] E. Cornfeld, E. Sela, and M. Goldstein. "Measuring fermionic entanglement: Entropy, negativity, and spin structure". In: *Phys. Rev. A* 062309 (2019). DOI: 10.1103/PhysRevA.99.062309. URL: http://dx.doi.org/10.1103/PhysRevA.99.062309.

[84] A. Elben et al. "Mixed-state entanglement from local randomized measurements". In: *Phys. Rev. Lett.* 125 (2005). DOI: 10.1103/PhysRevLett.125.200501. URL: https://doi.org/10.1103/PhysRevLett.125.200501.

[85] J. Gray et al. "Machine Learning Assisted Many-Body Entanglement Measurement". In: *Phys. Rev. Lett.* 121.150503 (2018). DOI: 10.1103/PhysRevLett.121.150503. URL: https://doi.org/10.1103/PhysRevLett.121.150503.

[86] K. Audenaert et al. "Entanglement properties of the harmonic chain". In: *Phys. Rev. A* 66.042327 (2002). DOI: 10.1103/PhysRevA.66.042327. URL: https://doi.org/10.1103/PhysRevA.66.042327.

[87] A. Ferraro et al. "Thermal Bound Entanglement in Macroscopic Systems and Area Law," in: *Phys. Rev. Lett.* 100.080502 (2008). DOI: https://doi.org/10.1103/PhysRevLett.100.080502. URL: 10.1103/PhysRevLett.100.080502.

[88] D. Cavalcanti et al. "Distillable entanglement and area laws in spin and harmonic-oscillator systems". In: *Phys. Rev. A* 78.012335 (2008). DOI: 110.1103/PhysRevA.78.012335. URL: https://doi.org/110.1103/PhysRevA.78.012335.

[89] J. Anders and W. Andreas. "Entanglement and separability of quantum harmonic oscillator systems at finite temperature". In: *Quantum Info. Comput.* 8.0245 (2008). DOI: 10.26421/QIC8.3-4-2. URL: https://doi.org/10.26421/QIC8.3-4-2.

[90] J. Anders. "Thermal state entanglement in harmonic lattices". In: *Phys. Rev. A* 77.062102 (2008). DOI: 10.1103/PhysRevA.77.062102. URL: https://doi.org/10.1103/PhysRevA.77.062102.

[91] S. Marcovitch et al. "Critical and noncritical long-range entanglement in Klein-Gordon fields". In: *Phys. Rev. A* 80.012325 (2009). DOI: 10.1103/PhysRevA.80.012325. URL: https://doi.org/10.1103/PhysRevA.80.012325.

[92] V. Eisler and Z. Zimborás. "Entanglement negativity in the harmonic chain out of equilibrium". In: *New J. Phys.* 16.123020 (2014). DOI: 10.1088/1367-2630/16/12/123020. URL: doi.org/10.1088/1367-2630/16/12/123020.

[93] N. E. Sherman et al. "Nonzero-temperature entanglement negativity of quantum spin models: Area law, linked cluster expansions, and sudden death". In: *Phys. Rev. E* 93.022128 (2016). DOI: 10.1103/PhysRevE.93.022128. URL: https://doi.org/10.1103/PhysRevE.93.022128.

[94] C. D. Nobili, A. Coser, and E. Tonni. "Entanglement negativity in a two dimensional harmonic lattice: area law and corner contributions". In: *J. Stat. Mech.* 2016.083102 (2016). DOI: 10.1088/1742-5468/2016/08/083102. URL: https://doi.org/10.1088/1742-5468/2016/08/083102.

[95] H. Wichterich, J. Molina-Vilaplana, and S. Bose. "Scaling of entanglement between separated blocks in spin chains at criticality". In: *Phys. Rev. A* 80.010304 (2009). DOI: 10.1103/PhysRevA.80.010304. URL: https://doi.org/10.1103/PhysRevA.80.010304.

[96] A. Bayat, S. Bose, and P. Sodano. "Entanglement Routers Using Macroscopic Singlets". In: *Phys. Rev. Lett.* 105.187204 (2010). DOI: 10.1103/PhysRevLett.105.187204. URL: https://doi.org/10.1103/PhysRevLett.105.187204.

[97] A. Bayat, P. Sodano, and S. Bose. "Negativity as the entanglement measure to probe the Kondo regime in the spin-chain Kondo model". In: *Phys. Rev. B* 81.064429 (2010). DOI: 10.1103/PhysRevB.81.064429. URL: https://doi.org/10.1103/PhysRevB.81.064429.

[98] A. Bayat et al. "Entanglement Probe of Two- Impurity Kondo Physics in a Spin Chain". In: *Phys. Rev. Lett.* 109.066403 (2012). DOI: 10.1103/PhysRevLett.109.066403. URL: https://doi.org/10.1103/PhysRevLett.109.066403.

[99] H. Wichterich, J. Vidal, and S. Bose. "Universality of the negativity in the Lipkin - Meshkov - Glick model". In: *Phys. Rev. A* 81.032311 (2010). DOI: 10.1103/PhysRevA.81.032311. URL: https://doi.org/10.1103/PhysRevA.81.032311.

[100] R. A. Santos, V. Korepin, and S. Bose. "Negativity for two blocks in the one-dimensional spin-1 Affleck-Kennedy-Lieb-Tasaki model". In: *Phys. Rev. A* 84.062307 (2011). DOI: 10.1103/PhysRevA.84.062307. URL: https://doi.org/10.1103/PhysRevA.84.062307.

[101] T. C. Luand and T. Grover. "Singularity in Entanglement Negativity Across Finite Temperature Phase Transitions". In: *Phys. Rev. B* 99.075157 (2019). DOI: 10.1103/PhysRevB.99.075157. URL: https://doi.org/10.1103/PhysRevB.99.075157.

[102] P. Ruggiero, V. Alba, and P. Calabrese. "Entanglement negativity in random spin chains". In: *Phys. Rev. B* 94.035152 (2016). DOI: 10.1103/PhysRevB.94.035152. URL: https://doi.org/10.1103/PhysRevB.94.035152.

[103] P. Ruggiero, V. Alba, and P. Calabrese. "Negativity Spectrum in the Random Singlet Phase". In: *Phys. Rev. B* 101.064207 (2020). DOI: 10.1103/PhysRevB.101.064207. URL: https://doi.org/10.1103/PhysRevB.101.064207.

[104] G. B. Mbeng, V. Alba, and P. Calabrese. "Negativity spectrum in 1D gapped phases of matter". In: *J. Phys. A* 50.194001 (2017). DOI: 10.1088/1751-8121/aa6734. URL: http://dx.doi.org/10.1088/1751-8121/aa6734.

[105] S. Wald, R. Arias, and V. Alba. "Entanglement and classical fluctuations at finite - temperature critical points". In: *J. Stat. Mech.* 033105 (2020). DOI: 10.1088/1742-5468/ab6b19. URL: http://dx.doi.org/10.1088/1742-5468/ab6b19.

[106] C.-M. Chung et al. "Entanglement negativity via replica trick: a Quantum Monte Carlo approach". In: *Phys. Rev. B* 90.064401 (2014). DOI: 10.1088/1742-5468/2013/05/P05013. URL: https://doi.org/10.1088/1742-5468/2013/05/P05013.

[107] V. Alba. "Entanglement negativity and conformal field theory: a Monte Carlo study". In: *Phys. Rev. A* P05013 (2013). DOI: 10.1088/1742-5468/2013/05/P05013. URL: https://doi.org/10.1088/1742-5468/2013/05/P05013.

[108] H. Shapourian et al. "Entanglement negativity spectrum of random mixed states: A diagrammatic approach". In: *ArXiv:2011.01277* (2021). URL: https://arxiv.org/abs/2011.01277.

[109] P. Calabrese, J. Cardy, and E. Tonni. "Entanglement Negativity in Quantum Field Theory". In: *Phys. Rev. Lett.* 109.13 (2012), p. 130502. DOI: 10.1103/PhysRevLett.109.130502. URL: https://link.aps.org/doi/10.1103/PhysRevLett.109.130502.

[110] P. Calabrese, J. Cardy, and E. Tonni. "Entanglement negativity in extended systems: a field theoretical approach". In: *J. Stat. Mech.* 88.P02008 (2013). DOI: 10.1088/1742-5468/2013/02/P02008. URL: http://dx.doi.org/10.1088/1742-5468/2013/02/P02008.

[111] P. Calabrese, L. Tagliacozzo, and E. Tonni. "Entanglement negativity in the critical Ising chain". In: *J. Stat. Mech.* P05002 (2013). DOI: 10.1088/1742-5468/2013/05/P05002. URL: https://doi.org/10.1088/1742-5468/2013/05/P05002.

[112] P. Calabrese, J. Cardy, and E. Tonni. "Finite temperature entanglement negativity in conformal field theory". In: *J. Phys. A* 48.015006 (2015). DOI: 10.1088/1751-8113/48/1/015006. URL: https://dx.doi.org/10.1088/1751-8113/48/1/015006.

[113] P. Ruggiero, V. Alba, and P. Calabrese. "Negativity spectrum of one-dimensional conformal field theories". In: *Phys. Rev. B* 94.195121 (2016). DOI: 10.1103/PhysRevB.94.195121. URL: http://dx.doi.org/10.1103/PhysRevB.94.195121.

[114] V. Alba, P. Calabrese, and E. Tonni. "Entanglement spectrum degeneracy and the Cardy formula in 1+1 dimensional conformal field theories". In: *J. Phys. A* 51.024001 (2018). DOI: 10.1088/1751-8121/aa9365. URL: https://doi.org/10.1088/1751-8121/aa9365.

[115] M. Kulaxizi, A. Parnachev, and G. Policastro. "Conformal Blocks and Negativity at Large Central Charge". In: *J. High Energ. Phys* 09 (2014), p. 010. DOI: 10.1007/JHEP09(2014)010. arXiv: 1407.0324 [hep-th].

[116] D. Bianchini and O. A. Castro-Alvaredo. "Branch point twist field correlators in the massive free Boson theory". In: *Nucl. Phys. B* 913.879 (2016). DOI: 10.1016/j.nuclphysb.2016.10.016.. URL: https://doi.org/10.1016/j.nuclphysb.2016.10.016..

[117] O. Blondeau-Fournier, O. A. Castro-Alvaredo, and B. Doyon. "Universal scaling of the logarithmic negativity in massive quantum field theory". In: *J. Phys. A* 49.125401 (2016). DOI: 10.1088/1751-8113/49/12/125401. URL: https://doi.org/10.1088/1751-8113/49/12/125401.

[118] O. A. Castro-Alvaredo et al. "Entanglement Content of Quantum Particle Excitations II. Disconnected Regions and Logarithmic Negativity". In: *J. High Energ. Phys.* 2019.58 (2019). DOI: 10.1007/JHEP11(2019)058. URL: https://doi.org/10.1007/JHEP11(2019)058.

[119] X. Wen et al. "Edge theory approach to topological entanglement entropy, mutual information, and entanglement negativity in Chern-Simons theories". In: *Phys. Rev. B* 93.245140 (2016). DOI: 10.1103/PhysRevB.93.245140. URL: https://doi.org/10.1103/PhysRevB.93.245140.

[120] X. Wen, P.-Y. Chang, and S. Ryu. "Topological entanglement negativity in Chern-Simons theories". In: *J. High Energ. Phys.* 2016.12 (2016). DOI: 10.1007/JHEP09(2016)012. URL: https://doi.org/10.1007/JHEP09(2016)012.

[121] C. Castelnovo. "Negativity and topological order in the toric code". In: *Phys. Rev. A* 88.4 (2013), p. 042319. DOI: 10.1103/PhysRevA.88.042319. URL: https://link.aps.org/doi/10.1103/PhysRevA.88.042319.

[122] Y. A. Lee and G. Vidal. "Entanglement negativity and topological order". In: *Phys. Rev. A* 88.4 (2013), p. 042318. DOI: 10.1103/PhysRevA.88.042318. URL: https://link.aps.org/doi/10.1103/PhysRevA.88.042318.

[123] O. Hart and C. Castelnovo. "Entanglement negativity and sudden death in the toric code at finite temperature". In: *Phys. Rev. B* 97.14 (2018), p. 144410. DOI: 10.1103/PhysRevB.97.144410. URL: https://link.aps.org/doi/10.1103/PhysRevB.97.144410.

[124] A. Coser, E. Tonni, and P. Calabrese. "Entanglement negativity after a global quantum quench". In: *Journal of Statistical Mechanics: Theory and Experiment* 2014.12 (2014), P12017. DOI: 10.1088/1742-5468/2014/12/p12017. URL: https://doi.org/10.1088/1742-5468/2014/12/p12017.

[125] V. Eisler and Z. Zimborás. "Entanglement negativity in the harmonic chain out of equilibrium". In: *New J. Phys.* 16.123020 (2014). DOI: 10.1088/1367-2630/16/12/123020. URL: https://doi.org/10.1088/1367-2630/16/12/123020.

[126] M. Hoogeveen and B. Doyon. "Entanglement negativity and entropy in non-equilibrium conformal field theory". In: *Nucl. Phys. B* 898.78 (2015). DOI: 10.1016/j.nuclphysb.2015.06.021. URL: https://doi.org/10.1016/j.nuclphysb.2015.06.021.

[127] V. Alba and P. Calabrese. "Quantum information dynamics in multipartite integrable systems". In: *Euro Phys. Lett.* 126.60001 (2019). DOI: 10.1209/0295-5075/126/60001. URL: https://doi.org/10.1209/0295-5075/126/60001.

[128] X. Wen, P.-Y. Chang, and S. Ryu. "Entanglement negativity after a local quantum quench in conformal field theories". In: *Phys. Rev. B* 92.075109 (2015). DOI: 10.1103/PhysRevB.92.075109. URL: https://doi.org/10.1103/PhysRevB.92.075109.

[129] M. J. Gullans and D. A. Huse. "Entanglement Structure of Current-Driven Diffusive Fermion Systems". In: *Phys. Rev. X* 9.021007 (2019). DOI: 10.1103/PhysRevX.9.021007. URL: https://doi.org/10.1103/PhysRevX.9.021007.

[130] J. Kudler-Flam, Y. Kusuki, and S. Ryu. "The quasi-particle picture and its breakdown after local quenches: mutual information, negativity, and reflected entropy". In: *J. High Energ. Phys.* 2021.146 (2021). DOI: 10.1007/JHEP03(2021)146. URL: https://doi.org/10.1007/JHEP03(2021)146.

[131] B. Shi, X. Dai, and Y.-M. Lu. "Entanglement negativity at the critical point of measurement-driven transition". In: *ArXiv:2012.00040* (2021). DOI: 10.1103/PhysRevB.102.064304. URL: https://arxiv.org/abs/2012.00040.

[132] E. Wybo, M. Knap, and F. Pollmann. "Entanglement dynamics of a many-body localized system coupled to a bath". In: *Phys. Rev. B* 102.064304 (2020). DOI: 10.1103/PhysRevB.102.064304. URL: https://doi.org/10.1103/PhysRevB.102.064304.

[133] M. Rangamani and M. Rota. "Comments on entanglement negativity in holographic field theories". In: *J. High Energ. Phys* 2014.60 (2014). DOI: 10.1007/JHEP10(2014)060. URL: https://doi.org/10.1007/JHEP10(2014)060.

[134] P. Chaturvedi, V. Malvimat, and G. Sengupta. "Entanglement negativity, Holography and Black holes". In: *Eur. Phys. J.* 78.499 (2018). DOI: 10.1140/epjc/s10052-018-5969-8. URL: https://doi.org/10.1140/epjc/s10052-018-5969-8.

[135] P. Chaturvedi, V. Malvimat, and G. Sengupta. "Covariant holographic entanglement negativity for Adjacent Subsystems in AdS_3/CFT_2". In: *Nucl. Phys. B* 945.114683 (2019). DOI: 10.1016/j.nuclphysb.2019.114683. URL: https://doi.org/10.1016/j.nuclphysb.2019.114683.

[136] P. Chaturvedi, V. Malvimat, and G. Sengupta. "Holographic quantum entanglement negativity". In: *J. High Energ. Phys.* 2018.5 (2018). DOI: 10.1007/JHEP05(2018)172. URL: https://doi.org/10.1007/JHEP05(2018)172.

[137] G. Sengupta and V. Malvimat. "Entanglement negativity at large central charge". In: *Phys. Rev. D* 103.10 (2021), p. 106003. DOI: 10.1103/PhysRevD.103.106003. URL: https://link.aps.org/doi/10.1103/PhysRevD.103.106003.

[138] J. Kudler-Flam and S. Ryu. "Entanglement negativity and minimal entanglement wedge cross sections in holographic theories". In: *Phys. Rev. D* 99.10 (2019), p. 106014. DOI: 10.1103/PhysRevD.99.106014. URL: https://link.aps.org/doi/10.1103/PhysRevD.99.106014.

[139] J. L. Cardy, O. A. Castro-Alvaredo, and B. Doyon. "Form Factors of Branch-Point Twist Fields in Quantum Integrable Models and Entanglement Entropy". In: *Journal of Statistical Physics* 130 (2007), pp. 129–168. DOI: https://doi.org/10.1007/s10955-007-9422-x.

[140] O. A. Castro-Alvaredo and B. Doyon. "Bi-partite entanglement entropy in massive $(1+1)$-dimensional quantum field theories". In: *Journal of Physics A: Mathematical and Theoretical* 42.50 (2009), p. 504006. DOI: 10.1088/1751-8113/42/50/504006. URL: https://doi.org/10.1088/1751-8113/42/50/504006.

[141] O. A. Castro-Alvaredo and B. Doyon. "Bi-partite entanglement entropy in integrable models with backscattering". In: *Journal of Physics A: Mathematical and Theoretical* 41.27 (2008), p. 275203. DOI: 10.1088/1751-8113/41/27/275203. URL: https://doi.org/10.1088/1751-8113/41/27/275203.

[142] O. A. Castro-Alvaredo and E. Levi. "Higher particle form factors of branch point twist fields in integrable quantum field theories". In: *Journal of Physics A: Mathematical and Theoretical* 44.25 (2011), p. 255401. DOI: 10.1088/1751-8113/44/25/255401. URL: https://doi.org/10.1088/1751-8113/44/25/255401.

[143] D. Bianchini, O. A. Castro-Alvaredo, and B. Doyon. "Entanglement entropy of non-unitary integrable quantum field theory". In: *Nuclear Physics B* 896 (2015), pp. 835–880. ISSN: 0550-3213. DOI: https://doi.org/10.1016/j.nuclphysb.2015.05.013. URL: https://www.sciencedirect.com/science/article/pii/S055032131500173X.

[144] P. Francesco, P. Mathieu, and D. Sénéchal. *Conformal Field Theory*. Springer-Verlag New York, 1997. DOI: 10.1007/978-1-4612-2256-9.

[145] P. Christe and M. Henkel. "Introduction to Conformal Invariance and Its Applications to Critical Phenomena". In: *Physics Today* 47.9 (1994), p. 94. DOI: 10.1063/1.2808642.

[146] F. C. Alcaraz, M. I. Berganza, and G. Sierra. "Entanglement of Low-Energy Excitations in Conformal Field Theory". In: *Phys. Rev. Lett.* 106.20 (2011), p. 201601. DOI: 10.1103/PhysRevLett.106.201601. URL: https://link.aps.org/doi/10.1103/PhysRevLett.106.201601.

[147] M. I. Berganza, F. C. Alcaraz, and G. Sierra. "Entanglement of excited states in critical spin chains". In: *Journal of Statistical Mechanics: Theory and Experiment* 2012.01 (2012), P01016. DOI: 10.1088/1742-5468/2012/01/p01016. URL: https://doi.org/10.1088/1742-5468/2012/01/p01016.

[148] D. Bianchini et al. "Entanglement entropy of non-unitary conformal field theory". In: *Journal of Physics A: Mathematical and Theoretical* 48.4 (2014), 04FT01. DOI: 10.1088/1751-8113/48/4/04ft01. URL: https://doi.org/10.1088/1751-8113/48/4/04ft01.

[149] O. B.-F., O. A. C.-A., and B. Doyon. "Universal scaling of the logarithmic negativity in massive quantum field theory". In: *Journal of Physics A: Mathematical and Theoretical* 49.12 (2016), p. 125401. DOI: 10.1088/1751-8113/49/12/125401. URL: https://doi.org/10.1088/1751-8113/49/12/125401.

[150] A.A. Belavin, A.M. Polyakov, and A.B. Zamolodchikov. "Infinite conformal symmetry in two-dimensional quantum field theory". In: *Nuclear Physics B* 241.2 (1984), pp. 333 –380. ISSN: 0550-3213. DOI: https://doi.org/10.1016/0550-3213(84)90052-X. URL: http://www.sciencedirect.com/science/article/pii/055032138490052X.

[151] B. Chen and J. Wu. "Rényi entropy of a free compact boson on a torus". In: *Phys. Rev. D* 91.10 (2015), p. 105013. DOI: 10.1103/PhysRevD.91.105013. URL: https://link.aps.org/doi/10.1103/PhysRevD.91.105013.

[152] C. P. Herzog and T. Nishioka. "Entanglement entropy of a massive fermion on a torus". In: *J. High Energ. Phys* 2013 (2013). DOI: 10.1007/JHEP03(2013)077. URL: https://doi.org/10.1007/JHEP03(2013)077.

[153] S. Datta and J. R. David. "Rényi entropies of free bosons on the torus and holography". In: *J. High Energ. Phys* 2014.81 (2014). DOI: 10.1007/JHEP04(2014)081. URL: https://doi.org/10.1007/JHEP04(2014)081.

[154] S. Mukhi, S. Murthy, and J. Q. Wu. "Entanglement, replicas, and Thetas". In: *J. High Energ. Phys* 2018.5 (2018). DOI: 10.1007/JHEP04(2014)081. URL: https://doi.org/10.1007/JHEP01(2018)005.

[155] J. J. Atick et al. "Multi-loop twist field correlation functions for ZN orbifolds". In: *Nuclear Physics B* 298.1 (1988), pp. 1–35. ISSN: 0550-3213. DOI: https://doi.org/10.1016/0550-3213(88)90302-1. URL: https://www.sciencedirect.com/science/article/pii/0550321388903021.

[156] F. Liu. "Free compact boson on branched covering of the torus". In: *Physics Letters B* 771 (2017), pp. 271–276. ISSN: 0370-2693. DOI: https://doi.org/10.1016/j.physletb.2017.05.058. URL: https://www.sciencedirect.com/science/article/pii/S0370269317304215.

[157] L. Alvarez-Gaumé, G. Moore, and C. Vafa. "Theta functions, modular invariance, and strings". In: *Commun.Math. Phys* 106 (1986), pp. 1–40. DOI: 10.1007/BF01210925. URL: https://doi.org/10.1007/BF01210925.

[158] T. Azeyanagi, T. Nishioka, and T. Takayanagi. "Near extremal black hole entropy as entanglement entropy via AdS_2/CFT_1". In: *Phys. Rev. D* 77.6 (2008), p. 064005. DOI: 10.1103/PhysRevD.77.064005. URL: https://link.aps.org/doi/10.1103/PhysRevD.77.064005.

[159] S.F. Lokhande and S. Mukhi. "Modular invariance and entanglement entropy". In: *J. High Energ. Phys.* 2015.106 (2015). DOI: 10.1007/JHEP06(2015)106. URL: https://doi.org/10.1007/JHEP06(2015)106.

[160] S. Mukhi and S. Murthy. "Fermions on replica geometries and the $\Theta - \theta$ relation". In: *Commun. Num. Theor. Phys* 13 (2019), 225 – 251. DOI: 10.4310/CNTP.2019.v13.n1.a8. URL: https://dx.doi.org/10.4310/CNTP.2019.v13.n1.a8.

[161] H. Shapourian and S. Ryu. "Finite-temperature entanglement negativity of free fermions". In: *J. Stat. Mech.* 043106 (2019). DOI: 10.1088/1742-5468/ab11e0. URL: https://doi.org/10.1088/1742-5468/ab11e0.

[162] J. L. Cardy. "Conformal Invariance and Surface Critical Behaviour". In: *Nucl. Phys. B* 240.514 (1984). DOI: 10.1016/0550-3213(84)90241-4. URL: https://doi.org/10.1016/0550-3213(84)90241-4.

[163] H. Q. Zhou et al. "Entanglement and boundary critical phenomena". In: *Phys. Rev. A* 74.5 (2006), p. 050305. DOI: 10.1103/PhysRevA.74.050305. URL: https://link.aps.org/doi/10.1103/PhysRevA.74.050305.

[164] I. Affleck and A. W. Ludwig. "Universal noninteger "ground-state degeneracy" in critical quantum systems". In: *Phys. Rev. Lett.* 67.2 (1991), pp. 161–164. DOI: 10.1103/PhysRevLett.67.161. URL: https://link.aps.org/doi/10.1103/PhysRevLett.67.161.

[165] E. Cornfeld and E. Sela. "Entanglement entropy and boundary renormalization group flow: Exact results in the Ising universality class". In: *Phys. Rev. B* 96.7 (2017), p. 075153. DOI: 10.1103/PhysRevB.96.075153. URL: https://link.aps.org/doi/10.1103/PhysRevB.96.075153.

[166] A. Coser, L. Tagliacozzo, and E. Tonni. "On Rényi entropies of disjoint intervals in conformal field theory". In: *Journal of Statistical Mechanics: Theory and Experiment* 2014.1 (2014), P01008. DOI: 10.1088/1742-5468/2014/01/p01008. URL: https://doi.org/10.1088/1742-5468/2014/01/p01008.

[167] M. Headrick. "Entanglement Rényi entropies in holographic theories". In: *Phys. Rev. D* 82.12 (2010), p. 126010. DOI: 10.1103/PhysRevD.82.126010. URL: https://link.aps.org/doi/10.1103/PhysRevD.82.126010.

[168] Pasquale Calabrese, John Cardy, and Erik Tonni. "Entanglement entropy of two disjoint intervals in conformal field theory: II". In: *Journal of Statistical Mechanics: Theory and Experiment* 2011.01 (2011), P01021. DOI: 10.1088/1742-5468/2011/01/p01021. URL: https://doi.org/10.1088/1742-5468/2011/01/p01021.

[169] Michele Caraglio and Ferdinando Gliozzi. "Entanglement entropy and twist fields". In: *Journal of High Energy Physics* 2008.11 (2008), pp. 076–076. DOI: 10.1088/1126-6708/2008/11/076. URL: https://doi.org/10.1088/1126-6708/2008/11/076.

[170] S. Furukawa, V. Pasquier, and J. Shiraishi. "Mutual Information and Boson Radius in a $c = 1$ Critical System in One Dimension". In: *Phys. Rev. Lett.* 102.17 (2009), p. 170602. DOI: 10.1103/PhysRevLett.102.170602. URL: https://link.aps.org/doi/10.1103/PhysRevLett.102.170602.

[171] V. Alba, L. Tagliacozzo, and P. Calabrese. "Entanglement entropy of two disjoint intervals in $c = 1$ theories". In: *Journal of Statistical Mechanics: Theory and Experiment* 2011.06 (2010), P06012. DOI: 10.1088/1742-5468/2011/06/p06012. URL: https://doi.org/10.1088/1742-5468/2011/06/p06012.

[172] H. Casini and M. Huerta. "Reduced density matrix and internal dynamics for multicomponent regions". In: *Classical and Quantum Gravity* 26.18 (2009), p. 185005. DOI: 10.1088/0264-9381/26/18/185005. URL: https://doi.org/10.1088/0264-9381/26/18/185005.

[173] J. Cardy. "Some results on the mutual information of disjoint regions in higher dimensions". In: *Journal of Physics A: Mathematical and Theoretical* 46.28 (2013), p. 285402. DOI: 10.1088/1751-8113/46/28/285402. URL: https://doi.org/10.1088/1751-8113/46/28/285402.

[174] N. Shiba. "Entanglement entropy of two spheres". In: *J. High Energ. Phys.* 2012.100 (2012). DOI: 10.1007/JHEP07(2012)100. URL: https://doi.org/10.1007/JHEP07(2012)100.

[175] P. Calabrese, J. Cardy, and E. Tonni. "Entanglement entropy of two disjoint intervals in conformal field theory". In: *Journal of Statistical Mechanics: Theory and Experiment* 2009.11 (2009), P11001. DOI: 10.1088/1742-5468/2009/11/p11001. URL: https://doi.org/10.1088/1742-5468/2009/11/p11001.

[176] A. Polkovnikov et al. "Colloquium: Nonequilibrium dynamics of closed interacting quantum systems". In: *Rev. Mod. Phys.* 83.3 (2011), pp. 863–883. DOI: 10.1103/RevModPhys.83.863. URL: https://link.aps.org/doi/10.1103/RevModPhys.83.863.

[177] C. Gogolin and J. Eisert. "Equilibration, thermalisation, and the emergence of statistical mechanics in closed quantum systems". In: *Reports on Progress in Physics* 79.5 (2016), p. 056001. DOI: 10.1088/0034-4885/79/5/056001. URL: https://doi.org/10.1088/0034-4885/79/5/056001.

[178] L. D'Alessio et al. "From quantum chaos and eigenstate thermalization to statistical mechanics and thermodynamics". In: *Advances in Physics* 65.3 (2016), pp. 239–362. DOI: 10.1080/00018732.2016.1198134. eprint: https://doi.org/10.1080/00018732.2016.1198134. URL: https://doi.org/10.1080/00018732.2016.1198134.

[179] P. Calabrese, F. H. L. Essler, and G. Mussardo. "Introduction to 'Quantum Integrability in Out of Equilibrium Systems'". In: *Journal of Statistical Mechanics: Theory and Experiment* 2016.6 (2016), p. 064001. DOI: 10.1088/1742-5468/2016/06/064001. URL: https://doi.org/10.1088/1742-5468/2016/06/064001.

[180] F. H. L. Essler and M. Fagotti. "Quench dynamics and relaxation in isolated integrable quantum spin chains". In: *Journal of Statistical Mechanics: Theory and Experiment* 2016.6 (2016), p. 064002. DOI: 10.1088/1742-5468/2016/06/064002. URL: https://doi.org/10.1088/1742-5468/2016/06/064002.

[181] P. Calabrese. "Entanglement and thermodynamics in non-equilibrium isolated quantum systems". In: *Physica A: Statistical Mechanics and its Applications* 504 (2018). Lecture Notes of the 14th International Summer School on Fundamental Problems in Statistical Physics, pp. 31–44. ISSN: 0378-4371. DOI: https://doi.org/10.1016/j.physa.2017.10.011. URL: https://www.sciencedirect.com/science/article/pii/S037843711731018X.

[182] J. M. Deutsch, H. Li, and A. Sharma. "Microscopic origin of thermodynamic entropy in isolated systems". In: *Phys. Rev. E* 87.4 (2013), p. 042135. DOI: 10.1103/PhysRevE.87.042135. URL: https://link.aps.org/doi/10.1103/PhysRevE.87.042135.

[183] L. F. Santos, A. Polkovnikov, and M. Rigol. "Entropy of Isolated Quantum Systems after a Quench". In: *Phys. Rev. Lett.* 107.4 (2011), p. 040601. DOI: 10.1103/PhysRevLett.107.040601. URL: https://link.aps.org/doi/10.1103/PhysRevLett.107.040601.

[184] M. Collura, M. Kormos, and P. Calabrese. "Stationary entanglement entropies following an interaction quench in 1D Bose gas". In: *Journal of Statistical Mechanics: Theory and Experiment* 2014.1 (2014), P01009. DOI: 10.1088/1742-5468/2014/01/p01009. URL: https://doi.org/10.1088/1742-5468/2014/01/p01009.

[185] N. Schuch et al. "Entropy Scaling and Simulability by Matrix Product States". In: *Phys. Rev. Lett.* 100.3 (2008), p. 030504. DOI: 10.1103/PhysRevLett.100.030504. URL: https://link.aps.org/doi/10.1103/PhysRevLett.100.030504.

[186] N. Schuch et al. "On entropy growth and the hardness of simulating time evolution". In: *New Journal of Physics* 10.3 (2008), p. 033032. DOI: 10.1088/1367-2630/10/3/033032. URL: https://doi.org/10.1088/1367-2630/10/3/033032.

[187] A. Perales and G. Vidal. "Entanglement growth and simulation efficiency in one-dimensional quantum lattice systems". In: *Phys. Rev. A* 78.4 (2008), p. 042337. DOI: 10.1103/PhysRevA.78.042337. URL: https://link.aps.org/doi/10.1103/PhysRevA.78.042337.

[188] P. Hauke et al. "Can one trust quantum simulators?" In: *Reports on Progress in Physics* 75.8 (2012), p. 082401. DOI: 10.1088/0034-4885/75/8/082401. URL: https://doi.org/10.1088/0034-4885/75/8/082401.

[189] J. Dubail. "Entanglement scaling of operators: a conformal field theory approach, with a glimpse of simulability of long-time dynamics in 1 + 1d". In: *Journal of Physics A: Mathematical and Theoretical* 50.23 (2017), p. 234001. DOI: 10.1088/1751-8121/aa6f38. URL: https://doi.org/10.1088/1751-8121/aa6f38.

[190] P. Calabrese and J. Cardy. "Time Dependence of Correlation Functions Following a Quantum Quench". In: *Phys. Rev. Lett.* 96.13 (2006), p. 136801. DOI: 10.1103/PhysRevLett.96.136801. URL: https://link.aps.org/doi/10.1103/PhysRevLett.96.136801.

[191] P. Calabrese and J. Cardy. "Quantum quenches in extended systems". In: *Journal of Statistical Mechanics: Theory and Experiment* 2007.06 (2007), P06008–P06008. DOI: 10.1088/1742-5468/2007/06/p06008. URL: https://doi.org/10.1088/1742-5468/2007/06/p06008.

[192] P. Calabrese and J. Cardy. "Evolution of Entanglement Entropy in One-Dimensional Systems". In: *J. Stat. Mech.* P04010 (2005). DOI: 10.1088/1742-5468/2005/04/P04010. URL: http://dx.doi.org/10.1088/1742-5468/2005/04/P04010.

[193] V. Alba and P. Calabrese. "Entanglement and thermodynamics after a quantum quench in integrable systems". In: *PNAS* 114.7947 (2017). DOI: 10.1073/pnas.1703516114. URL: https://doi.org/10.1073/pnas.1703516114.

[194] P. Calabrese. "Entanglement spreading in non-equilibrium integrable systems". In: *SciPost Phys. Lect. Notes* (2020), p. 20. DOI: 10.21468/SciPostPhysLectNotes.20. URL: https://scipost.org/10.21468/SciPostPhysLectNotes.20.

[195] T. Brydges et al. “Probing entanglement entropy via randomized measurements”. In: *Science* 364 (2019). DOI: 10.1126/science.aau4963. URL: http://dx.doi.org/10.1126/science.aau4963.

[196] E. Ilievski et al. “Quasilocal charges in integrable lattice systems”. In: *Journal of Statistical Mechanics: Theory and Experiment* 2016.6 (2016), p. 064008. DOI: 10.1088/1742-5468/2016/06/064008. URL: https://doi.org/10.1088/1742-5468/2016/06/064008.

[197] J. Cardy. “Quantum quenches to a critical point in one dimension: some further results”. In: *Journal of Statistical Mechanics: Theory and Experiment* 2016.2 (2016), p. 023103. DOI: 10.1088/1742-5468/2016/02/023103. URL: https://doi.org/10.1088/1742-5468/2016/02/023103.

[198] P. Calabrese and J. Cardy. “Quantum quenches in $1+1$ dimensional conformal field theories”. In: *Journal of Statistical Mechanics: Theory and Experiment* 2016.6 (2016), p. 064003. DOI: 10.1088/1742-5468/2016/06/064003. URL: https://doi.org/10.1088/1742-5468/2016/06/064003.

[199] B. Bertini, E. Tartaglia, and P. Calabrese. “Entanglement and diagonal entropies after a quench with no pair structure”. In: *Journal of Statistical Mechanics: Theory and Experiment* 2018.6 (2018), p. 063104. DOI: 10.1088/1742-5468/aac73f. URL: https://doi.org/10.1088/1742-5468/aac73f.

[200] A. Bastianello and P. Calabrese. “Spreading of entanglement and correlations after a quench with intertwined quasiparticles”. In: *SciPost Phys.* 5.033 (2018). DOI: 10.21468/SciPostPhys.5.4.033. URL: https://doi.org/10.21468/SciPostPhys.5.4.033.

[201] A. Bastianello and M. Collura. “Entanglement spreading and quasiparticle picture beyond the pair structure”. In: *SciPost Phys.* 8.045 (2020). DOI: 10.21468/SciPostPhys.8.3.045. URL: https://doi.org/10.21468/SciPostPhys.8.3.045.

[202] L. Piroli, B. Pozsgay, and E. Vernier. “What is an integrable quench?” In: *Nucl. Phys. B* 925.362 (2017). DOI: 10.1016/j.nuclphysb.2017.10.012. URL: https://doi.org/10.1016/j.nuclphysb.2017.10.012.

[203] E. H. Lieb and D.W. Robinson. “The finite group velocity of quantum spin systems”. In: *Commun.Math. Phys.* 28 (1972), 251–257. DOI: 10.1007/BF01645779. URL: https://doi.org/10.1007/BF01645779.

[204] V. Alba and P. Calabrese. “Quench action and Rényi entropies in integrable systems”. In: *Phys. Rev. B* 96.11 (2017), p. 115421. DOI: 10.1103/PhysRevB.96.115421. URL: https://link.aps.org/doi/10.1103/PhysRevB.96.115421.

[205] P. Calabrese. “Rényi entropies after releasing the Néel state in the XXZ spin-chain”. In: *J. Stat. Mech.* 113105 (2017). DOI: 10.1088/1742-5468/aa934c. URL: http://dx.doi.org/10.1088/1742-5468/aa934c.

[206] M. Mestyán, V. Alba, and P. Calabrese. “Rényi entropies of generic thermodynamic macrostates in integrable systems”. In: *J. Stat. Mech.* 083104 (2018). DOI: 10.1088/1742-5468/aad6b9. URL: https://doi.org/10.1088/1742-5468/aad6b9.

[207] O. A. Castro-Alvaredo et al. “Entanglement dynamics after a quench in Ising field theory: a branch point twist field approach”. In: *J. High Energ. Phys.* 2019.079 (2019). DOI: 10.1007/JHEP12(2019)079. URL: https://doi.org/10.1007/JHEP12(2019)079.

[208] K. Klobas and B. Bertini. "Entanglement dynamics in Rule 54: exact results and quasiparticle picture". In: *arXiv:2104.04513* (2021). URL: https://arxiv.org/abs/2104.04513.

[209] V. Alba and P. Calabrese. "Quantum information dynamics in multipartite integrable systems". In: *Euro Phys. Lett* 126.60001 (2019). DOI: 10.1209/0295-5075/126/60001. URL: https://doi.org/10.1209/0295-5075/126/60001.

[210] J. I. Latorre and A. Riera. "A short review on entanglement in quantum spin systems". In: *Journal of Physics A: Mathematical and Theoretical* 42.50 (2009), p. 504002. DOI: 10.1088/1751-8113/42/50/504002. URL: https://doi.org/10.1088/1751-8113/42/50/504002.

[211] I. Peschel. "Calculation of reduced density matrices from correlation functions". In: *Journal of Physics A: Mathematical and General* 36.14 (2003), pp. L205–L208. DOI: 10.1088/0305-4470/36/14/101. URL: https://doi.org/10.1088/0305-4470/36/14/101.

[212] I. Peschel and V. Eisler. "Reduced density matrices and entanglement entropy in free lattice models". In: *Journal of Physics A: Mathematical and Theoretical* 42.50 (2009), p. 504003. DOI: 10.1088/1751-8113/42/50/504003. URL: https://doi.org/10.1088/1751-8113/42/50/504003.

[213] I. Peschel. "Entanglement in solvable many-particle models". In: *Braz. J. Phys.* 42.267 (2012). URL: http://dx.doi.org/10.1007/s13538-012-0074-1.

[214] E. L. Basor and C. A. Tracy. "The Fisher-Hartwig conjecture and generalizations". In: *Physica A.* 177.167 (1991). URL: https://doi.org/10.1016/0378-4371(91)90149-7.

[215] E. L. Basor and K. E. Morrison. "The Fisher-Hartwig conjecture and Toeplitz eigenvalues". In: *Linear Algebra and Its Applications* 202.129 (1994). URL: https://doi.org/10.1016/0024-3795(94)90187-2.

[216] B. Q. Jin and V. E. Korepin. "Quantum Spin Chain, Toeplitz Determinants and the Fisher - Hartwig Conjecture". In: *Journal of Statistical Physics* 116 (2004), 79–95. URL: https://doi.org/10.1023/B:JOSS.0000037230.37166.42.

[217] P. Calabrese and F. H. L. Essler. "Universal corrections to scaling for block entanglement in spin-1/2XXchains". In: *Journal of Statistical Mechanics: Theory and Experiment* 2010.08 (2010), P08029. DOI: 10.1088/1742-5468/2010/08/p08029. URL: https://doi.org/10.1088/1742-5468/2010/08/p08029.

[218] H. M. Wiseman and J. A. Vaccaro. "Entanglement of Indistinguishable Particles Shared between Two Parties". In: *Phys. Rev. Lett.* 91.9 (2003), p. 097902. DOI: 10.1103/PhysRevLett.91.097902. URL: https://link.aps.org/doi/10.1103/PhysRevLett.91.097902.

[219] H. Barghathi, C. M. Herdman, and A. Del Maestro. "Rényi Generalization of the Accessible Entanglement Entropy". In: *Phys. Rev. Lett.* 121.15 (2018), p. 150501. DOI: 10.1103/PhysRevLett.121.150501. URL: https://link.aps.org/doi/10.1103/PhysRevLett.121.150501.

[220] H. Barghathi, E. Casiano-Diaz, and A. Del Maestro. "Operationally accessible entanglement of one-dimensional spinless fermions". In: *Phys. Rev. A* 100.2 (2019), p. 022324. DOI: 10.1103/PhysRevA.100.022324. URL: https://link.aps.org/doi/10.1103/PhysRevA.100.022324.

[221] M. C. Chung and I. Peschel. "Density-matrix spectra of solvable fermionic systems". In: *Phys. Rev. B* 64.6 (2001), p. 064412. DOI: 10.1103/PhysRevB.64.064412. URL: https://link.aps.org/doi/10.1103/PhysRevB.64.064412.

[222] H. F. Song et al. "Entanglement entropy from charge statistics: Exact relations for noninteracting many-body systems". In: *Phys. Rev. B* 83.16 (2011), p. 161408. DOI: 10.1103/PhysRevB.83.161408. URL: https://link.aps.org/doi/10.1103/PhysRevB.83.161408.

[223] H. F. Song et al. "Bipartite fluctuations as a probe of many-body entanglement". In: *Phys. Rev. B* 85.3 (2012), p. 035409. DOI: 10.1103/PhysRevB.85.035409. URL: https://link.aps.org/doi/10.1103/PhysRevB.85.035409.

[224] P. Calabrese, M. Mintchev, and E. Vicari. "Exact relations between particle fluctuations and entanglement in Fermi gases". In: *EPL (Europhysics Letters)* 98.2 (2012), p. 20003. DOI: 10.1209/0295-5075/98/20003. URL: https://doi.org/10.1209/0295-5075/98/20003.

[225] R. Süsstrunk and D. A. Ivanov. "Free fermions on a line: Asymptotics of the entanglement entropy and entanglement spectrum from full counting statistics". In: *EPL (Europhysics Letters)* 100.6 (2012), p. 60009. DOI: 10.1209/0295-5075/100/60009. URL: https://doi.org/10.1209/0295-5075/100/60009.

[226] P. Calabrese, P. Le Doussal, and S. N. Majumdar. "Random matrices and entanglement entropy of trapped Fermi gases". In: *Phys. Rev. A* 91.1 (2015), p. 012303. DOI: 10.1103/PhysRevA.91.012303. URL: https://link.aps.org/doi/10.1103/PhysRevA.91.012303.

[227] J. Keating and F. Mezzadri. "Random Matrix Theory and Entanglement in Quantum Spin Chains". In: *Commun. Math. Phys.* 252 (2005), 543–579. DOI: 10.1007/s00220-004-1188-2. URL: https://doi.org/10.1007/s00220-004-1188-2.

[228] V. Alba, M. Fagotti, and P. Calabrese. "Entanglement entropy of excited states". In: *J. Stat. Mech.* P10020 (2009). DOI: 10.1088/1742-5468/2009/10/P10020. URL: http://dx.doi.org/10.1088/1742-5468/2009/10/P10020.

[229] M. Fagotti and P. Calabrese. "Universal parity effects in the entanglement entropy of XX chains with open boundary conditions". In: *J. Stat. Mech.* P01017 (2011). DOI: 10.1088/1742-5468/2011/01/P01017. URL: http://dx.doi.org/10.1088/1742-5468/2011/01/P01017.

[230] F. Ares et al. "Excited state entanglement in homogeneous fermionic chains". In: *J. Phys. A* 47.245301 (2014). DOI: 10.1088/1751-8113/47/24/245301. URL: http://dx.doi.org/10.1088/1751-8113/47/24/245301.

[231] F. Ares, J. G. Esteve, and F. Falceto. "Entanglement of several blocks in fermionic chains". In: *Phys. Rev. A* 90.062321 (2014). DOI: 10.1103/PhysRevA.90.062321. URL: http://dx.doi.org/10.1103/PhysRevA.90.062321.

[232] F. Ares et al. "On the Mobius transformation in the entanglement entropy of fermionic chains". In: *J. Stat. Mech.* 90.043106 (2016). DOI: 10.1088/1742-5468/2016/04/043106. URL: http://dx.doi.org/.

[233] F. Ares et al. "Entanglement entropy and Möbius transformations for critical fermionic chains". In: *J. Stat. Mech.* 063104 (2017). DOI: 10.1088/1742-5468/aa71dc. URL: http://dx.doi.org/10.1088/1742-5468/aa71dc.

[234] P. Calabrese et al. “Parity effect in the scaling of block entanglement in gapless spin chains”. In: *Phys. Rev. Lett.* 095701 (2010). DOI: 10.1103/PhysRevLett.104.095701. URL: http://dx.doi.org/10.1103/PhysRevLett.104.095701.

[235] J. Cardy and P. Calabrese. “Unusual Corrections to Scaling in Entanglement Entropy”. In: *J. Stat. Mech.* P04023 (2010). DOI: 10.1088/1742-5468/2010/04/P04023. URL: http://dx.doi.org/10.1088/1742-5468/2010/04/P04023.

[236] P. Calabrese, J. Cardy, and I. Peschel. “Corrections to scaling for block entanglement in massive spin-chains”. In: *J. Stat. Mech.* P09003 (2010). DOI: 10.1088/1742-5468/2010/09/P09003. URL: http://dx.doi.org/10.1088/1742-5468/2010/09/P09003.

[237] K. Ohmori and Y. Tachikawa. “Physics at the entangling surface”. In: *J. Stat. Mech.* P04010 (2015). DOI: 10.1088/1742-5468/2015/04/P04010. URL: http://dx.doi.org/10.1088/1742-5468/2015/04/P04010.

[238] P. Calabrese, M. Mintchev, and E. Vicari. “Entanglement Entropy of One-Dimensional Gases”. In: *Phys. Rev. Lett.* 107.020601 (2011). DOI: 10.1103/PhysRevLett.107.020601. URL: https://doi.org/10.1103/PhysRevLett.107.020601.

[239] P. Calabrese, M. Mintchev, and E. Vicari. “The entanglement entropy of one-dimensional systems in continuous and homogeneous space”. In: *J. Stat. Mech.* P09028 (2011). URL: https://iopscience.iop.org/article/10.1088/1742-5468/2011/09/P09028.

[240] S. Murciano, P. Ruggiero, and P. Calabrese. “Entanglement and relative entropies for low-lying excited states in inhomogeneous one-dimensional quantum systems”. In: *J. Stat. Mech.* 034001 (2019). DOI: 10.1088/1742-5468/ab00ec. URL: http://dx.doi.org/10.1088/1742-5468/ab00ec.

[241] P. Calabrese, M. Mintchev, and E. Vicari. “Entanglement entropies in free fermion gases for arbitrary dimension”. In: *J. Stat. Mech.* 97.20009 (2012). DOI: 10.1209/0295-5075/97/20009. URL: https://doi.org/10.1209/0295-5075/97/20009.

[242] P. Calabrese, M. Mintchev, and E. Vicari. “Entanglement entropy of quantum wire junctions”. In: *J. Phys. A* 45.105206 (2012). DOI: 10.1088/1751-8113/45/10/105206. URL: https://doi.org/10.1088/1751-8113/45/10/105206.

[243] E. Vicari. “Entanglement and particle correlations of Fermi gases in harmonic traps”. In: *Phys. Rev. A* 85.062104 (2012). DOI: 10.1103/PhysRevA.85.062104. URL: https://doi.org/10.1103/PhysRevA.85.062104.

[244] V. Eisler and I. Peschel. “Free-fermion entanglement and spheroidal functions”. In: *J. Stat. Mech.* P04028 (2013). DOI: 10.1088/1742-5468/2013/04/P04028. URL: https://doi.org/10.1088/1742-5468/2013/04/P04028.

[245] A. Ossipov. “Entanglement Entropy in Fermi Gases and Anderson Orthogonality Catastrophe”. In: *Phys. Rev. Lett.* 113.130402 (2014). DOI: 10.1103/PhysRevLett.113.130402. URL: https://doi.org/10.1103/PhysRevLett.113.130402.

[246] P. Y. Chang and X. Wen. “Entanglement negativity in free-fermion systems: An overlap matrix approach”. In: *Phys. Rev. B* 93.195140 (2016). DOI: 10.1103/PhysRevB.93.195140. URL: https://doi.org/10.1103/PhysRevB.93.195140.

[247] B. Lacroix-A-Chez-Toine, S. N. Majumdar, and G. Schehr. “Entanglement Entropy and Full Counting Statistics for 2d-Rotating Trapped Fermions”. In: *Phys. Rev. A* 99.021602 (2019). DOI: 10.1103/PhysRevA.99.021602. URL: https://doi.org/10.1103/PhysRevA.99.021602.

[248] J. Dubail et al. "Conformal Field Theory for Inhomogeneous One-dimensional Quantum Systems: the Example of Non-Interacting Fermi Gases". In: *SciPost Phys.* 2.1 (2017), p. 002. DOI: 10.21468/SciPostPhys.2.1.002. URL: https://scipost.org/10.21468/SciPostPhys.2.1.002.

[249] N. Laflorencie et al. "Boundary Effects in the Critical Scaling of Entanglement Entropy in 1D Systems". In: *Phys. Rev. Lett.* 96.10 (2006), p. 100603. DOI: 10.1103/PhysRevLett.96.100603. URL: https://link.aps.org/doi/10.1103/PhysRevLett.96.100603.

[250] A. Bastianello. "Rényi entanglement entropies for the compactified massless boson with open boundary conditions". In: *J. High En. Phys.* 141 (2019). DOI: 10.1007/JHEP10(2019)141. URL: https://dx.doi.org/10.1007/JHEP10(2019)141.

[251] A. Bastianello, J. Dubail, and J.-M. Stéphan. "Entanglement entropies of inhomogeneous Luttinger liquids". In: *Journal of Physics A: Mathematical and Theoretical* 53.15 (2020), p. 155001. DOI: 10.1088/1751-8121/ab7580. URL: https://doi.org/10.1088/1751-8121/ab7580.

[252] F. Iglói and I. Peschel. "On reduced density matrices for disjoint subsystems". In: *EPL (Europhysics Letters)* 89.4 (2010), p. 40001. DOI: 10.1209/0295-5075/89/40001. URL: https://doi.org/10.1209/0295-5075/89/40001.

[253] V. Alba, L. Tagliacozzo, and P. Calabrese. "Entanglement entropy of two disjoint blocks in critical Ising models". In: *Phys. Rev. B* 81.6 (2010), p. 060411. DOI: 10.1103/PhysRevB.81.060411. URL: https://link.aps.org/doi/10.1103/PhysRevB.81.060411.

[254] M. Fagotti and P. Calabrese. "Entanglement entropy of two disjoint blocks in XY chains". In: *Journal of Statistical Mechanics: Theory and Experiment* 2010.04 (2010), P04016. DOI: 10.1088/1742-5468/2010/04/p04016. URL: https://doi.org/10.1088/1742-5468/2010/04/p04016.

[255] P. Deift, A. Its, and I. Krasovsky. "Asymptotics of Toeplitz, Hankel, and Toeplitz+Hankel determinants with Fisher-Hartwig singularities". In: *Ann. Math.* 174.1243 (2011). DOI: 10.4007/annals.2011.174.2.12. URL: http://dx.doi.org/10.4007/annals.2011.174.2.12.

[256] E. Basor and T. Ehrhardt. "Asymptotic Formulas for Determinants of a Special Class of Toeplitz + Hankel Matrices". In: *Large Truncated Toeplitz Matrices, Toeplitz Operators, and Related Topics. Operator Theory: Advances and Applications.* (2017). DOI: 10.1007/978-3-319-49182-0_9. URL: https://doi.org/10.1007/978-3-319-49182-0_9.

[257] M. Fagotti and P. Calabrese. "Evolution of entanglement entropy following a quantum quench: Analytic results for the *XY* chain in a transverse magnetic field". In: *Phys. Rev. A* 78.1 (2008), p. 010306. DOI: 10.1103/PhysRevA.78.010306. URL: https://link.aps.org/doi/10.1103/PhysRevA.78.010306.

[258] A. Coser, E. Tonni, and P. Calabrese. "Spin structures and entanglement of two disjoint intervals in conformal field theories". In: *J. Stat. Mech.* 053109 (2016). DOI: 10.1088/1742-5468/2016/05/053109. URL: https://doi.org/10.1088/1742-5468/2016/05/053109.

[259] P. Fendley, H. Saleur, and N. Warner. "Exact solution of a massless scalar field with a relevant boundary interaction". In: *Nuclear Physics B* 430.3 (1994), pp. 577–596. ISSN: 0550-3213. DOI: https://doi.org/10.1016/0550-3213(94)90160-0. URL: https://www.sciencedirect.com/science/article/pii/0550321394901600.

[260] O. A. Castro-Alvaredo and B. Doyon. "Bi-partite entanglement entropy in massive QFT with a boundary: the Ising model". In: *J. Stat. Phys.* 134.105 (2009). DOI: 10.1007/s10955-008-9664-2. URL: http://dx.doi.org/10.1007/s10955-008-9664-2.

[261] V. Eisler and Z. Zimborás. "On the partial transpose of fermionic Gaussian states". In: *New J. Phys.* 17.053048 (2015). DOI: 10.1088/1367-2630/17/5/053048. URL: https://doi.org/10.1088/1367-2630/17/5/053048.

[262] A. Coser, E. Tonni, and P. Calabrese. "Partial transpose of two disjoint blocks in XY spin chains". In: *J. Stat. Mech.* P08005 (2015). DOI: 10.1088/1742-5468/2015/08/P08005. URL: https://doi.org/10.1088/1742-5468/2015/08/P08005.

[263] A. Coser, E. Tonni, and P. Calabrese. "Towards the entanglement negativity of two disjoint intervals for a one dimensional free fermion". In: *J. Stat. Mech.* 033116 (2016). DOI: 10.1088/1742-5468/2016/03/033116. URL: https://doi.org/10.1088/1742-5468/2016/03/033116.

[264] V. Eisler and Z. Zimborás. "Entanglement negativity in two-dimensional free lattice models". In: *Phys. Rev. B* 93.11 (2016), p. 115148. DOI: 10.1103/PhysRevB.93.115148. URL: https://link.aps.org/doi/10.1103/PhysRevB.93.115148.

[265] P.-Y. Chang and X. Wen. "Entanglement negativity in free-fermion systems: An overlap matrix approach". In: *Phys. Rev. B* 93.19 (2016), p. 195140. DOI: 10.1103/PhysRevB.93.195140. URL: https://link.aps.org/doi/10.1103/PhysRevB.93.195140.

[266] Christopher P Herzog and Yihong Wang. In: 2016.7 (2016), p. 073102. DOI: 10.1088/1742-5468/2016/07/073102. URL: https://doi.org/10.1088/1742-5468/2016/07/073102.

[267] J. Eisert et al. "Entanglement negativity bounds for fermionic Gaussian states". In: *Phys. Rev. B* 97.16 (2018), p. 165123. DOI: 10.1103/PhysRevB.97.165123. URL: https://link.aps.org/doi/10.1103/PhysRevB.97.165123.

[268] H. Shapourian, K. Shiozaki, and S. Ryu. "Many-body topological invariants in fermionic symmetry-protected topological phases: Cases of point group symmetries". In: *Phys. Rev. B* 95.20 (2017), p. 205139. DOI: 10.1103/PhysRevB.95.205139. URL: https://link.aps.org/doi/10.1103/PhysRevB.95.205139.

[269] K. Shiozaki et al. "Many-body topological invariants for fermionic short-range entangled topological phases protected by antiunitary symmetries". In: *Phys. Rev. B* 98.3 (2018), p. 035151. DOI: 10.1103/PhysRevB.98.035151. URL: https://link.aps.org/doi/10.1103/PhysRevB.98.035151.

[270] H. Shapourian, R. S. K. Mong, and S. Ryu. "Anyonic Partial Transpose I: Quantum Information Aspects". In: *arXiv:2012.02222* (2021). URL: https://arxiv.org/abs/2012.02222.

[271] H. Shapourian and S. Ryu. "Entanglement negativity of fermions: Monotonicity, separability criterion, and classification of few-mode states". In: *Phys. Rev. A* 99.2 (2019), p. 022310. DOI: 10.1103/PhysRevA.99.022310. URL: https://link.aps.org/doi/10.1103/PhysRevA.99.022310.

[272] J. K. Flam, H. Shapourian, and S. Ryu. "The negativity contour: a quasi-local measure of entanglement for mixed states". In: *SciPost Phys.* 8.4 (2020), p. 63. DOI: 10.21468/SciPostPhys.8.4.063. URL: https://scipost.org/10.21468/SciPostPhys.8.4.063.

[273] R. Simon. "Peres-Horodecki Separability Criterion for Continuous Variable Systems". In: *Phys. Rev. Lett.* 84.12 (2000), pp. 2726–2729. DOI: 10.1103/PhysRevLett.84.2726. URL: https://link.aps.org/doi/10.1103/PhysRevLett.84.2726.

[274] S. Groha, F. Essler, and P.Calabrese. "Full counting statistics in the transverse field Ising chain". In: *SciPost Phys.* 4.6 (2018), p. 43. DOI: 10.21468/SciPostPhys.4.6.043. URL: https://scipost.org/10.21468/SciPostPhys.4.6.043.

[275] R. Balian and E. Brezin. "Nonunitary Bogoliubov transformations and extension of Wick's theorem". In: *Il Nuovo Cimento B* 64.37 (1969), 37–55. DOI: 10.1007/BF02710281. URL: https://link.springer.com/article/10.1007/BF02710281.

[276] M. Kiefer-Emmanouilidis et al. "Bounds on the entanglement entropy by the number entropy in non-interacting fermionic systems". In: *SciPost Phys.* 8.6 (2020), p. 83. DOI: 10.21468/SciPostPhys.8.6.083. URL: https://scipost.org/10.21468/SciPostPhys.8.6.083.

[277] M. Kiefer-Emmanouilidis et al. "Evidence for Unbounded Growth of the Number Entropy in Many-Body Localized Phases". In: *Phys. Rev. Lett.* 124.24 (2020), p. 243601. DOI: 10.1103/PhysRevLett.124.243601. URL: https://link.aps.org/doi/10.1103/PhysRevLett.124.243601.

[278] M. Kiefer-Emmanouilidis et al. "Unlimited growth of particle fluctuations in many-body localized phases". In: *Annals of Physics* (2021), p. 168481. ISSN: 0003-4916. DOI: https://doi.org/10.1016/j.aop.2021.168481. URL: https://www.sciencedirect.com/science/article/pii/S0003491621000877.

[279] V. Alba and P. Calabrese. "Quantum information scrambling after a quantum quench". In: *Phys. Rev. B* 100.11 (2019), p. 115150. DOI: 10.1103/PhysRevB.100.115150. URL: https://link.aps.org/doi/10.1103/PhysRevB.100.115150.

[280] Maurizio Fagotti. "On conservation laws, relaxation and pre-relaxation after a quantum quench". In: *Journal of Statistical Mechanics: Theory and Experiment* 2014.3 (2014), P03016. DOI: 10.1088/1742-5468/2014/03/p03016. URL: https://doi.org/10.1088/1742-5468/2014/03/p03016.

[281] G. Perfetto, L. Piroli, and A. Gambassi. "Quench action and large deviations: Work statistics in the one-dimensional Bose gas". In: *Phys. Rev. E* 100.3 (2019), p. 032114. DOI: 10.1103/PhysRevE.100.032114. URL: https://link.aps.org/doi/10.1103/PhysRevE.100.032114.

[282] V. Alba. "Entanglement and quantum transport in integrable systems". In: *Phys. Rev. B* 97.24 (2018), p. 245135. DOI: 10.1103/PhysRevB.97.245135. URL: https://link.aps.org/doi/10.1103/PhysRevB.97.245135.

[283] B. Bertini et al. "Entanglement evolution and generalised hydrodynamics: noninteracting systems". In: *Journal of Physics A: Mathematical and Theoretical* 51.39 (2018), 39LT01. DOI: 10.1088/1751-8121/aad82e. URL: https://doi.org/10.1088/1751-8121/aad82e.

[284] V. Alba, B. Bertini, and M. Fagotti. "Entanglement evolution and generalised hydrodynamics: interacting integrable systems". In: *SciPost Phys.* 7.1 (2019), p. 5. DOI: 10.21468/SciPostPhys.7.1.005. URL: https://scipost.org/10.21468/SciPostPhys.7.1.005.

[285] V. Alba. "Towards a generalized hydrodynamics description of Rényi entropies in integrable systems". In: *Phys. Rev. B* 99.4 (2019), p. 045150. DOI: 10.1103/PhysRevB.99.045150. URL: https://link.aps.org/doi/10.1103/PhysRevB.99.045150.

[286] P. Ruggiero et al. "Quantum Generalized Hydrodynamics". In: *Phys. Rev. Lett.* 124.14 (2020), p. 140603. DOI: 10.1103/PhysRevLett.124.140603. URL: https://link.aps.org/doi/10.1103/PhysRevLett.124.140603.

[287] A. Nahum et al. "Quantum Entanglement Growth under Random Unitary Dynamics". In: *Phys. Rev. X* 7.3 (2017), p. 031016. DOI: 10.1103/PhysRevX.7.031016. URL: https://link.aps.org/doi/10.1103/PhysRevX.7.031016.

[288] A. Nahum, S. Vijay, and J. Haah. "Operator Spreading in Random Unitary Circuits". In: *Phys. Rev. X* 8.2 (2018), p. 021014. DOI: 10.1103/PhysRevX.8.021014. URL: https://link.aps.org/doi/10.1103/PhysRevX.8.021014.

[289] T. Zhou and A. Nahum. "Entanglement Membrane in Chaotic Many-Body Systems". In: *Phys. Rev. X* 10.3 (2020), p. 031066. DOI: 10.1103/PhysRevX.10.031066. URL: https://link.aps.org/doi/10.1103/PhysRevX.10.031066.

[290] B. Bertini, P. Kos, and T. Prosen. "Entanglement Spreading in a Minimal Model of Maximal Many-Body Quantum Chaos". In: *Phys. Rev. X* 9.2 (2019), p. 021033. DOI: 10.1103/PhysRevX.9.021033. URL: https://link.aps.org/doi/10.1103/PhysRevX.9.021033.

[291] S. Gopalakrishnan and A. Lamacraft. "Unitary circuits of finite depth and infinite width from quantum channels". In: *Phys. Rev. B* 100.6 (2019), p. 064309. DOI: 10.1103/PhysRevB.100.064309. URL: https://link.aps.org/doi/10.1103/PhysRevB.100.064309.

[292] B. Bertini and P. Calabrese. "Prethermalization and thermalization in entanglement dynamics". In: *Phys. Rev. B* 102.9 (2020), p. 094303. DOI: 10.1103/PhysRevB.102.094303. URL: https://link.aps.org/doi/10.1103/PhysRevB.102.094303.

[293] L. Piroli et al. "Exact dynamics in dual-unitary quantum circuits". In: *Phys. Rev. B* 101.9 (2020), p. 094304. DOI: 10.1103/PhysRevB.101.094304. URL: https://link.aps.org/doi/10.1103/PhysRevB.101.094304.

[294] Ranjan Modak, Vincenzo Alba, and Pasquale Calabrese. "Entanglement revivals as a probe of scrambling in finite quantum systems". In: *Journal of Statistical Mechanics: Theory and Experiment* 2020.8 (2020), p. 083110. DOI: 10.1088/1742-5468/aba9d9. URL: https://doi.org/10.1088/1742-5468/aba9d9.

[295] A. Chan, A. De Luca, and J. T. Chalker. "Solution of a Minimal Model for Many-Body Quantum Chaos". In: *Phys. Rev. X* 8.4 (2018), p. 041019. DOI: 10.1103/PhysRevX.8.041019. URL: https://link.aps.org/doi/10.1103/PhysRevX.8.041019.

[296] A. J. Friedman et al. "Spectral Statistics and Many-Body Quantum Chaos with Conserved Charge". In: *Phys. Rev. Lett.* 123.21 (2019), p. 210603. DOI: 10.1103/PhysRevLett.123.210603. URL: https://link.aps.org/doi/10.1103/PhysRevLett.123.210603.

[297] T. Rakovszky, F. Pollmann, and C. W. von Keyserlingk. "Sub-ballistic Growth of Rényi Entropies due to Diffusion". In: *Phys. Rev. Lett.* 122.25 (2019), p. 250602. DOI: 10.1103/PhysRevLett.122.250602. URL: https://link.aps.org/doi/10.1103/PhysRevLett.122.250602.

[298] R. Blumenhagen and E. Plauschinn. *Introduction to Conformal Field Theory. With Applications to String Theory*. Springer-Verlag Berlin Heidelberg, 2009. DOI: 10.1007/978-3-642-00450-6.